FOSSIL ENERGY

DOE/BC/14936-9
(DE98000456)

APPLICATION OF ADVANCED RESERVOIR CHARACTERIZATION, SIMULATION AND PRODUCTION OPTIMIZATION STRATEGIES TO MAXIMIZE RECOVERY IN SLOPE AND BASIN CLASTIC RESERVOIRS, WEST TEXAS (DELAWARE BASIN)

Annual Report
March 31, 1996 to March 30, 1997

By
Shirley P. Dutton
George B. Asquith
Mark D. Barton
Andrew G. Cole
John Gogas
Mohammed A. Malik
Sigrid J. Clift
Jose I. Guzman

November 1997

Performed Under Contract No. DE-FC22-95BC14936

Bureau of Economic Geology
University of Texas at Austin
Austin, Texas

National Petroleum Technology Office
U. S. DEPARTMENT OF ENERGY
Tulsa, Oklahoma

DOE/BC/14936-9
Distribution Category UC-122

Application Of Advanced Reservoir Characterization, Simulation And Production Optimization Strategies To Maximize Recovery In Slope And Basin Clastic Reservoirs, West Texas (Delaware Basin)

Annual Report

By
Shirley P. Dutton
George B. Asquith
Mark D. Barton
Andrew G. Cole
John Gogas
Mohammed A. Malik
Sigrid J. Clift
Jose I. Guzman

November 1997

Work Performed Under Contract No. DE-FC22-95BC14936

Prepared for
BDM-Oklahoma/
U.S. Department of Energy
Assistant Secretary for Fossil Energy

Jerry Casteel, Project Manager
National Petroleum Technology Office
P.O. Box 3628
Tulsa, OK 74101

Prepared by:
Bureau of Economic Geology
The University of Texas at Austin
Austin, TX 78713-8924

CONTENTS

Figures

Tables

ABSTRACT

The objective of this Class III project is to demonstrate that detailed reservoir characterization of clastic reservoirs in basinal sandstones of the Delaware Mountain Group in the Delaware Basin of West Texas and New Mexico is a cost-effective way to recover more of the original oil in place by strategic infill-well placement and geologically based field development. The study focused on Geraldine Ford field, which produces from the upper Bell Canyon Formation (Ramsey sandstone), and West Ford field, which produces from the upper Cherry Canyon and lower Bell Canyon Formations. Reservoirs in these and other Delaware Mountain Group fields have low producibility (average recovery <14 percent of the original oil in place) because of a high degree of vertical and lateral heterogeneity caused by depositional processes and postdepositional diagenetic modification.

Outcrop analogs were studied to better interpret the depositional processes that formed the reservoirs at Geraldine Ford and West Ford fields and to determine the dimensions of reservoir sandstone bodies. Stratal relationships examined in laterally continuous outcrop exposures of upper Bell Canyon sandstones in Culberson County, Texas, indicate that the sandstones were deposited by high- and low-density turbidity currents in a basinal deep-water setting. The fundamental depositional element is the channel with attached levees and lobes. These elements appear to initially step into the basin, aggrade, then step back toward the shelf.

Core descriptions, subsurface mapping, and study of the outcrop analog indicate that reservoir sandstones at the Ford Geraldine unit were deposited in a similar channel-levee and lobe system. Ramsey sandstone channels are about 1,200 ft wide and 15 to 35 ft thick, and they are flanked by levee deposits. Lobe facies were deposited at the mouths of channels. Uniform grain size in the sediment source area resulted in channel, levee, and lobe facies having similar porosity and permeability relationships. The main control on reservoir quality in these sandstones is the

volume of authigenic calcite and chlorite. Calcite cement occurs in all facies but is more abundant near the top and base of sandstones.

Petrophysical characterization of the Ford Geraldine unit was accomplished by integrating core and log data and quantifying petrophysical properties from wireline logs. Core-porosity to log-data transforms and core-porosity to core-permeability transforms were derived for the reservoir. Water saturations were calculated by the modified Archie equation: $S_w = [(1/Ø^{1.83}) \times (R_w/R_t)]^{1/1.90}$. These data were used to construct maps of porosity, permeability, net pay, water saturation, porous hydrocarbon volume, and other reservoir properties.

Interpretation of the 3-D seismic volume indicates that Ramsey sandstone thickness in the Ford Geraldine unit is ≤1/4 wavelength of the seismic data. The coherency cube is effective in delineating the field outline, and a residual map of the top of the Lamar Limestone identified a residual high that is associated with Ramsey sandstone thickness. The amplitude family of attributes had the highest correlations with the reservoir properties of average porosity and porosity × thickness. The best correlation coefficients were less than 0.4 when all the wells were used, but higher correlations were found in smaller areas within the unit.

In preparation for simulation of the pilot area, conditional simulation was used to generate interwell permeability distributions. A spherical semivariogram with a dimensionless correlation length of 0.3 gave the most geologically realistic 3-D geostatistical permeability distribution. The 3-D permeabilities were scaled up by using direct fine-scale simulation, assuming steady-state flow. The conditionally simulated stochastic permeabilities generated for the demonstration area conform reasonably well with the main geologic features of the reservoir.

Production and other reservoir data were used to make preliminary estimates of tertiary recovery for the demonstration area. Using the average 7.9-percent tertiary performance of the rest of the unit, it is estimated that 904,000 STB of oil can be recovered from the demonstration area with a CO_2 flood. This is a conservative estimate; the results of the planned flow simulations are expected to confirm or exceed this estimate.

EXECUTIVE SUMMARY

Slope and basin clastic reservoirs in sandstones of the Delaware Mountain Group in the Delaware Basin of West Texas and New Mexico contained more than 1.8 billion barrels (Bbbl) of oil at discovery. Recovery efficiencies of these reservoirs have averaged only 14 percent since production began in the 1920's, and thus a substantial amount of the original oil in place remains unproduced. In this project, the Bureau of Economic Geology, The University of Texas at Austin, and Conoco, Inc., are deploying advanced reservoir characterization strategies to characterize Geraldine Ford and Ford West fields, which produce from the two most prolific horizons in the Delaware Mountain Group in Texas. Work performed during the second year of the contract focused more on reservoir characterization of the Ford Geraldine unit because it has more available data and a larger volume of oil in place than Ford West field, making it the more attractive target for enhanced recovery. The goal of the study is to demonstrate that reservoir characterization, using 3-D seismic data, high-resolution sequence stratigraphy, and other techniques, and integrated with reservoir simulation, can optimize infill drilling and Enhanced Oil Recovery (EOR) projects. Through technology transfer workshops and other presentations, the knowledge gained in the study of these two fields with 89 MMbbl of remaining oil in place can then be applied to increase production from the more than 100 other Delaware Mountain Group reservoirs, which together contain 1.6 Bbbl of remaining oil.

Interpretation of the processes that deposited the sandstones of the Delaware Mountain Group has long been controversial, and this controversy is of practical importance because different depositional models predict very different sandstone distribution, geometry, and continuity. Applying the correct depositional model is critical to effective reservoir development, but subsurface data commonly do not provide the interwell-scale information needed to differentiate between competing depositional models. Thus, a key component of our reservoir characterization effort was to investigate well-exposed analogs of the subsurface reservoirs.

Stratal relationships indicate that upper Bell Canyon sandstones exposed in outcrop 24 mi west of the Ford Geraldine unit were deposited in channels with levees and attached lobes. Channels are up to 60 ft thick and 1,000 ft across, but they may amalgamate to form bodies that are 3,000 ft across. The channels have erosive bases and are composed largely of cross-stratified sandstones. The channels are flanked by wedge-shaped bodies interpreted as channel levees, which are composed of thin-bedded sandstones and siltstones. They are 5 to 15 ft thick and several thousand feet long. Away from the channels the levees thin and interfinger with organic-rich siltstones interpreted as interchannel deposits. Basinward the channels bifurcate and terminate in lobes that are up to 30 ft thick and between 1 and 10 mi wide. The lobes have a broad lenticular geometry and dip gently into the basin, where they interfinger with sheets of laminated siltstones. This depositional model developed from outcrop can be widely applied by operators to reservoirs that produce from Delaware Mountain Group sandstones.

The model was used to interpret the processes that deposited the Ramsey sandstone reservoirs at the Ford Geraldine unit and to map the geometry and dimensions of the architectural elements within it. On the basis of core descriptions, subsurface mapping, and the depositional model, the reservoir sandstones are interpreted to consist of sheetlike lobe deposits overlain and incised by lenticular 1,200-ft-wide channels. Adjacent levee and overbank deposits vertically and laterally separate channel sandstone bodies. Ramsey sandstones are bounded by laterally continuous, organic-rich siltstones deposited by settling from suspension. The siltstone beds provide the greatest amount of depositional heterogeneity in the reservoir because of the grain size and permeability contrast between sandstones and siltstone facies. The sandstone facies all have similar grain sizes, and thus there may not be much permeability contrast or inhibition of flow between sandstone facies, for example, at contacts between channel and levee facies or where channels incise into lobe facies. Delaware Mountain Group sandstones are unusual in having a very narrow range of detrital grain sizes and no detrital clay. Because grain size is so constant in the sandstone facies, the main control on reservoir quality is the volume of authigenic cement, particularly calcite and chlorite. Calcite cement occurs in all facies but is more abundant near the top and base of

sandstones, suggesting that the laminated siltstones were the source of calcite. Additional petrographic work is needed to determine the controls on calcite and chlorite cement distribution within the Ford Geraldine unit.

Because most of the wells in the Ford Geraldine unit were drilled and logged in the 1950's and early 1960's, special techniques had to be used to maximize the information that could be derived from the old logs. A new technique was developed to determine the value of saturation exponent (n), which is used to calculate hydrocarbon saturation of a reservoir from geophysical logs. This approach uses water saturations measured by core analysis; these data are generally available in mature fields that have few or no relative permeability curves. Because many of the wells with resistivity logs in the unit have only a deep laterolog, it was necessary to correct the deep laterolog to true formation resistivity (R_t) using a transform. Without applying this transform, water saturations in the wells with only a deep laterolog would be overestimated. For Bell Canyon sandstones in the Ford–Geraldine area, water saturations should be calculated by the following modified Archie equation:

$$S_w = [(1/Ø\text{^}1.83) \times (R_w/R_t)]\text{^}1/1.90.$$

Using published information and log and core data, net-pay cutoffs of volume of clay $\leq$ 15 percent, porosity $\geq$ 15 percent, and water saturation < 60 percent were determined for the Ramsey sandstone.

The acquisition of 3-D seismic data for this project was designed specifically to target Delaware Mountain Group reservoirs. An older 2-D seismic grid was used to determine the survey design; a minimum of 48 nominal fold is needed to image Bell and Cherry Canyon reservoirs. For the first time a key subsurface horizon above the Ramsey reservoir sandstone, the top of the Lamar Limestone, was imaged with 3-D seismic data. This surface had not previously been imaged satisfactorily because of shallow statics problems in the area. Residual mapping of the Lamar assisted in visualizing areas of thick Ramsey sandstone development. Interpretation of the data included coherence cube evaluation to highlight discontinuities—perhaps one of the first uses of

the coherency cube in a Delaware Mountain Group reservoir. This technique was effective in delineating the field outline. Ramsey sandstone thickness in the Ford Geraldine unit is ≤1/4 wavelength of the seismic data. The amplitude family of attributes had the highest correlations with the reservoir properties of average porosity and porosity × thickness.

On the basis of reservoir characterization of the Ford Geraldine unit and West Ford field, the northern end of the Ford Geraldine unit was chosen as the proposed demonstration area. This area was chosen over West Ford field for the following reasons: (1) the greater amount of available data from the Ford Geraldine unit, including cores, logs, and core-analysis data; (2) a larger volume of oil in place in the Ford Geraldine unit than in Ford West field; and (3) the greater applicability of outcrop information to the upper Bell Canyon reservoir interval in the Ford Geraldine unit than to the lower Bell Canyon/upper Cherry Canyon reservoir in West Ford field.

In preparation for simulation of the pilot area, conditional simulation was used to generate interwell permeability distributions. A spherical semivariogram with a dimensionless correlation length of 0.3 gave the most geologically realistic 3-D geostatistical permeability distribution. The 3-D permeabilities were scaled up by using direct fine-scale simulation, assuming steady-state flow. The conditionally simulated stochastic permeabilities generated for the demonstration area conform reasonably well with the main geologic features of the reservoir.

Production and other reservoir data were used to make preliminary estimates of tertiary recovery for the demonstration area. Using the average 7.9 percent tertiary performance of the rest of the unit, it is estimated that 904,000 STB of oil can be recovered from the demonstration area with a CO_2 flood. This is a conservative estimate; the results of the planned flow simulations are expected to confirm or exceed this estimate.

INTRODUCTION

Summary of Project Objectives

The objective of this project is to demonstrate that detailed reservoir characterization of slope and basin clastic reservoirs in sandstones of the Delaware Mountain Group in the Delaware Basin of West Texas and New Mexico is a cost-effective way to recover a higher percentage of the original oil in place through strategic placement of infill wells and geologically based field development. One of the most important lessons learned from 75 yr of reservoir development experience in the Permian Basin is that comprehensive geologic and engineering investigations of reservoir character (that is, description of the geologic controls on engineering attributes and the effects of internal heterogeneity on the distribution of hydrocarbons) are essential prerequisites for designing efficient production strategies (Ruppel and others, 1995). Primary production, infill drilling, waterflooding, and enhanced oil recovery operations undertaken without thorough reservoir characterization will not realize maximum potential production. The goal of this project is to demonstrate that reservoir characterization incorporating 3-D seismic and reservoir simulation can optimize infill drilling and enhanced oil recovery (such as CO_2 flood) projects and thus increase production and prevent premature abandonment of slope and basin clastic reservoirs in mature fields.

Project Description

This project involves reservoir characterization of two Late Permian slope and basin clastic reservoirs in the Delaware Basin, West Texas, followed by a field demonstration in one of the fields. The fields being investigated are Geraldine Ford and Ford West (4100) fields in Reeves and Culberson Counties, Texas (fig. 1). Geraldine Ford field, which is operated as the Ford Geraldine unit by Conoco, Inc., produces at 2,600 ft below ground surface from a stratigraphic trap in the upper part of the Bell Canyon Formation of the Delaware Mountain Group. The 99 MMbbl of

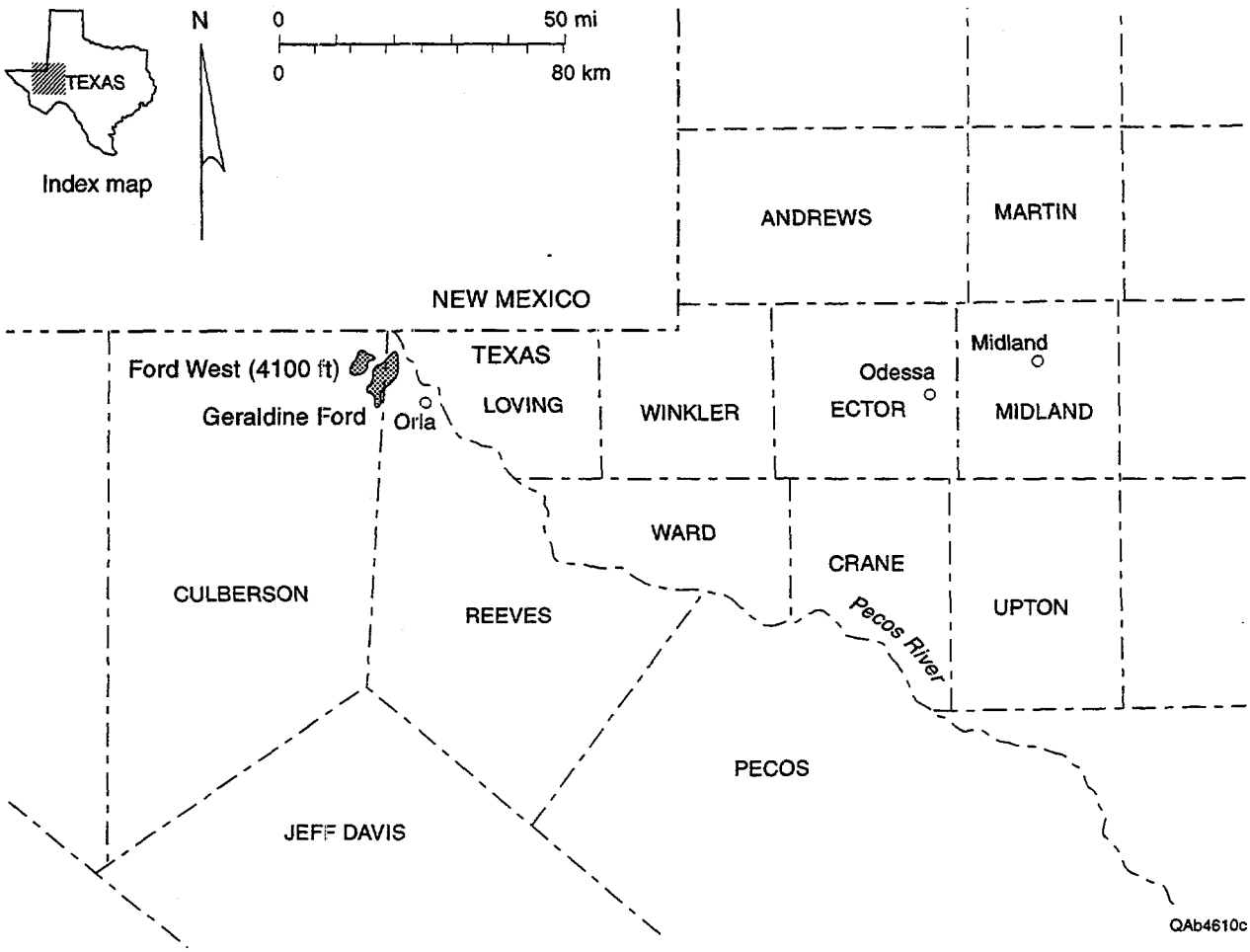

Figure 1. Location of Geraldine Ford and Ford West fields in Reeves and Culberson Counties, Texas.

original oil in place (Pittaway and Rosato, 1991) makes it the largest Delaware Mountain Group field in the basin. Some 13 yr of primary production and 28 yr of secondary (waterflood) and tertiary (CO_2 flood) development in the Ford Geraldine unit have resulted in a recovery efficiency of only 28 percent. This recovery efficiency is higher than that of most reservoirs in this play because the Ford Geraldine unit is one of the first to undergo tertiary development. Thus, secondary and tertiary recovery programs at the Ford Geraldine unit resulted in incremental recovery, but overall recovery efficiency remains poor because reservoir heterogeneity causes serious producibility problems.

The other field being studied, Conoco's Ford West field, is still in primary production from deeper (3,400 ft) slope and basin clastic reservoirs. This field is located 2 mi to the west of Geraldine Ford and produces from a similar style trap in the upper part of the underlying Cherry Canyon and basal Bell Canyon Formations (fig. 2). After 21 yr of development, an estimated 5 percent of the original oil in place has been recovered at Ford West. Although the reservoir zones in Geraldine Ford and Ford West fields are among the most prolific slope and basin clastic reservoirs in the Delaware Basin, at these low recovery efficiencies much of the oil will remain in the ground unless new recovery methods are developed.

Project Structure

Project objectives are divided into two major phases, reservoir characterization and implementation. The objectives of the reservoir characterization phase of the project were to provide a detailed understanding of the architecture and heterogeneity of the two fields, the Ford Geraldine unit and Ford West field. Reservoir characterization utilized 3-D seismic data, high-resolution sequence stratigraphy, subsurface field studies, outcrop characterization, and other techniques. Once reservoir characterization was completed, a pilot area of approximately 1 mi^2 at the northern end of the Ford Geraldine unit was chosen for reservoir simulation. This report summarizes the results of the second year of reservoir characterization.

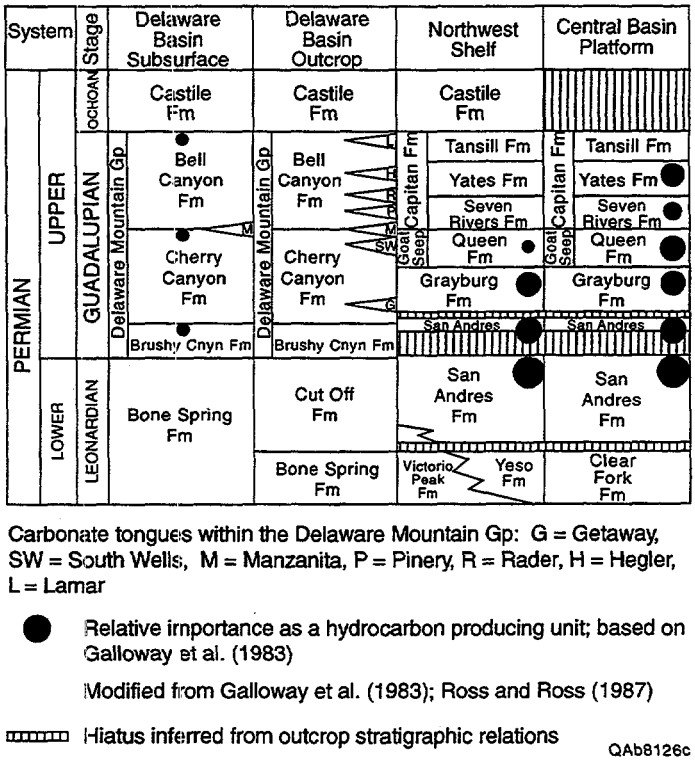

Figure 2. Stratigraphic nomenclature of the Delaware Mountain Group in the Delaware Basin subsurface and outcrop areas and time-equivalent formations on the surrounding shelves.

The objectives of the upcoming implementation phase of the project are to (1) apply the knowledge gained from reservoir characterization and simulation studies to increase recovery from the pilot area, (2) demonstrate that economically significant unrecovered oil remains in geologically resolvable untapped compartments, and (3) test the accuracy of reservoir characterization and flow simulation as predictive tools in resource preservation of mature fields. A geologically designed, enhanced-recovery program (CO_2 flood, waterflood, or polymer flood) and well-completion program will be developed, and one to three infill wells will be drilled and cored. Through technology transfer workshops and other presentations, the knowledge gained in the comparative study of these two fields can then be applied to increase production from the more than 100 other Delaware Mountain Group reservoirs.

Characterization of Reservoir Heterogeneity

The architecture of sandstones in clastic reservoirs has a direct impact on hydrocarbon recovery efficiency. Internal features within reservoir sandstone units define the geometry of fluid pathways that control the efficiency of hydrocarbon migration to the well bore and therefore provide fundamental constraints on the ultimate volume of oil and gas that remains in the ground when the reservoir is abandoned (Tyler and others, 1992). Understanding the details of reservoir architecture and its inherent control on fluid migration is critical to efficient targeting of the remaining recoverable oil resource in mature reservoirs.

Slope and basin clastic systems are characterized by a high degree of vertical heterogeneity, which results in low recovery efficiency, generally less than 20 percent (Tyler and Gholston, 1988). Delaware Mountain Group reservoirs are no exception. Original oil in place in the Delaware Sandstone play was estimated to be 1.8 Bbbl (M. Holtz, personal communication, 1994). By 1994, cumulative production from this play was approximately 251 MMbbl, an average recovery efficiency of 14 percent.

Lateral heterogeneity in slope and basin clastic systems has not generally been considered a major control on recovery efficiency (Tyler and Gholston, 1988), but recent work suggests it is

more important than has previously been recognized. Outcrops studies of deep-basin turbidite deposits of the Jackfork Group in Arkansas (Slatt and others, 1992) have demonstrated that lateral heterogeneity is commonly greater than can be recognized from gamma-ray logs spaced 500 to 600 ft apart, and deep-water sandstones may be mistakenly interpreted from subsurface data as being more laterally continuous than they actually are. Identifying the vertical and lateral heterogeneity in the Delaware Mountain Group sandstone reservoirs and taking that information into account to design the pilot project are the goals of the reservoir characterization phase of this project.

Summary of Progress

This annual report documents technical work during the second year of the contract, from April 1996 through March 1997. Work performed during the first year of the contract focused on tasks associated with project start-up activities, data collection, and initial reservoir characterization. A major task accomplished the first year was designing, acquiring, and processing a 3-D seismic survey from a 36-mi^2 area over Geraldine Ford and Ford West fields and the nonproductive area in between. Work performed this year focused on reservoir characterization and identification of heterogeneity. Evaluation of large-scale reservoir heterogeneity was done primarily using geophysical data. Intermediate- to small-scale heterogeneity caused by depositional and diagenetic processes were studied using well logs, outcrop data, cores, thin sections, and SEM imaging.

Major tasks accomplished this year were (1) study of Bell Canyon sandstones in outcrop (2) subsurface mapping of reservoir intervals in the Ford Geraldine unit and West Ford field and interpretation of depositional and diagenetic processes, (3) petrophysical analysis of Ramsey sandstone reservoirs in the Ford Geraldine unit, (4) interpretation of the 3-D seismic data set and correlation of seismic, petrophysical, and production parameters, (5) selection of the pilot area, and (6) stochastic permeability characterization and preliminary enhanced-recovery predictions of the pilot area.

DELAWARE MOUNTAIN GROUP OIL PLAY

The Permian Basin is the most prolific, and one of the oldest, oil-producing basins in the continental United States, and it still contains an estimated 35 Bbbl of remaining mobile oil (Holtz and Major, 1994). Upper Permian (Guadalupian) Delaware Mountain Group strata (fig. 2) comprise a 3,500-ft-thick succession of slope and basin reservoirs in the Delaware Basin that are important contributors to Permian Basin production. The Delaware Basin, the western subbasin of the Permian Basin, is located in West Texas and southeastern New Mexico (fig. 3) and extends from Pecos County, Texas, northward to Eddy County, New Mexico. Fields in the Delaware play produce oil and gas from slope and basin sandstone deposits that form long, linear trends (fig. 4). Structural contours on limestone beds capping the reservoir sandstones indicate monoclinal dip to the east and northeast (fig. 4). Most hydrocarbons are trapped by stratigraphic traps formed by an updip lateral facies change from higher permeability reservoir sandstones to low-permeability siltstones. Fields show minor structural closure because linear trends of thick sandstones formed compactional anticlines by differential compaction during burial (Ruggiero, 1985).

Individual fields in the Delaware play produce from lenticular sandstone bodies interbedded vertically with organic-rich siltstone, carbonate mudstone, and laminated siltstone (Gardner, 1992; Bureau of Economic Geology, 1993). Reservoir sandstones are depositionally and diagenetically complex, with extreme heterogeneity demonstrated by an average 14-percent recovery efficiency from fields in the play. Deeper pool potential also exists in Delaware Mountain Group fields. Early exploration typically drilled into the upper part of the Bell Canyon Formation only, leaving many deeper horizons in densely drilled fields untapped (Gardner, 1992).

The Delaware play is now mature and has a drilling history of progressive deeper pool discoveries in the Bell Canyon, Cherry Canyon, and Brushy Canyon Formations (fig. 2). In the 1920's, reservoirs were discovered in the Ramsey sandstone, the upper part of the Bell Canyon Formation. Geraldine Ford field, located about 2 mi south of the Texas–New Mexico state line in Reeves and Culberson Counties, Texas (fig. 1), was discovered in 1956 from shallow (2,600 ft)

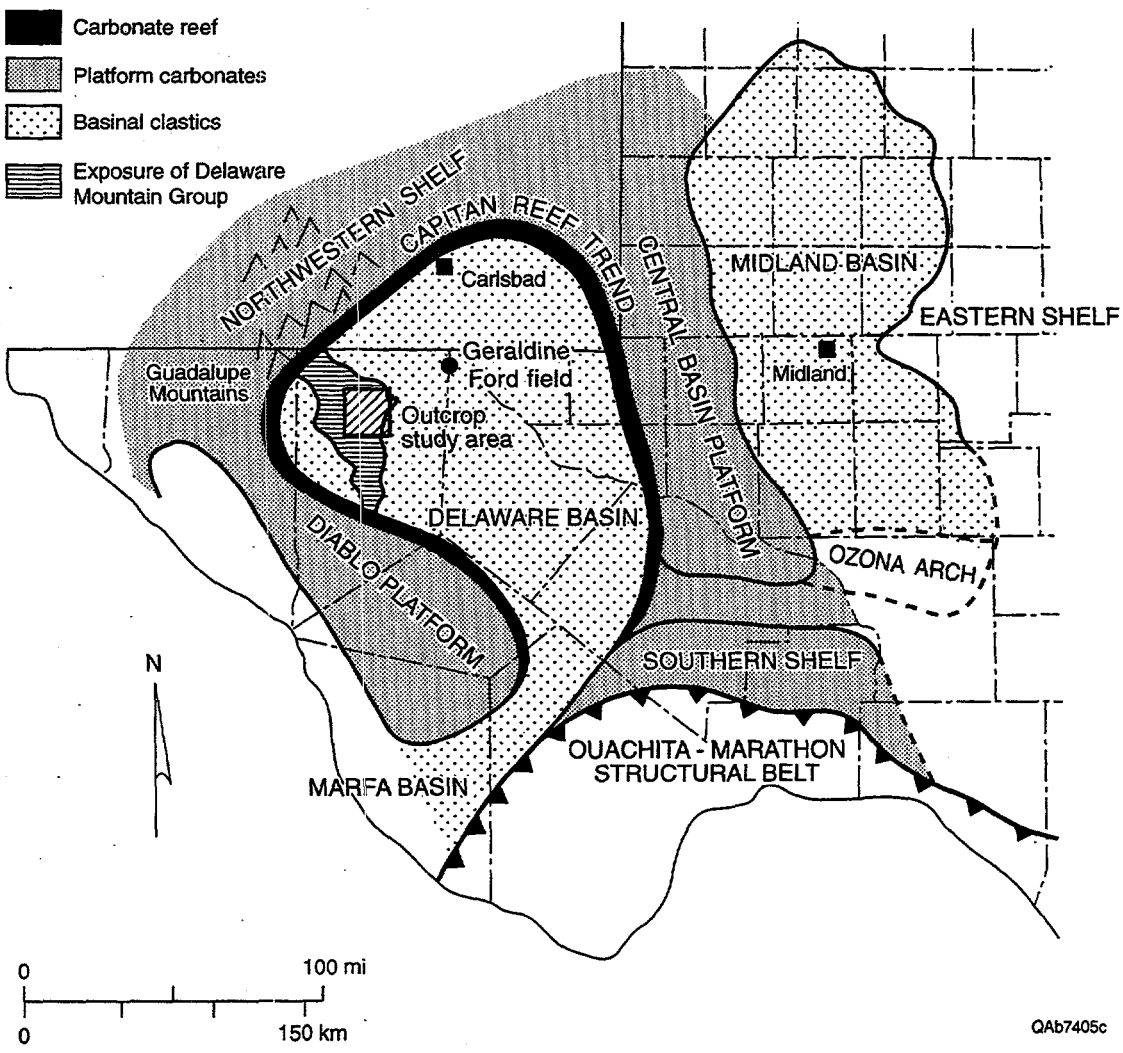

Figure 3. Map showing location of Delaware Basin and paleogeographic setting during the Late Permian.

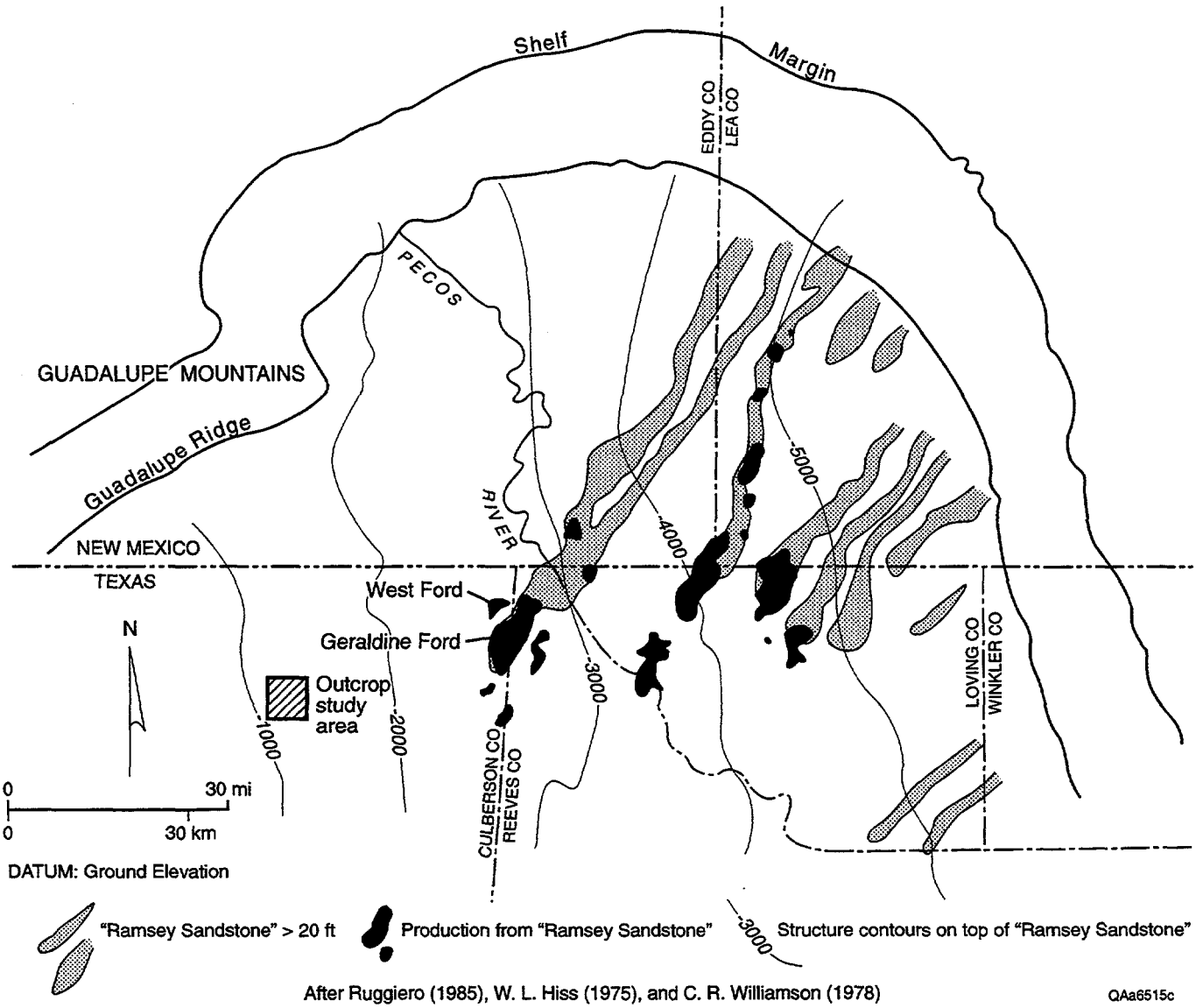

Figure 4. Production from Geraldine Ford and other upper Bell Canyon fields in the Delaware Basin from the distal (southwest) ends of east-dipping, northeast-oriented linear trends of thick Ramsey sandstone deposits. Modified from Ruggiero (1985), after Hiss (1975) and Williamson (1978).

Ramsey sandstone reservoirs (fig. 5). The main reservoir at Geraldine Ford field is the Ramsey sandstone, but there is also some production from the underlying Olds sandstone (fig. 5). The field was unitized in 1958 and is operated by Conoco as the Ford Geraldine unit. As of May, 1994, there were 115 producer and 75 injector wells in the field (fig. 6), and cumulative production was 25.6 MMbbl. By the late 1970's, more than 100 fields produced from the Bell Canyon Formation (Williamson, 1977, 1978).

In 1952, deeper reservoirs were discovered in the Cherry Canyon Formation (fig. 7). By 1985, 39 Cherry Canyon fields had been developed (Linn, 1985). Ford West field, which was discovered in 1976, produces from the upper part of the Cherry Canyon Formation and the lower Bell Canyon Formation. More recently, deeper pool discoveries have been made in the Brushy Canyon Formation (DeMis and Cole, 1996).

The Delaware Basin is an ideal location for a reservoir-characterization study of slope and basin clastic reservoirs. More than 70 yr of exploration and development in the Delaware play provides a wealth of subsurface data. Furthermore, nearby outcrops showing the internal structure of reservoir strata are present within 24 mi of Ford West and Geraldine Ford fields (figs. 3, 4). The present Delaware Basin configuration approximates the Upper Permian depositional basin. Geraldine Ford and Ford West fields are located near the paleogeographic center of the Upper Permian Delaware Basin, about 65 mi from the paleoshelf margin. The outcrops selected for this study are also from a basin-floor setting, many miles from the shelf edge. The Ford Geraldine unit was the major focus of the reservoir characterization phase because of the abundance of subsurface data available from this field compared with those of Ford West and because the outcrop analogs are from the upper Bell Canyon Formation.

Two major issues that were unresolved after the first year of the project were the depositional processes that formed the reservoirs at Geraldine Ford and West Ford fields and the dimensions of reservoir sandstone bodies. These two questions were addressed this year by study of well-exposed outcrops of Bell Canyon sandstone, mapping based on subsurface log and core data, and interpretation of the 3-D seismic data set.

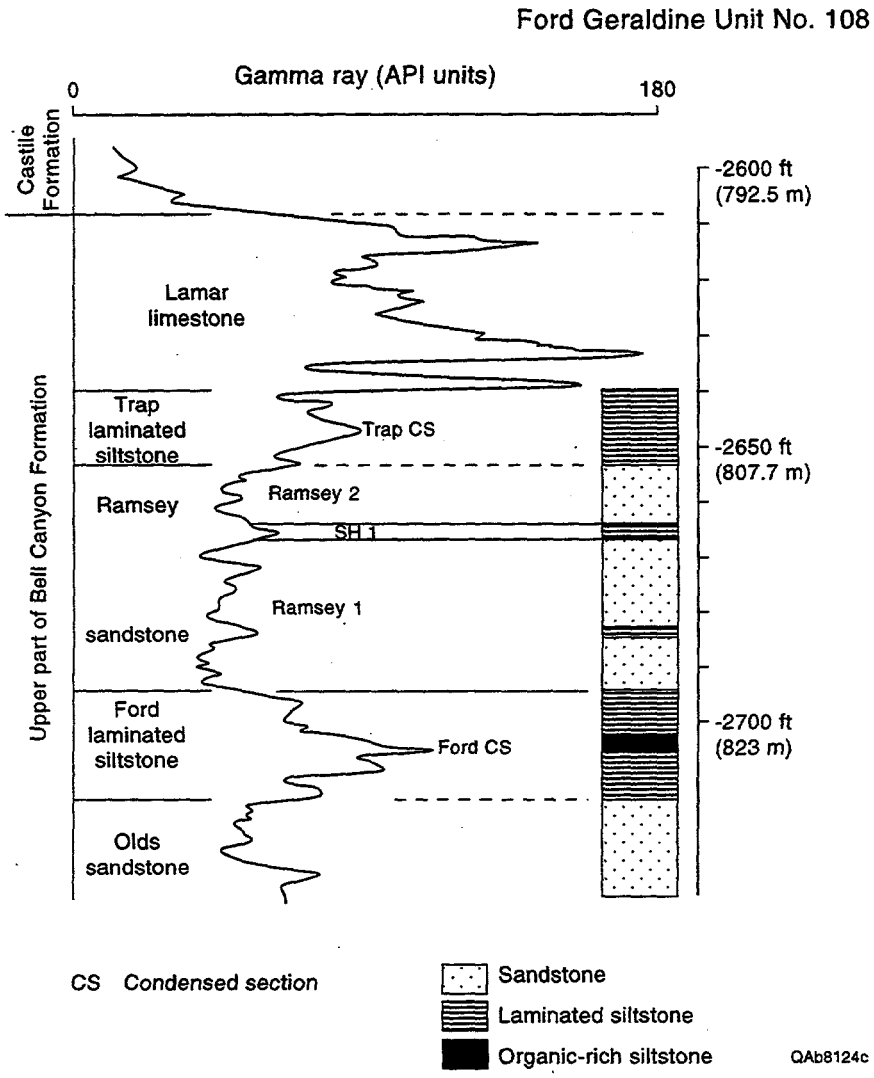

Figure 5. Typical log from the Ford Geraldine unit well No. 108 (modified from Ruggiero, 1985). Well location is shown in figure 6.

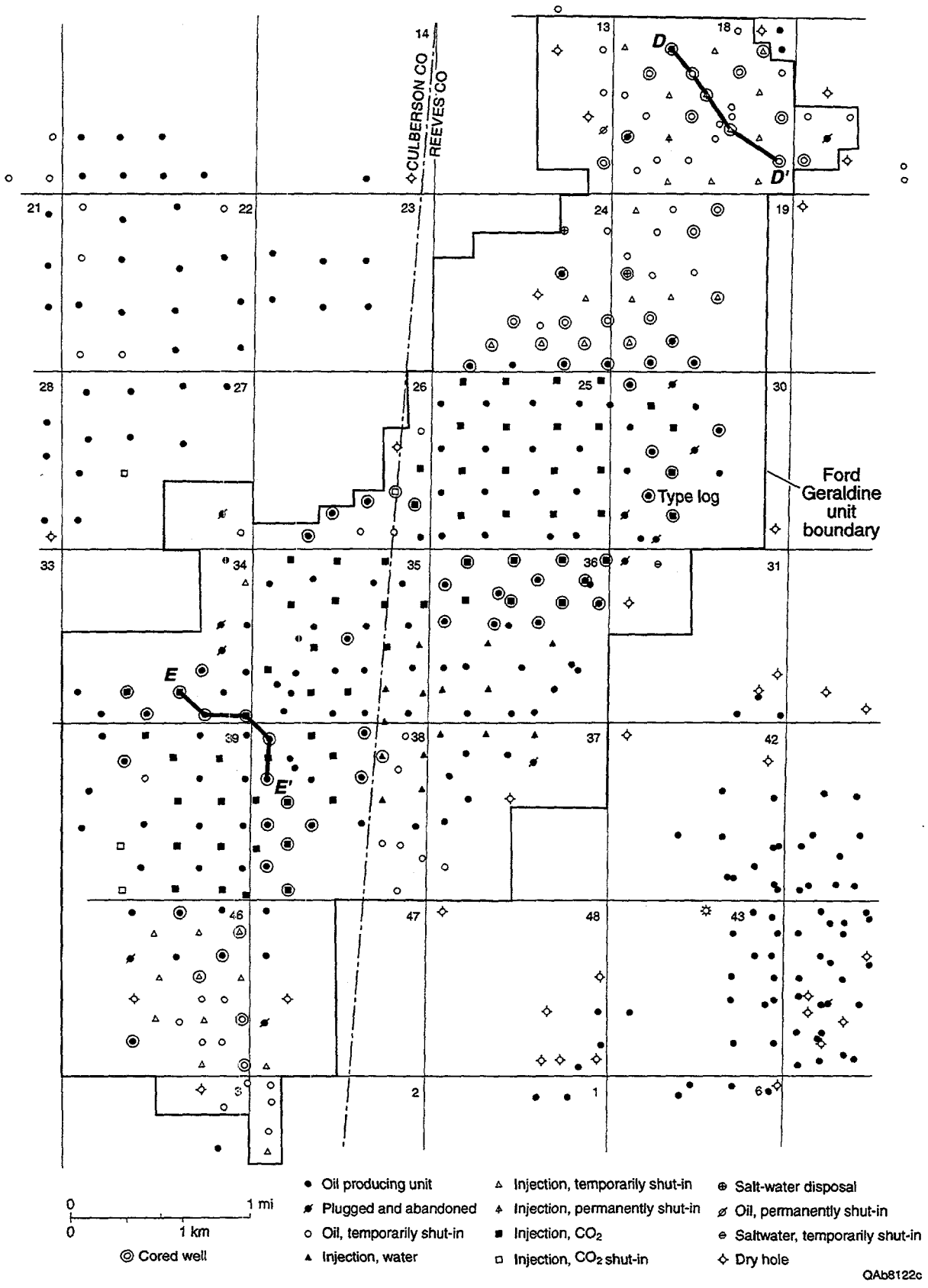

Figure 6. Status of wells in the Ford Geraldine unit and distribution of core control. Type log is shown in figure 5, cross section D–D′ in figure 39, and cross section E–E′ in figure 40.

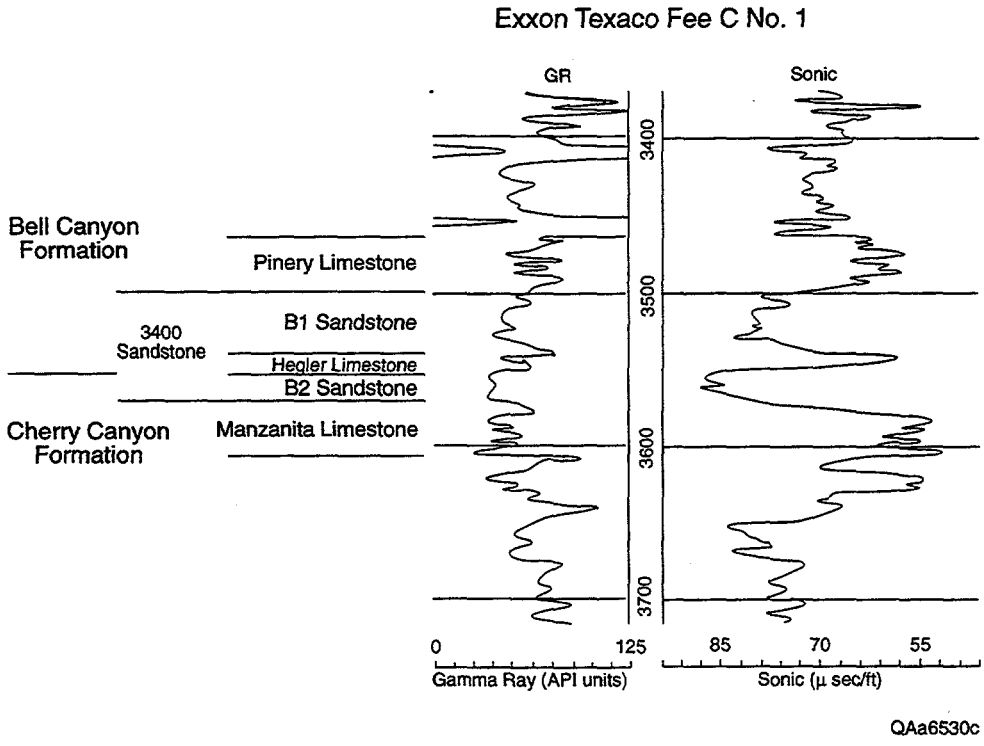

Figure 7. Typical log for Ford West field from the Exxon Texaco Fee C No. 1 (from Linn, 1985). Well location shown in figure 51.

OUTCROP CHARACTERIZATION OF BELL CANYON SANDSTONE RESERVOIR ANALOGS

Introduction

The objective of this section is to describe the architecture of upper Bell Canyon sandstones as seen in outcrop exposures. Outcrops were examined to address two primary issues. The first was to determine by what processes upper Bell Canyon sandstones and siltstones were deposited. The second was to identify the fundamental architectural elements and document their geometry, dimensions, and composition. Motivation for this study comes from a need to better understand the production performance of the Ford Geraldine unit and other Delaware Mountain Group reservoirs.

Regional Setting and Stratigraphic Framework

The Bell Canyon Formation is a deep-water siliciclastic unit that accumulated in the Delaware Basin during the Late Permian. The Delaware Basin, located in West Texas and southeast New Mexico, was a circular basin about 120 mi in diameter (fig. 3). The basin was semirestricted, with its southern end partially open to the seaway and its northern end surrounded by an extensive carbonate shelf and reef complex. Shelf to basin floor correlations of time equivalent strata indicate water depths were between 1,000 and 2,000 ft (Kerans and others, 1992).

The Bell Canyon is the youngest formation in the Delaware Mountain Group, which also includes the Brushy Canyon and Cherry Canyon Formations (figs. 2, 8). The Bell Canyon Formation is composed of sandstones, siltstones, and minor amounts of carbonate. Detrital clay-size material is almost completely absent. Maximum thickness of the Bell Canyon Formation is about 1,200 ft near the center of the basin. Sandstones and siltstones of the Bell Canyon Formation thin near the margins of the basin where they interfinger with and onlap adjacent carbonate slope deposits of the Capitan Formation (fig. 8). Time-equivalent shelf strata include, in ascending stratigraphic order, the Seven Rivers, Yates, and Tansill Formations.

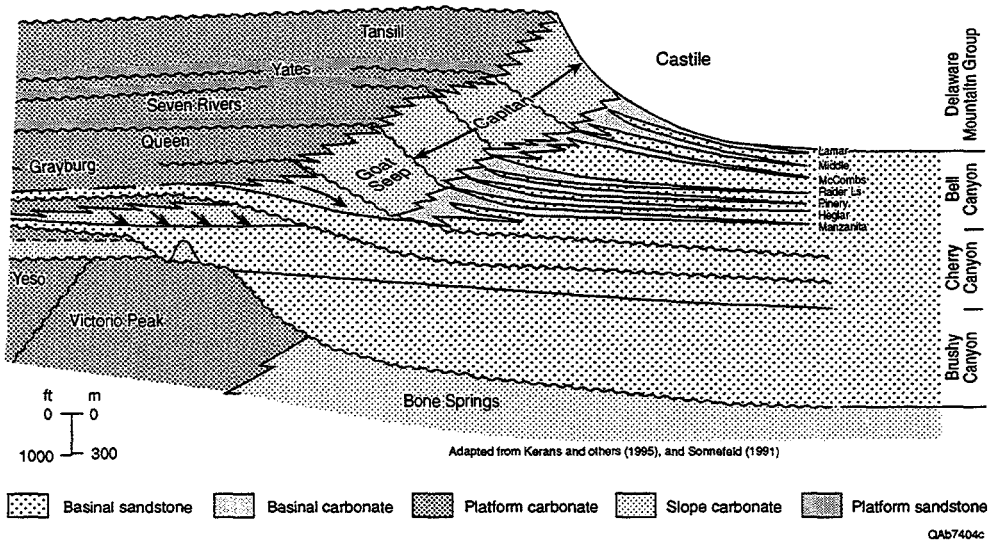

Figure 8. Cross section through northwestern part of the Delaware Basin illustrating Late Permian stratigraphy.

The Bell Canyon Formation contains six limestone tongues. From oldest to youngest they include the Hegler, Pinery, Rader, McCombs, Middle, and Lamar Limestones. These tongues extend basinward from the shelf margin and divide the Bell Canyon into six sandstone bodies that have been informally labeled BC1 through BC6 in ascending stratigraphic order (fig. 9). The sandstone bodies are 50 to 300 ft thick, and they are further subdivided by organic-rich siltstones into genetic units referred to as high-order cycles (Gardner, 1992). The high-order cycles are 20 to 100 ft thick and show a trend of upward-increasing followed by upward-decreasing sandstone content.

The regular interbedding of sandstones with organic-rich siltstones and limestones has been interpreted by some workers to record frequent changes in relative sea level (Meissner, 1972). During highstands in relative sea level, sands were trapped behind a broad, flooded shelf and prevented from entering the basin. Thin, widespread, organic-rich siltstones accumulated on the basin floor by the slow settling of marine algal material and airborne silt. Associated limestones were deposited by sediment gravity flows that originated by the slumping of carbonate debris along the flanks of a rapidly aggrading carbonate platform. During subsequent lowstands in relative sea level the carbonate shelf was exposed and sandstones bypassed to the basin floor. Textural characteristics of the sands, such as the absence of detrital clay-size material and the lack of channels on the shelf, suggest that wind was an important agent in transporting the sands to the shelf margin (Fischer and Sarnthein, 1988). Paleocurrent indicators indicate that the sands entered the basin from the Northwestern Shelf and Central Basin Platform (fig. 3).

Models of Basinal Sandstone Deposition

It has been shown that production from many Bell Canyon reservoirs is from the distal end of long, linear sandstones bodies that extend basinward from the shelf margin (fig. 4) (Williamson, 1978). Although this feature has been recognized for some time, the processes that formed the sandstone bodies have been the source of controversy. A variety of depositional models have been

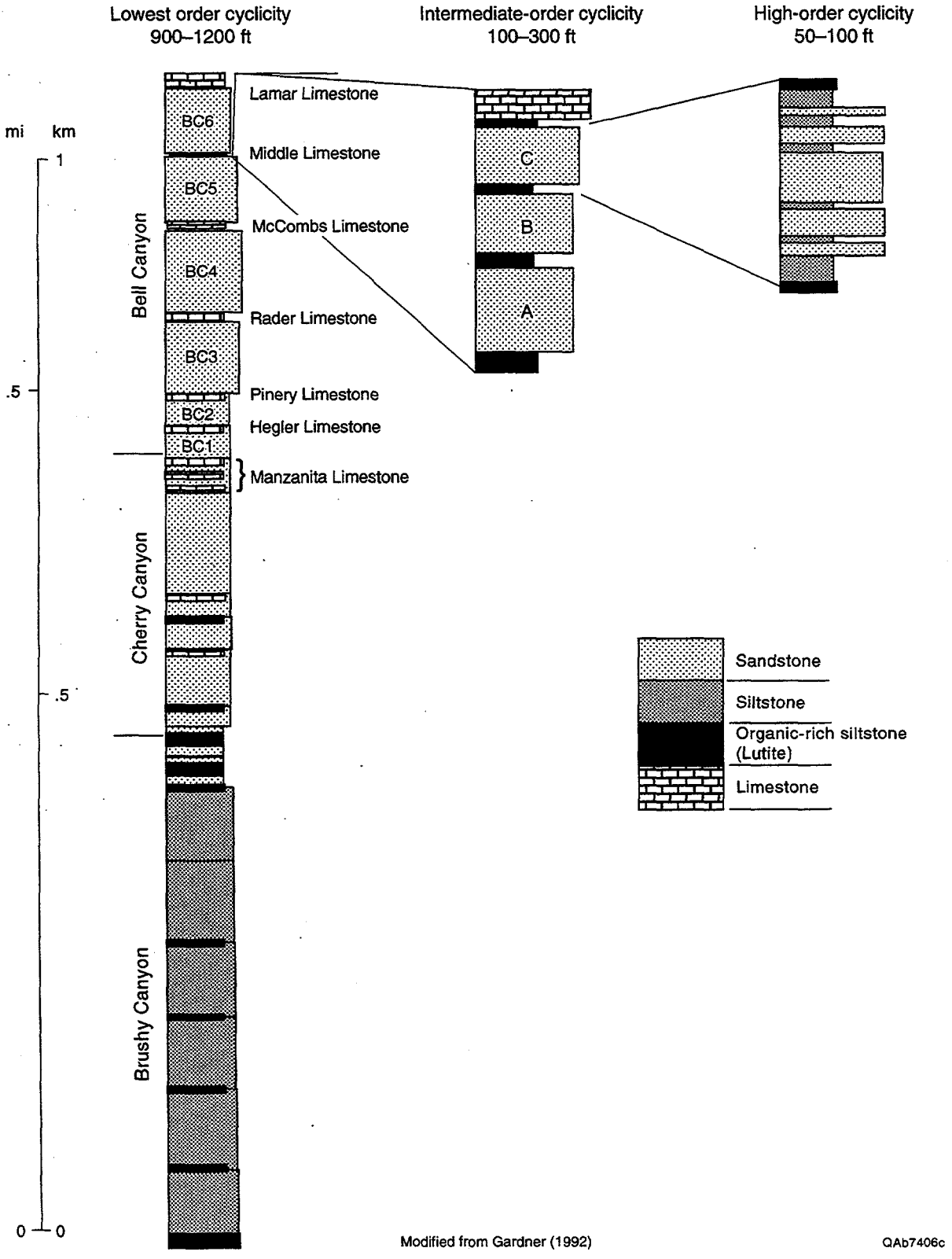

Figure 9. Diagram illustrating stratigraphic cyclicity of Bell and Cherry Canyon Formations. Three scales classified as low, intermediate, and high have been recognized (Gardner, 1992; Kerans and others, 1992). The cycles are bounded by regionally correlatable carbonate mudstones and organic-rich siltstones.

proposed, including deposition by turbidity currents, debris flows, and saline density currents (fig. 10).

In the turbidity-current model, sands are transported into the basin by turbulent sediment gravity flows (Payne, 1976; Berg, 1979; Zelt and Rossen, 1995). These flows originated along the shelf edge by the slumping of sands. The slumped sands produce sediment-rich water masses that due to their greater density move downslope and into the basin as turbulent flows. In the turbidity-current model, sands are deposited in channels with well-developed levees. The channels bifurcate basinward and terminate in fan-shaped lobes. This model predicts that basinal deposits are interstratified with broad lenticular lobes and channels with levees (fig. 11). The lobes coarsen upward and are composed of graded sandstones that may display partial Bouma sequences. The lobes are capped by fine-grained interchannel deposits or are replaced and overlain by channels with attached levees.

In the debris-flow model sands are also carried into the basin by dense sediment-gravity flows that originated along the shelf margin (fig. 10). However, in the debris-flow model the sediment-gravity flows behave as laminar flows instead of turbulent flows. In the debris-flow model, sands are deposited in narrow, elongate lobes. Channels are poorly defined and lack well-developed levees. The debris-flow model predicts that basinal deposits are interstratified with lenticular mounds (fig. 11). The mounds display abrupt contacts and are composed largely of structureless sandstones.

In the density-current model, sands are transported into the basin by dense saline currents (Harms, 1968; Williamson, 1977; Harms and Williamson, 1988). The dense saline waters originated on the shelf by evaporation (fig. 10). Density differences cause the hypersaline waters to move off the shelf and into the basin. In doing so, the currents entrain sediment and scour out channels. In the density-current model, sands are restricted to infilled scours. The infilled scours consist of basinal deposits that are interstratified with channel-form sandstone bodies that lack levees or distal lobes (fig. 11). The channel sandstones overlie an erosive base and display traction-produced stratification.

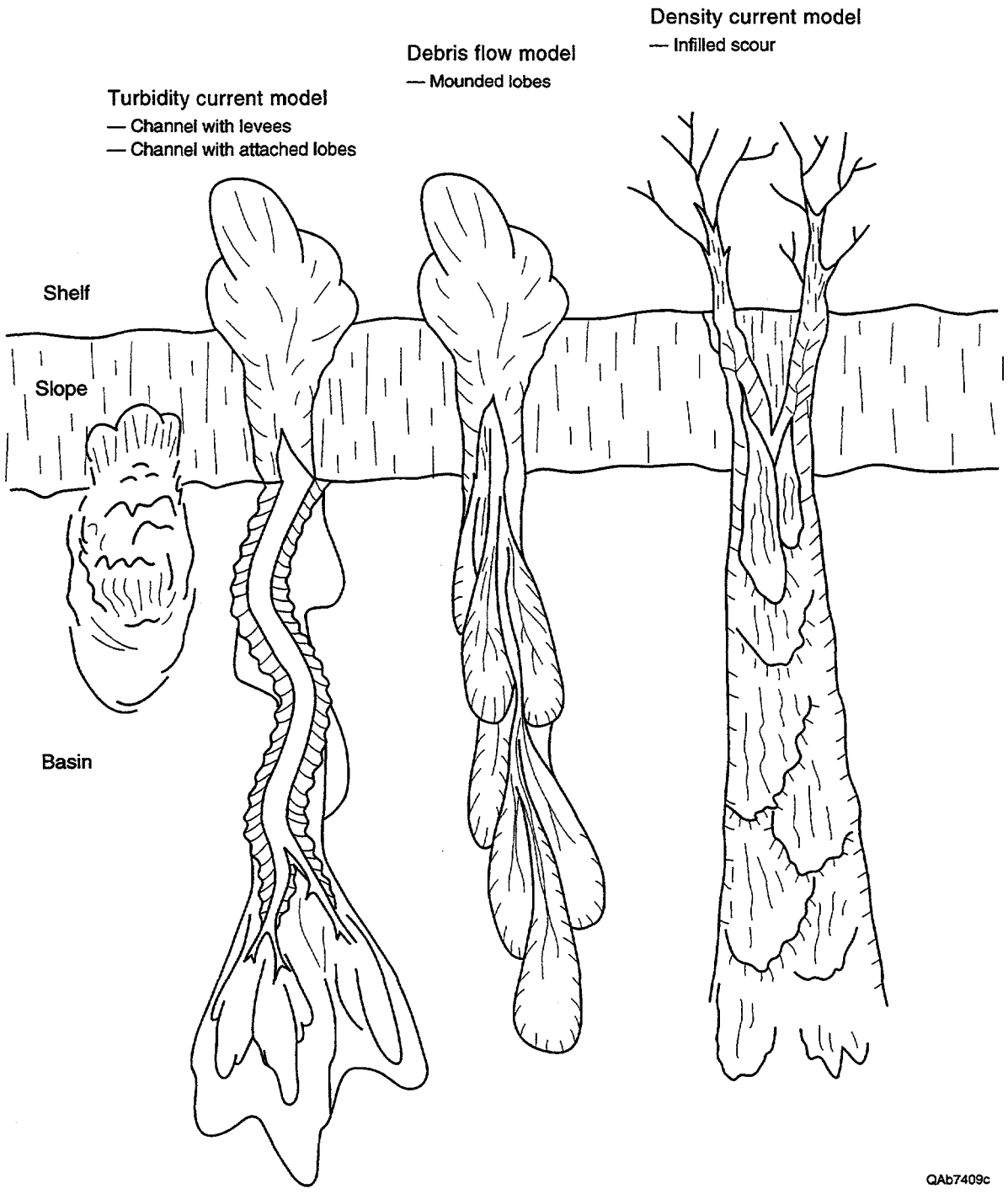

Figure 10. Diagram illustrating plausible depositional models for Bell Canyon sandstones. Three models are illustrated. They include deposition by (1) turbidity currents, (2) debris flows, and (3) saline density currents.

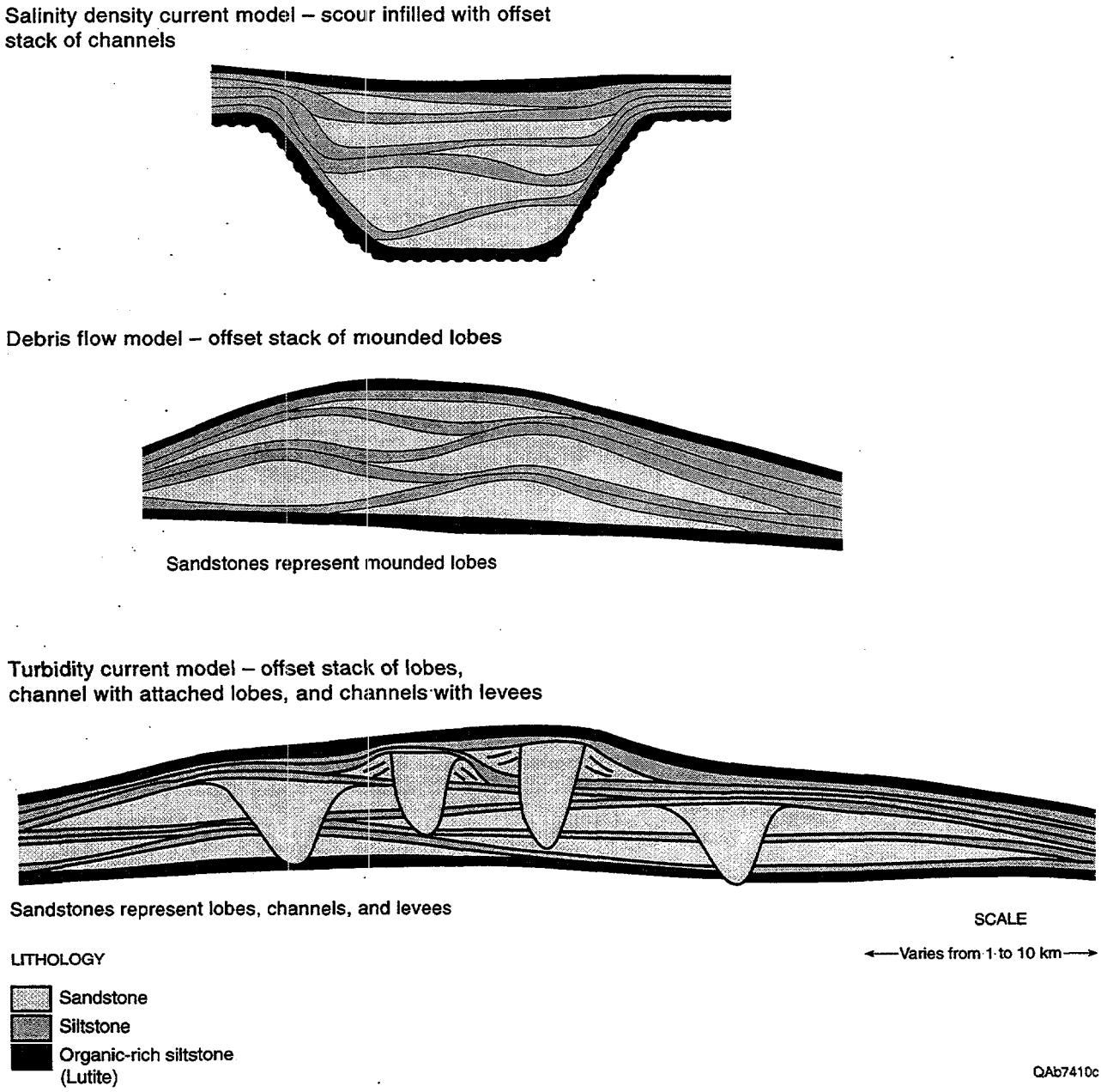

Figure 11. Diagram illustrating sand-body architecture predicted by turbidity-current, debris-flow, and saline-density-current models.

Data and Methods

Outcrop work was undertaken to document stratigraphic relationships within the Bell Canyon Formation, which is well exposed in the Delaware Mountains of West Texas (fig. 12). The Delaware Mountains extend from the base of the Guadalupe Mountains south and east for a distance of about 50 mi. The trend of the outcrop belt roughly parallels the direction of sediment transport, which is to the south and southeast in the western part of the Delaware Basin. Sandstones exposed at the base of the Guadalupe Mountains were deposited at the base of the carbonate slope (Capitan Formation), whereas those exposed to the south and east were deposited on the basin floor.

The outcrops examined in this study are located on the Cowden Ranch in Culberson County, Texas, about 20 mi southeast of the Guadalupe Mountains. Outcrop work focused on stratigraphic relationships within the uppermost high-order cycle in BC4 (fig. 9). The top of this high-order cycle is represented by the Middle Limestone and the base by the first regionally correlative organic-rich siltstone. The scale and position of this stratigraphic unit is directly analogous to that of the highly productive Ramsey interval, which is part of the uppermost high-order cycle in BC5.

Stratigraphic relationships were documented by describing facies and correlating the discontinuities that bound them. Data consisted of measured logs and photomosaics that provided complete coverage of the outcrops. Outcrop exposure of the high-order cycle investigated in this study and the location of measured logs are shown in figure 13. Stratigraphic relationships are illustrated in three cross sections labeled A–A′, B–B′, and C–C′. Cross sections A–A′ and B–B′ are about 1.5 mi long and aligned parallel to the depositional strike of the system. Cross section C–C′ is about 6 mi long and aligned parallel to the depositional axis of the system.

Outcrop Descriptions

In this section the facies architecture of a single high-order cycle is described. The outcrop descriptions are presented in a hierarchical fashion beginning with the smallest units of observation

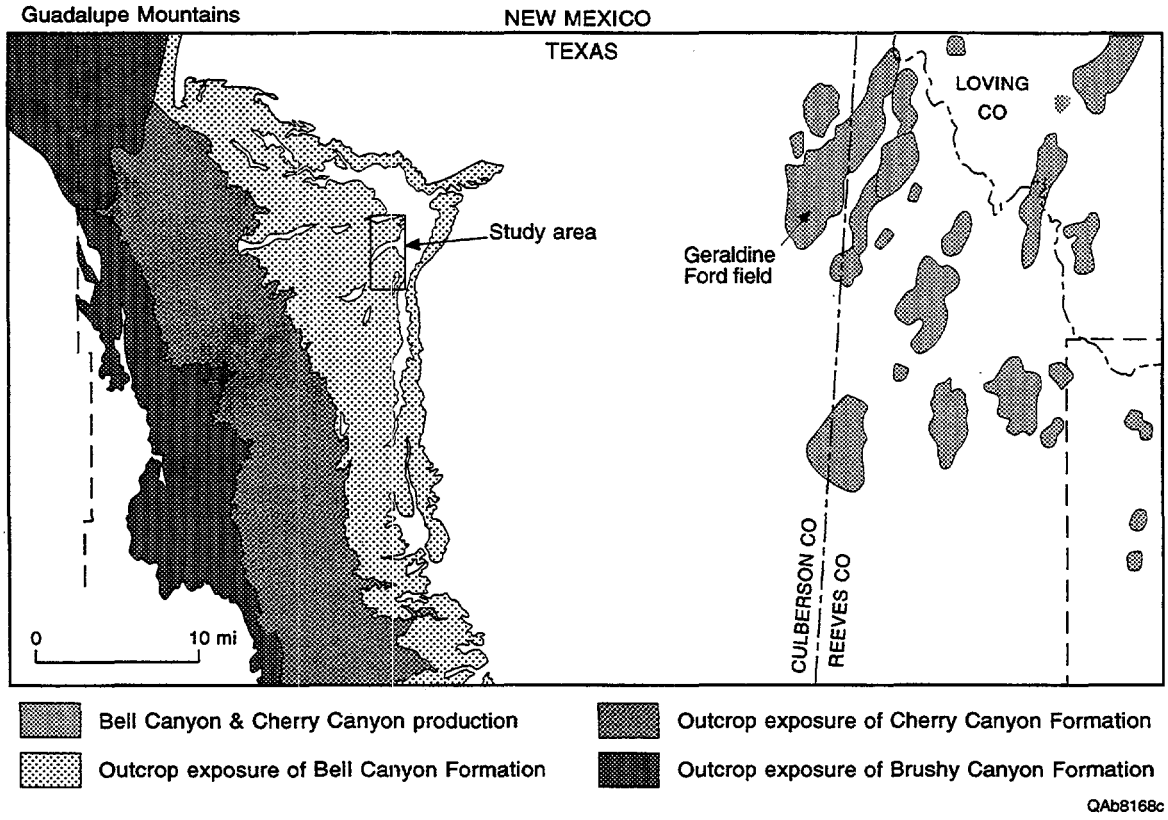

Figure 12. Map of west Texas showing the location of the outcrop study area. The study area was located on the Cowden Ranch in Culberson County, Texas. Outcrop work focused on stratigraphic relationships within the uppermost cycle of BC4 (see figure 9).

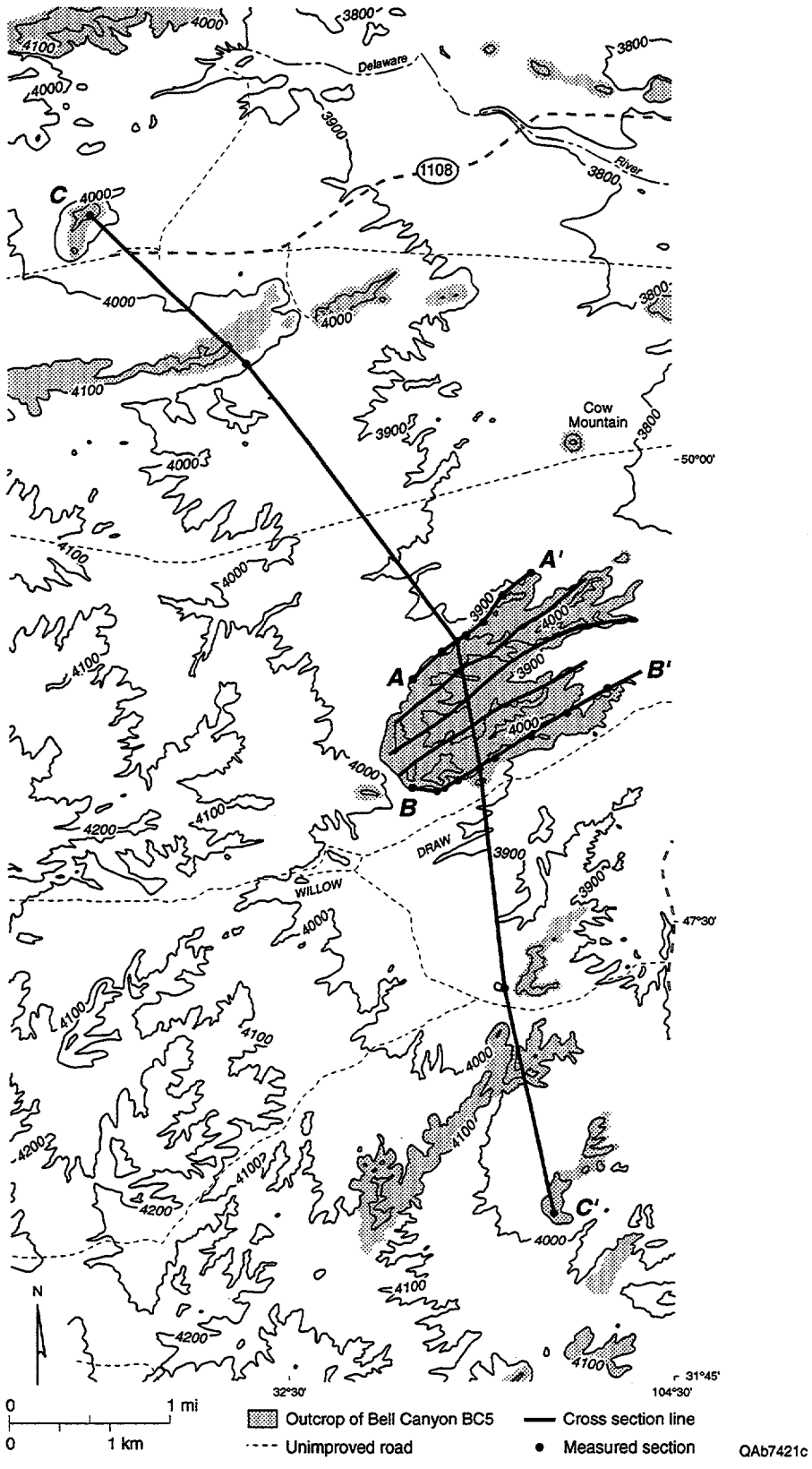

Figure 13. Map of study area showing outcrop exposures of BC4, location of measured sections, and cross sections. Cross sections A–A′ is shown in figure 23, B–B′ in figure 27, and C–C′ in figure 29.

(facies) and building up to the recognition of the distinct rock bodies (architectural elements or lithosomes).

Facies

Facies are the basic descriptive units in this study. Six facies, numbered 1 through 6, were recognized and mapped on the outcrop. They include (1) limestone, (2) organic-rich siltstone, (3) laminated siltstone, (4) sandstones and siltstones that are graded or displayed partial Bouma sequences, (5) structureless or convoluted sandstone, and (6) sandstone having dune scale cross-stratification.

Facies 1 consists of centimeter- to decimeter-thick beds of graded carbonate mudstone (fig. 14). The mudstones are rich in platform allochems such as fusilinids, crinoids, and brachiopods. The limestones are restricted to the top of the high-order cycle. Regional mapping shows that they correlate with the Middle limestone tongue and thicken to the west where they merge with carbonate slope deposits of the Capitan Formation. The well-developed grading and presence of platform allochems suggest that facies 1 was deposited by sediment-gravity flows that originated along the flanks of the carbonate platform by slumping of carbonate debris.

Facies 2 is an organic-rich siltstone that is often referred to as a lutite. It has a dark, massive appearance and may contain centimeter-thick beds of graded and ripple-laminated sandstone (fig. 15). Analysis of the organic matter (Williamson, 1978) has shown that much of it is derived from marine algal matter. The organic-rich siltstones are interpreted to have been deposited from the slow settling of pelagic matter and airborne silt. The thin, graded sandstones are interpreted to record deposition from infrequent, low-density turbidity currents.

Facies 3 is a siltstone that displays extremely even-parallel lamination (fig. 16). It is commonly referred to as a laminite. The lamination is produced by the regular alteration of dark, organic-rich siltstone laminae, that are a fraction of 1 mm thick, with tan to light-gray siltstone laminae that are up to 5 mm thick. The composition of this facies varies in a systematic fashion from organic rich to organic poor depending on regular increases or decreases in the thickness of

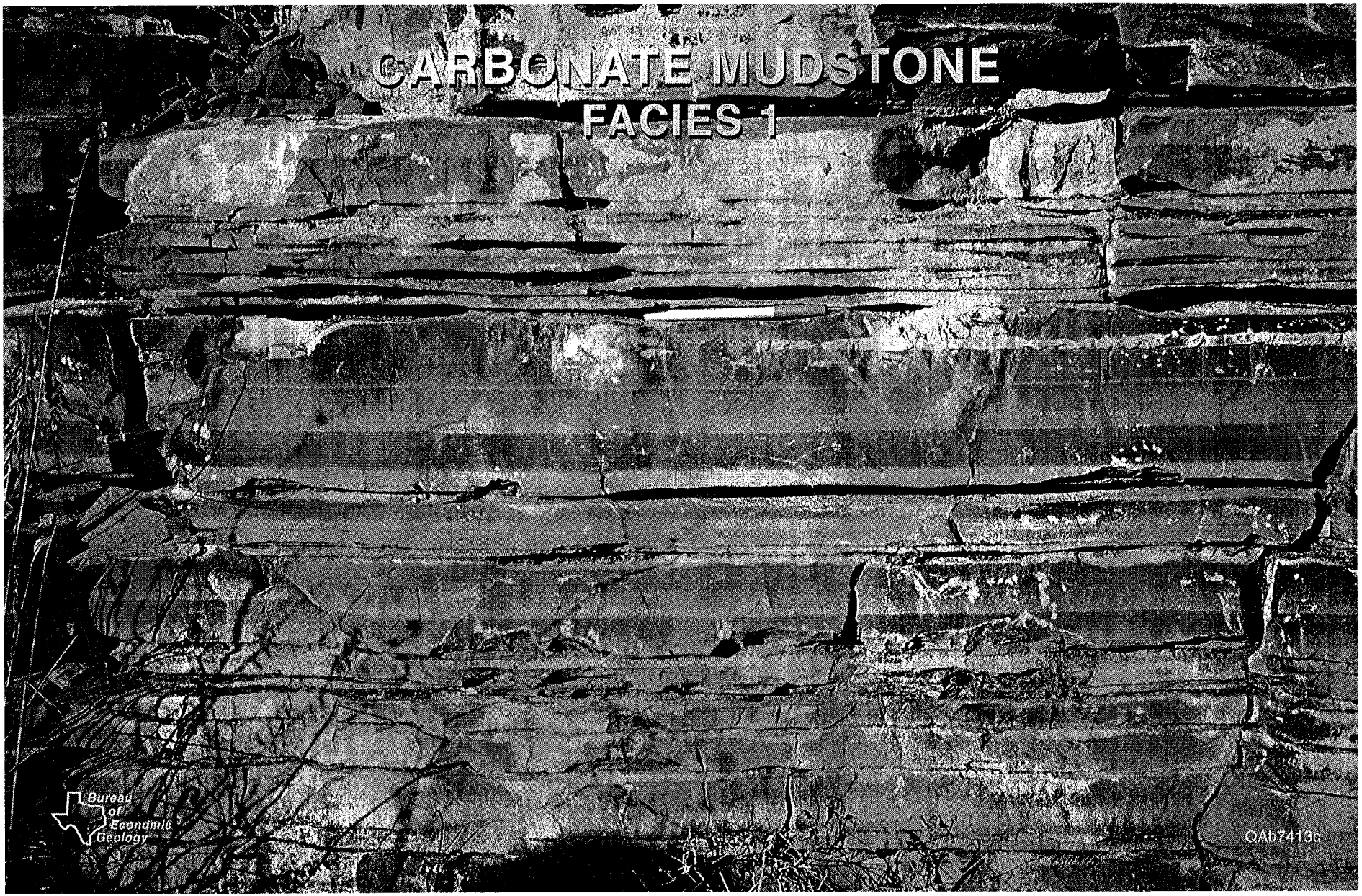

Figure 14. Photograph of facies 1 showing centimeter- to decimeter-thick beds of graded carbonate mudstone.

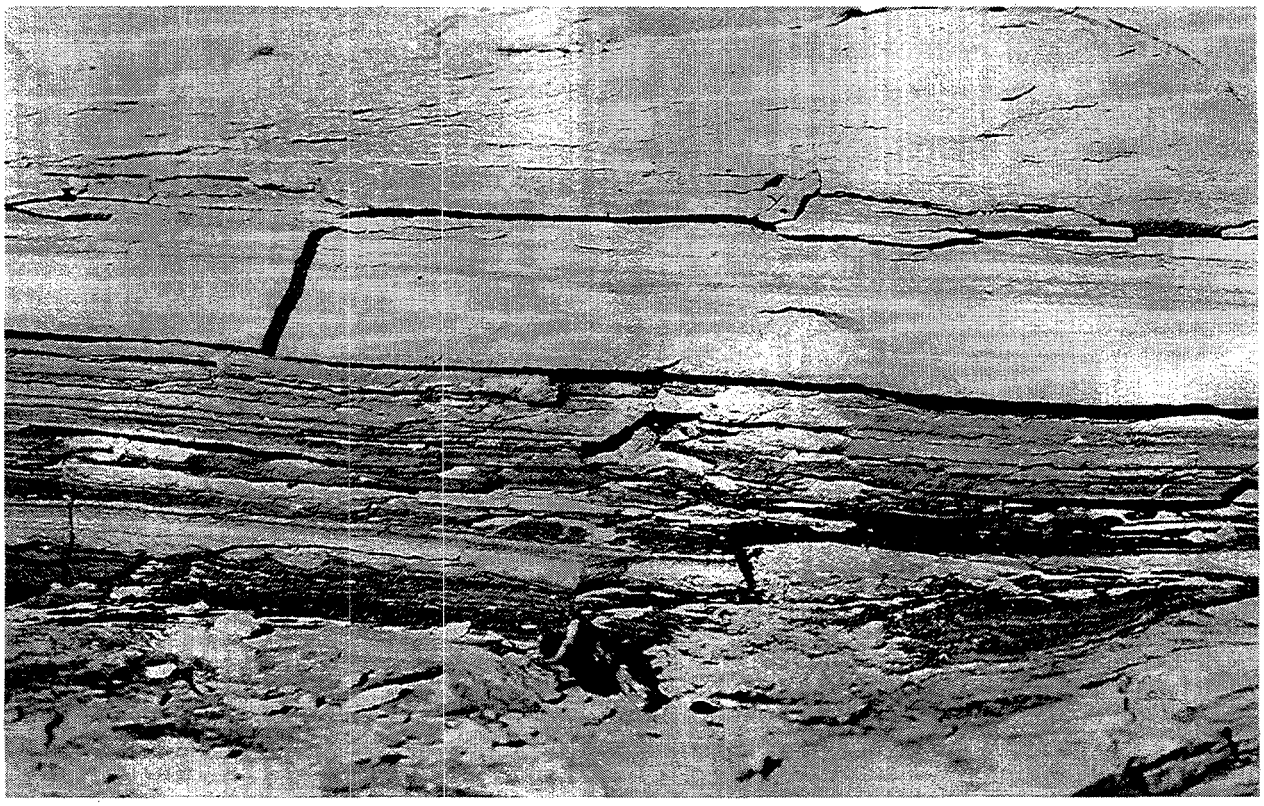

QAb7412c

Figure 15. Photograph of facies 2 showing dark, organic-rich siltstone interstratified with thin beds of graded sandstone and siltstone.

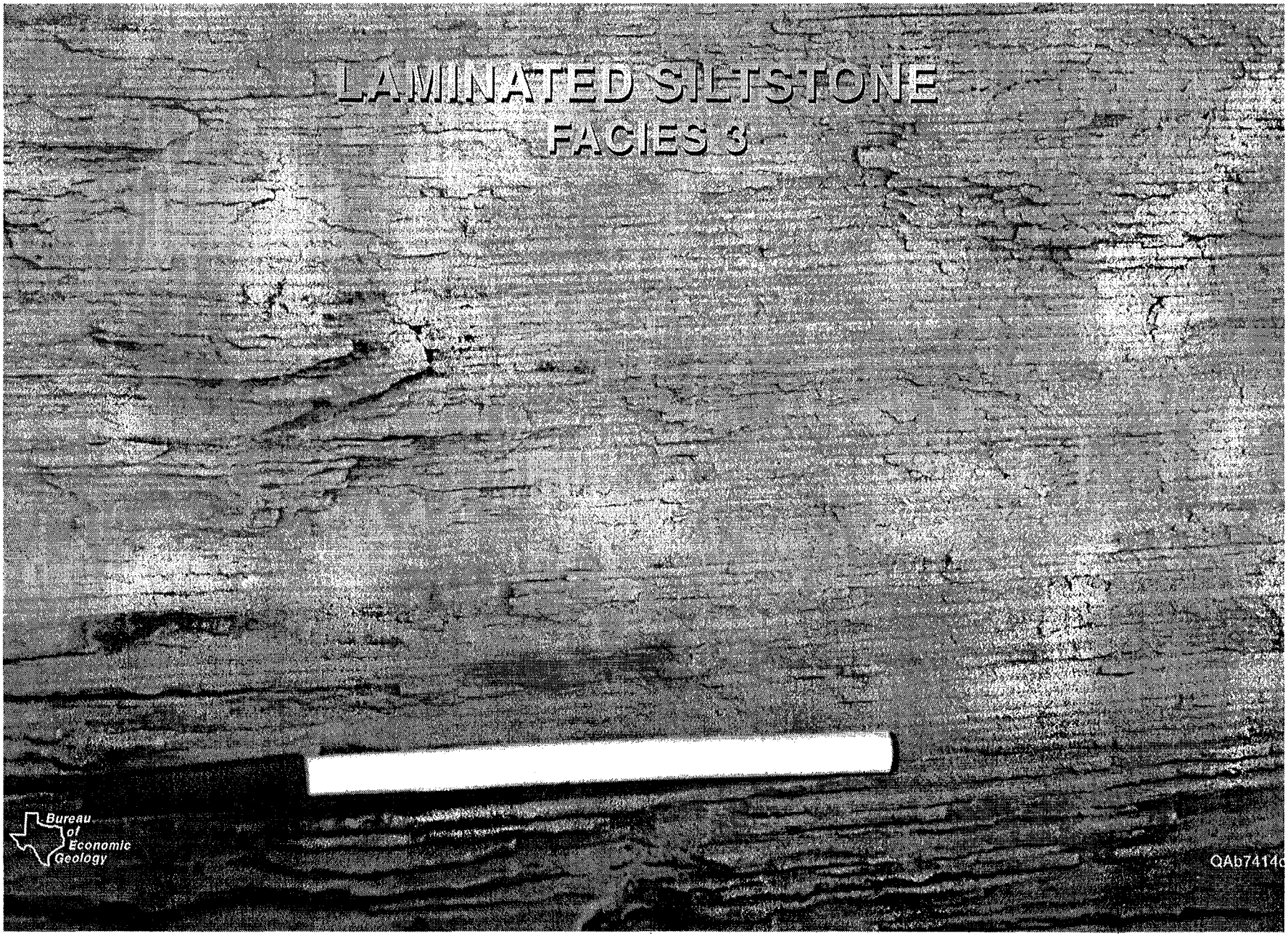

Figure 16. Photograph of facies 3 showing siltstone with extremely even, parallel lamination.

the organic-poor siltstone laminae. The laminated siltstones may be disrupted in discrete zones by burrows that are generally parallel to bedding. Other features include truncated laminae and isolated, low-amplitude ripples that display rounded crests.

The laminated siltstone facies has been interpreted by some workers to record seasonal fluctuations in the settling of pelagic matter and airborne silt. Alternatively, the organic-poor siltstone laminae may record the settling of silt from frequent low-density interflows or turbidity currents. The presence of truncated laminae and low-amplitude ripples suggests that the sediments were occasionally reworked by weak bottom currents.

Facies 4 consists of sandstones and siltstones that are graded or display partial Bouma sequences (fig. 17). Most sandstone beds are less then 1 ft thick and commonly display erosional bases. Most individual beds grade from sandstone at the base to siltstone at the top. The most common sequence of stratification types is similar to the Bouma Tbcd and Tcd divisions that begin with a horizontally laminated sandstone or ripple-drift cross-laminated sandstone and pass upward into a wavy-laminated siltstone. The sequence of stratification types and abundance of ripple-drift cross-lamination indicates that facies 4 was deposited from frequent, low-density turbidity currents (Lowe, 1982).

Facies 5 consists of sandstones that are structureless or convoluted (fig. 18). Sandstone beds are commonly greater then 1 ft thick and display abrupt, nonerosional bases. Many of the sandstones are convoluted owing to loading and dewatering structures that are contemporaneous with deposition (fig. 19). Other common features include siltstone clasts that float in a matrix of fine sand and are concentrated near the top of the bed. The lack of lamination, presence of floating clasts, and abundance of water escape and load structures suggest that the sandstones were rapidly deposited from concentrated, sediment-gravity flows (high-density turbidity currents) or sandy debris flows (Lowe, 1982).

Facies 6 consists of sandstones displaying dune-scale cross-stratification. The cross-stratification varies from infilled scours to climbing dunes. The infilled scours have a scoop-shaped geometry with sides inclined up to 75° in dip. In plane view the scours have an elliptical shape that

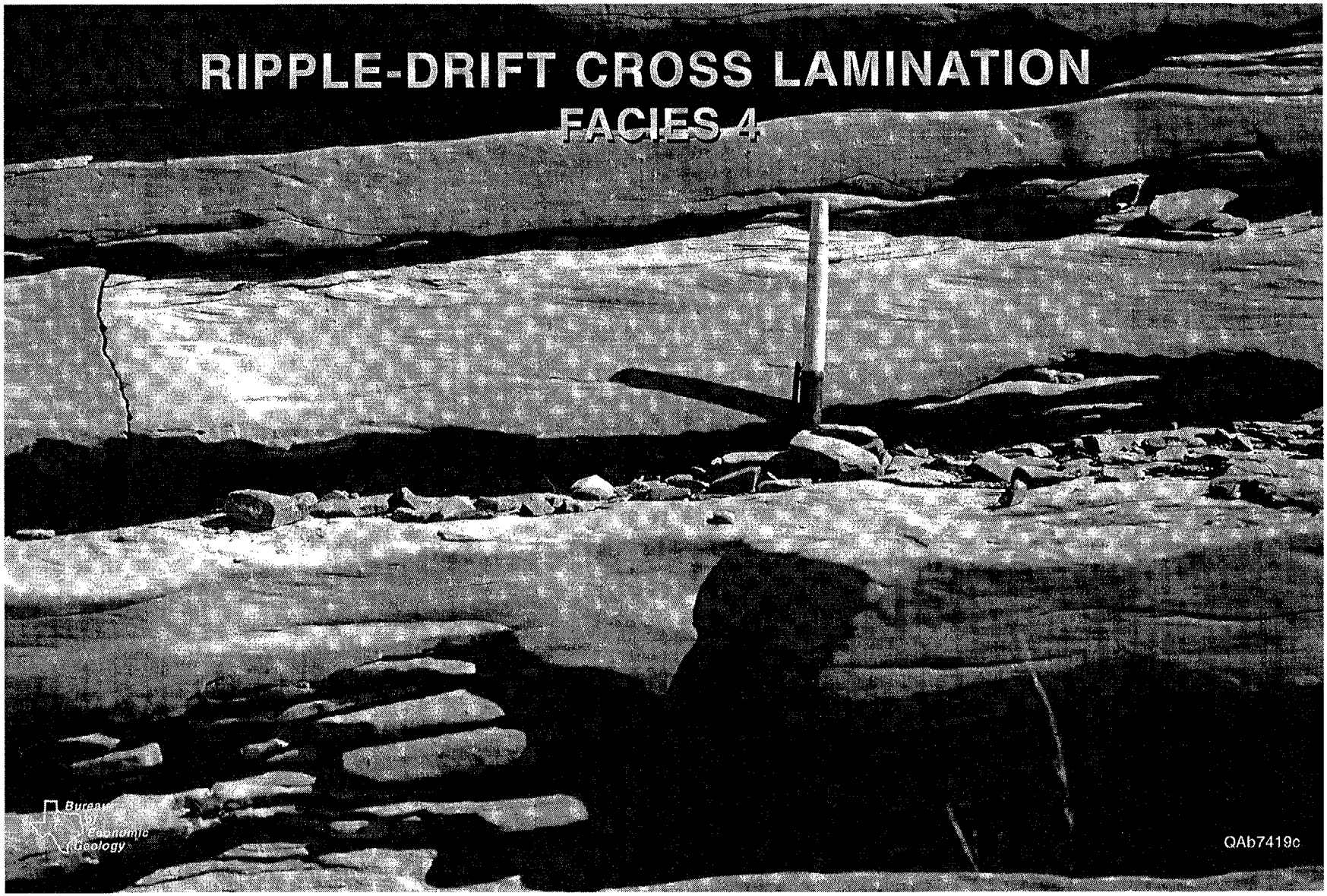

Figure 17. Photograph of facies 4 showing ripple-drift, cross-laminated sandstones interbedded with wavy-laminated siltstones.

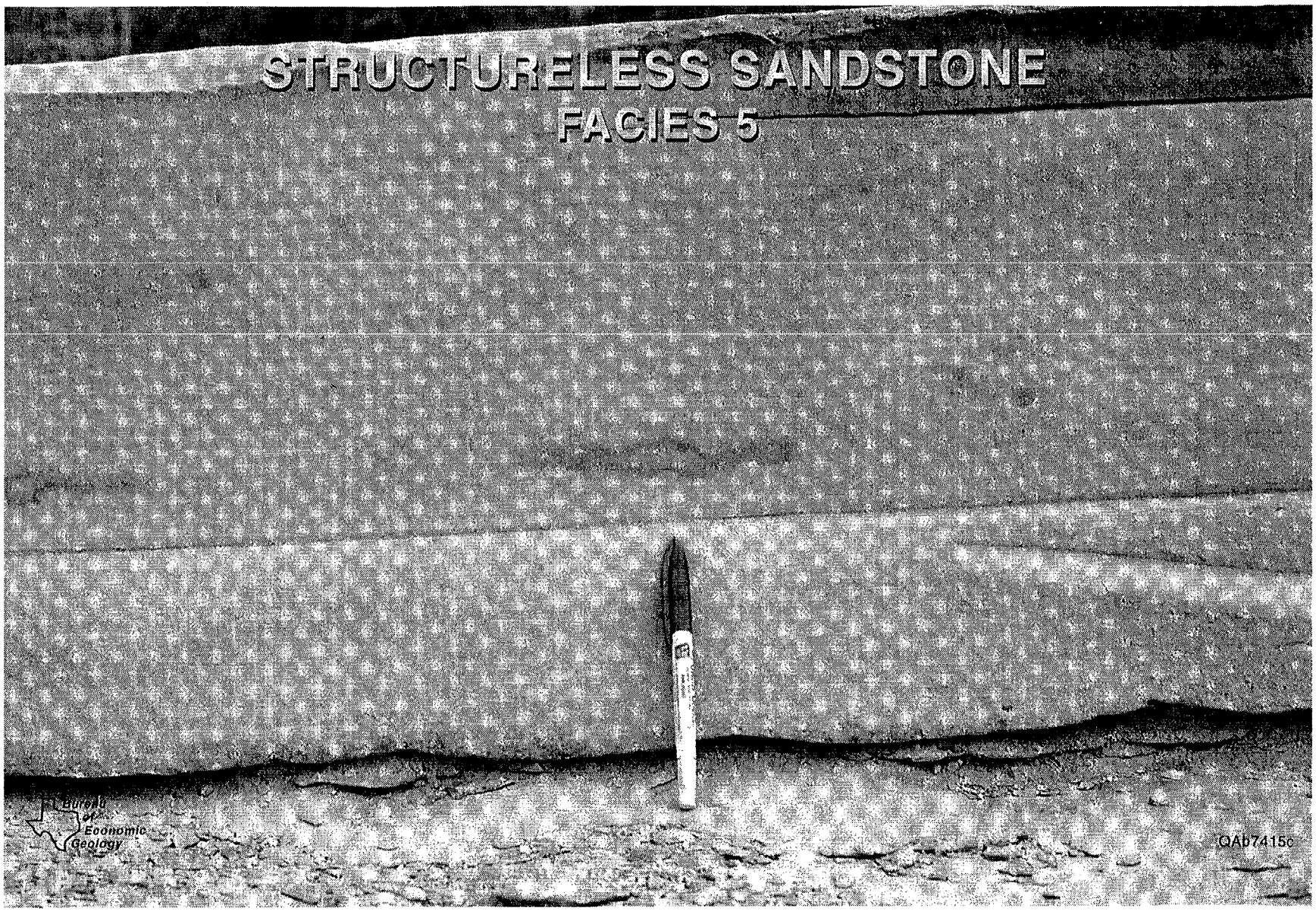

Figure 18. Photograph of facies 5 showing structureless sandstone with abrupt nonerosional contacts.

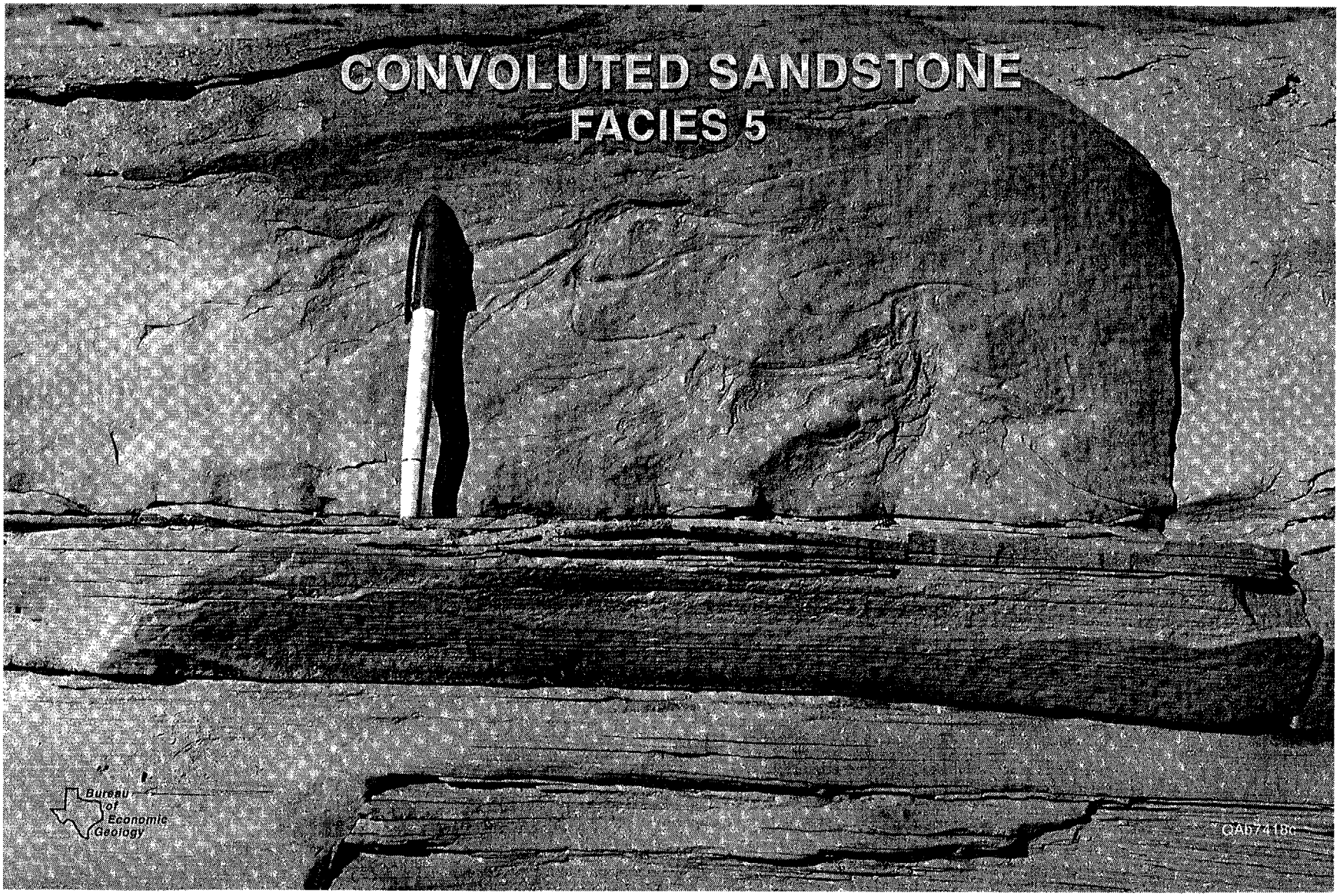

Figure 19. Photograph of facies 5 showing convoluted sandstones. The pullover structures are related to syndepositional loading and dewatering features and suggest flow was from left to right on the photograph.

is about 4 ft long and 2 ft across. The scours are infilled from the flanks by laminae that onlap the sides of the scour or overlap the margins (fig. 20). The infilled scours have been interpreted by some workers to represent the downcurrent migration of sand dunes. However, the observations that the scours are draped and infilled from the sides suggests that they are the product of fluid scour followed by the rapid fallout of sand from suspension.

The climbing dune-scale cross-lamination, often referred to as mega-ripple drift, is similar to ripple-drift cross-lamination only larger in scale. The most common form showed full preservation of laminae on the stoss side of the dune (fig. 21). The climbing dunes formed sets up to 10 ft thick. The scale and form of the cross-lamination suggests that these sands were rapidly deposited from high-viscosity flows (Lowe, 1982).

Outcrop Correlations

Outcrop correlations show how facies are organized into bodies of strata or architectural elements. These bodies are recognized on the basis of their geometry, composition, and bounding surfaces. Measured logs and the correlation of facies between them are illustrated in cross sections A–A′, B–B′, and C–C′ (see figure 13 for the location of the cross sections). Cross sections A–A′ and B–B′ are about 1.5 mi long and aligned perpendicular to the direction of sediment transport, which was predominantly to the southeast. Facies and bounding surfaces were correlated between logs spaced about 1,000 ft apart. Cross section C–C′ is about 6 mi long and aligned parallel to the dominant direction of sediment transport. In cross section C–C′, facies and bounding surfaces were correlated between logs spaced about 5,000 ft apart.

Several descriptive logs collected from the outcrop are shown in figure 22 to illustrate some general characteristics of the high-order cycle and to show how facies are organized vertically. The high-order cycle is bounded by organic-rich siltstones that are 1 to 2 ft thick. The organic-rich siltstones are transitional with facies 3 and continuous across the study area except where the basal organic-rich siltstone has been eroded and replaced by channel-form sandstone bodies. Thickness

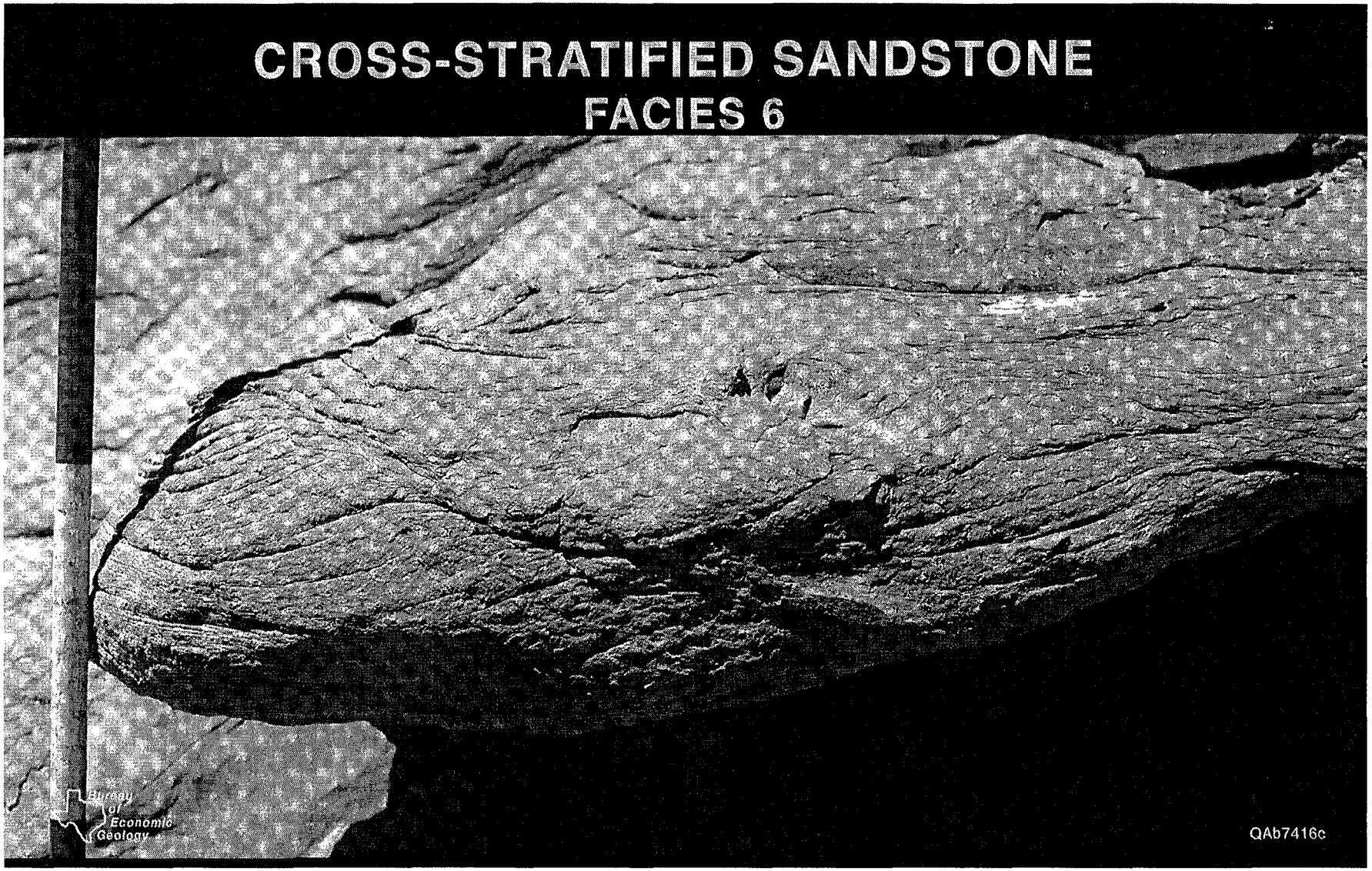

Figure 20. Photograph of facies 6 showing scoop-shaped scours infilled from the sides by laminae that overlap the margins of the scour.

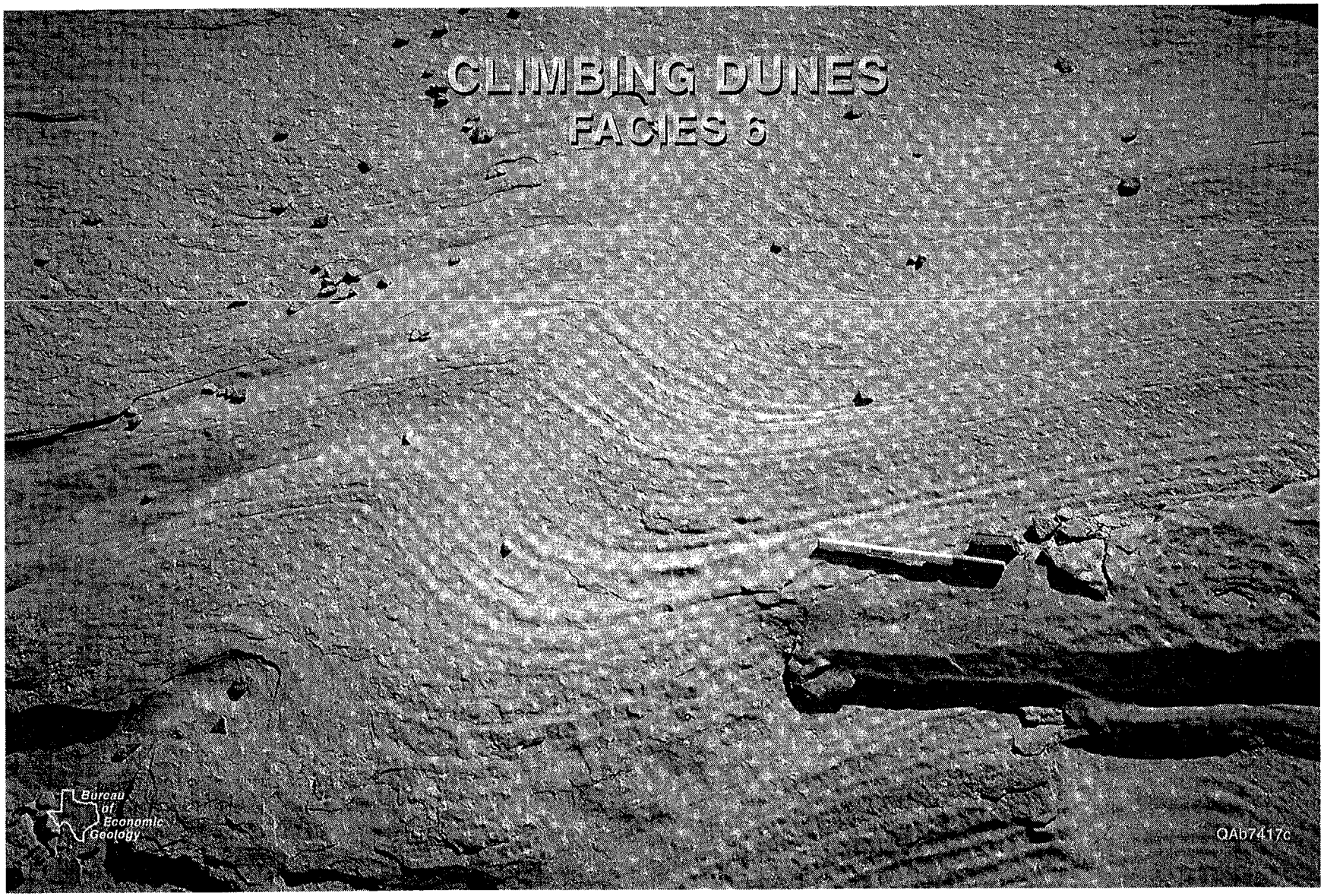

Figure 21. Photograph of facies 6 showing climbing dune scale, cross-lamination.

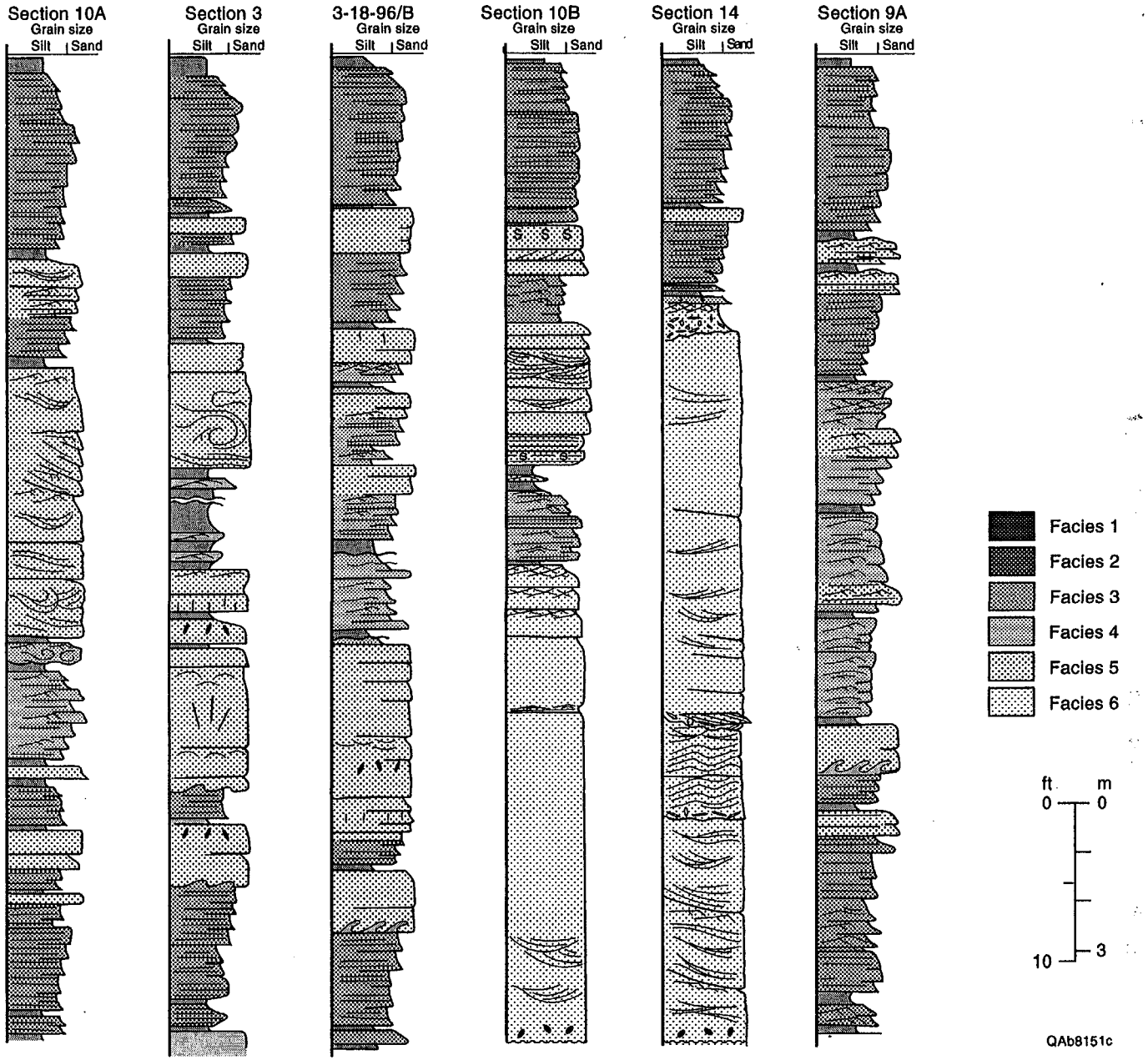

Figure 22. Representative measured sections collected from outcrop exposures of the uppermost high-order cycle in BC4.

of the cycle ranged from 50 to 85 ft with sandstone content varying from 10 to 75 percent. Differential compactional was observed over the sandstone thicks.

Within the high-order cycle facies are organized in a complex but systematic fashion. Rather than a single vertical succession, the high-order cycle is characterized by multiple (3 to 7) facies successions. Many of the successions are bounded by centimeter-thick lutites. The lower part of the cycle consists of an upward-coarsening succession of facies 3, 5, and in some cases facies 6. The upward-coarsening succession is overlain by a thin, upward-fining to upward-coarsening succession of facies 2 and 4 or is eroded and partially replaced by a thick, upward-fining succession of facies 6, 5, and 4. The upper part of the cycle consists of an upward-fining succession of facies 3 and 5.

Cross section A–A′

Within cross section A–A′ (fig. 23) facies are organized in two basic patterns that include (1) layered sheets and (2) winged channels. The layered sheets occur in the upper and lower half of the cycle and are composed of siltstone sheets that alternate with sandstone sheets. Contacts between the sheets are abrupt but nonerosional. The siltstone sheets are composed largely of laminated siltstones that tend to coarsen upward. They are between 3 and 8 ft thick and show little variation in composition or thickness laterally except where they have been truncated and replaced by the channel-form bodies.

The sandstone sheets are 2 to 14 ft thick and tend to thin to the east. The sandstone sheets tend to thicken upward in the lower portion of the cycle and thin upward in the upper portion of the cycle. The sandstone sheets are composed largely of structureless and convoluted sandstones. Trough cross-stratified sandstones occur at the top of some sandstone sheets and infill broad shallow scours.

The layered sheets are overlain and in places replaced by winged channels interstratified with organic-rich siltstones. The channels are up to 60 ft thick and 1,000 ft wide. The channels are amalgamated to form a composite body that is 3,000 ft wide. The channels are stacked from left to

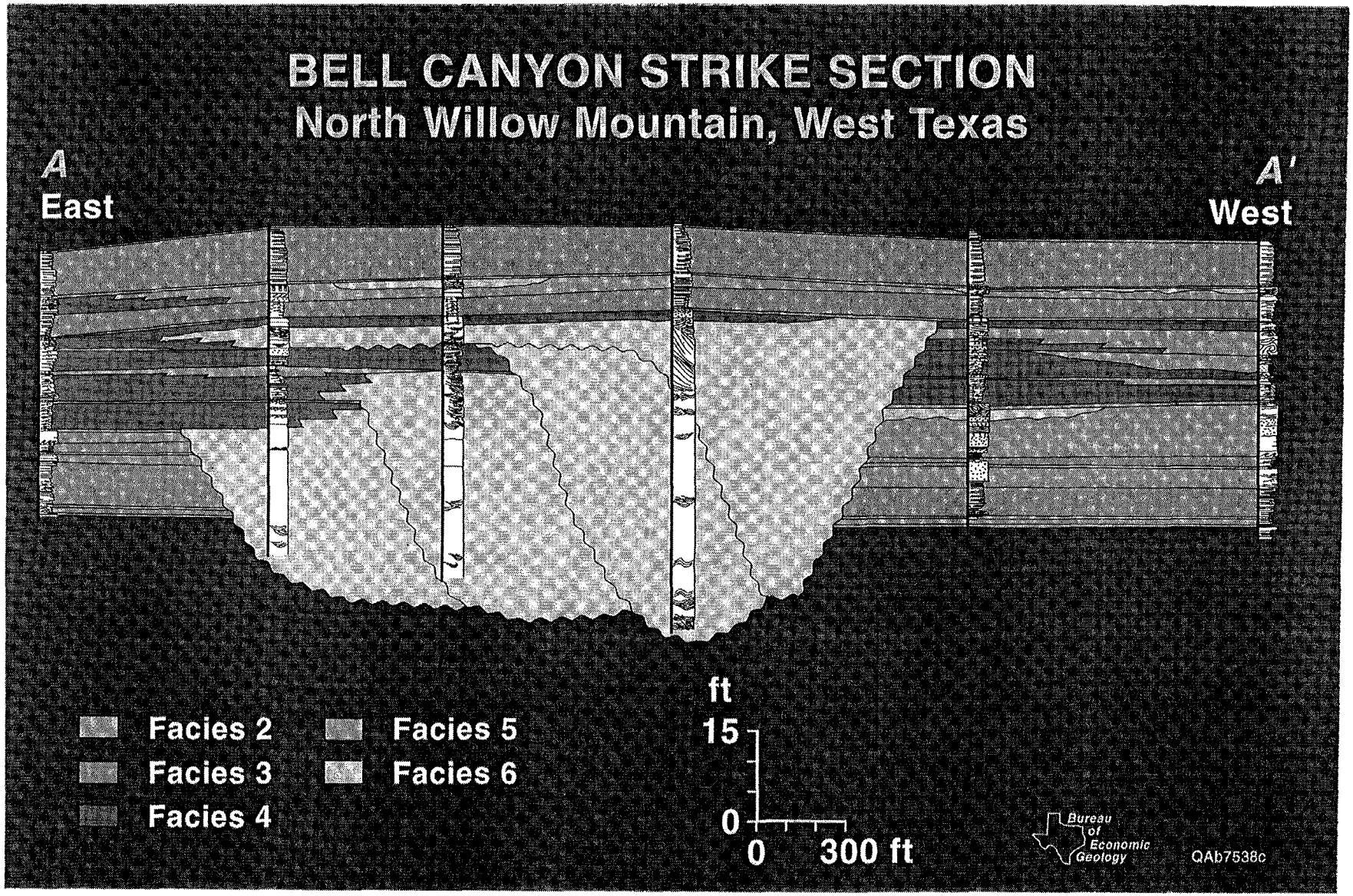

Figure 23. Outcrop cross section A–A′ showing measured logs and the correlation of facies between them.

right in an offset fashion (fig. 24). Offset between channels is 10 to 15 ft vertically and 600 to 700 ft laterally.

The channel fills are relatively homogeneous and composed of cross-stratified sandstones that may show a weak, upward-fining trend. Rounded siltstone clasts that are several centimeters in diameter may be concentrated near the base of the channels. Siltstone drapes at the base of the channel, similar to those documented in the Brushy Canyon by Harms (1974), were not observed.

The channel margins varied from abrupt cut banks (fig. 25) to gradual transitions with nonchannelized wings (fig. 26). The channel wings are made up of beds that overextend the channel margins. The wings are 5 to 15 ft thick and several thousand feet in length. Within an individual bed, facies change from cross-stratified sandstones in the channel to graded and ripple-laminated sandstones and siltstones outside the channel. Away from the channel the wings thin, fine, and interfinger with organic-rich siltstones. The interval of winged channels is succeeded by sheets of siltstone and sandstone that thin and fine upward.

Cross section B–B′

Cross section B–B′ (fig. 27) is located about 1 mi basinward of cross section A–A′. Facies are organized in the same general pattern as seen in cross section A–A′. The lower and upper portions of the high-order cycle are composed of layered sheets of sandstone and siltstone that are separated by an interval of winged channels and organic-rich siltstones. There are, however, some differences that are worth noting in the interval of winged channels between the two cross sections.

In cross section B–B′ the channels are smaller, ranging up to 45 ft in depth, and not as deeply incised into the underlying layered sheet as seen in cross section A–A′. The channels are also less amalgamated and more widely spaced. In particular, outcrop mapping has shown the two uppermost channels in cross section B–B′, which are about 1 mi apart, to represent the bifurcation of the uppermost channel seen in cross section A–A′.

The channel wings also show some significant changes between the two cross sections. The channel wings tend to be thicker, wider, and sandier in cross section B–B′ than in cross section

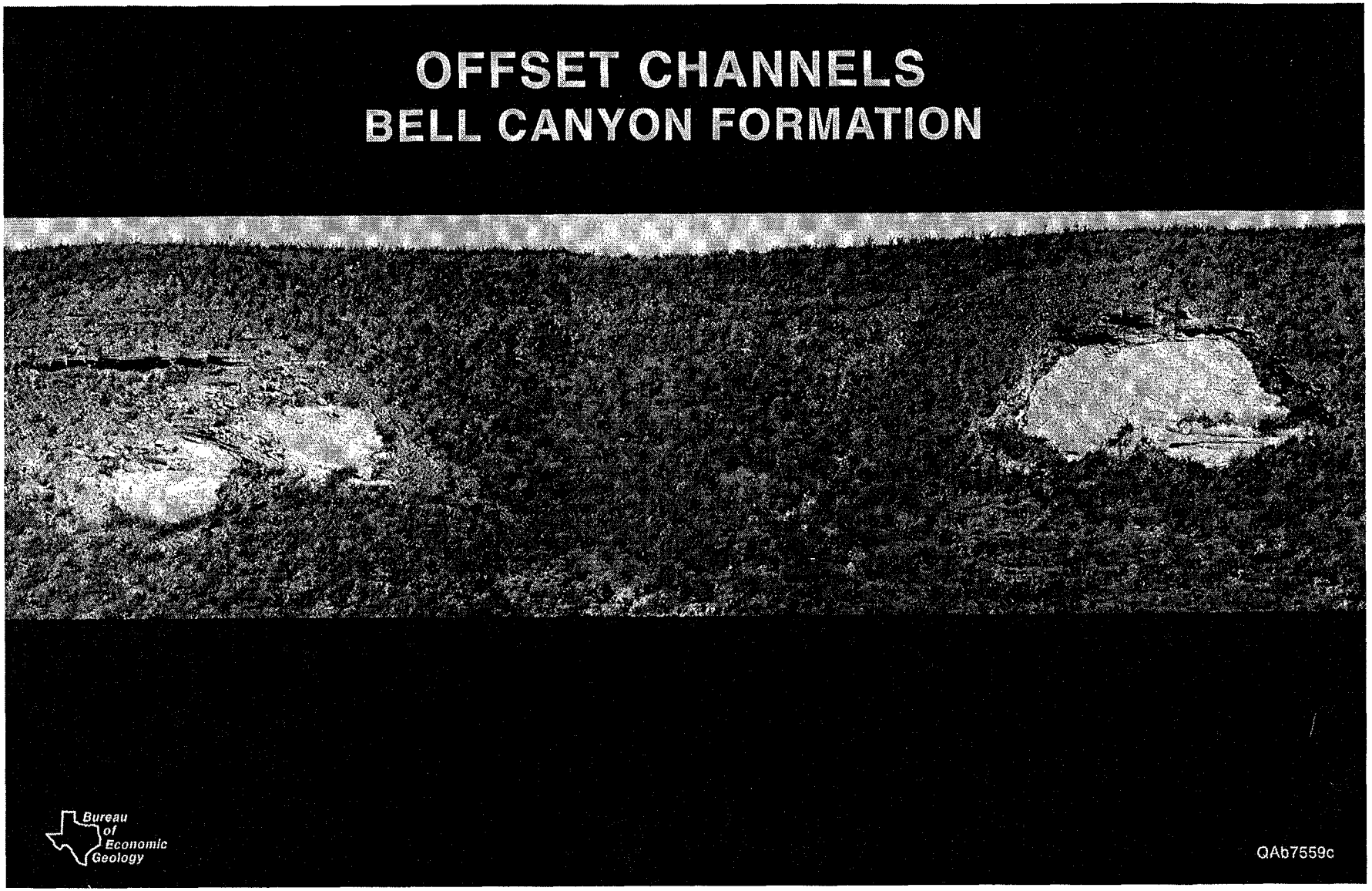

Figure 24. Photograph from cross section A–A′ showing offset stacking pattern of channels.

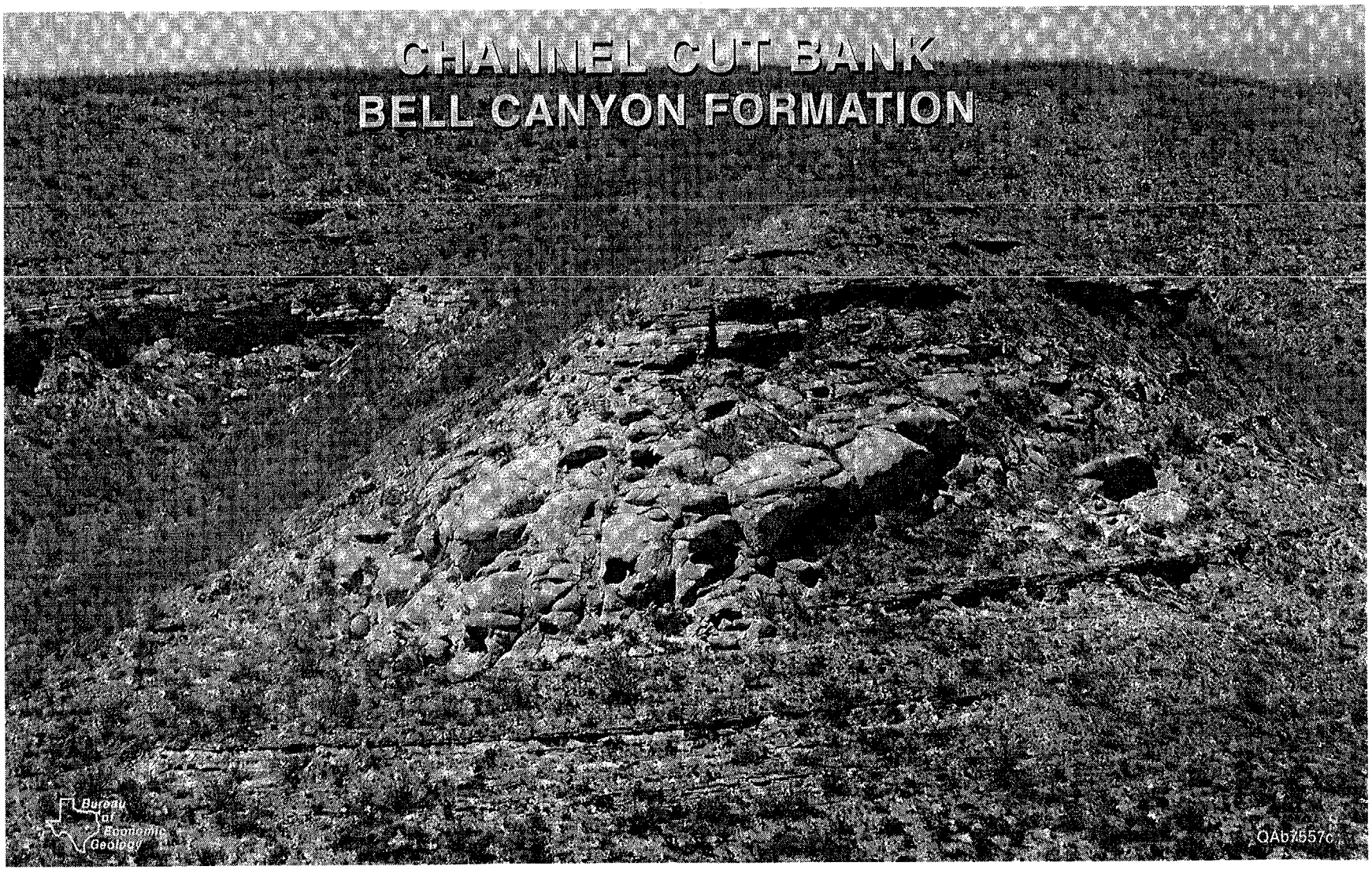

Figure 25. Photograph from cross section A–A′ showing steep channel cut bank.

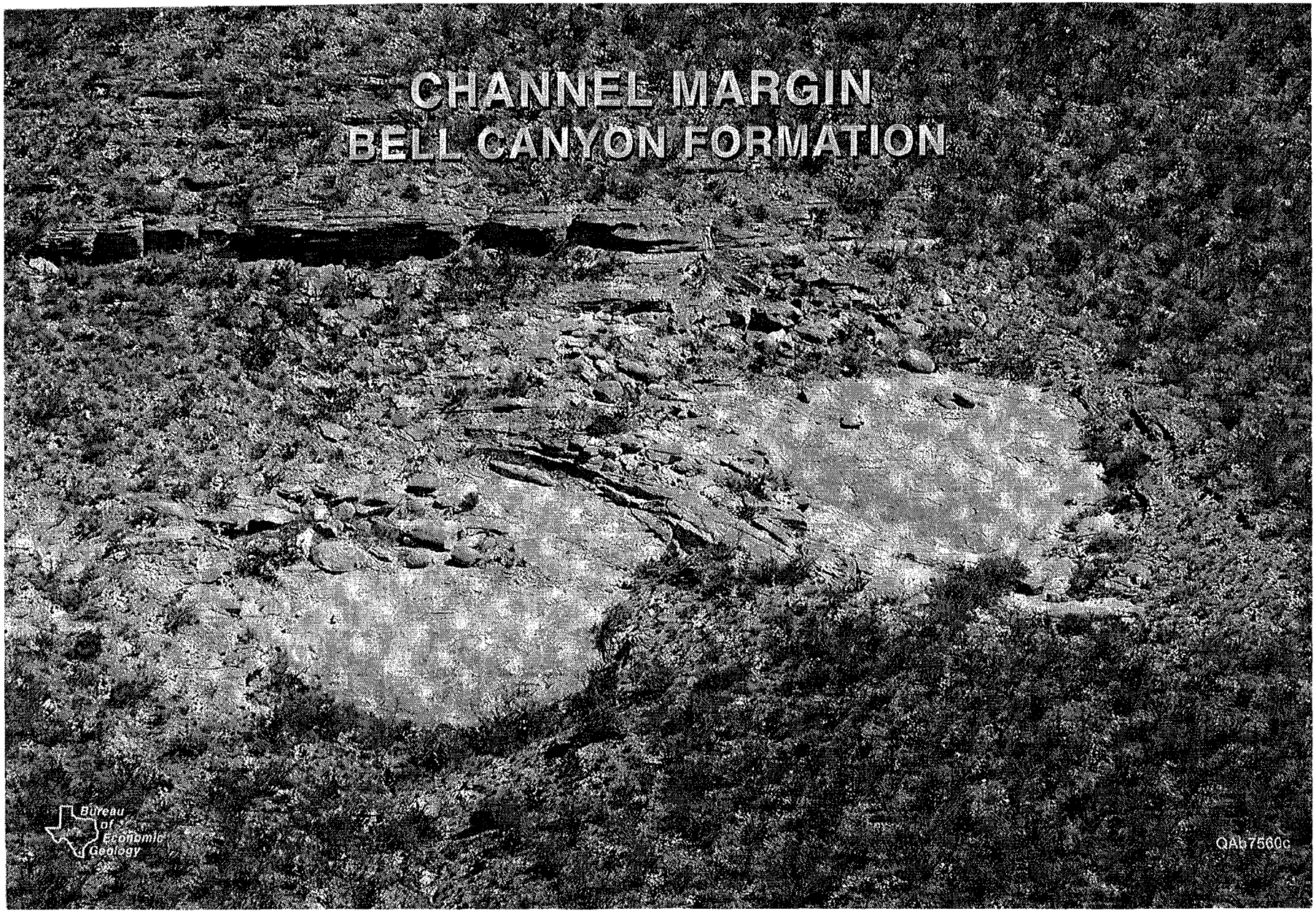

Figure 26. Photograph from cross section A–A′ showing beds that overextend channel margin.

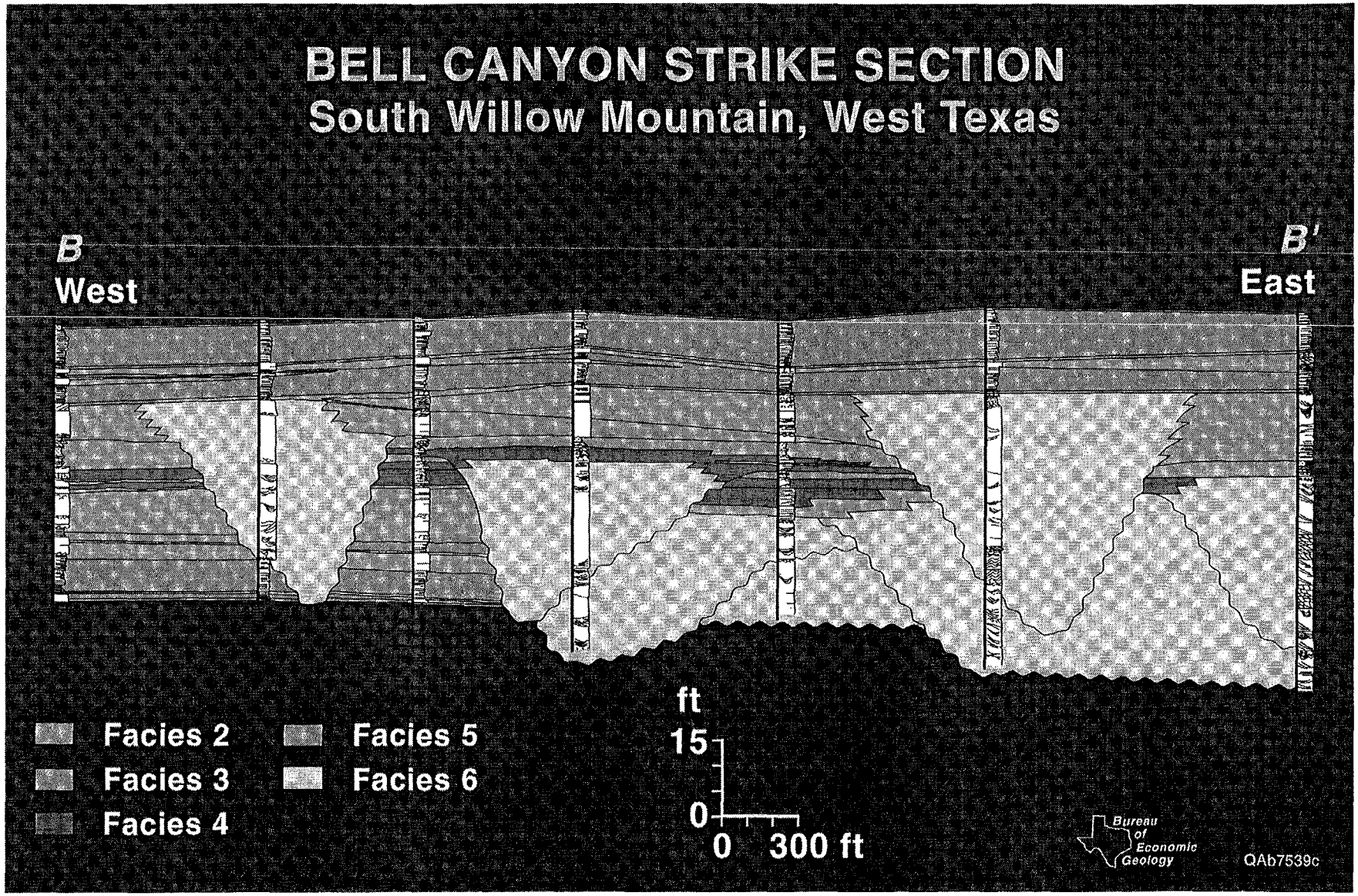

Figure 27. Outcrop cross section B–B′ showing measured logs and the correlation of facies between them.

A–A′. In the upper channel system the wings overlap to form a composite sheet sandstone. The wings are composed of massive and cross-stratified sandstones instead of thin-bedded, ripple-laminated and graded, sandstones and siltstones (fig. 28).

Cross section C–C′

Cross section C–C′ (fig. 29) is about 6 mi in length and aligned parallel to the direction of sediment transport, which was to the south. Due to differences in scale and orientation, several features are observed in cross section C–C′ that were not observed in cross sections A–A′ or B–B′. Overall, the high-order cycle thins basinward from about 85 ft in the north to about 55 ft in the south. Sandstones in the lower half of the cycle, which appear as sheets in cross sections A–A′ and B–B′, appear as lenticular bodies that dip gently to the south or basinward and pinch out into laminated siltstones. In the upper portion of the high-order cycle the sandstone sheets thicken toward the north or the shelf. Channelized sandstone occurs at several different stratigraphic levels. Basinward, or toward the south, they terminate in broad lenticular sandstone bodies. Systematic changes in facies that progress upward from laminated siltstones at the base to massive and channelized sandstones at the top define four sediment bodies. Shifts in facies between the sediment bodies suggest that they initially step basinward, then turn around and step toward the shelf.

Depositional Model

Stratal relationships indicate that the sandstones were deposited in channels with levees and attached lobes (fig. 30). In cross section A–A′ channels with beds that overextended the channel margin (channel wings) are observed. These bodies are interpreted as channels with attached levees. In cross section B–B′ it was observed that basinward the channels bifurcate and are flanked by channel wings composed largely of structureless sandstones. The structureless sandstones form broad lenticular bodies that dipped gently basinward and pinch out into laminated siltstones. These

Figure 28. Photograph from cross section B–B′ showing winged channel.

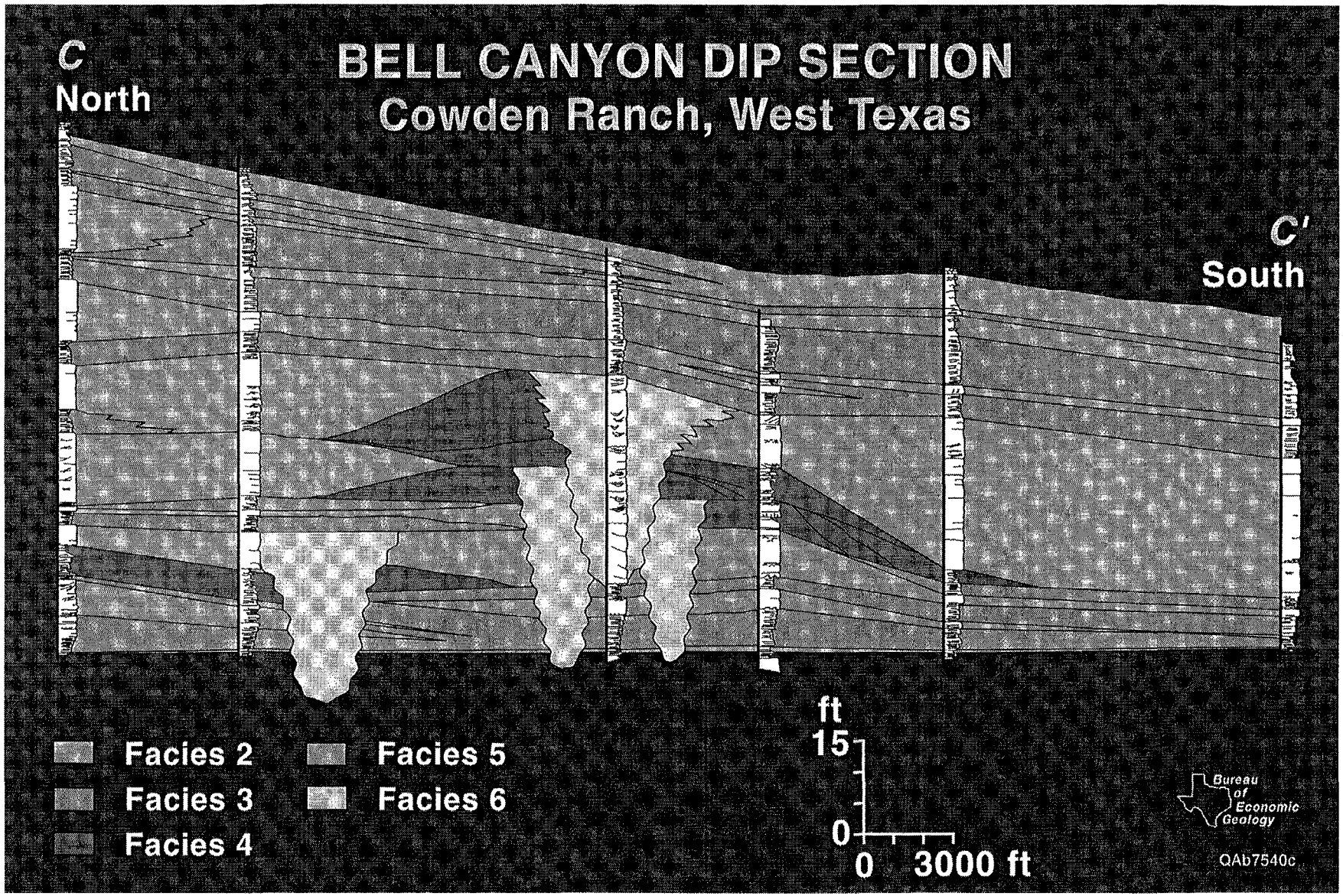

Figure 29. Outcrop cross section C–C′ showing measured logs and the correlation of facies between them.

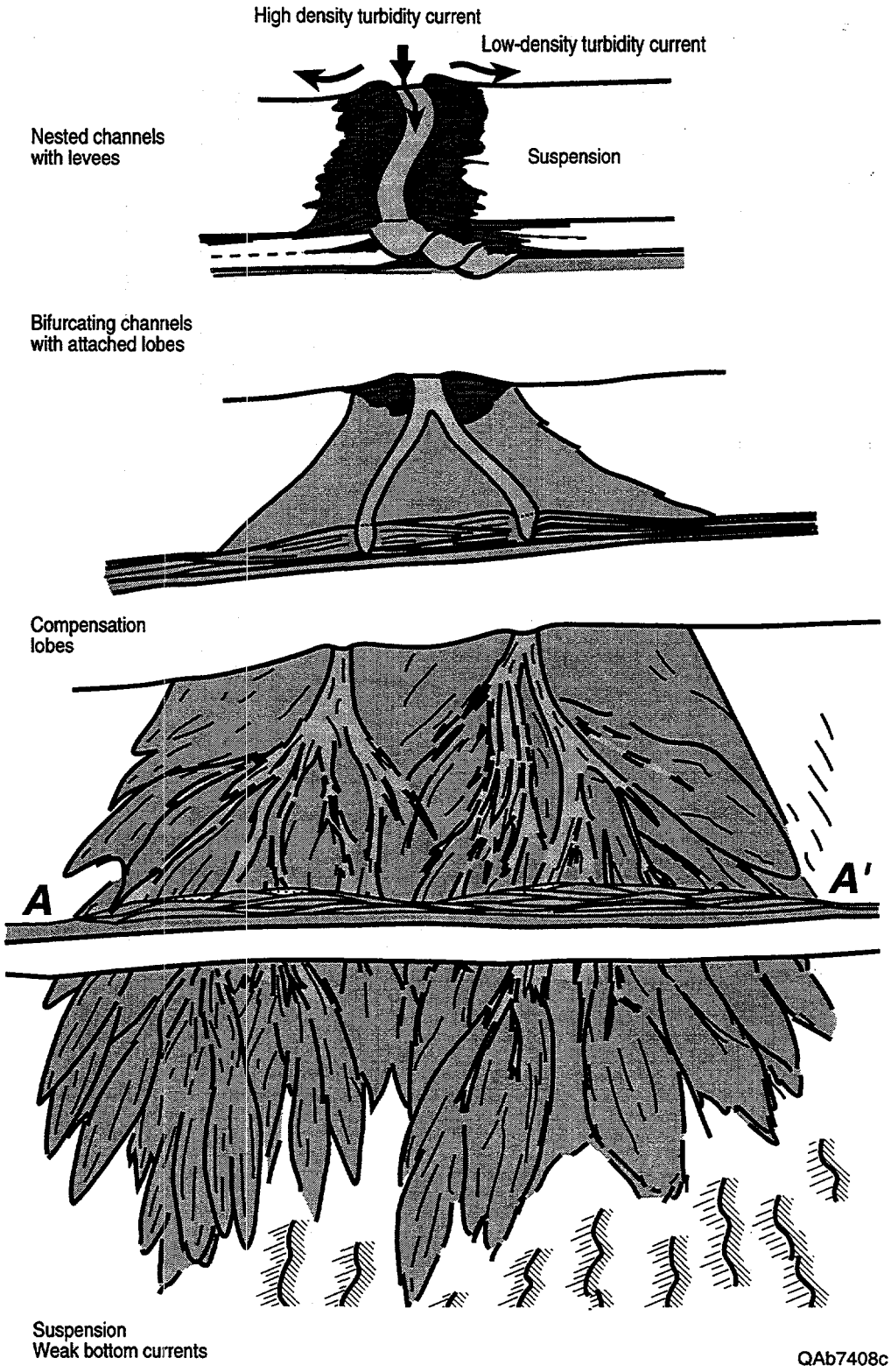

Figure 30. Diagram illustrating depositional model for upper Bell Canyon Formation. Bell Canyon sandstones are interpreted to have been deposited in submarine channels with levees and attached lobes.

sandstone bodies are interpreted as channels with attached lobes. Relationships seen in cross section C–C′ suggest that the high-order cycle is composed of multiple channel levees with attached lobes (fig. 31). These elements appear to initially step into the basin, then aggrade, then step back toward the shelf.

Facies characteristics indicate that the sandstones were transported into the basin by turbulent sediment-gravity flows. Climbing dune-scale cross-lamination within the channels suggests that they were deposited at moderate rates from flows with a high concentration of suspended sediment (high-density turbidity current). The abundance of sandstones and siltstones that are graded or display partial Bouma sequences within the channel levees suggests that they were deposited from low-density turbidity currents that overtop the channel margins. The lack of well-developed lamination and abundance of loading and dewatering structures within sandstones that compose the channel lobes suggest that they were rapidly deposited by high-density turbidity currents at the mouth of the channels. Interchannel areas are composed of organic-rich siltstones and are interpreted to record the slow settling of airborne silt and pelagic material. The thin organic-rich siltstones that bound many of the successions are interpreted as an abandonment facies associated with channel avulsion and lobe switching. The sheetlike laminated siltstones are interpreted as a basinal facies deposited by the settling of airborne silt and pelagic material combined with minor reworking by weak bottom currents and suspension deposition from density interflows or turbidity currents.

Architectural Elements

The cross sections indicate that the high-order cycle can be subdivided into bodies of strata or architectural elements that are distinctive with regard to their composition, geometry, and bounding surfaces. Distinctive architectural elements include channels, levees, lobes, interchannel bodies, pelagic drapes, and basinal sheets. The composition, geometry, and dimensions of each element are summarized in tables 1 and 2.

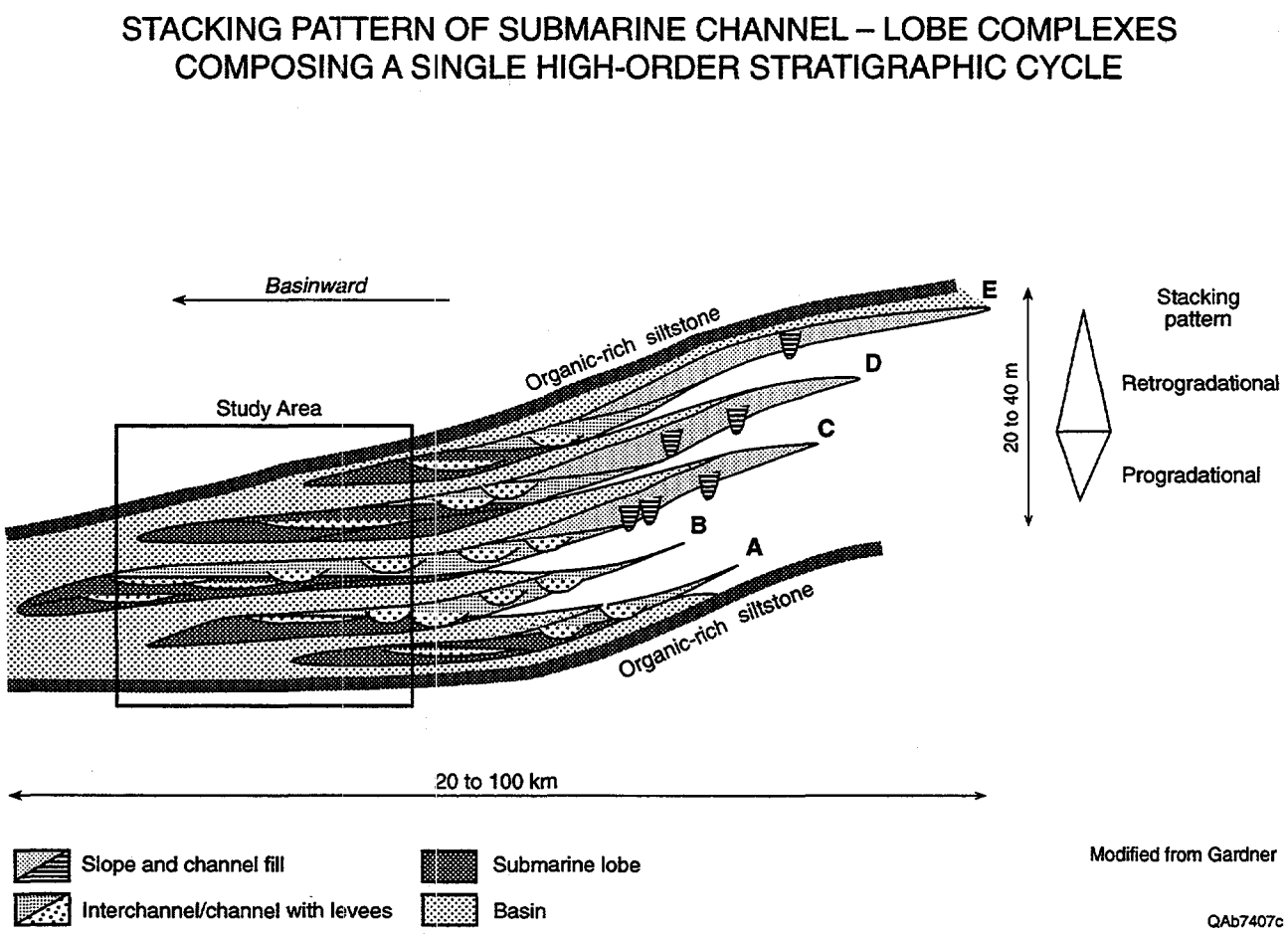

Figure 31. Diagram illustrating the vertical stacking pattern of the submarine channels and lobes.

Table 1. Description of architectural elements.

Element	Facies succession	Depositional setting
Channel	Erosive-base, uniform to upward-fining succession. Dominated by facies 6 with lesser amounts of facies 5 and 4.	Deposition from waning traction currents or high-density sediment gravity flows.
Levee	Upward-coarsening to upward-fining succession. Dominated by facies 2 with minor amounts of facies 4.	Spillover deposition from low-density sediment-gravity flows along channel margin.
Interchannel	Irregular succession. Dominated by facies 2 with minor amounts of facies 4.	Suspension deposition in interchannel areas protected from bottom currents.
Lobe	Sharp-base, uniform to upward-coarsening succession. Dominated by facies 5 with minor amounts of facies 6.	Deposition from high-density sediment-gravity flows at mouth of channel.
Pelagic drape	Facies 2.	Pelagic drape preserved following channel avulsion and lobe abandonment.
Basinal	Upward-coarsening to upward-fining succession. Facies 3.	Suspension deposition from density interflows with minor amounts of reworking by weak bottom currents.

Table 2. Geometric attributes of architectural elements.

Element	Geometry	Thickness (m)	Width
Channel	Lens	5–20	100–1000 m
Levee	Wedge	1–5	100–1000 m
Interchannel	Irregular	0.1–2	1–10 km
Lobe	Lobate	1–10	1–10 km
Pelagic drape	Discontinuous drape	0.01–0.2	> 10 km
Basinal laminate	Sheet	1–5	> 10 km

Channels are up to 60 ft in thickness and 1,000 ft across. They may amalgamate to form bodies that are 3,000 ft across. The channels have erosive bases and are composed largely of cross-stratified sandstones that may show a weak upward-fining trend. The channels are flanked by wedge-shaped bodies interpreted as channel levees, which are composed of thin-bedded sandstones and siltstones. They are 5 to 15 ft thick and several thousand feet in length. Away from the channels the levees thin and interfinger with organic-rich siltstones interpreted as interchannel deposits. The interchannel deposits are up to 6 ft thick and display an irregular geometry.

Basinward the channels bifurcate and terminate in lobes. The lobes are up to 30 ft thick and between 1 and 10 mi in width. Large lobes may represent composite lobes formed by the overlap of smaller lobes. The lobes have a broad lenticular geometry and dip gently into the basin. The lobes display abrupt nonerosional contacts and are composed of structureless sandstones that may show a weak upward-coarsening or bed-thickening trend. Basinward the lobes interfinger with sheets of laminated siltstones. The laminated siltstone sheets are 3 to 10 ft thick and show little variation in thickness except where they have been truncated and replaced by channels. Pelagic drapes that bound many of the successions are several centimeters to several decimeters in thickness. They are preserved as locally discontinuous but laterally persistent layers.

Conclusions

In summary, the Bell Canyon Formation represents a sand-rich, deep-water system that accumulated in the semirestricted Delaware Basin. Outcrop investigations of the upper Bell Canyon Formation indicate that sandstones were deposited on the basin floor by high- and low-density turbidity currents. Based on composition, geometry, and bounding surfaces, the fundamental depositional elements are submarine channels with levees and attached lobes. Within a high-order cycle, additional stratigraphic complexity results from abrupt lateral shifts in the stacking pattern of the submarine channel and lobe elements.

RESERVOIR CHARACTERIZATION OF FORD GERALDINE UNIT

A major goal of the project this year was reservoir characterization of the Ford Geraldine unit, which involved the following tasks: (1) correlating and subdividing the high-order cycle that includes the Ramsey sandstone; (2) mapping the geometry of reservoir sandstone bodies and bounding siltstones; (3) describing cores in order to interpret depositional environments, calibrate log responses, and construct a depositional model; and (4) evaluating diagenetic processes that may affect the production performance of reservoirs. Reservoir characterization focused on this unit because it has more available data and a larger volume of oil in place than does Ford West field, making it the more attractive target.

The Ramsey sandstone at the Ford Geraldine unit dips to the northeast (fig. 32), almost directly opposite original depositional dip, because Late Cretaceous movement associated with the Laramide Orogeny tilted the Delaware Basin eastward (Hills, 1984). Production from Geraldine Ford field and other upper Bell Canyon fields in the Delaware Basin occurs from the distal (southwest) ends of east-dipping, northeast-oriented linear trends of thick Ramsey sandstone deposits (fig. 4). Most hydrocarbons in these fields are trapped by stratigraphic traps formed by an updip lateral facies change from higher permeability reservoir sandstones to low-permeability siltstones. Several of the fields, including Geraldine Ford, show minor structural closure because linear trends of thick sandstones formed compactional anticlines by differential compaction during burial (Ruggiero, 1985).

Information about Bell Canyon sandstones gathered from well-exposed outcrops has guided interpretation of the reservoir at the Ford Geraldine unit. The Ramsey sandstone is the uppermost high-order cycle in the BC5 interval of the Bell Canyon. The scale and position of the Ramsey sandstone is directly analogous to that of the uppermost high-order cycle in the BC4 interval examined in outcrop (previous section). In addition, previous studies of Geraldine Ford field and other nearby Bell Canyon fields by Williamson (1978, 1979), Berg (1979), Ruggiero (1985, 1993), and Gardner (1992, in press) provided the foundation for this study.

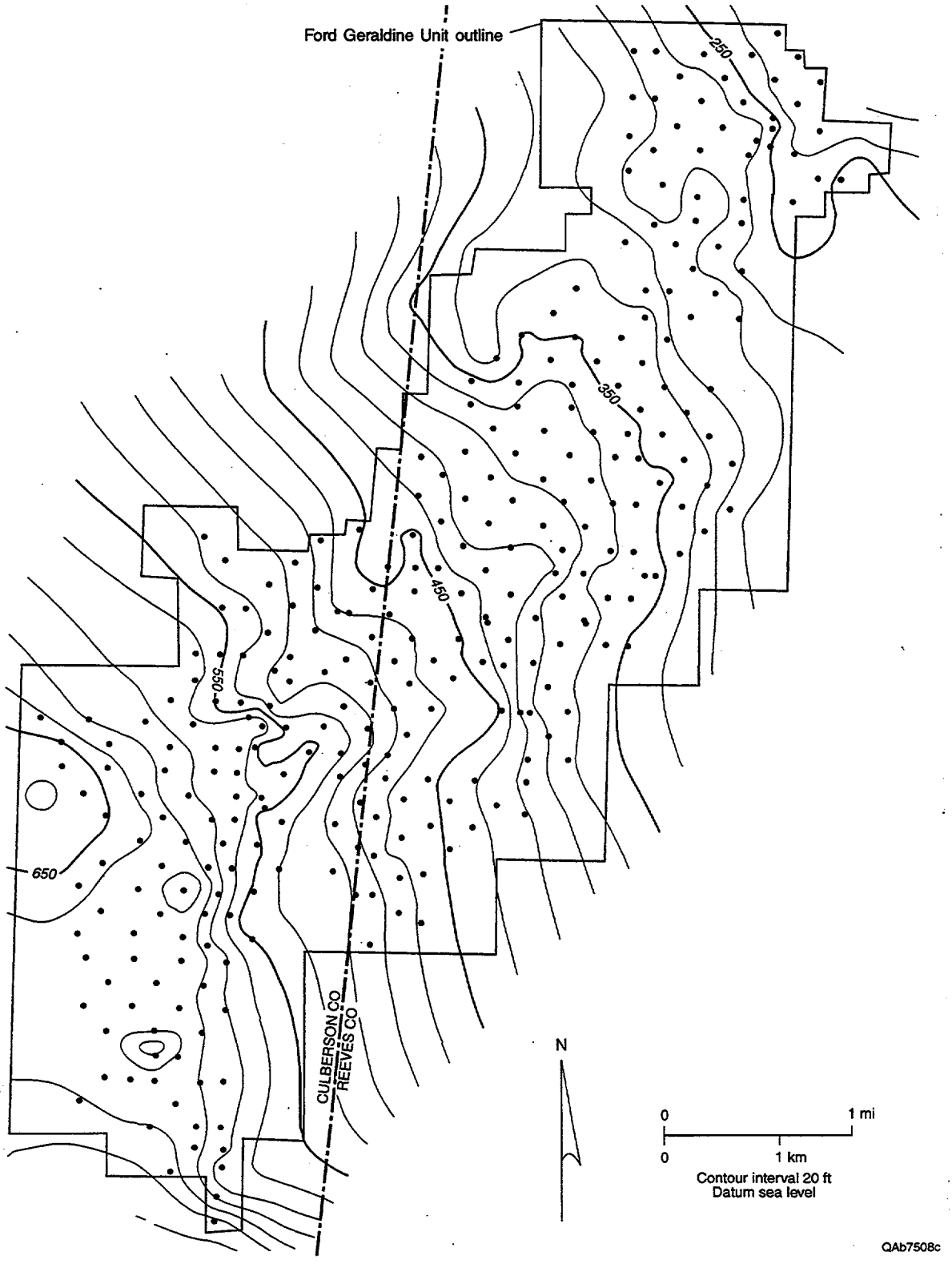

Figure 32. Structure contours on the top of the Lamar Limestone dip to the east and northeast. The trap at Geraldine Ford field is formed by pinch-out of permeable sandstone into low-permeability siltstone up structural dip. The field has minor structural closure because of differential compaction over the reservoir sandstone body.

Methods

An excellent subsurface data base for reservoir characterization is available from the Ford Geraldine unit. Logs were available from 305 of the 340 wells in the field, including 182 wells that had some type of porosity log. A total of 3,615 ft of core of the Ramsey sandstone and adjacent siltstones from 70 wells was slabbed and described this year, and these data were supplemented by descriptions of 681 ft of additional core from 13 wells by Ruggiero (1985). Core analyses (permeability, porosity, water saturation, and oil saturation) from nearly 8,000 samples from 120 cores throughout the Ford Geraldine unit were entered into a spreadsheet.

The tops shown in figure 5 were correlated in all logs in the Ford Geraldine unit. The API well numbers, log curves, elevation datum, total depth, latitude and longitude, and tops for each well were entered into the Landmark software OpenWorks™ during the first year of the project. Core-analysis, perforation, and production data were added to OpenWorks™ this year.

The composition of Ramsey sandstones was determined from 15 thin sections made from samples representing a wide range of permeability. The chips used to make the thin sections were taken immediately adjacent to core-analysis plugs so that petrographic parameters could be compared with porosity and permeability. Composition of Ramsey sandstones was determined by standard thin-section point counts (200 points) of thin sections stained for potassium feldspar and carbonates. Point counts of cements differentiated between those falling within molds of dissolved grains and those in primary pores.

A JEOL T-300 SEM was used to examine, qualitatively describe, and photograph the grains, cements, and pore structure of about 20 representative samples from the Ramsey 1 and 2 sandstones. Qualitative compositional analysis by a Tracor energy dispersive system (EDS) aided in mineral identification.

Depositional Models

Ramsey sandstones in Geraldine Ford field were interpreted by Ruggiero (1985, 1993) as having been deposited in a submarine channel that funneled bottom-hugging saline density currents into the basin from breaks in the shelf margin. In this model a channel 1 to 2 mi wide and 40 to 100 ft deep was cut prior to deposition of the Olds sandstone (fig. 5). The Olds and Ramsey sandstones that filled the channel form the reservoir at Geraldine Ford field. Following the model of Harms (1974) and Harms and Williamson (1988), Ruggiero concluded that saline-density currents laden with fine-grained sandstone swept off the shelf and flowed down slope, confined within the channel. Ruggiero interpreted the major correlative units as being laterally continuous across the entire channel (Ruggiero, 1985, 1993). He concluded that bottom-hugging saline-density currents had enough volume to fill the entire channel in a sheetlike fashion from margin to margin (figs. 11, 33). This interpretation of the depositional processes is of particular importance to the model for reservoir architecture in the Ford Geraldine unit, because it suggests a high degree of lateral continuity within sandstones (fig. 33).

A different depositional model for Bell Canyon sandstones was developed on the basis of the outcrop study conducted for this project (Barton, 1997; previous section). Stratal relationships indicate that sandstones in the upper Bell Canyon in outcrop were deposited in channels with levees and attached lobes (fig. 30). This model predicts greater lateral heterogeneity within the reservoir sandstones, caused by the juxtaposition of sandstone channel, levee, and lobe facies and their interfingering with interchannel facies composed of organic-rich siltstones. Reservoir characterization of Ramsey sandstones at Geraldine Ford field summarized in this section indicates that the channel-levee and lobe model best fits the data.

Texture

Ramsey sandstones in the Ford Geraldine unit have a very narrow range of grain sizes. The average grain size in sandstone samples is 0.092 mm (3.44 Ø), and the range is 0.085 to

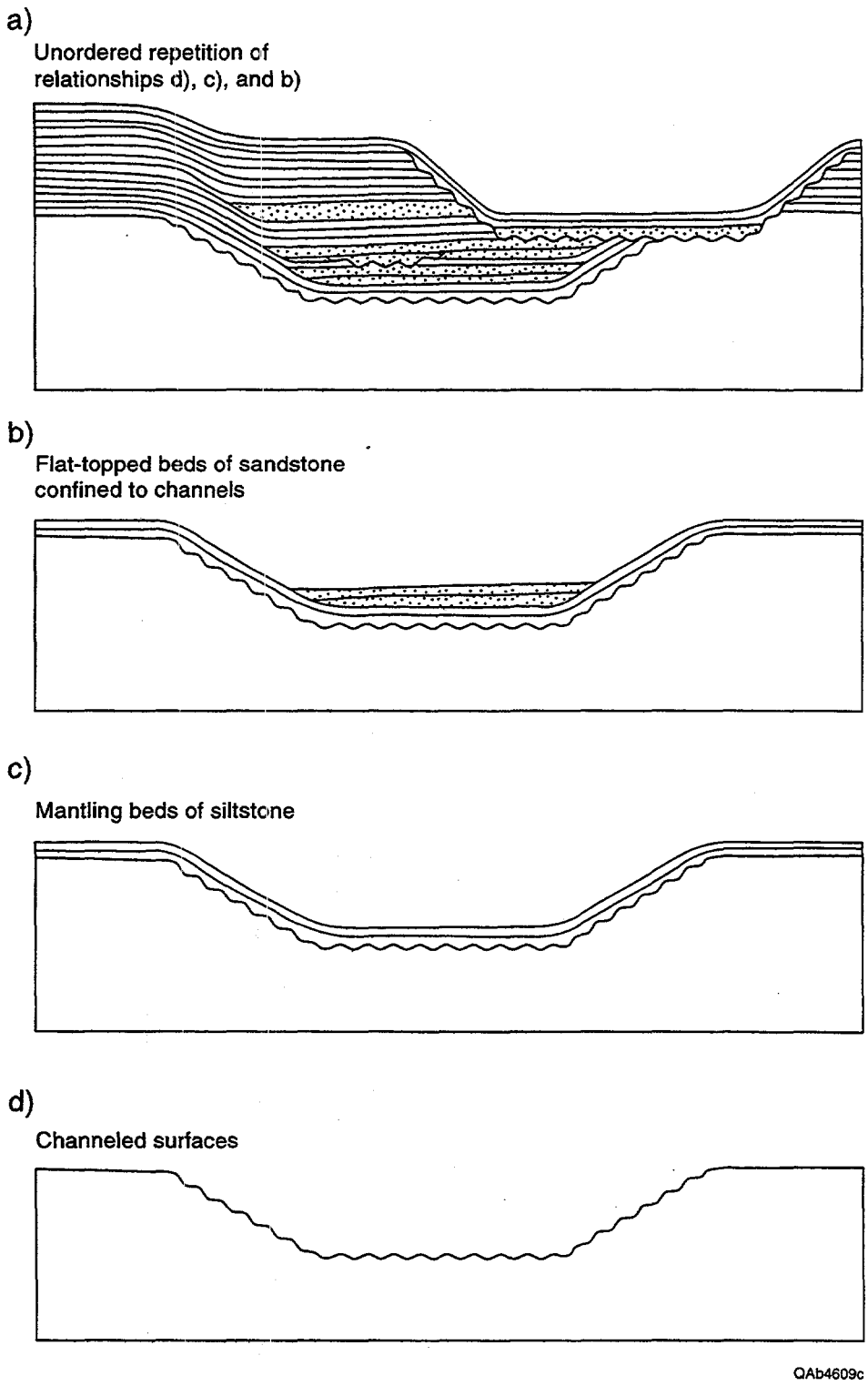

Figure 33. Interpreted sequence of events during deposition of Delaware Mountain Group sediments by saline-density currents (modified from Harms, 1974). In this model, channels (d) were scoured by strong currents of dense water flowing basinward under less dense, deep water. Deposition of silt (c) occurred by settling from intermediate density water flowing basinward into density-stratified, deep water. The final stage of the sequence (b) was deposition within pre-existing channels of sand tractionally carried by thin, upper-to-lower flow regime currents of dense, low turbidity water flowing basinward under less dense, deep water.

0.107 mm. The proportion of silt-size grains in the sandstones ranges from 4 to 20 percent. The sandstones are mostly well sorted, having an average standard deviation of 0.44 Ø. Sorting ranges from 0.37 to 0.52 Ø. Clay minerals in Ramsey sandstone are interpreted as authigenic; thus, as has been noted by other previous workers (for example, Williamson, 1978; Berg, 1979), the Ramsey sandstones are unusual in their lack of detrital clay.

A laminated siltstone sample from the base of the Trap siltstone immediately above the Ramsey 2 sandstone has an average grain size of 0.059 mm (4.09 Ø), and it contains 38 percent sand grains. A lutite sample near the base of the Lamar Limestone has an average grain size of 0.033 mm (4.94 Ø), and it contains 46 percent silt, 46 percent organic matter, and 8 percent sand.

Characterization of Depositional Heterogeneity

Interpretation of the processes that deposited the reservoir sandstones at Geraldine Ford field was based strongly on the outcrop characterization of analogous reservoir sandstones in the upper Bell Canyon. All five facies identified in upper Bell Canyon sandstones in outcrop were observed in the 70 Ramsey sandstone cores examined from Geraldine Ford field (fig. 6). These facies were also observed by Ruggiero (1985) in the 13 cores he described. The five facies were (1) massive, organic-rich siltstone (lutite); (2) laminated siltstone (laminite); (3) sandstones that are graded or display partial Bouma sequences; (4) structureless or convoluted sandstone; and (5) cross-stratified sandstone. Massive sandstones are volumetrically the most abundant sandstone facies in the core, although that may in part be an artifact of the narrow range in grain sizes, which makes sedimentary structures indistinct and difficult to see in core. On outcrop, weathering processes may help to accentuate the sedimentary structures and make them more visible. Thus, some sandstones described as massive in the core may actually contain sedimentary structures that could not be distinguished.

The Ramsey sandstone is a 0- to 60-ft thick sandstone that is bounded by the Ford and Trap laminated siltstones. Lutites in the underlying Ford siltstone and the overlying Trap siltstone (fig. 5) are interpreted to represent condensed sections that mark the top and base of a genetic unit,

equivalent to a high-order cycle (Gardner, 1992; Kerans and others, 1992). In the northern part of the Geraldine Ford unit, the Ramsey is divided into two sandstones (Ramsey 1 and Ramsey 2) separated by a 1- to 3-ft-thick laminated siltstone (SH1) (Ruggiero, 1985). In the southern part of the Ford Geraldine unit, only the Ramsey 1 sandstone is present. Thus, the Ramsey high-order cycle is subdivided into the following five units, from oldest to youngest: (1) upper Ford siltstone, from the Ford condensed section to the top of the Ford siltstone; (2) Ramsey 1 sandstone; (3) SH1 siltstone; (4) Ramsey 2 sandstone; and (5) lower Trap siltstone, from the base of the Trap siltstone to the Trap condensed section (fig. 5).

Mapping of Genetic Units

Upper Ford Siltstone

The upper Ford is composed of organic-rich siltstone laminae interbedded on a millimeter scale with organic-poor siltstone laminae. The average grain size of the silt coarsens upward from the Ford condensed section to the top of the Ford, and the percentage of sand, amount of burrowing, and the thickness of organic-poor laminae all increase toward the sandstone. Rarely do ripples and truncated laminae occur within the upper Ford siltstone. Gamma-ray response decreases over this interval, probably because much of the radioactivity is contained in organic matter within the organic-rich layers. The upper Ford thins from the northwestern side of the field (13 to 15 ft) to the southeast (11 to 13 ft) (fig. 34). Porosity in the Ford siltstone ranges from 1.1 to 20.3 percent and averages 16.9 percent. Permeability ranges from 1 to 33 md, and geometric mean permeability is 2 md.

Ramsey 1 Sandstone

The Ramsey 1 sandstone occurs across all of the Ford Geraldine unit (fig. 35). It pinches out at the northwest and southeast margins of the field and reaches a maximum thickness of >35 ft along a curving northeast-southwest trend. At the southwest end of the field, the single trend of

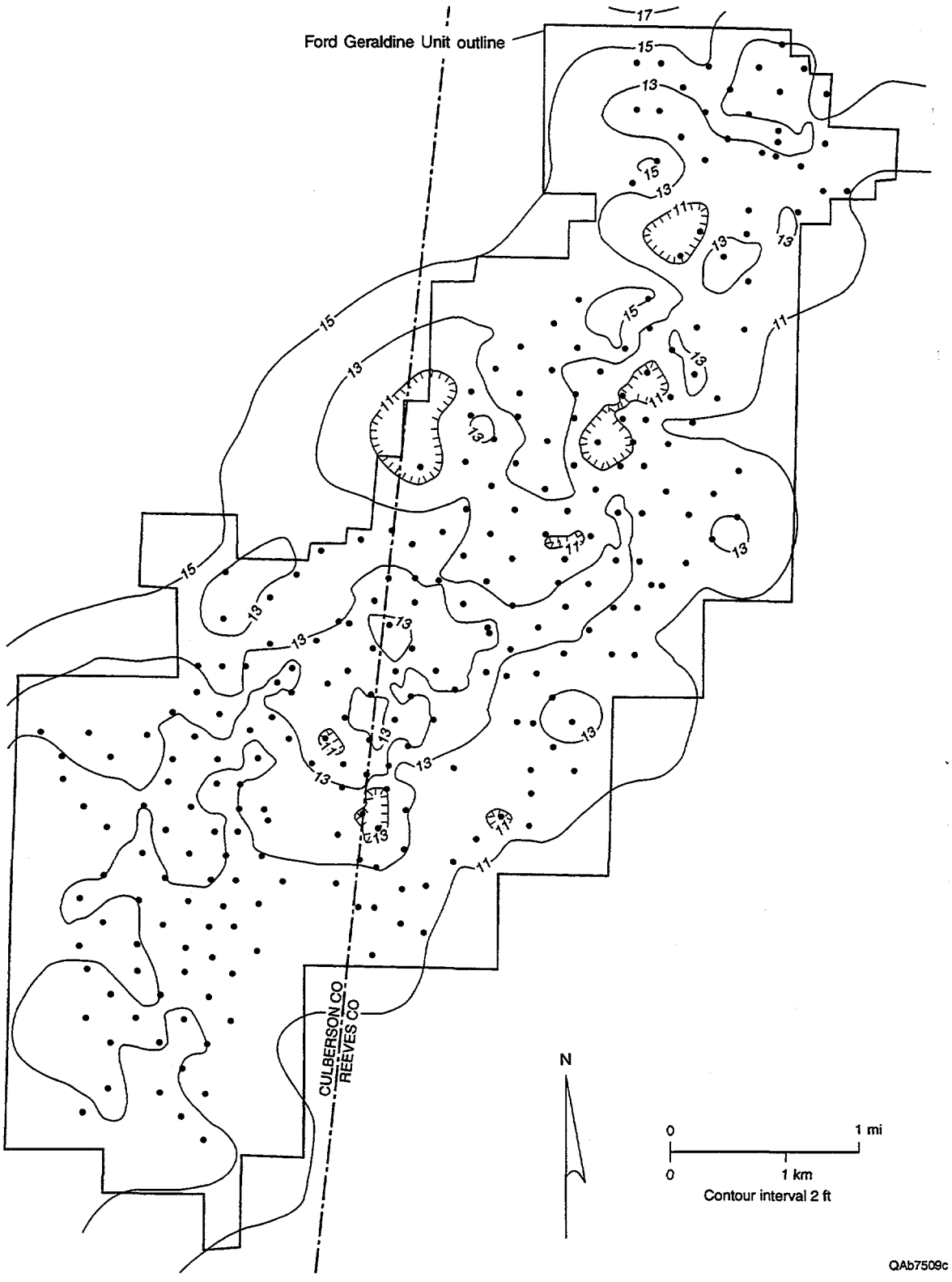

Figure 34. Isopach map of the upper Ford laminated siltstone, measured from the Ford condensed section to the top of the Ford. The relatively uniform thickness of the Ford interval suggests it was either deposited as widespread windblown silt or deposited in a broad lobe that extends beyond the margins of the field.

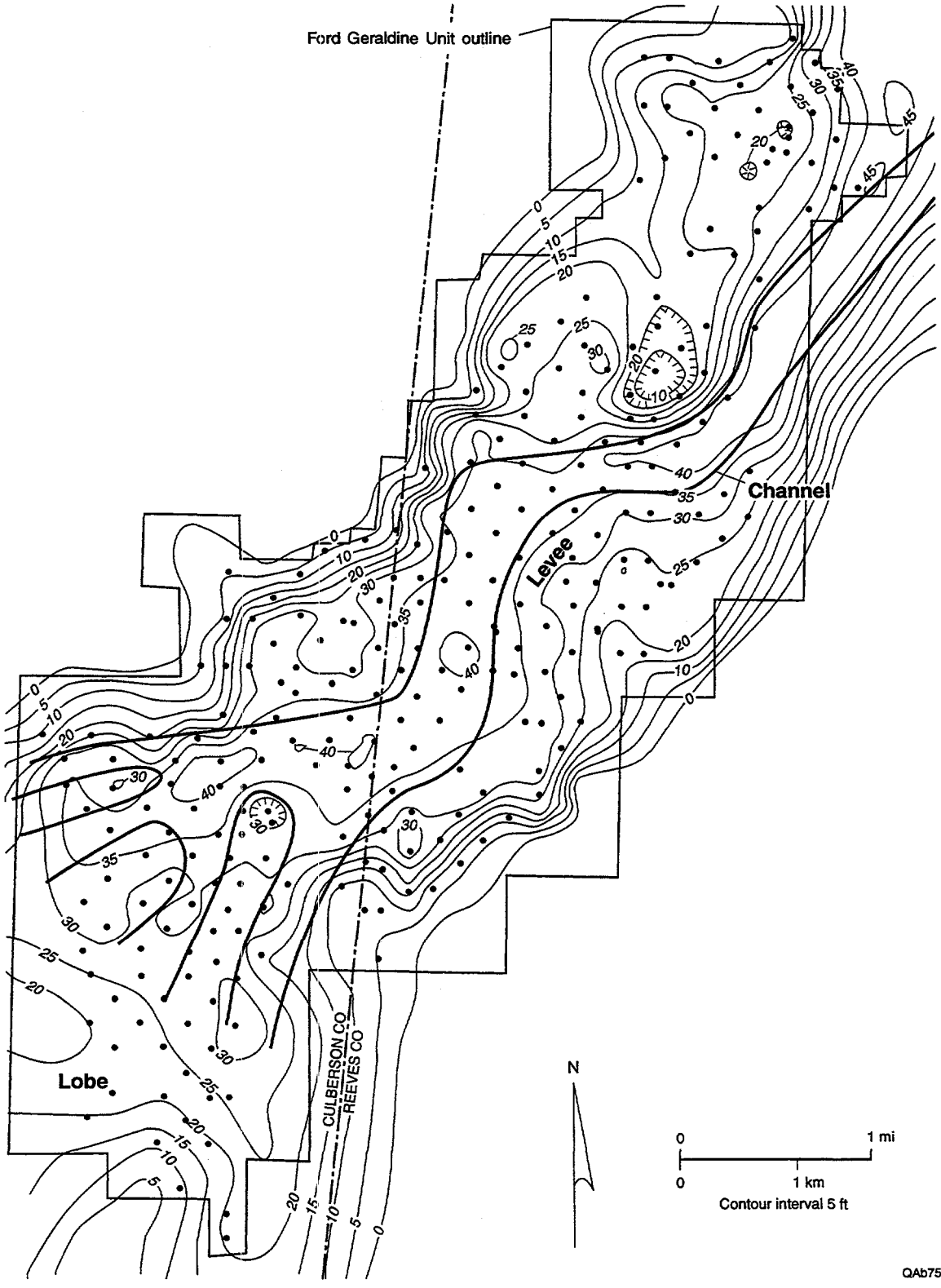

Figure 35. Isopach map of the Ramsey 1 sandstone, the main reservoir interval at Geraldine Ford field. It is interpreted as a channel-levee system that progrades over an elongate lobe. At the southwestern end of the field, the channel apparently breaks up into many smaller branches with attached lobes.

thick sandstone splits into several smaller trends (fig. 35). The Ramsey 1 sandstone interval is 83 to 100 percent sandstone, with some thin interbeds of laminated siltstone and lutite. The average grain size of Ramsey 1 sandstones is 0.093 mm (3.42 Ø), which is near the boundary between upper and lower very fine sandstone. The range of average grain sizes is quite narrow, from 0.087 to 0.103 mm (3.28 to 3.51 Ø).

Core descriptions show that sandstones from all three sandstone facies occur in the Ramsey 1. Massive sandstones are common in all parts of the interval and throughout the field. Crossbedded sandstones are most common along the trend of thickest sandstone through the center of the field. Sandstones with partial Bouma sequences, particularly rippled sandstones, and siltstone interbeds occur most commonly in the sandstone wedge that follows the margins of the thick sandstone and pinches out at the edges of the field. Massive and contorted sandstones with abundant dewatering structures occur commonly in the lower Ramsey 1 interval.

Ruggiero (1985, 1993) subdivided the Ramsey 1 interval into three sandstones that he correlated across most of the field. In this study, the siltstones within the Ramsey 1 that Ruggiero used to correlate were determined to have only local distribution, so fieldwide subdivision of the Ramsey 1 was not deemed appropriate.

In most wells the gamma-ray response is distinctly lower in the Ramsey 1 sandstone than in the underlying Ford siltstone; in some wells the gamma response continues to decrease upward in the lower Ramsey 1 interval. Porosity in the Ramsey 1 sandstone ranges from 2.9 to 29.9 percent and averages 21.8 percent. Permeability ranges from 0.01 to 400 md, and geometric mean permeability is 19 md.

SH1 Siltstone

The SH1 siltstone represents a break in sandstone deposition within the Ramsey interval, when laminated siltstone was deposited (fig. 36). The SH1 siltstone can only be differentiated from the Trap siltstone at the northern end of the field, where they are separated by the Ramsey 2 sandstone (fig. 5), but it is interpreted as being of widespread extent. Where it can be mapped

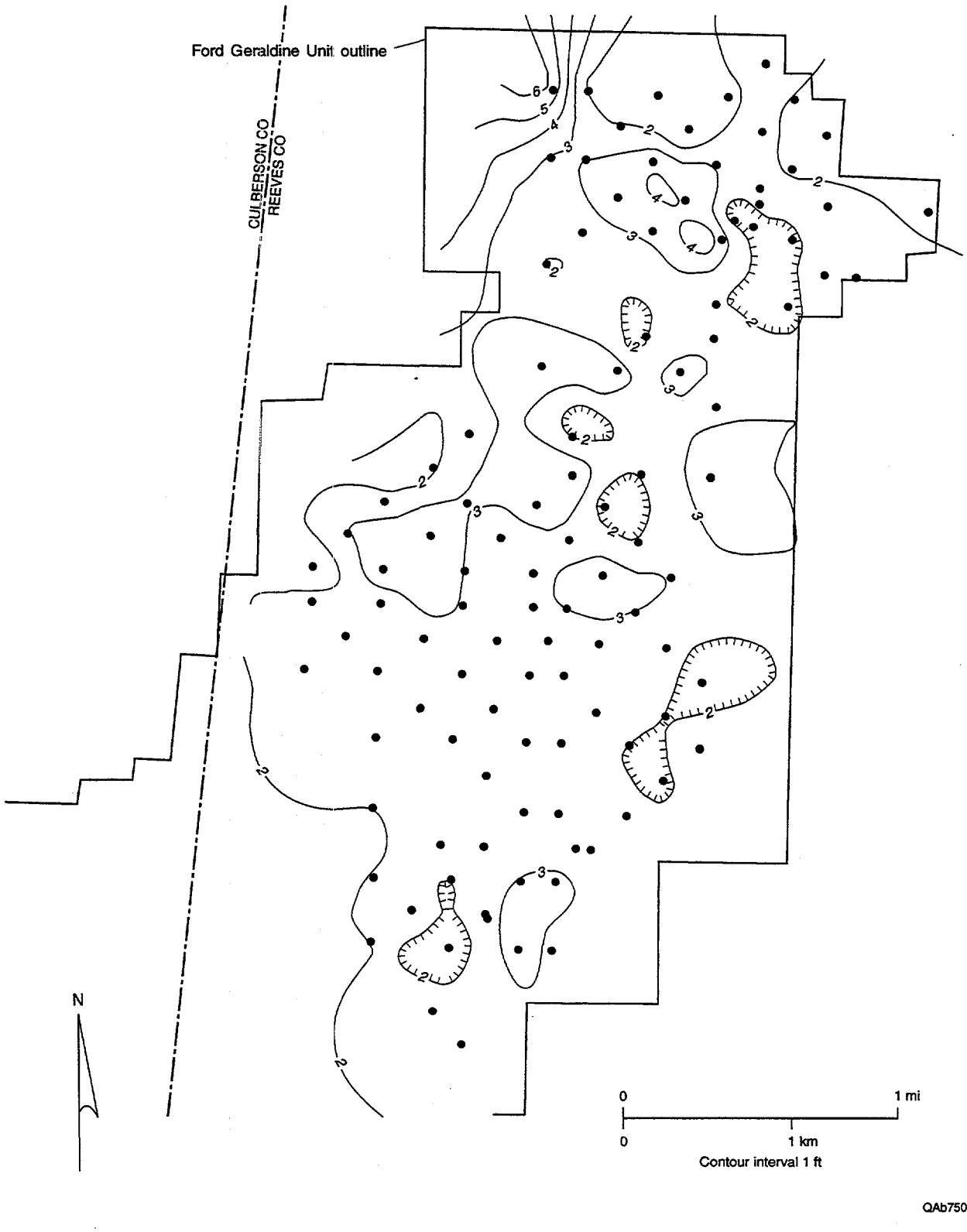

Figure 36. Isopach map of the SH1 laminated siltstone, which was deposited during a break in sandstone deposition. It can only be differentiated from the Trap siltstone at the northern end of the field, where it is overlain by the Ramsey 2 sandstone, but is interpreted as being of widespread extent. Like the Ford and Trap laminites, the SH1 siltstone was probably deposited by windblown silt settling out of suspension or deposited as a distal fan lobe.

separately, it is mostly 2 to 4 ft thick, increasing to >6 ft at the northwestern edge of the unit (fig. 36). The SH1 siltstone is composed of laminated siltstone similar to that of the Ford; burrows are common. Some ripples and truncated laminae occur in the siltstone, and in a few wells, a lutite occurs at the base of the SH1 interval.

Ramsey 2 Sandstone

The younger sandstone in the Ramsey cycle, called the Ramsey 2 (Ruggiero, 1985), occurs only at the northern end of the unit (fig. 37). This sandstone is thinner than the Ramsey 1, having a maximum thickness of >14 ft along a sinuous, bifurcating northeast-southwest trend. The Ramsey 2 sandstone did not extend as far into the basin in the Ford Geraldine area as did the Ramsey 1 sandstone; the main area of Ramsey 2 sandstone deposition was in the Sullivan–Screwbean area, another linear Ramsey sandstone trend to the east and south (Ruggiero, 1985). The Ramsey 2 sandstone interval is 86 to 100 percent sandstone, with some thin interbeds of laminated siltstone and lutite. The average grain size of Ramsey 2 sandstones is 0.091 mm (3.46 Ø), almost exactly the same as the average grain size of Ramsey 1 sandstones. The range of average grain sizes is similarly narrow, from 0.085 to 0.099 mm (3.34 to 3.56 Ø).

As was true of the Ramsey 1, core descriptions show that sandstones from all three sandstone facies occur in the Ramsey 2. Crossbedded sandstones are most common along the trend of thickest sandstone. Sandstones with partial Bouma sequences, particularly rippled sandstones and sandstones with contorted ripples, occur adjacent to the margins of the thick Ramsey 2 sandstone. Massive and contorted sandstones with dewatering structures occur commonly in the areas of thinner Ramsey 2 sandstone, particularly at the northwest edge of the unit (fig. 37). Many of the thickest areas of Ramsey 2 sandstone correspond to areas of thin Ramsey 1 sandstone, suggesting that Ramsey 2 sandstones were deposited in the adjacent topographic depressions created by deposition of the preceding Ramsey 1 beds. Porosity in the Ramsey 2 sandstone ranges from 10.2 to 25.3 percent and averages 20.5 percent. Permeability ranges from 2 to 230 md, and geometric mean permeability is 17 md.

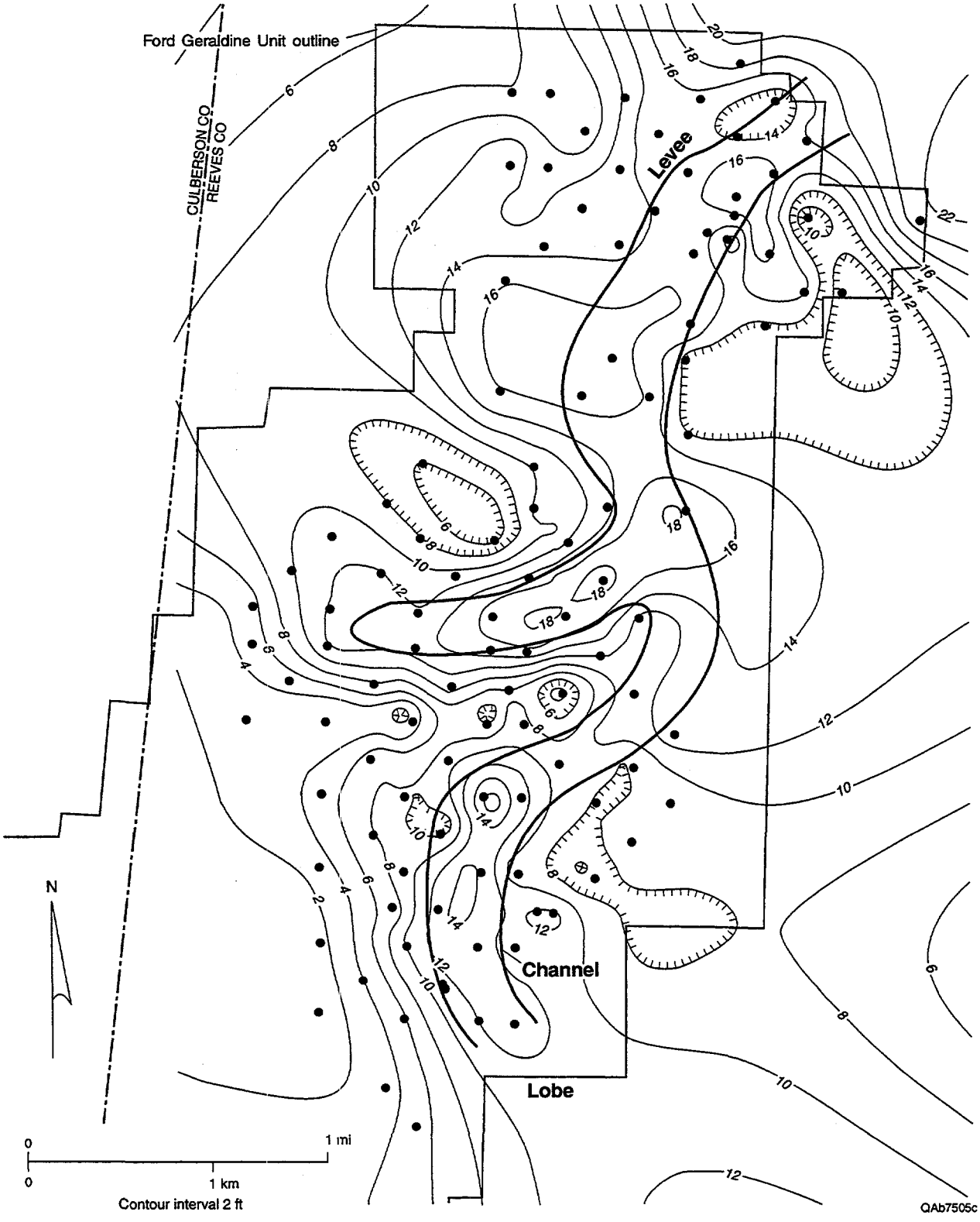

Figure 37. Isopach map of the Ramsey 2 sandstone. This sandstone is also interpreted as a channel-levee system that prograded over lobe deposits, but it did not prograde as far into the basin as did the Ramsey 1 sandstone. Many of the thickest areas of Ramsey 2 sandstone correspond to thin Ramsey 1, suggesting that Ramsey 2 sandstones were deposited in the adjacent topographic depressions created by deposition of the preceding Ramsey 1 beds.

Lower Trap Siltstone

The Ramsey cycle is capped by the Trap laminated siltstone. An isopach map of the lower Trap siltstone, measured from the top of the Ramsey sandstone (1 or 2, depending on location in the field) to the Trap condensed section (fig. 5), shows a distinct thickness change between the north and south parts of the unit (fig. 38). The lower Trap siltstone is thicker at the south end of the field (mostly 8 to 10 ft, compared with 6 to 8 ft at the north end) because there the SH1 siltstone cannot be differentiated and its thickness is thus added to the Trap thickness. Like the Ford siltstone, the Trap is composed of organic-rich siltstone laminae interbedded on a millimeter scale with organic-poor siltstone laminae. The average grain size of the silt decreases upward from the base of the Trap to the Trap condensed section, and the percentage of sand, amount of burrowing, and the thickness of organic-poor laminae all decrease away from the sandstone. Ripples and truncated laminae occur within the lower Trap siltstone. Gamma-ray response increases over this interval as the amount organic matter increases toward the condensed section. Porosity in the Trap siltstone ranges from 4.3 to 21.7 percent and averages 12.7 percent. Permeability ranges from 0.01 to 45 md, and geometric mean permeability is 0.4 md.

Distribution of Facies

Vertical and lateral distribution of facies described in core is illustrated on representative cross sections through cored wells from the northern and central parts of the Ford Geraldine unit (figs. 39, 40). As mentioned previously, much of the core appears massive, but sandstones with graded beds or partial Bouma sequences, sandstones with dewatering structures and convoluted bedding, and cross-laminated sandstones all occur in the Ramsey 1 and 2 sandstones. Laminated siltstones and lutites occur within the Ramsey sandstone interval and in the adjacent Ford and Trap units.

On the basis of facies distribution in the widely spaced subsurface cores, combined with information on facies distribution of Bell Canyon sandstones mapped in continuous outcrops, the

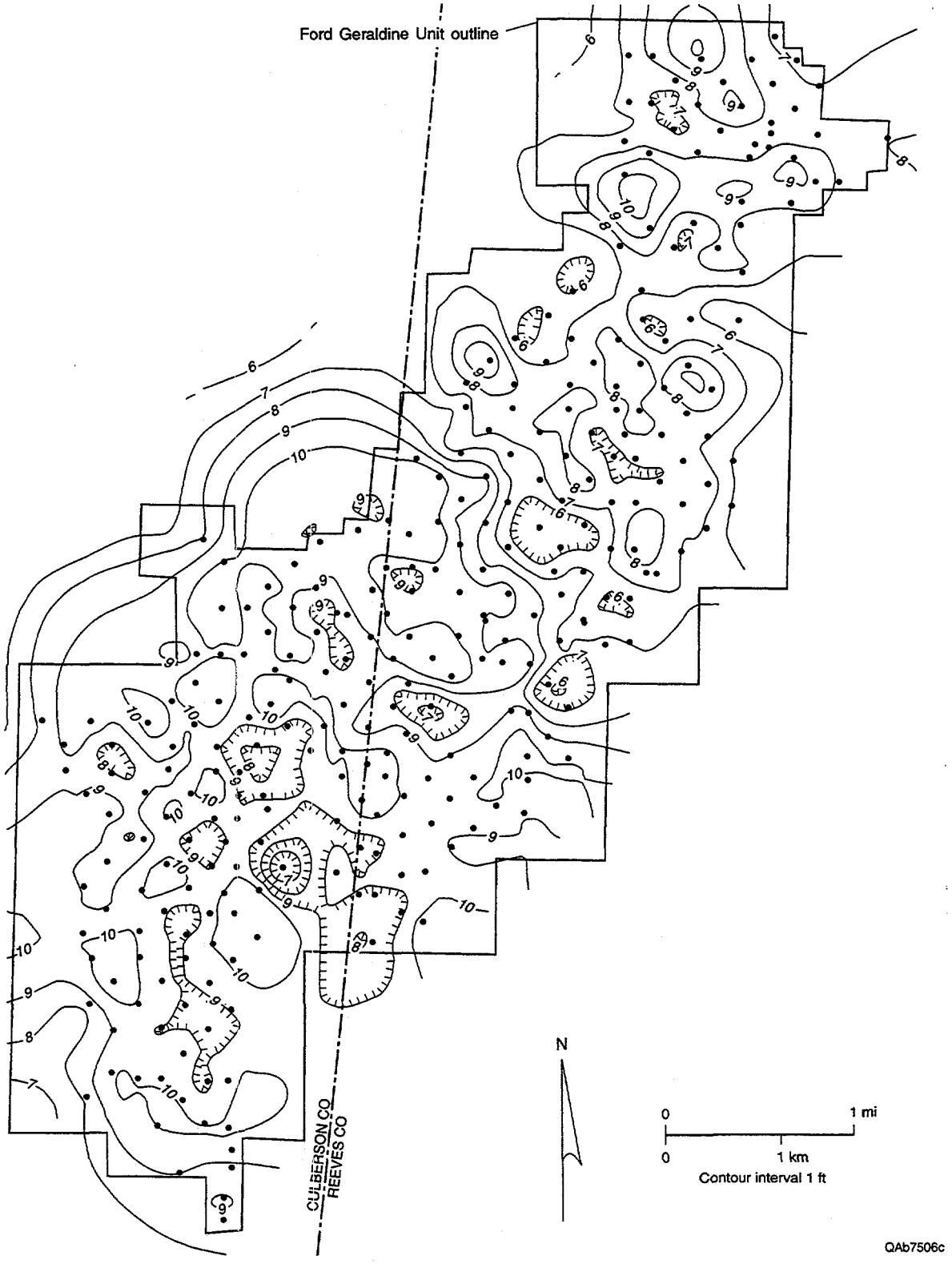

Figure 38. Isopach of the lower Trap laminated siltstone, measured from the top of the Ramsey sandstone (1 or 2, depending on location in the field) to the Trap condensed section. The lower Trap is thicker at the southern end of the field because the SH1 siltstone cannot be differentiated and thus its thickness is added to the Trap thickness.

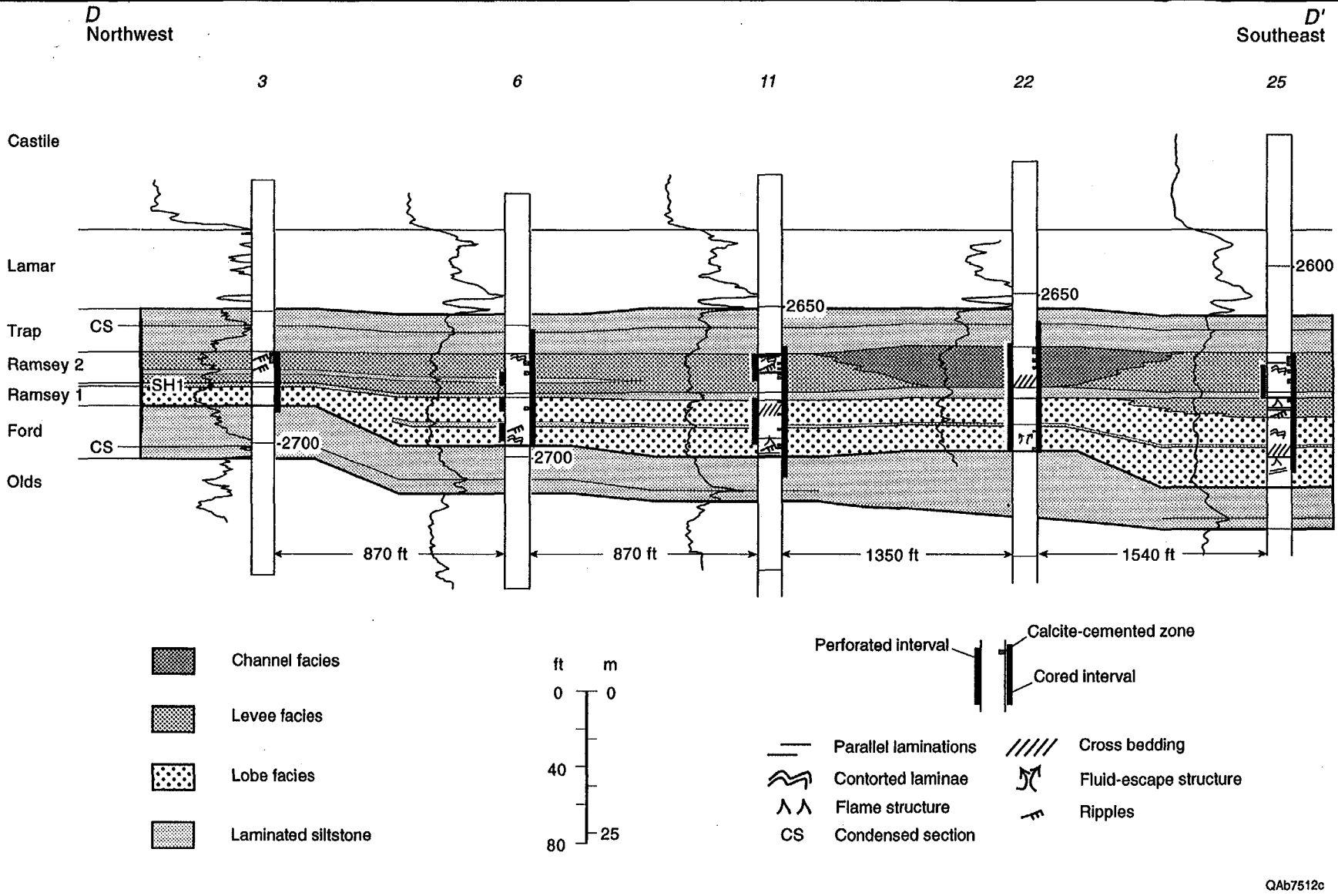

Figure 39. Cross section D–D′ through the northern end of Geraldine Ford field, where the SH1 laminated siltstone separates the reservoir into Ramsey 1 and Ramsey 2 sandstones. Deposition of Ramsey sandstones is interpreted to have occurred by sandy high- and low-density turbidity currents that carried a narrow range of sediment size, mostly very fine sand to coarse silt. On the basis of core descriptions and study of the outcrop analog, we interpret Ramsey sandstones as having been deposited on the basin floor in a sand-rich, channel-levee system with attached lobes.

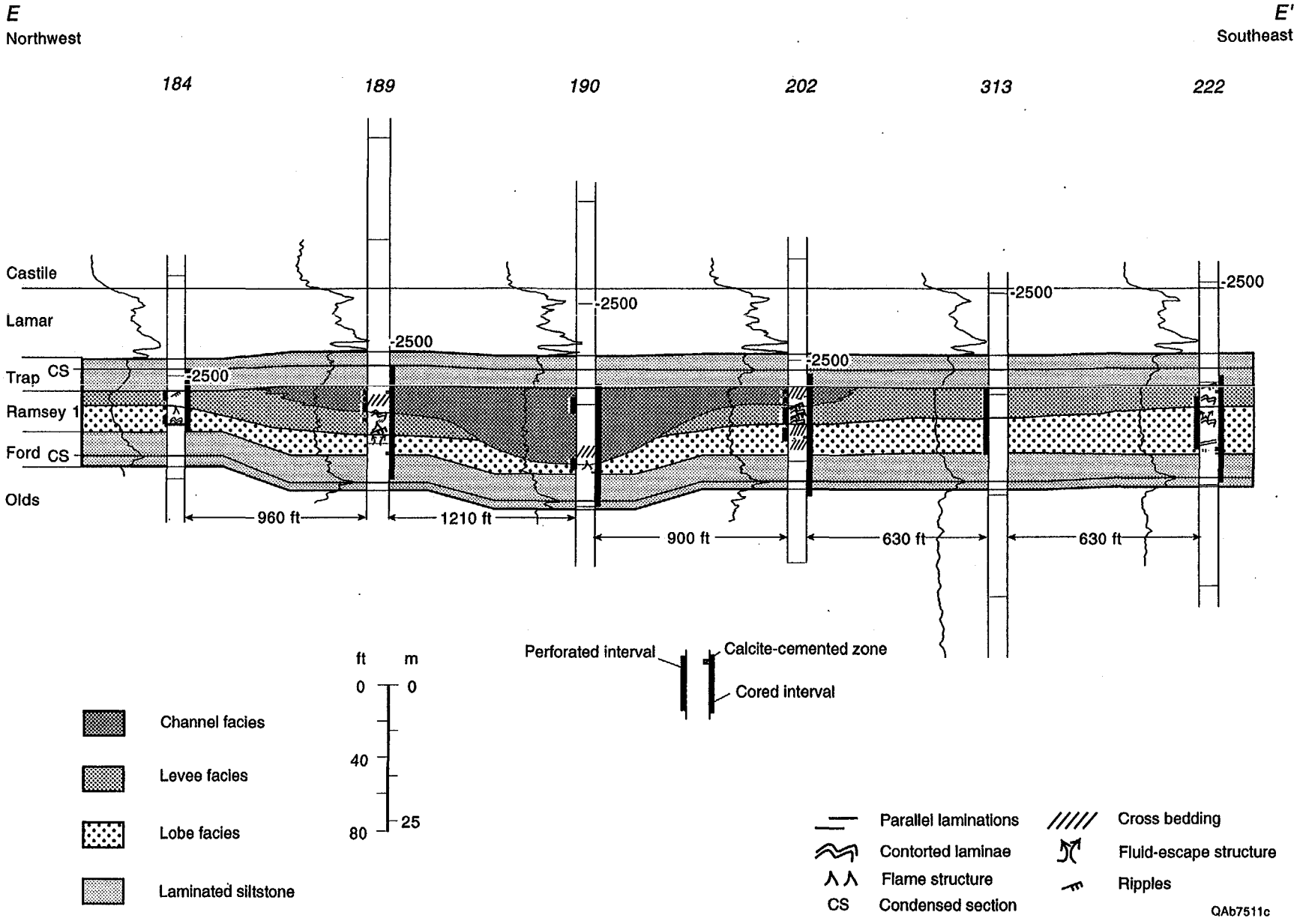

Figure 40. Cross section E–E′ through the southern part of Geraldine Ford field, where only the Ramsey 1 sandstone is present. Channel, levee, and lobe facies are similar to those in cross section D–D′.

Ramsey sandstone at Ford Geraldine unit is interpreted as consisting of channel, levee, and lobe deposits (figs. 39, 40).

Channel Facies

Channel facies consist of massive and crossbedded sandstones (fig. 41) interpreted to have been deposited from high-density turbidity currents (Lowe, 1982). Massive sandstones were probably deposited rapidly from suspension, whereas the crossbedded sandstones may result from a lower fallout rate from suspension (Kneller, 1996). Crossbedded Bell Canyon sandstones in outcrop are interpreted as the product of infilling of scoured zones, not migrating bedforms (see previous section). This may have occurred during the first phase of sediment deposition from a high-density turbidity current (Lowe, 1982), when the current is locally erosive and deposits show scours and lenticularity. During this stage, bedforms can form, including dunelike features, but flow unsteadiness "prevents the evolution of highly organized dunes" (Lowe, 1982, p. 283). B. Kneller (personal communication, 1996) reported that traction structures, including climbing dunes, can form from high-density turbidity currents when the suspended-load fallout rate is relatively low.

As interpreted from the cross sections and isopach map, channels in the Ramsey 1 sandstone are 30 to 35 ft thick and 1,200 ft across (figs. 35, 40). Ramsey 2 channels are thinner, mostly 15 to 20 ft thick, but also about 1,200 ft wide. In outcrop, many channels were seen to be nested and laterally offset from each other. Similar nesting of multiple channels may occur in the Ford Geraldine unit, but the core control is not sufficiently close to distinguish separate channels. The aspect ratio (width:thickness) of Ramsey 1 channel deposits is 40:1 to 34:1, and in Ramsey 2, 80:1 to 60:1. Within channels, the ratio of net-to-gross sandstone is 100 percent. Log response is generally blocky. The main Ramsey 1 channel thins and bifurcates into about four channels at the southwest part of the unit (fig. 35). The Ramsey 2 channel bifurcates farther updip, at the north end of the unit (fig. 37), reflecting the backstepping of the younger sandstone in this area. The

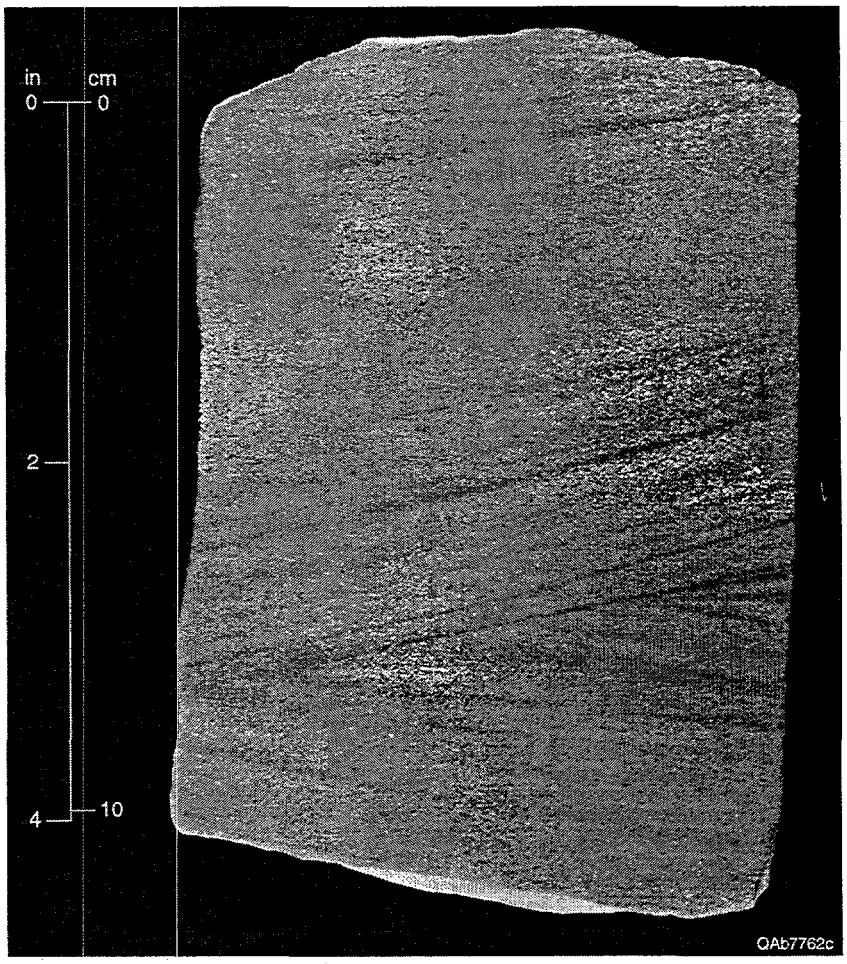

Figure 41. Photo of cross-laminated facies 6 sandstone from well FGU-130, 2670.0 to 2670.4 ft. Sandstone is interpreted as having been deposited in the channel facies.

average porosity in 272 channel sandstone samples is 22.1 percent. Geometric mean permeability is 16 md, and median permeability is 21 md.

Levee Facies

Levee facies occur as a sediment wedge along the margins of the channels (figs. 30, 39, 40). These channel-margin deposits consist of sandstones with partial Bouma sequences, particularly ripples (fig. 42) and convoluted ripples, and interbedded siltstones. They are interpreted as channel levees formed by overbanking of low-density turbidity currents. Thickness of the levee facies decreases away from the channels, and the volume of interbedded siltstones increases. Log response is more serrated than in the channels because of the presence of interbedded siltstones. The average porosity in 318 levee sandstones is 22.3 percent. Geometric mean permeability is 19 md, and median permeability is 29 md.

Lobe Facies

Lobe facies occur in broad sheets at the mouths of channels and are deposited by unconfined high-density turbidity currents (fig. 30). Lobe facies are characterized by massive sandstones and graded sandstones with dewatering features such as dish structures, flame structures, and vertical pipes (figs. 43 through 45), features that indicate rapid deposition and fluid escape. They were deposited at high, suspended-load fallout rates. In a prograding system such as the Ramsey sandstone, lobe facies would have prograded into the Ford Geraldine area first, then been overlain and partly eroded by the narrower prograding channel-levee system (figs. 39, 40). Thus, lobe deposits are found at the distal ends of the Ramsey 1 and 2 sandstone channels and also underlying and laterally adjacent to the Ramsey 1 and 2 channels and levees (fig. 35, 37, 39, 40). Deposition of lobe sandstones was periodic, and laminated siltstones are interbedded with the lobe sandstone sheets. Some lobe deposits show an upward-coarsening log pattern, but many have a massive log

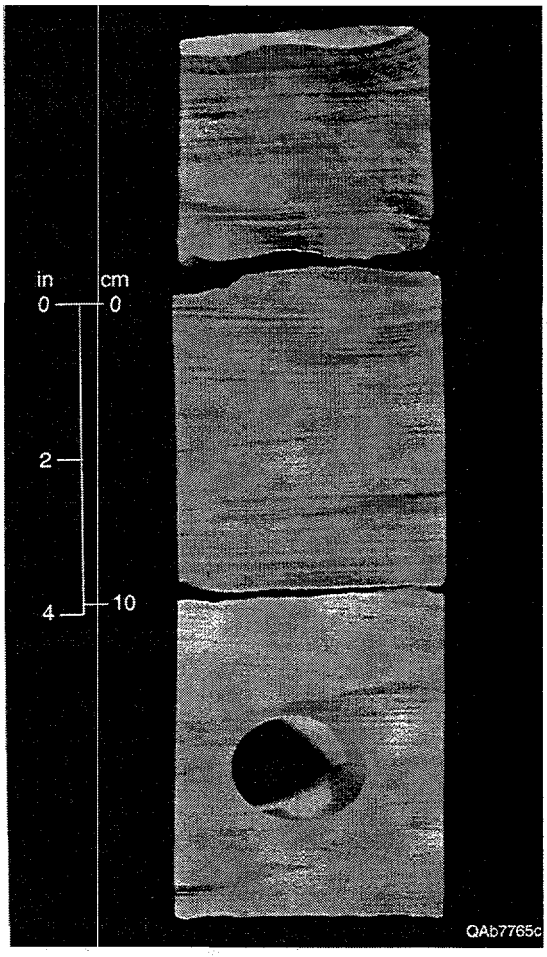

Figure 42. Photo of climbing ripples in facies 4 sandstone from well FGU-14, 2728.2 to 2729.1 ft. Sandstone is interpreted as having been deposited in the levee facies.

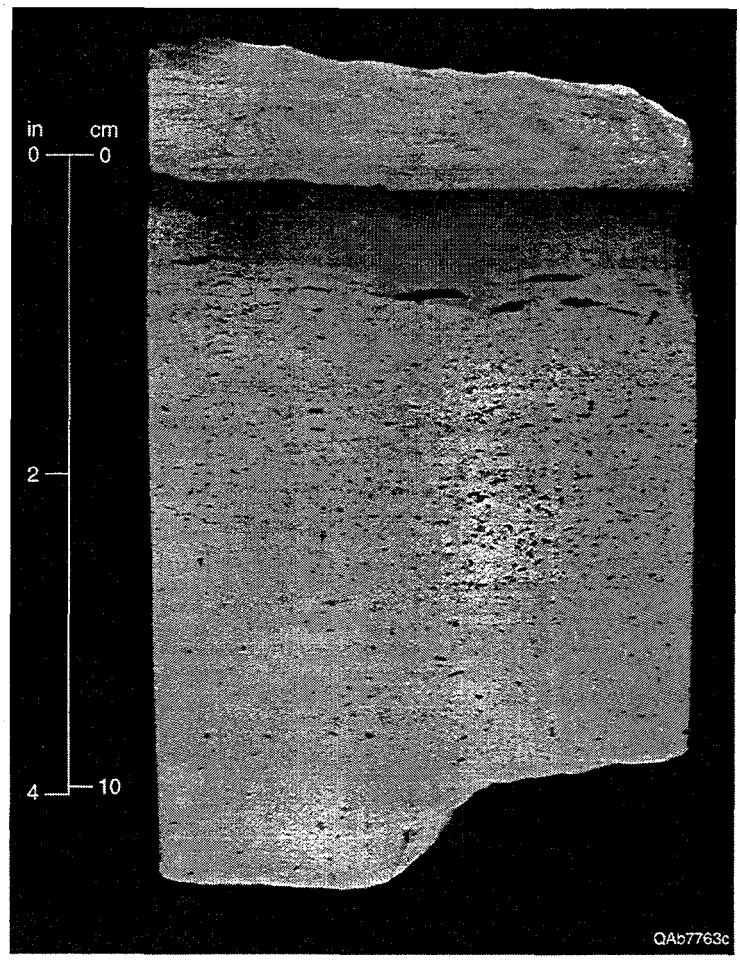

Figure 43. Photo of facies 4 graded sandstone with floating clasts and overlying lutite. From well FGU-3, 2685.5 to 2685.9 ft. Sandstone is interpreted as having been deposited in the lobe facies.

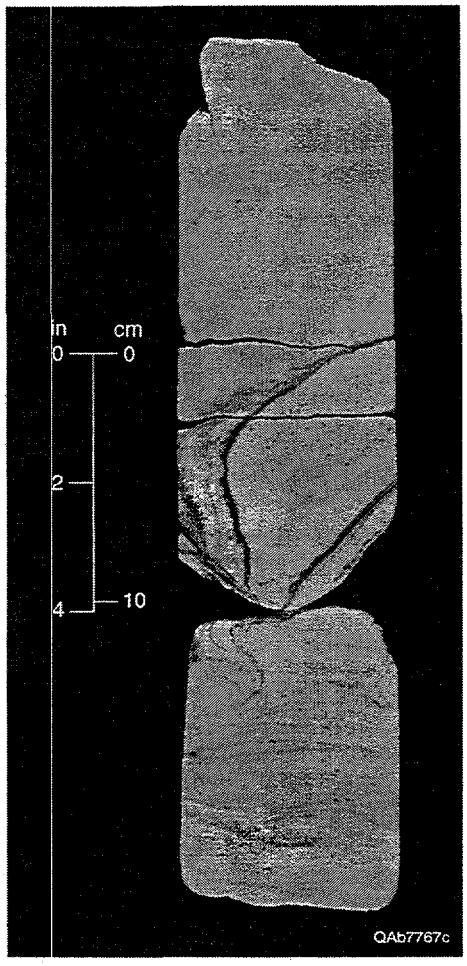

Figure 44. Photo of facies 5 sandstone with convoluted beds interpreted as loading and dewatering features at the base and massive sandstone above. From well FGU-22, 2705.8 to 2706.9 ft. Sandstone is interpreted as having been deposited in the lobe facies.

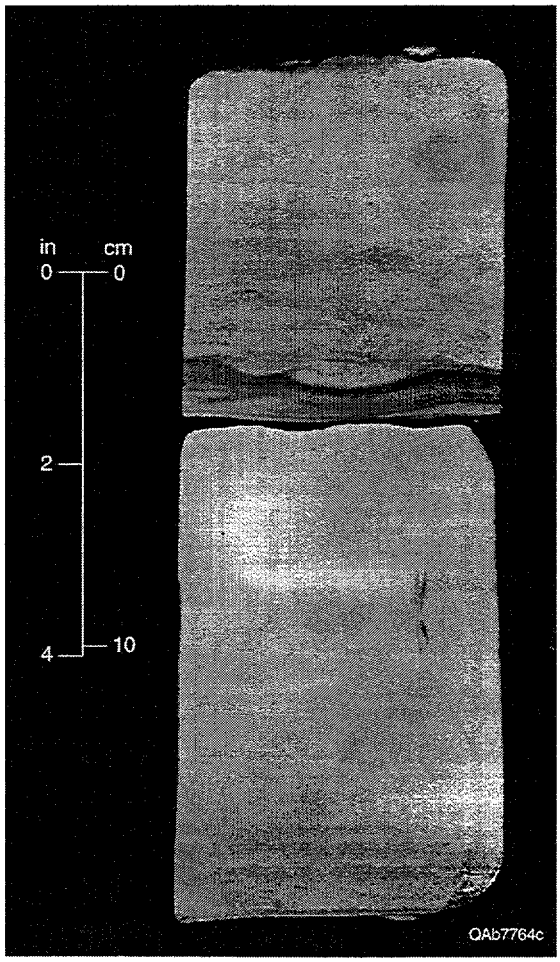

Figure 45. Photo of facies 5 sandstone with flame structure, which is interpreted as a loading and dewatering feature. From well FGU-6, 2664.8 to 2665.5 ft. Sandstone is interpreted as having been deposited in the lobe facies.

response. The average porosity in 310 lobe sandstones is 21.3 percent. Geometric mean permeability is 13 md, and median permeability is 21 md.

Laminated Siltstone Facies

The laminated siltstone facies consists of organic-rich siltstone laminae interbedded on a millimeter scale with organic-poor siltstone laminae (fig. 46). The depositional origin of the laminated siltstones is uncertain. The pattern of upward coarsening into the Ramsey sandstone and then upward fining above it suggests that the laminated siltstones are part of the progradation and retrogradation of the channel-levee and lobe system; the siltstones may represent the most distal part of the lobe. Alternatively, the siltstones may represent windblown silt from the shelf margins. Periods of relative sea-level fall may have exposed increasingly larger areas on the shelf and allowed the wind to carry away greater volumes of silt, resulting in thicker organic-poor siltstone layers. The relatively uniform thickness of the Ford and Trap siltstone intervals (fig. 34, 38) could be explained either as deposition of widespread windblown silt or deposition as the distal part of a broad lobe that extends beyond the margins of the field. The average porosity in 214 laminated siltstones is 15.7 percent, and geometric mean permeability is 0.54 md.

Lutite Facies

The organic-rich siltstones are interpreted as condensed sections that formed in the Ford and Trap intervals during times of very slow siltstone deposition. They contain abundant organic matter, including spores. The organic matter is probably derived from settling from suspension of planktonic organisms. Other lutites interfinger with the levee deposits and represent interchannel deposits. The average porosity in 8 lutites is 13.1 percent, and geometric mean permeability is 0.12 md.

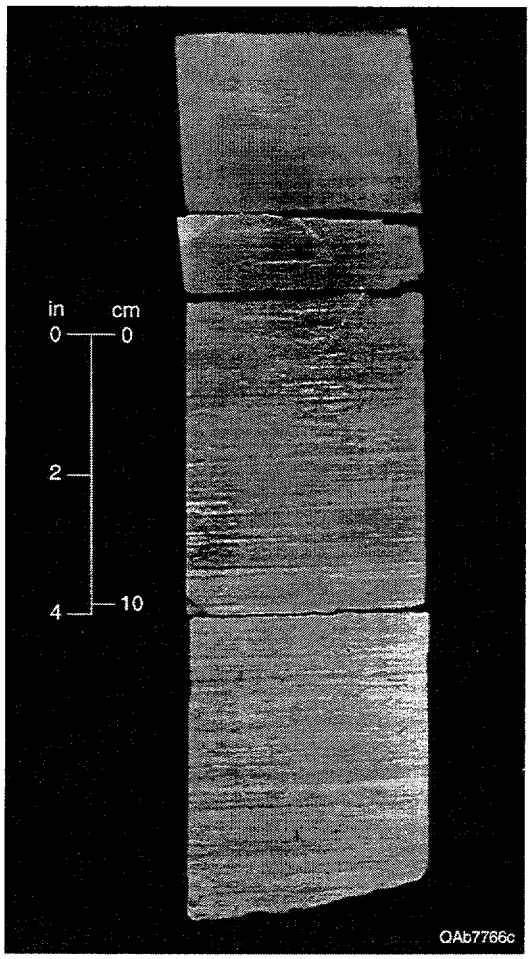

Figure 46. Facies 3 laminated siltstone (laminite) fining upward into facies 2 organic-rich siltstone (lutite). From well FGU-40, 2741.0 to 2742.0 ft.

Proposed Depositional Model for Ford Geraldine Unit

On the basis of core descriptions and study of the outcrop analog, Ramsey sandstones at Ford Geraldine unit are interpreted as having been deposited by sandy high- and low-density turbidity currents that carried a narrow range of sediment size, mostly very fine sand to coarse silt. The sands were deposited in a basin-floor setting by a channel-levee system with attached lobes (fig. 30). Channel facies are approximately 1,200 ft wide and 15 to 35 ft deep. They consist of massive and crossbedded sandstones interpreted to have been deposited from high-density turbidity currents (Lowe, 1982). Channel margins are characterized by rippled and convoluted sandstones interbedded with minor siltstones. Channel-margin deposits are interpreted as channel levees formed by overbanking of low-density turbidity currents. Lobe sandstones are interpreted as being deposited at the mouth of the channel by high-density turbidity currents. They were identified by massive and graded sandstones with load and dewatering structures such as dish structures, flame structures, and vertical pipes—features that indicate rapid deposition and fluid escape.

The narrow range of sediment size in the Ramsey sandstones, mostly very fine sand, supports the interpretation of Fischer and Sarnthein (1988) and Gardner (1992) of an eolian sediment source for sandstones of the Delaware Mountain Group. In their model, fine sand was transported from source areas in the ancestral Rockies by migration of eolian ergs, and silt and clay were transported as dust by the wind (Fischer and Sarnthein, 1988). Clay was carried by the wind beyond the Delaware Basin, thus accounting for the lack of clay-sized sediment in the Delaware Mountain Group deposits. Silt-sized dust was deposited in the basin by fallout from the wind and settling through the water column, forming topography-mantling laminated siltstones. During lowstands of sea level, dune sands were driven across the exposed shelf to the shelf edge, where they accumulated in unstable, shallow-water sand wedges. Slumping of the sand wedges gave rise to turbidity currents that carved channels and filled them with well-sorted sandstone. During

highstands in sea level, the platform was flooded and the dunes prevented from migrating to the shelf edge.

Mapping of Ramsey 1 and Ramsey 2 sandstone distribution shows that the younger Ramsey 2 sandstone does not prograde as far basinward as does the older Ramsey 1 sandstone. Kerans and others (1992) interpreted this to have been a time of relative rise of sea level, during which progressively less sand would be allowed into the basin, consistent with landward stepping of the Ramsey 2 sandstone.

Instead of filling a large channel, as suggested by the saline-density current model (Ruggiero, 1985, 1993), Ramsey sandstones were probably deposited on the basin floor (Barton, 1997). Younger sandstones were deposited in topographically low areas created by deposition of the preceding bed, resulting in offset stacking of lobes (fig. 11) called compensation lobes by Mutti and Normark (1987). The confinement of sandstones within narrow linear trends (fig. 4) may in part result from reef topography on the highly aggradational carbonate platform (Williamson, 1978; Gardner, in press).

The proposed channel-levee and lobe model for Ramsey sandstone deposition suggests that greater lateral heterogeneity of reservoir sandstones exists at Ford Geraldine unit than previously thought (Ruggiero, 1985). Progradation, aggradation, and retrogradation of the system resulted in lateral and vertical offset of channel, levee, and lobe facies (fig. 39, 40). Laminated siltstones and lutites provide the greatest amount of depositional heterogeneity because of the grain size and permeability contrast between sandstones and siltstone facies. The sandstones facies all have similar grain sizes, and thus there may not be much permeability contrast and inhibition of flow at sandstone-on-sandstone contacts, for example, where channels incise into lobe facies.

Characterization of Diagenetic Heterogeneity

Diagenesis commonly influences sandstone reservoir quality by overprinting and modifying depositional permeability distribution. In many sandstones, the original depositional features, particularly grain size, sorting, and volume of ductile grains, remain the most important predictors

of permeability in a sandstone even after burial diagenesis. However, in some sandstones diagenesis is so extensive that it becomes the dominant control on permeability. In the Ramsey sandstones, diagenesis is not unusually extensive, but because detrital grain size is so constant in the sandstone facies, the main control on reservoir quality in these sandstones is the volume of authigenic cement.

Petrography of the Ramsey Sandstones

The composition of Ramsey sandstones at the Ford Geraldine unit was determined from 15 thin sections from sandstones with a wide range of permeability, in order to quantify the petrographic characteristics of grain size, detrital mineralogy, authigenic cements, and porosity.

Ramsey sandstones at Geraldine Ford field are arkoses having an average composition of $Q_{62}F_{33}R_6$ (fig. 47). Detrital quartz composes an average of 42 percent of the total rock volume. Orthoclase and other potassium feldspars are the most abundant feldspars, having an average volume of 13 percent; plagioclase has an average volume of 10 percent. Many plagioclase grains have been partly vacuolized, sericitized, and chloritized. Rock fragments, including plutonic and metamorphic rock fragments and chert, average 4 percent of the whole-rock volume. Fossil fragments and carbonate rock fragments (<1 percent) occur in several sandstone samples, particularly in the calcite-cemented zones.

Cements and replacive minerals constitute between 4 and 30 percent of the sandstone volume in Ramsey sandstones, with calcite and chlorite being the most abundant. Calcite cement (average = 9 percent, range 1 to 29 percent) occurs both in primary pores and in secondary pores where it has replaced feldspar grains. Juddging from thin-section staining, some of the calcite cement apparently contains minor amounts of iron. Some calcite shows evidence of dissolution. Chlorite (average = 3 percent) forms rims around detrital grains, extending into pores and pore throats. Authigenic quartz, anhydrite, leucoxene, siderite, ankerite, illite or mixed-layer illite-smectite (probably mixed-layer illite-smectite, from X-ray analyses by Williamson, 1978), pyrite, and feldspar overgrowths (both K-feldspar and Na-feldspar) also occur in the Ramsey sandstones,

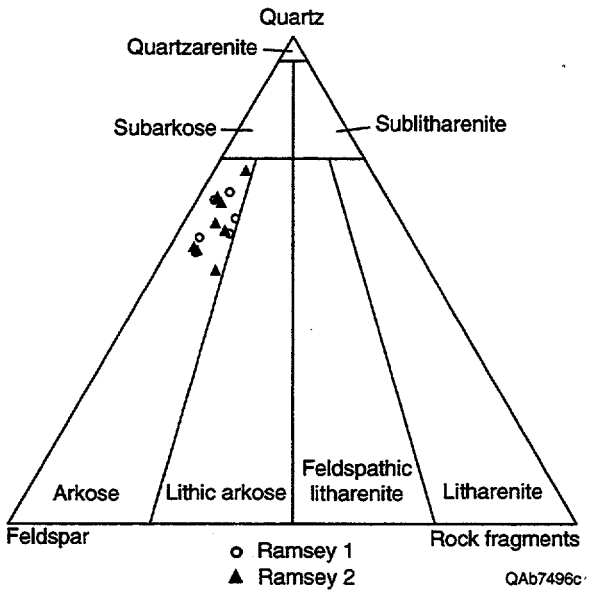

Figure 47. Ramsey sandstones at Geraldine Ford field—arkoses having an average composition of $Q_{62}F_{33}R_6$. Sandstone classification of Folk (1974).

generally in volumes of <1 percent. Quartz occurs as small crystals on quartz grain surfaces, as isolated euhedral crystals, and as syntaxial overgrowths on detrital quartz grains. Quartz generally appears to have overgrown and included authigenic clay.

Average porosimeter porosity in the petrographic samples is 17.6 percent, the same as the average porosity determined by point counts of the thin sections. On the basis of thin-section identification, average primary porosity has been found to be 15.0 percent, and average secondary porosity, 2.6 percent.

Diagenetic Controls on Reservoir Quality

By comparing core analyses with point-count data from thin sections, the influence of parameters such as grain size, detrital mineralogy, and volume of authigenic cements on porosity and permeability were analyzed. No statistically significant correlation at the 90-percent confidence level exists between porosity or permeability and depositional properties such as grain size, percent sand-size grains, sorting, or ductile grain volume. This is unusual for a sandstone but probably is a result of the narrow range of detrital grain sizes available in the eolian source area. Whereas most sandstones have ranges of grain size and volumes of detrital clay matrix in different facies, little variation among facies exists in the Ramsey sandstones. As a result, porosity and permeability have very similar distributions in channel, levee, and lobe facies (fig. 48). Porosity and log permeability distributions are negatively skewed, and the low values represent sandstones that have been cemented by calcite.

There is a statistically significant relationship between volume of cement and both porosity (fig. 49) and permeability. Calcite is the most important component of total cement, and it has the greatest impact on reservoir quality. In samples with more than 15 percent calcite cement, permeability is reduced to less than 3 md and porosity to less than 15 percent. Thus, the main controls on porosity and permeability in the Ramsey sandstones are authigenic cements, particularly calcite, and, to a lesser extent, chlorite.

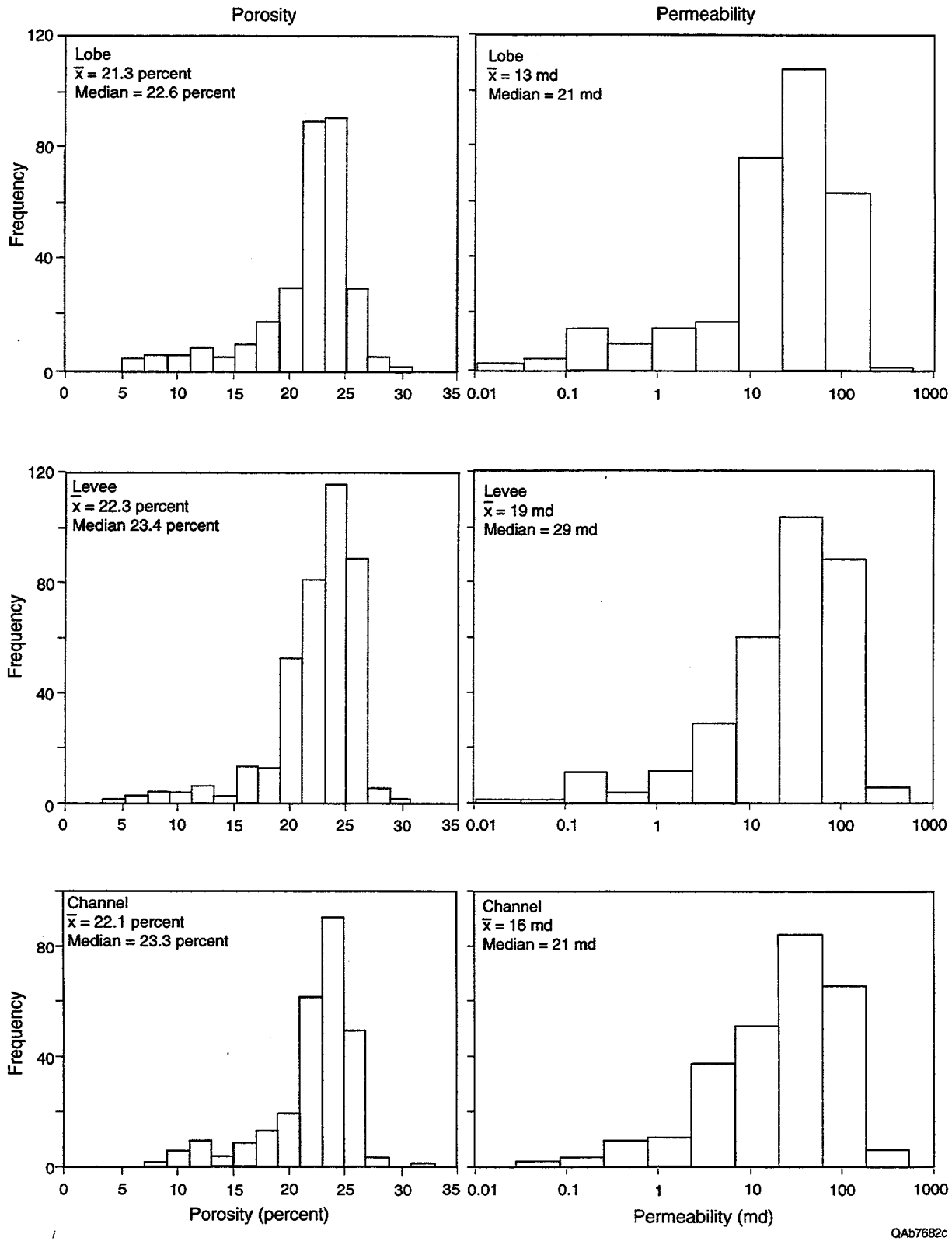

Figure 48. Distribution of porosity and permeability in channel, levee, and lobe facies. Porosity and permeability in the three facies are similar because of the narrow range of grain sizes in the system. The low values represent sandstones that have been cemented by calcite.

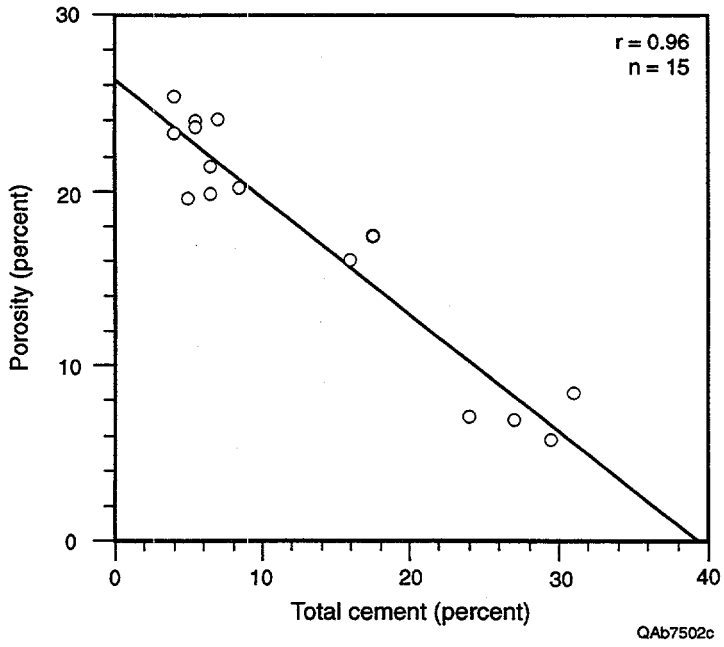

Figure 49. The main controls on porosity and permeability in the Ramsey sandstones—authigenic cements, particularly calcite, and, to a lesser extent, chlorite.

The distribution of calcite cement in Geraldine Ford field can to some extent be determined from the cores because highly calcite cemented zones have a distinct, white color. Calcite-cemented intervals were noted and described along with other sedimentary features in the core and thus can be mapped on cross sections (figs. 39, 40). Highly calcite cemented sandstones occur in all three sandstone facies—channel, levee, and lobe. Most cemented zones in the core are approximately 0.5 to 1 ft thick; their dimensions are unknown, but we assume they are not laterally extensive or continuous. Although they can occur anywhere within the vertical Ramsey sandstone section, they are more common near the top and base of sandstones (figs. 39, 40). The source of some of the calcite may be the adjacent siltstones, which would explain the greater abundance of calcite near the sandstone–siltstone contacts. There may also have been at least a partial internal source of calcite in the sandstones, the detrital carbonate rock fragments and fossils. Additional petrographic work is planned to determine whether detrital carbonate content varies with facies or stratigraphic level.

Although calcite-cemented zones commonly occur near the top of the Ramsey sandstone, high permeability values are also common near the top of the sandstone (Dutton and others, 1996). In the Ramsey 2 sandstone, the highest permeability values occur at the top of the unit, with lowest average permeability immediately (≈1 ft) below. The high permeability values at the top of the sandstone might indicate permeability enhancement as a result of dissolution of calcite cement (Dutton and others, 1996).

No significant difference exists in the porosity-versus-permeability relationship in channel, levee, or lobe facies (fig. 50). Extensively calcite cemented sandstones, which have permeabilities <1 md, occur in all three facies. Sandstones with intermediate permeabilities between 1 and 10 md are interpreted as containing chlorite cement and moderate amounts of calcite (fig. 50). High-permeability sandstones occur in all facies but have small volumes of calcite and chlorite cement. Additional petrographic work is needed to determine the controls on calcite and chlorite cement distribution within the Ford Geraldine unit.

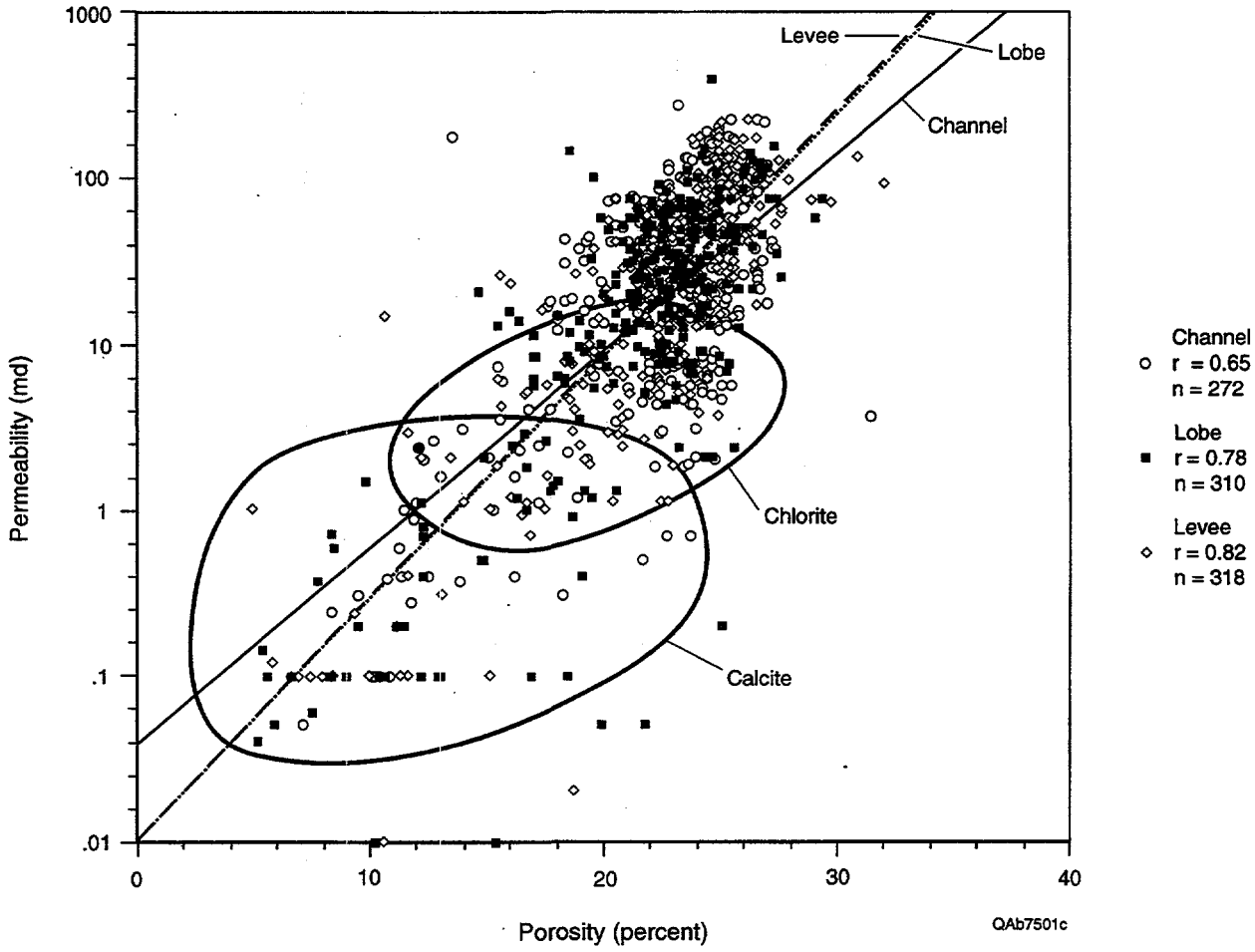

Figure 50. Graph showing no significant difference in the porosity-versus-permeability relationship in channel, levee, and lobe facies. Calcite- and chlorite-cemented sandstones occur in all three facies.

Conclusions

Ramsey sandstone at the Ford Geraldine unit was deposited in a channel-levee and lobe system by high- and low-density turbidity currents in a basinal deep-water setting. Ramsey 1 sandstones represent progradation and aggradation, and Ramsey 2 represents retrogradation (back stepping) of the system. Ramsey channels are about 1,200 ft wide and 15 to 35 ft thick, and they are flanked by levee deposits. Lobe facies were deposited at the mouths of channels.

Uniform grain size in the sediment source area resulted in channel, levee, and lobe facies having similar porosity and permeability relationships. Because grain size is so constant, the main control on reservoir quality in these sandstones is the volume of authigenic calcite and chlorite. Calcite cement occurs in all facies but is more abundant near the top and base of sandstones, suggesting that the laminites were the source of calcite.

RESERVOIR CHARACTERIZATION OF FORD WEST FIELD

Ford West field, an updip extension of Geraldine Ford field, is located 3 mi south of the Texas–New Mexico state line in Culberson County, Texas (fig. 51). The field produces from two principal reservoir zones (fig. 52), the lower B2 sandstone reservoir in the uppermost part of the Cherry Canyon Formation and the overlying B1 sandstone in the lower part of the Bell Canyon Formation.

Three cores through the B2 sandstone (fig. 51) and 16 logs formed the West Ford data base for the project. Conoco leases are in sections 16 and 22, and by March 1997, only three producing wells remained in those leases. Because of the limited amount of data available and because the outcrop analogs were from the upper Bell Canyon Formation, and thus more applicable to Geraldine Ford field, reservoir characterization of West Ford field was not as extensive as that of Geraldine Ford field.

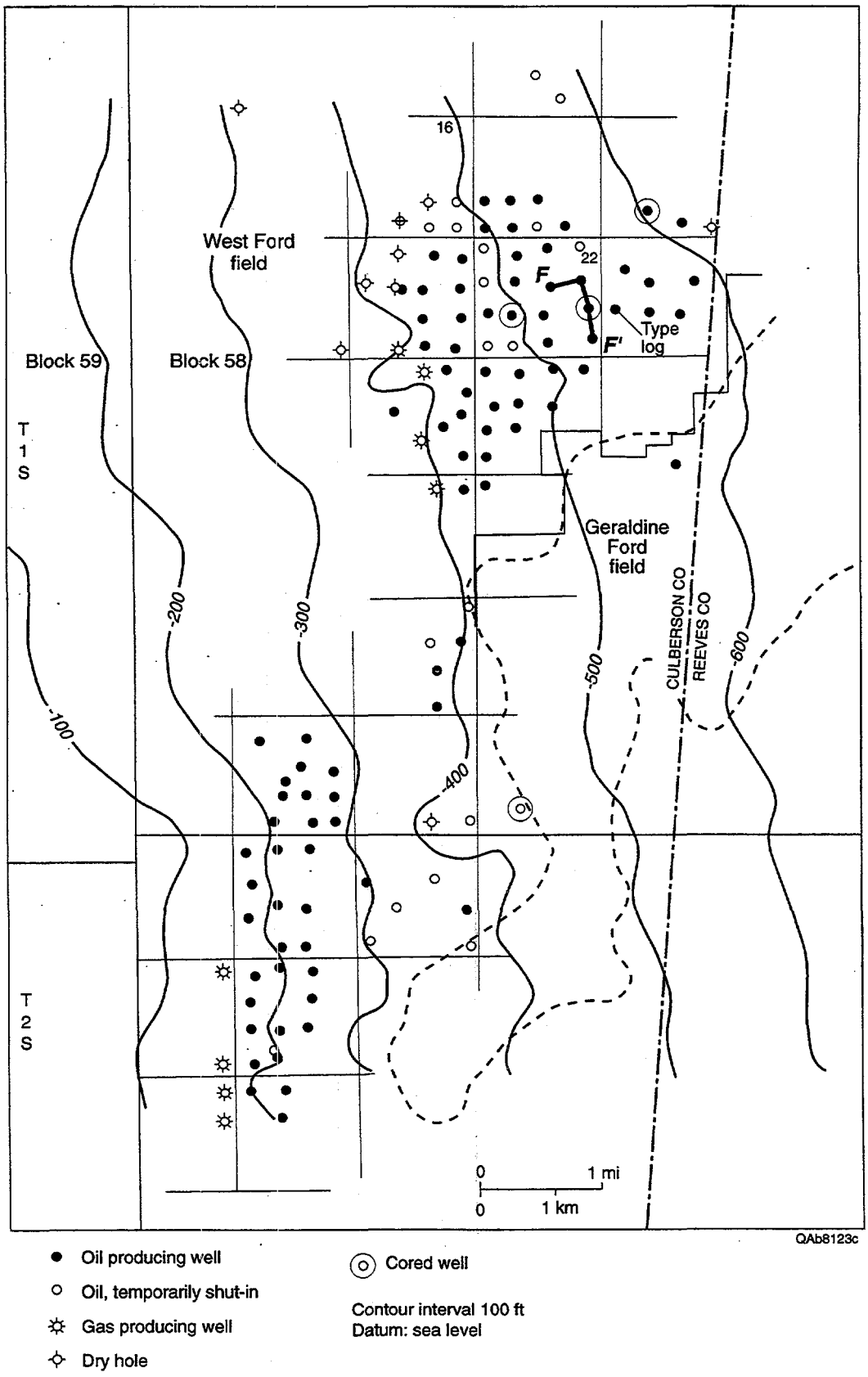

Figure 51. Location map of Ford West field, which produces from the upper Cherry Canyon Formation and lowermost Bell Canyon Formation, Delaware Mountain Group (modified from Linn, 1985). Three cores were described from Ford West field. Cross section F–F′ shown in figure 52, and type log shown in figure 7.

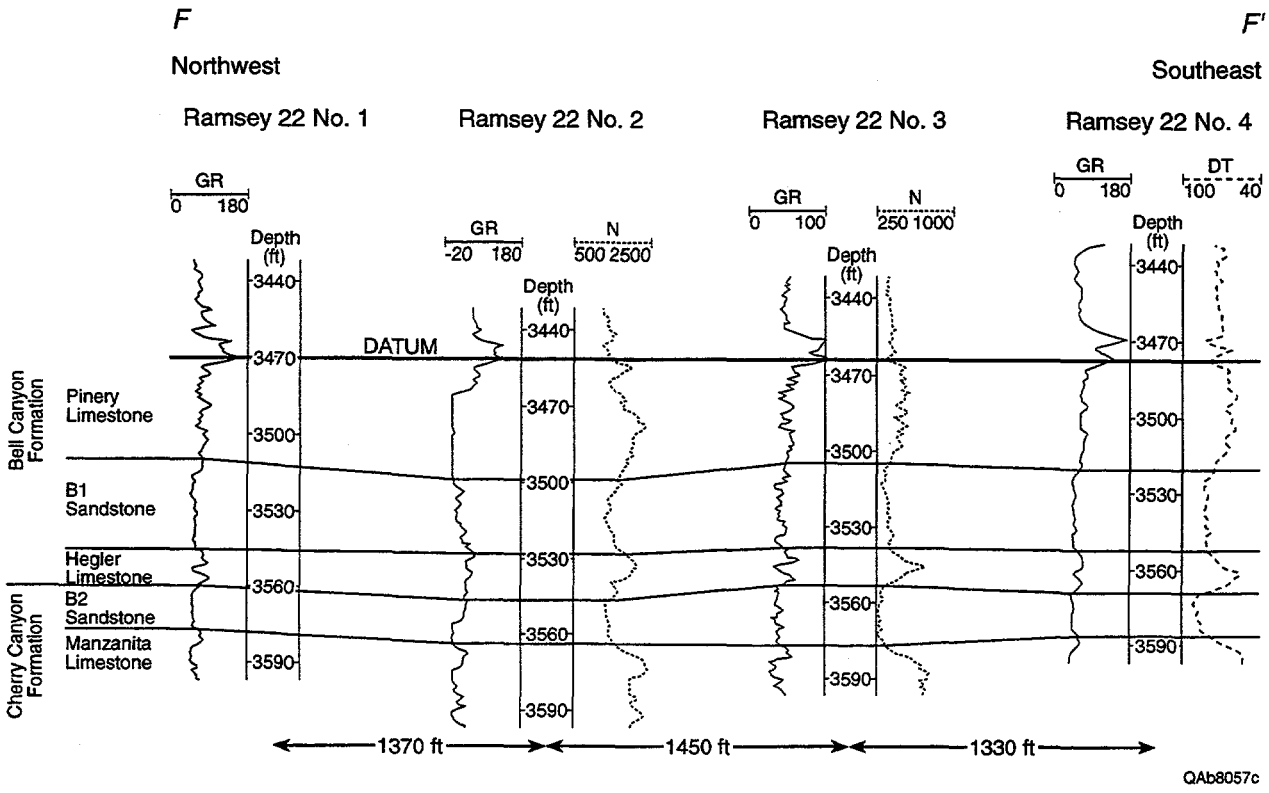

Figure 52. Strike cross section F–F′ of the upper Cherry Canyon and lower Bell Canyon interval in Ford West field. Location of cross section shown in figure 51.

Characterization of Depositional Heterogeneity

The sandstones in West Ford field have a very narrow range of grain sizes. The average grain size in B2 sandstone samples is 0.093 mm (3.44 Ø) (Linn, 1985). B1 sandstones are slightly finer grained, averaging 0.088 mm (Linn, 1985). Both are very well sorted.

Sandstones in West Ford field were interpreted as turbidite deposits (Linn, 1985), and the channel-levee and lobe depositional model developed for the Ramsey sandstone may apply to the West Ford reservoirs as well. A northeast-southwest trend of thick B2 sandstone in the southeast part of section 22 is interpreted as a channel (fig. 53). Thinner sandstones along the margins of the channel may be levee and lobe facies. The B1 sandstone is thickest at the northwest margin of the study area, possibly where a channel cuts the study area, and thins to the southeast.

Regional mapping of the distribution of the B1 and B2 sandstones shows that the younger B1 sandstone progrades farther basinward with respect to the older B2 sandstone (Linn, 1985). Kerans and others (1992) interpreted this to have been a time of relative fall of sea level, which would be consistent with basinward stepping of the B1 sandstone.

Characterization of Diagenetic Heterogeneity

The composition of Delaware sandstones at West Ford field was determined from four thin sections from B2 sandstones with a range of permeability. B2 sandstones at West Ford field are arkoses having an average composition of $Q_{66}F_{27}R_7$. Detrital quartz composes an average of 47 percent of the total rock volume, slightly higher than in the Ramsey sandstones. Orthoclase and other potassium feldspars are the most abundant type of feldspar, having an average volume of 13 percent; plagioclase has an average volume of 7 percent. Rock fragments, including plutonic, metamorphic, and carbonate rock fragments average 5 percent of the whole-rock volume. Carbonate rock fragments have an average volume of 1 percent and are somewhat more abundant than in the Ramsey sandstones.

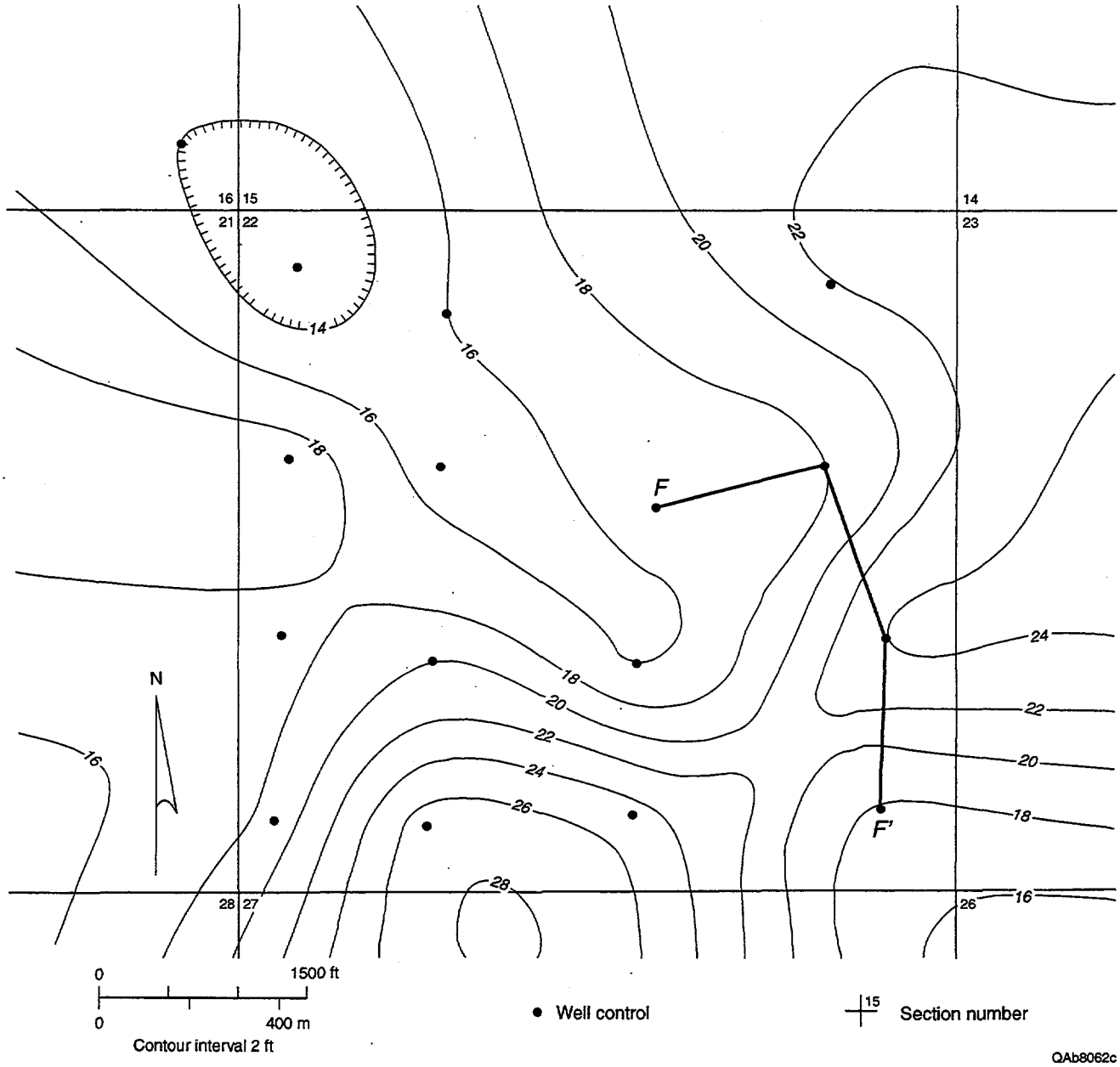

Figure 53. Isopach of upper Cherry Canyon B2 sandstone. The northeast-southwest trend of thick B2 sandstone in the southeast part of section 22 is interpreted as a channel.

Cements and replacive minerals constitute between 11 and 18 percent of the sandstone volume in B2 sandstones, with calcite and chlorite being the most abundant. Calcite cement (average = 6 percent, range 1 to 16 percent) occurs both in primary pores and in secondary pores, where it has replaced feldspar grains. On the basis of thin-section staining, some of the calcite cement apparently contains minor iron. Some calcite shows evidence of dissolution. Chlorite (average = 6 percent, range 2 to 9 percent) forms rims around detrital grains, extending into pores and pore throats.

Average porosimeter porosity in the petrographic samples is 22.1 percent; average thin-section porosity is 15.1 percent. On the basis of thin-section identification, average primary porosity has been found to be 14.6 percent, and average secondary porosity, 1.3 percent. Core-analysis data from 33 B2 sandstone samples from two wells show an average porosity of 22.6 percent and geometric mean permeability of 19.5 md.

PETROPHYSICS OF THE RAMSEY SANDSTONE, FORD GERALDINE UNIT

Introduction

Petrophysical characterization of the Ford Geraldine unit was accomplished by integrating core and log data and quantifying petrophysical properties from wireline logs (fig. 54); the goal was a set of maps of porosity, permeability, net pay, water saturation, porous hydrocarbon volume, and other reservoir properties across the unit. Petrophysical analysis of the Ramsey sandstone at the Ford Geraldine unit is complicated by the incomplete nature of the logging suites. A review of available log suites from the Ford Geraldine unit wells showed that 118 wells have no porosity logs, and of the remaining 187 wells, 84 of them have only old neutron logs. Only 38 wells have both porosity and resistivity logs.

Because the old gamma-ray and neutron logs were run by many different companies at different scales and sensitivities, the gamma-ray logs were normalized to API units and the neutron logs to porosity units (fig. 54). Normalization of the gamma-ray logs was completed last year, and

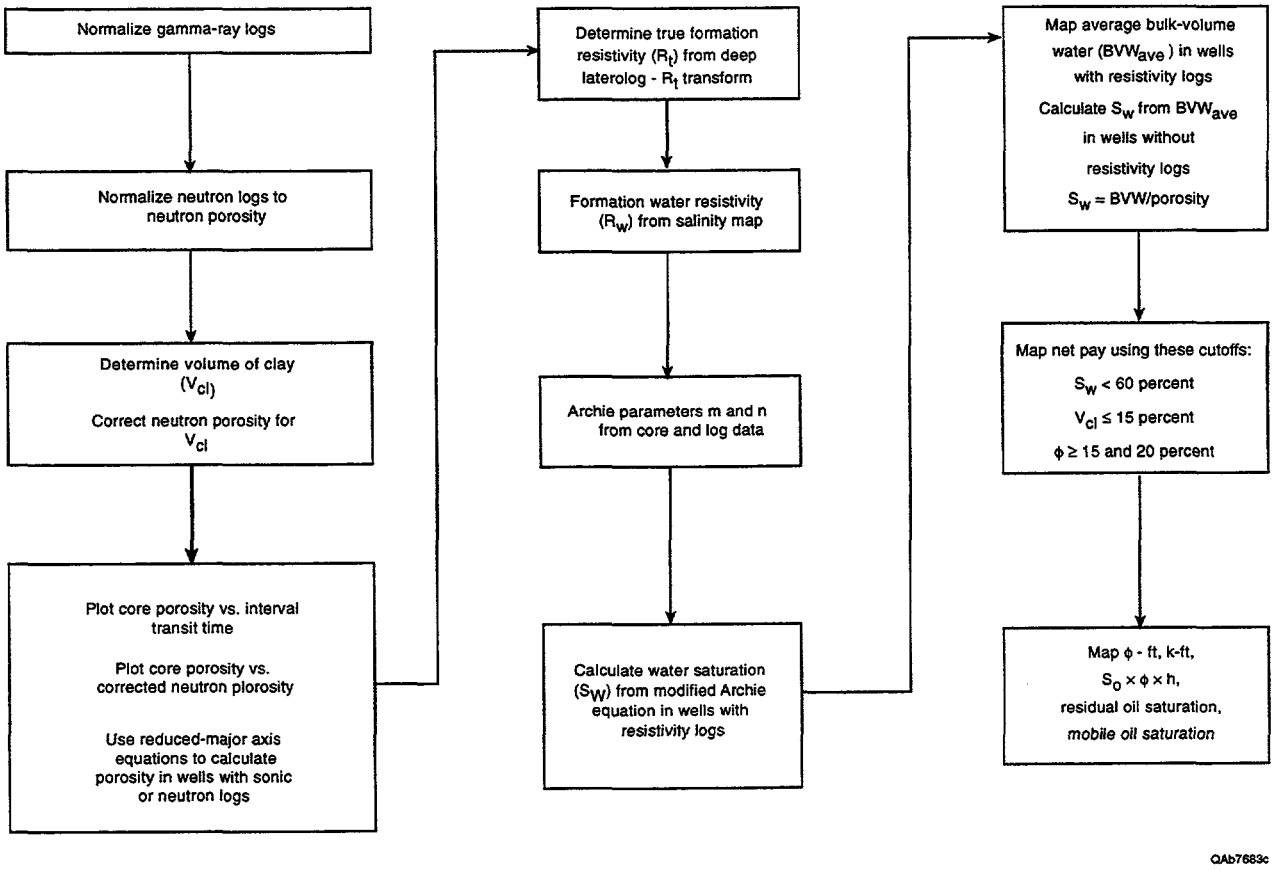

Figure 54. Flow chart of petrophysical analysis. Because most of the wells in the Ford Geraldine unit were drilled and logged in the 1950's and early 1960's, special techniques had to be used to maximize the information that could be derived from the old logs.

the neutron logs were normalized this year. The next step in the petrophysical analysis was to construct cross plots of neutron porosity and interval transit time (ITT) versus core porosity in order to determine log-to-core porosity transforms. In addition, core-porosity-versus-core-permeability cross plots were constructed to determine a porosity cutoff and to determine a porosity-versus-permeability transform (fig. 55).

Additional tasks included: (1) mapping water resistivity (R_w) across the unit, (2) determining the Archie parameters m (cementation exponent) and n (saturation exponent), and (3) developing a transform for converting the deep laterolog to R_t when an R_{xo} device is unavailable (fig. 54).

Volume of Clay

The presence of authigenic or detrital clay minerals in a reservoir can cause erroneous values for porosity derived from logs (Asquith and Gibson, 1982). Because the Ramsey sandstone contains abundant authigenic clays, it was necessary to make a correction for volume of clay in the calculation of neutron porosity.

To determine volume of clay (V_{cl}), the values for gamma-ray response in a clean sandstone (GR_{cl}) and the gamma-ray response in a shale (GR_{sh}) must be obtained. In the Delaware sandstones, determining an accurate value for GR_{sh} is difficult because of the lack of thick shale sequences. The gamma-ray response of organic-rich siltstones was substituted for GR_{sh}. In addition, the presence of potassium feldspar in the sandstones can also affect the gamma-ray log response. However, work on Brushy Canyon sandstones at Hat Mesa (Thomerson, 1992) and Red Tank (Green, 1996) fields in New Mexico has demonstrated that the presence of potassium feldspar in both the sandstones and the adjacent siltstones appears to affect gamma-ray logs equally.

Figure 56 is a cross plot of interval transit time (ITT) versus gamma-ray response (GR) from 25 wells in the Ford Geraldine unit. From this plot, a GR_{cl} value of 40 API, GR_{sh} of 90 API, and ITT_{sh} of 72μsec/ft were selected. The V_{cl} for the Ramsey sandstone was then calculated by the following formulas:

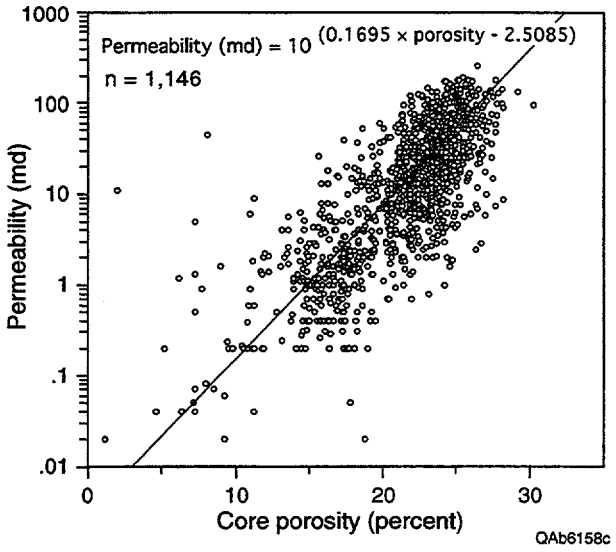

Figure 55. Cross plot of core porosity versus core permeability for the Ramsey sandstone in the Ford Geraldine unit, Reeves and Culberson Counties, Texas.

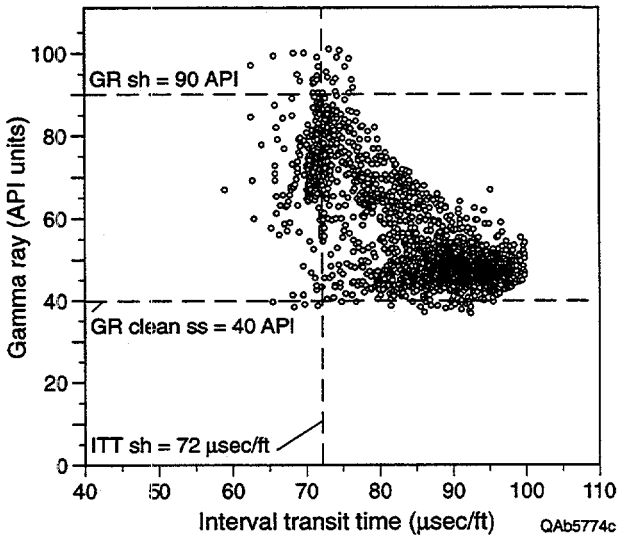

Figure 56. Cross plot of interval transit time (ITT) versus gamma ray (GR) for the Ramsey sandstone interval, Ford Geraldine unit. The data in this figure are from 12 wells, and the cross plot is used to determine GR_{cl} (40 API), GR_{sh} (90 API), and ITT_{sh} (72 µsec/ft).

$IGR=(GR-40)/(90-40)$ and

$V_{cl} = 0.33[2^{\wedge}(2 \times IGR) - 1.0]$ (Atlas Wireline, 1985),

where IGR is gamma-ray index and V_{cl} is volume of clay.

Porosity

The first step in the determination of accurate porosity values for the Ramsey sandstone was the normalization of the old neutron logs to modern neutron-porosity logs. First, neutron porosities from wells with modern neutron logs were determined in the overlying evaporite and an overlying shale. Next, because these neutron porosities were run on a limestone matrix, they were then converted to a sandstone matrix. The converted neutron-porosity values were 4 percent (evaporite) and 20 percent (shale). Neutron counts were then determined in each well for the same evaporite and shale in the wells with old neutron logs. Neutron counts for the evaporite and the shale vary greatly as a result of 10 different companies having run the neutron logs and each company having run different neutron detectors at different times. Therefore, to accurately normalize these old neutron logs, the normalization procedure had to be applied on each individual well using the evaporite and shale neutron counts from that well. The individual old neutron logs were normalized by the following equations:

$PHI_n = [m \times LOG(\text{Ramsey neutron counts})]+B$,

where

$m = (0.20–0.04)/[LOG(\text{shale neutron counts})–LOG(\text{evaporite neutron counts})]$, and

$B = 0.20–[m \times LOG(\text{shale neutron counts})]$.

Once normalized, the old and modern neutron porosities were then correlated to core porosities in order to derive a neutron-porosity-versus-core-porosity transform (fig. 57). In order to correct the neutron porosity for clay, the volume of clay (V_{cl}) calculated from the gamma-ray logs was used to correct neutron porosity as follows:

$PHI_{nc} = PHI_n \times (1.0 - V_{cl})$,

where:

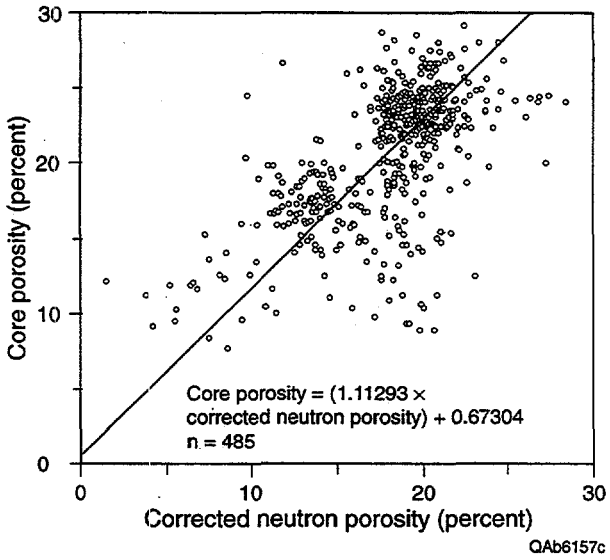

Figure 57. Cross plot of normalized and clay-corrected neutron porosity versus core porosity with porosity transform for the Ramsey sandstone in the Ford Geraldine unit.

PHI_n=neutron porosity,

V_{cl}=volume of clay, and

PHI_{nc}=neutron porosity corrected for clay.

In addition to the neutron-porosity-versus-core-porosity transform, an ITT-versus-core-porosity transform was also constructed (fig. 58). From these two plots (figs. 57, 58), reduced-major axis equations were calculated that can be used to calculate porosity in wells with sonic or neutron logs.

Calculation of Water Saturation

Resistivity logs are electric logs that are used to determine hydrocarbon versus water-bearing zones (Asquith and Gibson, 1982). Data from resistivity logs can be used to calculate a formation's water saturation if several parameters, including true formation resistivity (R_t), formation water resistivity (R_w), cementation exponent (m), and saturation exponent (n) are known (Archie, 1942).

True Formation Resistivity

During an examination of the logging suites in the Ford Geraldine unit, it was noted that commonly only a Deep Laterolog (LLD) was run, with no accompanying log to measure either resistivity of the flushed zone ([R_{xo}, which is measured by a Microlaterolog [MLL] or a Microspherically Focused Log [MSFL]) or resistivity of the invaded zone (Ri, which is measured by a Shallow Laterolog [LLS]). When both an LDD and an R_{xo} or an LLS log are available, the LDD can be corrected for invasion by the following equations:

$R_t = 1.67 \times LLD - 0.67 \times MLL$ (Hilchie, 1979) and

$Rt = 2.4 \times LLD - 1.4 \times LLS$ (Asquith, 1979),

where:

R_t = true formation resistivity (LLD corrected for invasion),

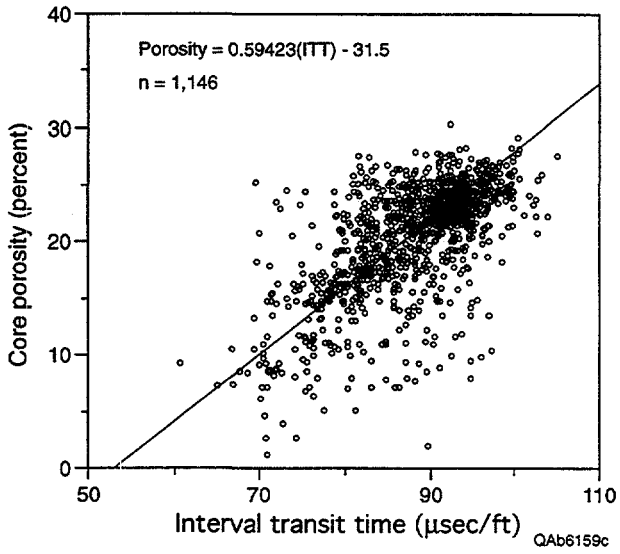

Figure 58. Cross plot of interval transit time (ITT) versus core porosity with porosity transform for the Ramsey sandstone in the Ford Geraldine unit.

LLD = Deep Laterolog,

MLL = R_{xo} or flushed zone resistivity, and

LLS = Shallow Laterolog.

Using R_t values calculated from the above equations and concomitant LLD values, an LLD versus R_t cross plot was constructed (fig. 59). Scatter on the plot is less at low LLD resistivities (2 to 8 ohm-m), which is the typical range of LLD values for Delaware sandstones. The calculated linear regression equation for the data ($R_t = 1.3002 \times LLD + 0.3397$) can be used to correct LLD to R_t in wells lacking an R_{xo} or an LLS log.

To illustrate the importance of using this LLD–R_t transform (fig. 59) to obtain R_t in wells with only an LLD log, hydrocarbon pore-feet in the FGU-153 well were calculated (a) with and (b) without using the R_t correction.

(a) FGU-153 Ramsey Sandstone (2580 to 2605 ft)

$R_t = 1.3002 \times LLD + 0.3397$

Hydrocarbon Pore-Feet = 2.3 Ø-ft

(b) FGU-153 Ramsey Sandstone (2,580 to 2,605 ft)

$R_t = LLD$

Hydrocarbon Pore-Feet = 1.8 Ø-ft

This calculation was done using the Archie equation (Archie, 1942) assuming a = 0.62, m = 2.15, and n = 2 in the Archie equation. Net-pay cutoffs used are V_{cl}=15 percent, porosity = 15 percent, and S_w=50 percent. The difference in hydrocarbon pore-feet of 0.5 Ø-ft (that is, 2.3–1.8) is not insignificant because it volumetrically represents 155,160 bbl of original oil in place (OOIP) per 40 acres.

Formation Water Resistivity

Formation water resistivities (R_w) were calculated across the Ford Geraldine unit from a map of prewaterflood salinity (fig. 60). The R_w values at 75°F ranged from 0.11 to 0.18 ohm-m, with

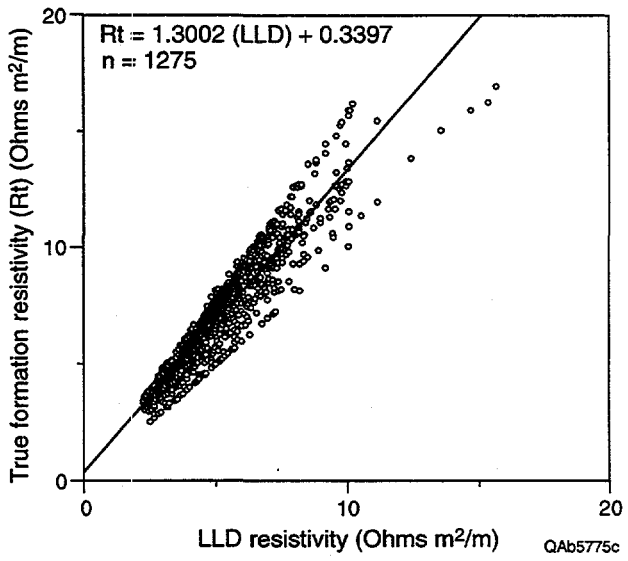

Figure 59. Cross plot of deep laterolog versus true formation resistivity (R_t) for 1,275 data points from 16 Ford Geraldine unit wells having a deep laterolog (LLD) plus a microlaterolog (MLL) or a shallow laterolog (LLS). The transform equation R_t=1.2963 × LLD + 0.3743 can be used to calculate R_t from LLD in wells where MLL and LLS logs are unavailable.

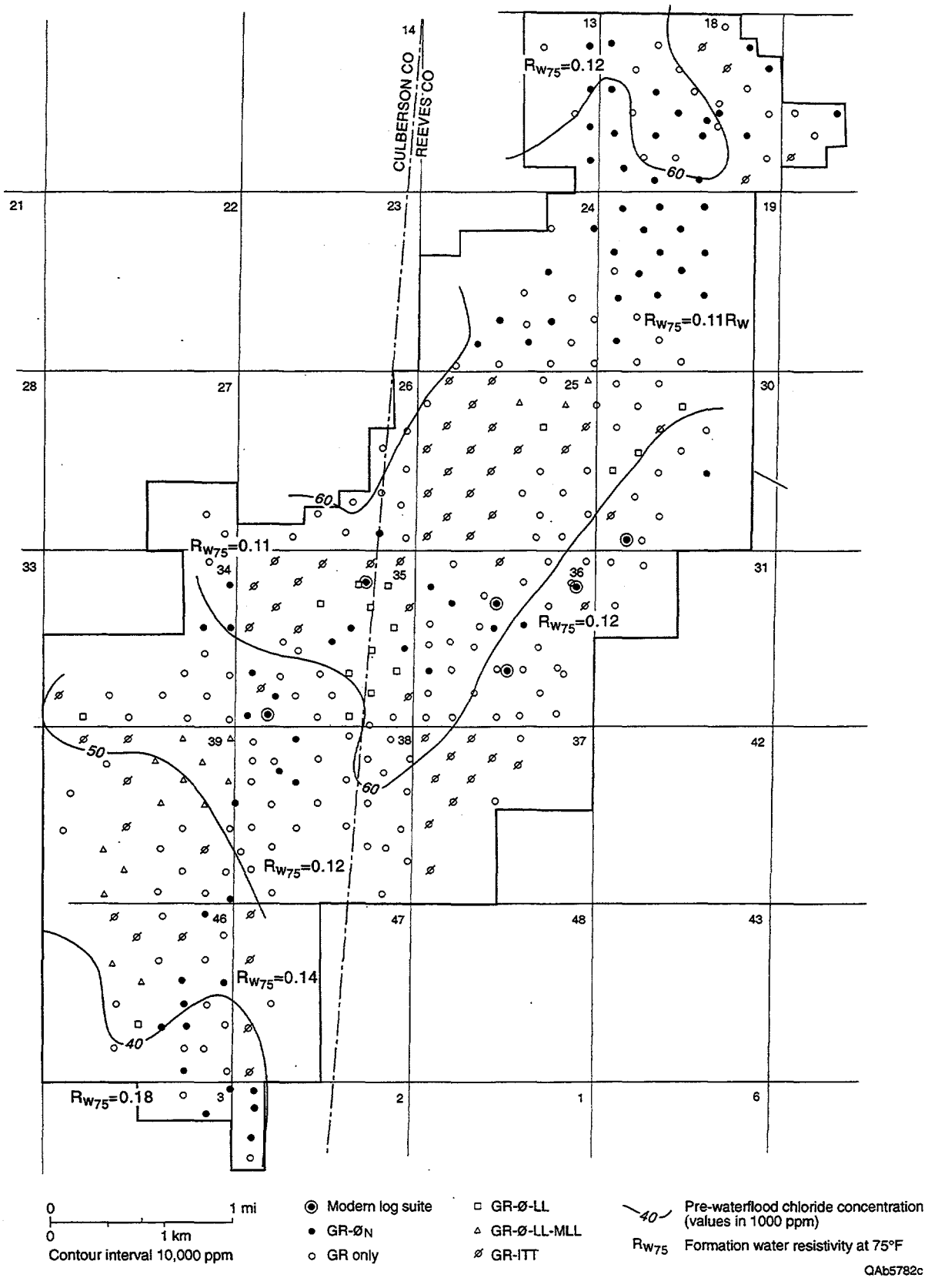

Figure 60. Prewaterflood isosalinity map with formation water resistivities (R_W) at 75°F for the Ford Geraldine unit. Modified from Ruggiero (1985).

the highest values to the southwest. It is important to remember that these values represent prewaterflood resistivities.

Archie Parameters m and n

Analyses of core from the FGU-156 well included five measurements of cementation exponent (m) (table 3). To verify these measured values of m, data from the FGU-95 well were used to calculate log-derived m values. The FGU-95 well was selected because it was the most downdip (structural) well that contained both sonic and R_{xo} logs. Using sonic and R_{xo} data from the FGU-95 well, core-corrected sonic porosity and formation resistivity factor were calculated at 82 depths ($Fr = R_{xo}/R_{mf}$, where R_{mf} is resistivity of the mud filtrate). The porosity and Fr data from the FGU-156 and FGU-95 wells were then combined with 160 core-derived porosity and Fr values from the Bell Canyon and Cherry Canyon sandstones, and a porosity-versus-Fr cross plot was constructed (fig. 61). The 160 additional Bell Canyon and Cherry Canyon porosity and Fr data are from the Ford Geraldine area and were measured at the Texas Tech University Center for Applied Petrophysical Studies. The slope of the best fit line (m) with an Fr value of 1.0 and porosity of 100 percent (that is, a = 1.0) is 1.83 (fig. 61). It is important to note on figure 61 that all three data sets cluster together, indicating similar m values. The high log-derived Fr values (above the line) are from thin tight streaks where the R_{xo} log with a resolution of 2 inches records the true resistivity, but the sonic log with a resolution of 1 ft records an average porosity. The result is an Fr value too high for the recorded porosity.

Saturation exponents (n) were also measured in the FGU-156 well (table 4).

These saturation exponents (n) are very low and need to be verified by the following equation:

$$n = LOG(F \times R_w/R_t)/LOG(S_w),$$

where:

n = saturation exponent,

F = 1/Core Porosity^1.83 from FGU-156 well,

R_w = formation water resistivity at formation temperature (0.092 ohm-m),

Table 3. Cementation exponents (m) measured in core from the FGU-156 well.

Depth (ft)	Porosity (%)	Fr[1]	m
2,575	14.7	38.1	1.89
2,583	25.2	12.7	1.84
2,599	26.0	13.9	1.95
2,605	9.1	67.5	1.83

[1]Formation resistivity factor

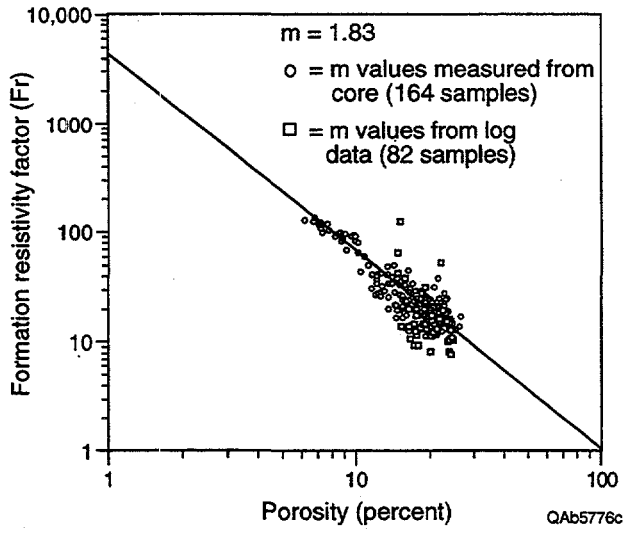

Figure 61. Cross plot of porosity versus formation resistivity factor ($Fr=R_o/R_w$) for Bell Canyon and Cherry Canyon sandstones in wells from the Ford Geraldine area. The data from core analysis includes four measurements from the FGU-165 well. The other 160 core measurements are from wells in the Ford Geraldine area. The log-derived porosity and Fr data are from the FGU-95 well. Porosity in the FGU-95 well was calculated from the sonic log corrected to core porosity, and Fr was calculated by the equation $Fr=R_{xo}/R_{mf}$.

Table 4. Saturation exponents (n) measured in core from the FGU-156 well.

Depth (ft)	Saturation exponent
2,575	1.09
2,583	1.41
2,599	1.46
	Avg. 1.32

R_t = true formation resistivity $R_t = 1.67 \times LLD - 0.67 \times MLL$, and

S_w = water saturation from relative permeability curves (table 5).

The S_w values in table 5 are the water saturation values from five relative permeability curves from the FGU-156 well, where relative permeability to water (K_{rw}) is equal to zero. The point where $K_{rw} = 0$ was selected because the FGU-156 well initially produced 158 bopd and only 18 bwpd.

Now all the parameters needed to calculate saturation exponent had been obtained except R_t. However, obtaining a value for R_t in the FGU-156 well was impossible because resistivity logs were not run. To overcome this lack, R_t values were obtained from the FGU-153 well (table 6), which is 1/3 mi to the northeast of FGU-156. Obtaining R_t values from the FGU-153 well was justified for the following reasons: (1) the wells are close and in the same R_w area, (2) R_t values were only selected from depths with similar porosities in both of the wells (see below), and (3) R_t values in the Bell Canyon sandstones do not vary much.

The calculated average saturation exponent (n) of 1.90 is more realistic than the core-measured value of 1.32 because using a saturation exponent of 1.32 would result in water saturations less than irreducible water saturation. For example, using the data at a depth of 2,583 ft (table 7), a saturation exponent of 1.90 results in water saturation of 34.9 percent, whereas a saturation exponent of 1.32 results in water saturation of 21.9 percent.

For the Bell Canyon sandstones in the Ford-Geraldine area, water saturations should therefore be calculated by the following modified Archie equation:

$$S_w = [(1/Ø\text{^}1.83) \times (R_w/R_t)]\text{^}1/1.90.$$

To test the validity of this formula, 1,415 porosities and water saturations were calculated in 15 wells and cross plotted. Figure 62 is a bulk volume water (BVW) cross plot of porosity and water saturations for the 15 wells. The lower curved line in figure 62 is a BVW value of 0.07, which should be the critical BVW value for the Ramsey sandstone in the Ford Geraldine area. A critical BVW value means that for a well to produce water free, the BVW should be 0.07 and plot along the 0.07 BVW line.

Table 5. Porosity and water saturation measured on core from the FGU-156 well.

Depth	**Core porosity (%)**	**S_w (%)**
2,575	15.6	47
2,583	26.2	38
2,583	25.8	37
2,593	23.8	40
2,599	26.0	39

Table 6. R_t from FGU-153 well.

Depth (ft)	**Sonic porosity (%)**	**MLL**	**LLD**	**R_t**
2,582	18.1	1.67	6.21	9.25
2,586	25.5	0.89	4.87	7.54
2,596	27.1	0.97	5.12	7.90
2,598	26.3	1.39	4.41	6.44
2,600	23.3	0.91	5.13	7.96

Table 7. Data for calculating saturation exponent in well FGU-156. (a = 1.0; m = 1.83; R_w = 0.092 @ T_f).

Depth	Core porosity (%)	R_t	S_w (%)	n
2,575	15.65	9.25	47	1.60
2,583	26.2	7.90	38	2.07
2,583	25.8	7.54	37	1.94
2,593	23.8	7.96	40	2.00
2,599	26.0	6.44	39	1.89
			Avg.	1.90

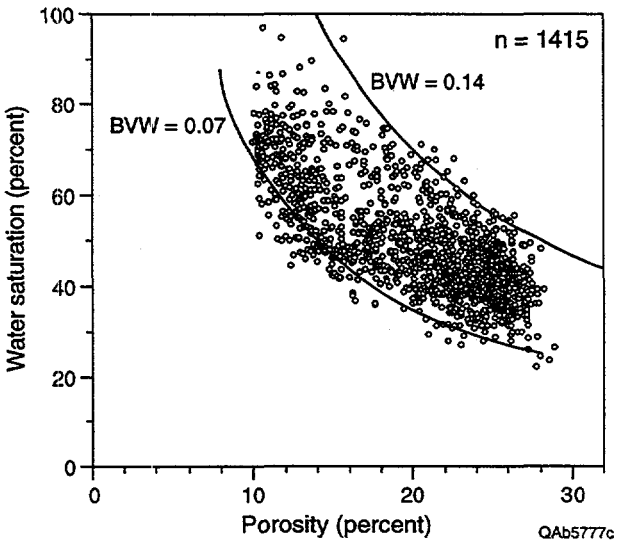

Figure 62. Cross plot of porosity versus water saturation (S_w) for wells in the Ford Geraldine unit. The porosity is core-corrected sonic and neutron porosities, and the water saturations are calculated by $S_W = [1/Ø^{1.83} \times (R_W/R_t)]^{1/1.90}$. The 0.07 bulk volume water (BVW) line is the critical BVW for the Ramsey sandstone in the Ford Geraldine unit.

Figure 63 is a BVW cross plot of data from the FGU-91 and FGU-187 wells. The FGU-91 well is located 3.4 mi northeast of the FGU-187 well and is structurally 294 ft downdip to the FGU-187 well. The BVW values for the FGU-187 well are lower than the BVW values for the FGU-91 well, and the BVW values for the FGU-187 well have a pattern that is more parallel and closer to the 0.07 BVW line (fig. 63). The BVW data from these two wells (fig. 63) indicate that the FGU-187 well should have a much lower water cut as compared with the FGU-91 well. A review of the production data indicates that monthly production with the highest amount of oil was 1,360 bbl of oil + 206 bbl of water (1/93) for the FGU-187 well and 1,161 bbl of oil + 1,285 bbl of water (1/94) for the FGU-91 well. Therefore, for their best oil-production months, the FGU-187 had a 13-percent water cut and the FGU-91 had a 53-percent water cut.

Figure 64 is a cross plot of core porosity versus core water saturations for Ramsey sandstone in the Ford Geraldine unit. A comparison of figure 64 (core data) with figure 62 (log data) reveals that the BVW trends in both cross plots are similar, thus indicating that the water saturations calculated by the modified Archie equation (a = 1.00, m = 1.83, and n = 1.90) are reliable.

Net-Pay Cutoffs

For the Ramsey sandstone in the Ford Geraldine unit, three net-pay cutoffs were selected. These cutoffs are volume of clay (V_{cl}), porosity (Ø), and water saturation (S_w). As discussed earlier, accurate values for V_{cl} are difficult to determine for the Delaware sandstones due to the lack of adjacent shales. Therefore, the selection of a V_{cl} cutoff was based on the work of Dewan (1984), which suggests a V_{cl} cutoff of 15 percent for reservoirs with dispersed authigenic clay. The dispersed authigenic clay cutoff was used because of the common occurrence of authigenic clay in the Delaware sandstones (Williamson, 1978; Thomerson, 1992; Walling, 1992; Asquith and others, 1995; and Green, 1996).

Examination of the core-porosity-versus-core-permeability cross plot (fig. 55) for the Ramsey sandstone in the Ford Geraldine unit resulted in the selection of the following porosity cutoffs:

Ø ≤ 15 percent for a permeability of 1.0 md and

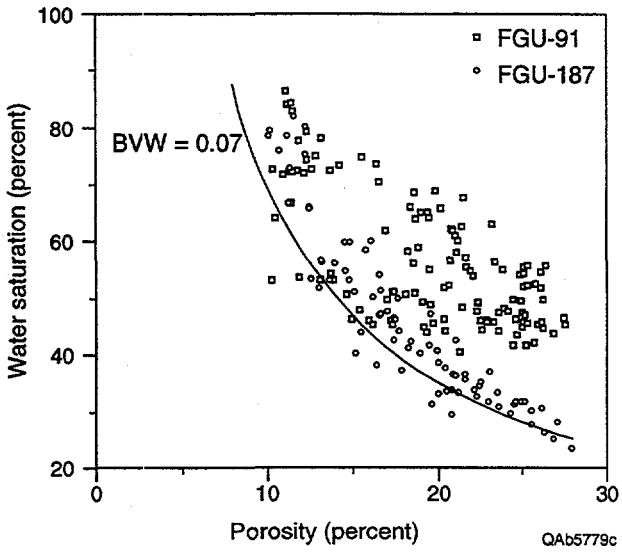

Figure 63. BVW cross plot for the FGU-91 and FGU-187 wells in the Ford Geraldine unit. The FGU-187 well is 294 ft structurally higher than the FGU-91 well. The data from the FGU-187 well plot closer and more parallel to the 0.07 BVW line when compared with the FGU-91 well data.

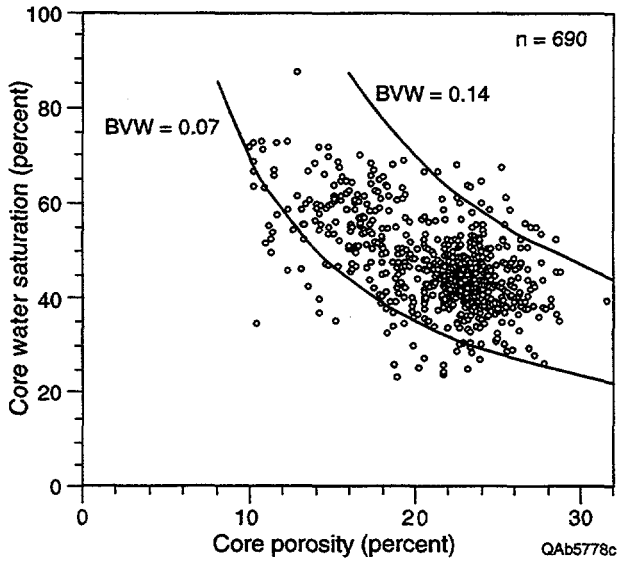

Figure 64. Cross plot of core porosity versus core water saturation for the Ramsey sandstone in the Ford Geraldine unit. Note how similar the BVW trends from core data are to the BVW trends from log-derived data in figure 62.

$\emptyset \leq 20$ percent for a permeability of 5.0 md.

For the water saturation (S_w) cutoff, five K_{ro}–K_{rw} relative permeability curves from the FGU-156 well were used. The first step was to normalize the five relative permeability curves using the method outlined by Schneider (1987). Figure 65 shows the resulting normalized Ramsey sandstone relative permeability curves. Note that on figure 65 at a water saturation (S_w) of 60 percent, the relative permeability to oil (K_{ro}) should be approximately eight times the relative permeability to water (K_{rw}). Therefore, for the Ramsey sandstone in the Ford Geraldine unit, a water saturation cutoff of 60 percent was selected.

It is of interest to note the very low relative permeability to water (K_{rw}) on the normalized relative permeability curves (fig. 65). The low K_{rw} has also been noted in other Delaware studies (Jenkins, 1961; Green, 1996). The low K_{rw} values are probably due to the very fine grain size and the presence of authigenic clay coatings.

It is not known why the Delaware sandstones commonly produce abundant water when K_{rw} is low. The answer might be that fracture treatments grow out of the productive zone into adjacent water-bearing zones due to a lack of thick seals between sandstones.

Residual Oil Saturation

Using relative permeability curves, the following residual oil saturation (ROS) values were determined (table 8). A linear regression line fitted to the data (fig. 66) results in the relationship $ROS = -0.7397 \times \emptyset + 41.4075$. By combining the modified Archie water saturations with residual oil saturations, original mobile oil saturations can be calculated as:

$$MOS = (1.0 - S_w) - ROS,$$

where:

MOS = original mobile oil saturation,

S_w = modified Archie water saturation (a=1.00, m=1.83, n=1.90), and

ROS = residual oil saturation calculated from the equation

$$ROS = -0.7397 \times \emptyset + 41.4075.$$

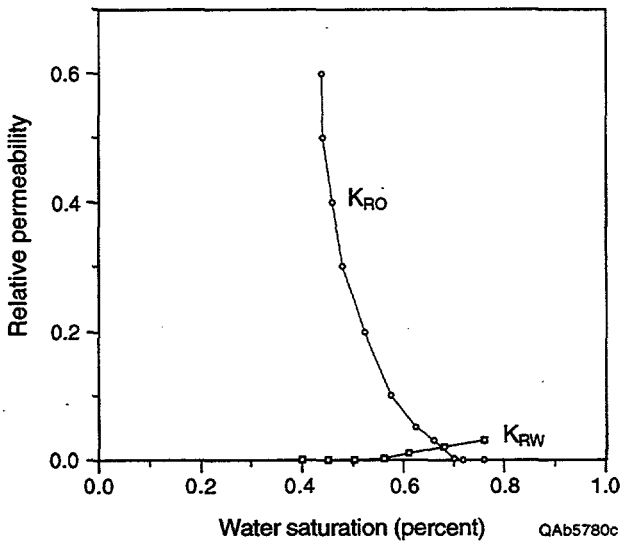

Figure 65. Normalized relative permeability curves for the five curves measured in the FGU-156 well. The method of normalization was based on the work of Schneider (1987).

Table 8. Residual oil saturation calculated from relative permeability curves, FGU-156 well.

Depth (ft)	Porosity (%)	ROS (%)
2,575	15.6	30.0
2,583	26.2	22.3
2,583	25.8	21.3
2,593	23.8	23.3
2,599	26.0	23.3

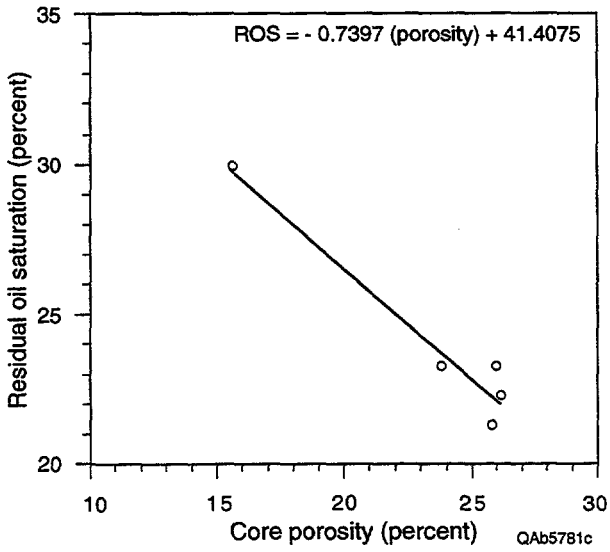

Figure 66. Cross plot of core porosity versus residual oil saturation (ROS) for the FGU-156 well, Ford Geraldine unit. The ROS values are from relative permeability curves in the FGU-156 well.

Petrophysical Maps

After the old neutron and gamma-ray logs were normalized, the Vcl determined, the Rw mapped, the Rt determined, the core-porosity to log-data and core-porosity to core-permeability transforms derived, and the reliable values for cementation (m) and saturation (n) exponents calculated, the petrophysical maps were constructed.

The map of average porosity (fig. 67) for the Ramsey sandstone in the Ford Geraldine unit exhibits a general northeast-southwest trend of high porosity, but the areas of highest porosity values are broken up. In contrast, the map of porosity-feet (fig. 68) exhibits a strong linear northeast-southwest trend of high porosity-feet (8 to 10 ft), with the greatest thickness (>10 ft) in the northeast part of the unit (shelfward). The trend of porosity-feet follows the trend of total thickness of the Ramsey sandstone (fig. 69). The decrease in average porosity and porosity-feet to the northwest and southeast is the result of a loss of reservoir rock along the edges of the Ramsey channel complex. The separation of high average porosity into different areas may be caused by diagenesis or it may represent discrete lobes along the flanks of the channel, but further work is necessary to evaluate these hypotheses.

Using the core-porosity-to-permeability transform (fig. 55) together with core-porosity-to-log-porosity transforms (figs. 57, 58), average permeability (fig. 70) and permeability-feet maps (fig. 71) were constructed. Like the map of average porosity (fig. 67), the average permeability and permeability-feet maps have a general northeast trend, but zones of highest permeability and permeability-feet are separated into isolated pods. The permeability-feet map exhibits a strong linear trend of high (>1,000) permeability-feet to the northeast that reflects the total Ramsey sandstone thickness (fig. 69). Some of the highest average permeability occurs along the margins of the field (fig. 70), in what is interpreted to be the levee facies. Lower permeability occurs near the center of the field, following the trend of the Ramsey 1 channel facies (fig. 35). Increased volumes of authigenic chlorite or calcite cement in the channel facies may explain this trend.

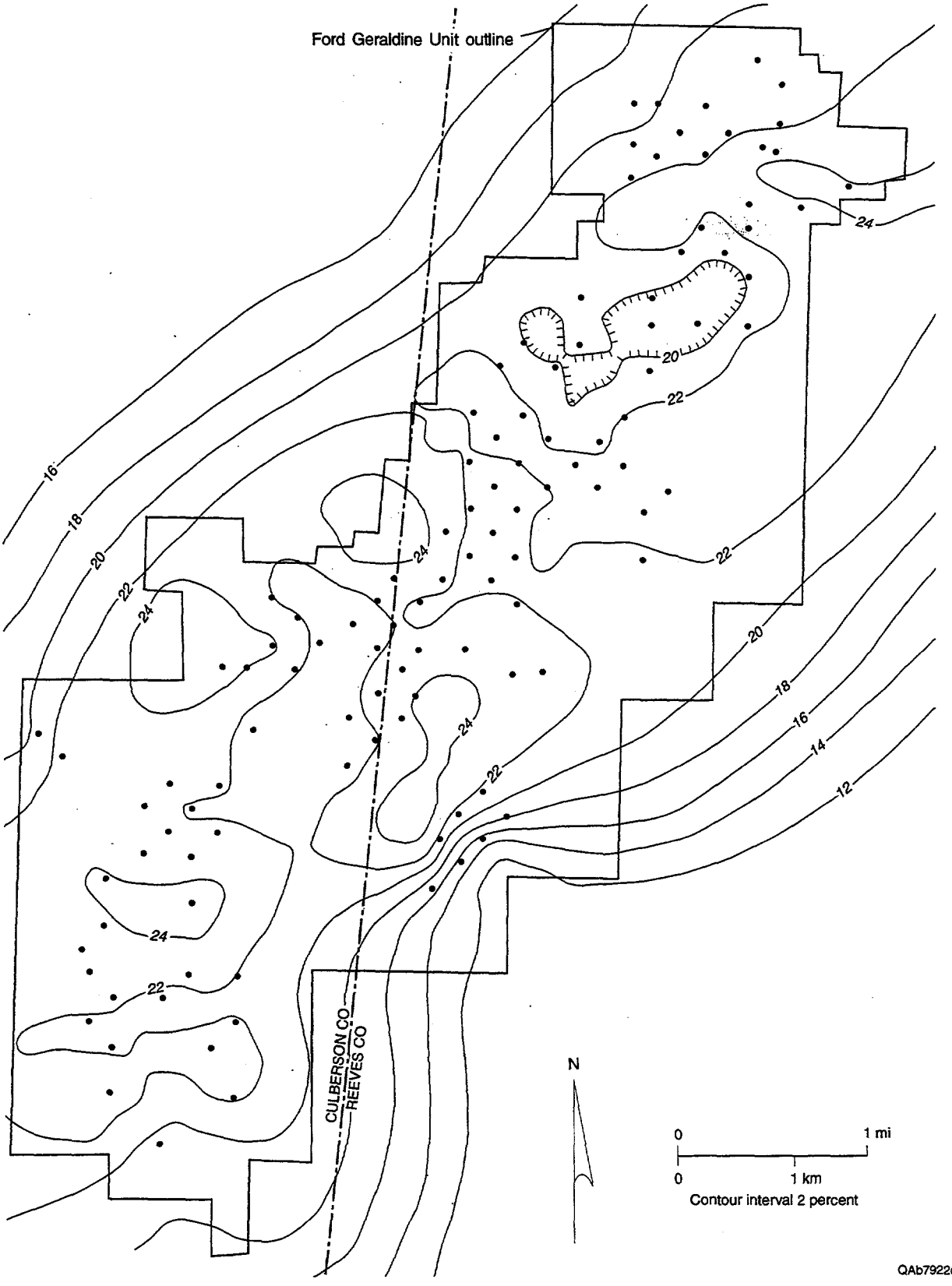

Figure 67. Map of average porosity for the Ramsey sandstone in the Ford Geraldine unit, Reeves and Culberson Counties, Texas. The porosities were determined by core-log porosity transforms (figs. 56, 57).

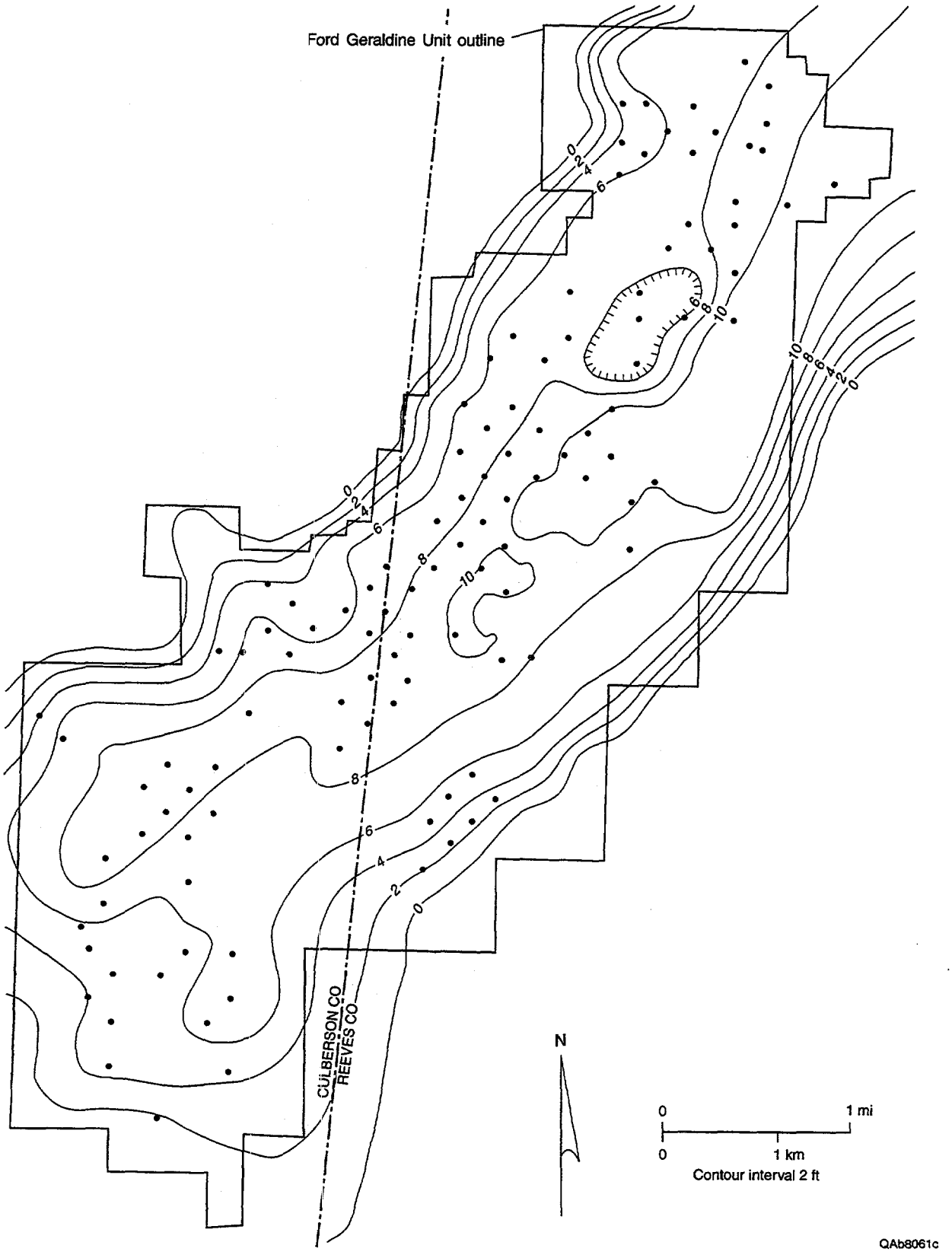

Figure 68. Map of porosity × thickness for the Ramsey sandstone in the Ford Geraldine unit, Reeves and Culberson Counties, Texas. The narrow, linear northeast-southwest trend of high porosity-feet down the central axis of the unit corresponds to the area of thick total Ramsey sandstone.

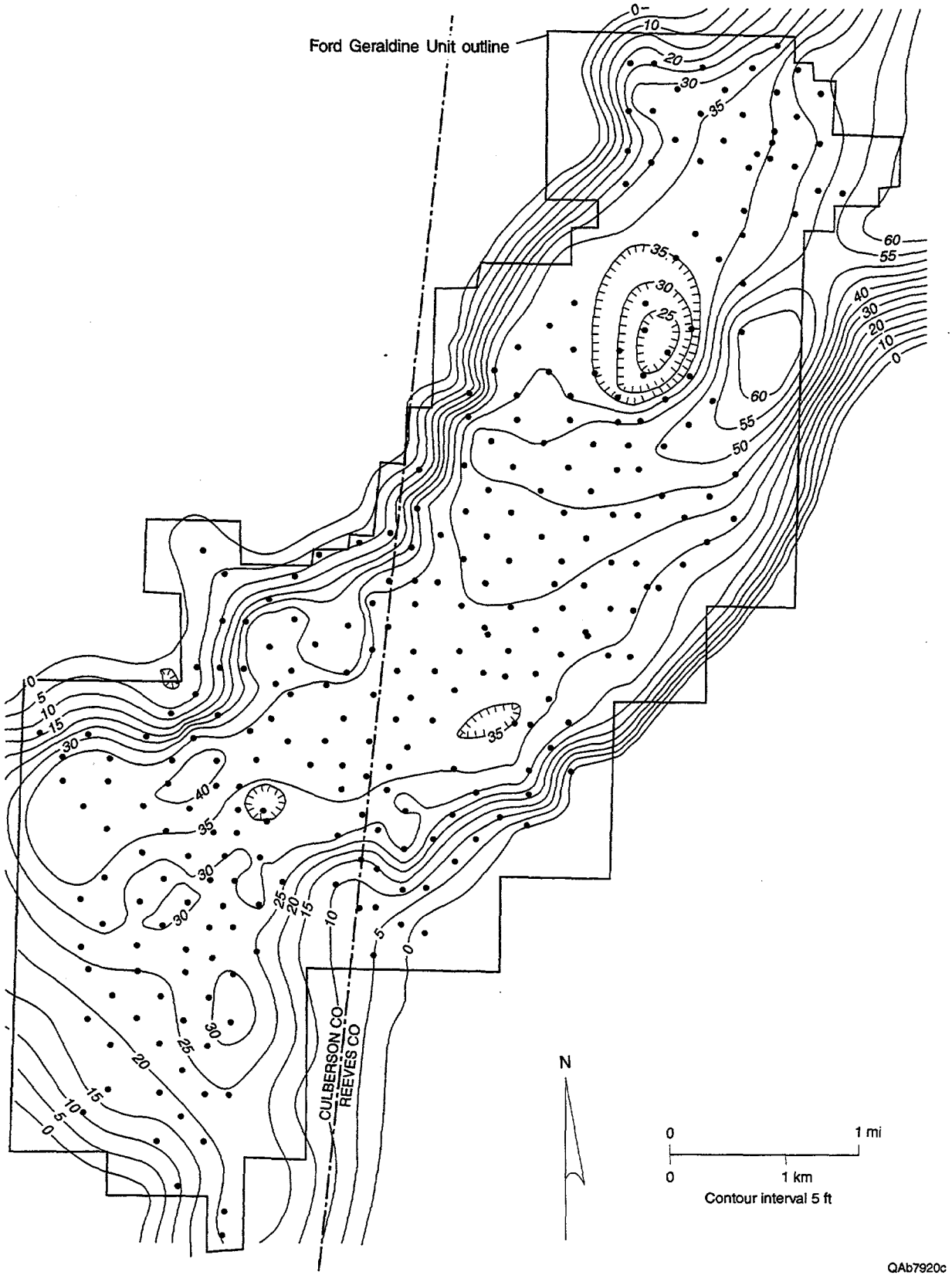

Figure 69. Map of thickness of the total Ramsey sandstone interval, from the top of the Ford siltstone to the base of the Trap siltstone.

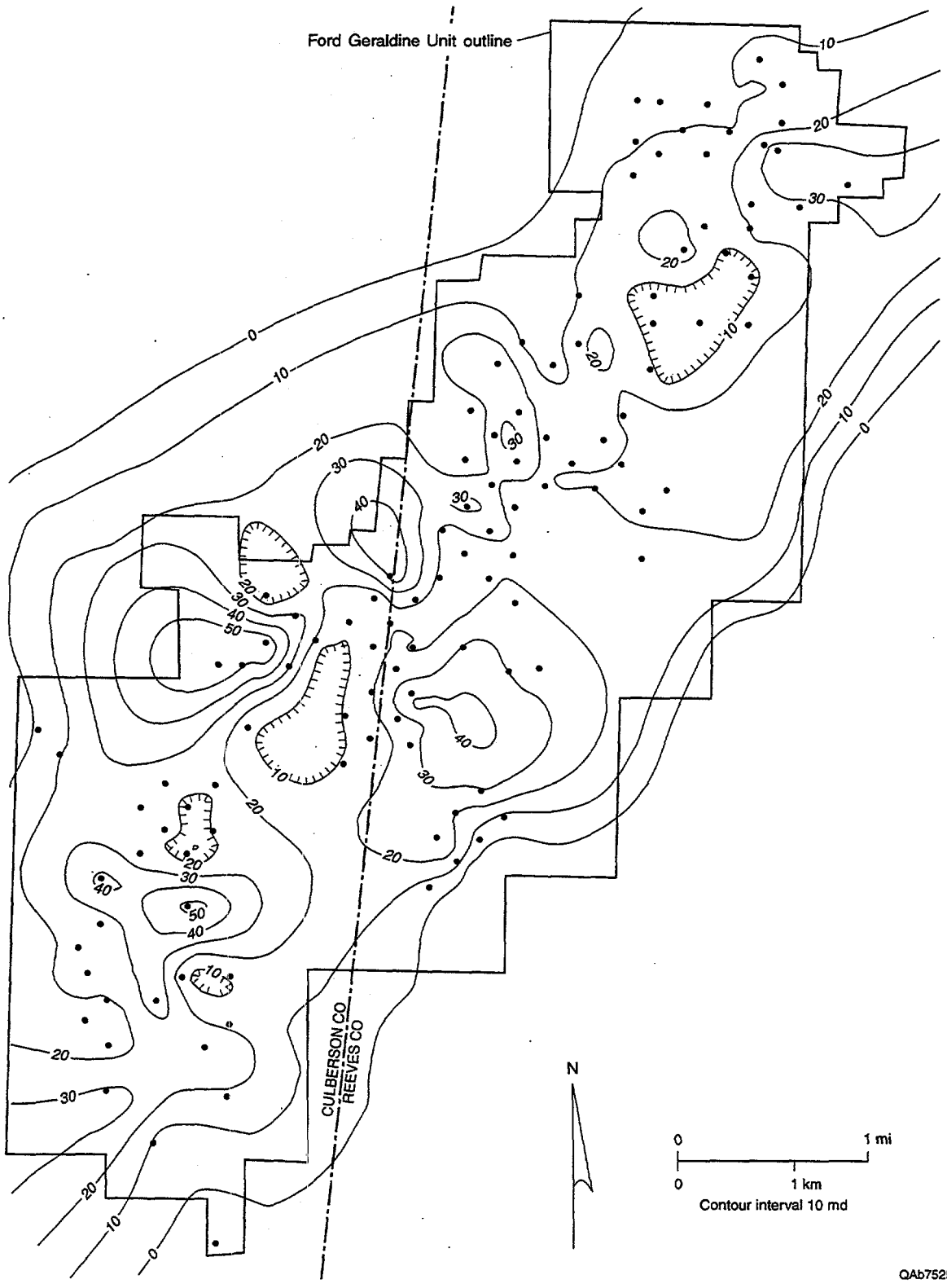

Figure 70. Map of geometric mean permeability for the Ramsey sandstone interval, calculated from log-porosity data and the core-porosity-versus-core-permeability transform. Some of the highest permeability occurs along the margins of the field, in the levee facies. Lower permeability occurs near the center of the field, along the trend of the Ramsey 1 channel facies.

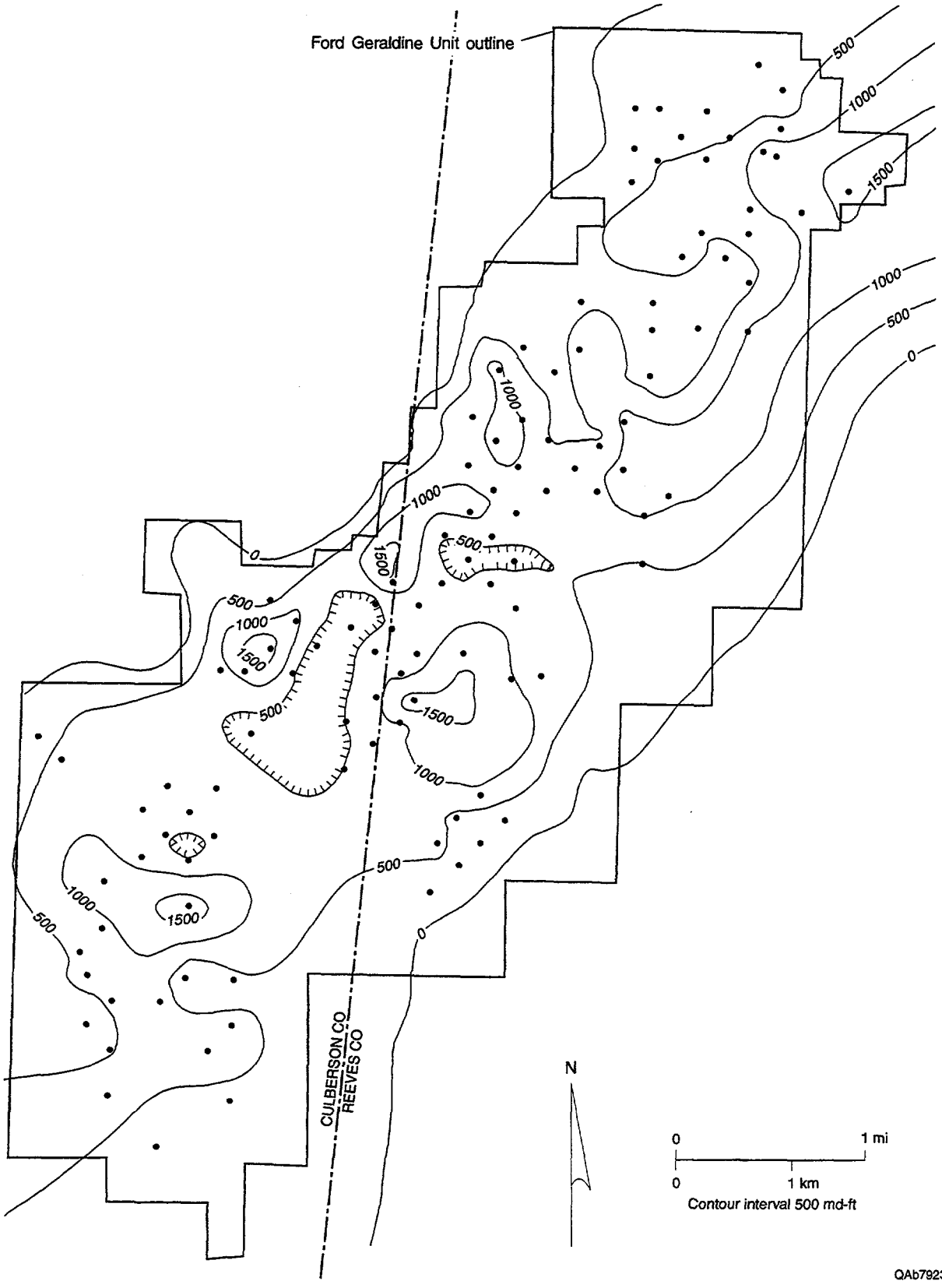

Figure 71. Map of permeability × thickness for the Ramsey sandstone in the Ford Geraldine unit, Reeves and Culberson Counties, Texas. The linear trend of high permeability-feet (>1,000) to the northeast breaks up to isolated "pods" of high permeability-feet to the southwest.

The average bulk volume water (BVW) map (fig. 72) was constructed in order to determine water saturations (S_w) northeast of sections 25 and 30, where no resistivity logs were run (fig. 60). To obtain S_w in the northeast part of the unit, average BVW values were extrapolated to the northeast (fig. 72), and BVW values assigned to wells with porosity logs. Water saturations (S_w) were calculated in these wells by the formula $S_w = BVW_{avg}/\emptyset$, then these S_w values were averaged and mapped (fig. 73). The BVW (fig. 72) and S_w (fig. 73) maps both show an increase to the northeast, which is to be expected because that direction is down structural dip (fig. 32).

Mobile oil saturations (MOS) were calculated by the formula

$$MOS = (1.0 - Sw) - ROS.$$

The values for residual oil saturation (ROS) were calculated using the porosity-ROS transform (fig. 66). The MOS map (fig. 74) has high MOS values concentrated to the southwest (updip) and in the central portions of the Ford Geraldine unit, where the better reservoirs are located (figs. 67 through 69).

The map of net pay (fig. 75) was based on the following cutoffs: Vcl≤15 percent, $\emptyset \geq 15$ percent, and $S_w < 60$ percent. As expected, there is a greater thickness of net pay to the southwest (updip) and in the central portions of the unit (fig. 74). The map of hydrocarbon pore-feet ($S_o \times \emptyset \times H$) (fig. 76) shows a strong northeast-southwest trend of high $S_o \times \emptyset \times H$ values (>5 ft) down the central portions of the unit that correlates best with the porosity-feet map (fig. 68). The slight loss of $S_o \times \emptyset \times H$ to the northeast is to be expected due to the more downdip position.

An isopach map of initial potential of the Ford Geraldine unit wells (fig. 77) shows areas of high initial potential (>300 bopd) in areas at the northern and southern ends of the unit. In many cases, the areas of high potential do not coincide with thickest Ramsey sandstone (fig. 69). Some areas of high initial potential also have high primary recovery, but not all. The map of primary oil recovery (fig. 78) has two separate areas of high oil recovery. One is located in the southwest, updip part of the unit and the other is located in the northeast, downdip part of the unit. An examination of the Ramsey sandstone isopach maps (figs. 35, 37) reveals that there is a lower

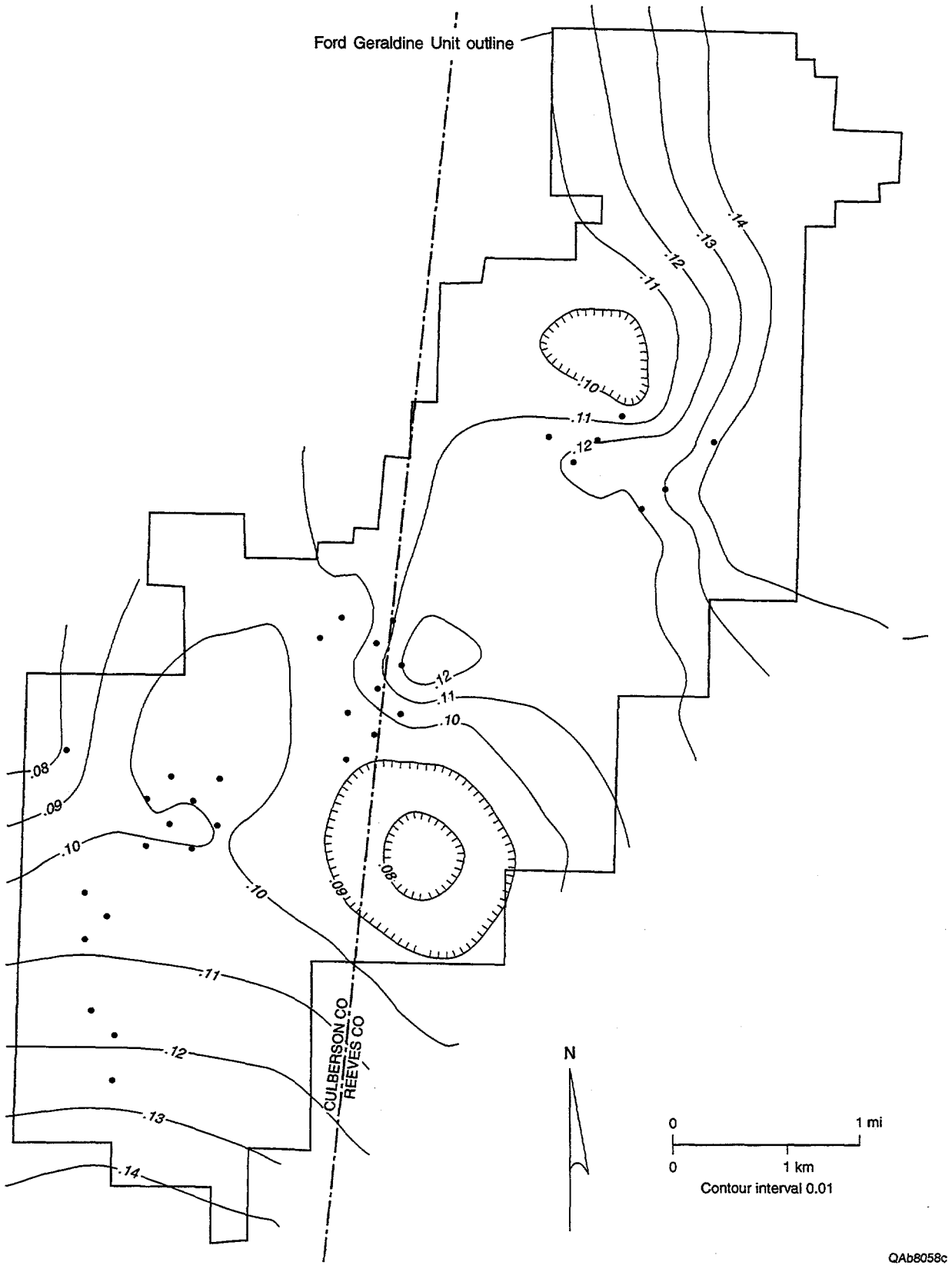

Figure 72. Map of bulk volume water (BVW) for the Ramsey sandstone in the Ford Geraldine unit, Reeves and Culberson Counties, Texas. The BVW values in the northeast part of the unit are extrapolated from BVW values to the south, where resistivity logs are available (see figure 60).

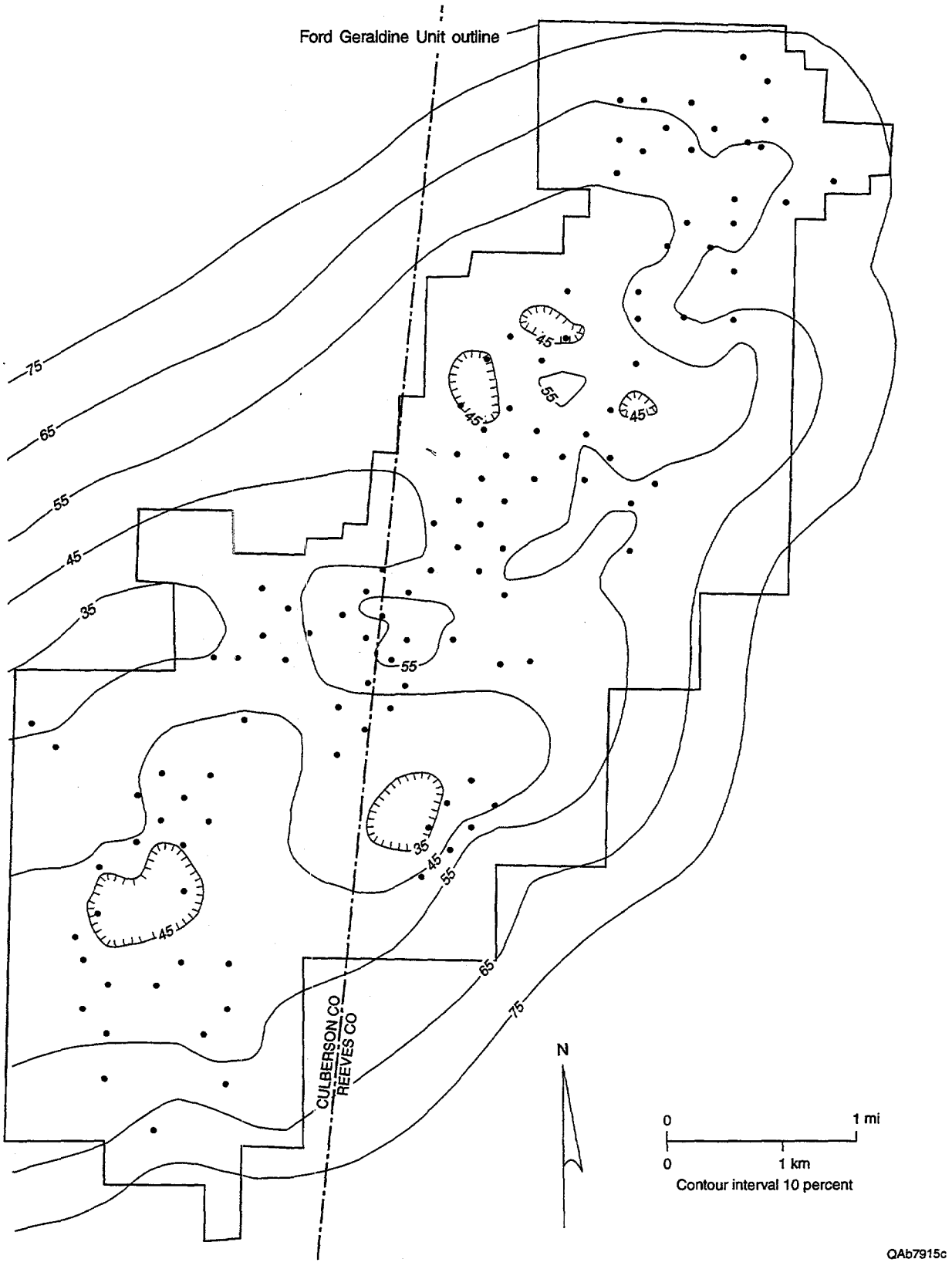

Figure 73. Map of water saturation (S_w) for the Ramsey sandstone in the Ford Geraldine unit, Reeves and Culberson Counties, Texas. The water saturations (S_w) in the northeast part of the unit were calculated from the average BVW values by the formula $S_w = BVW_{avg}/\emptyset$.

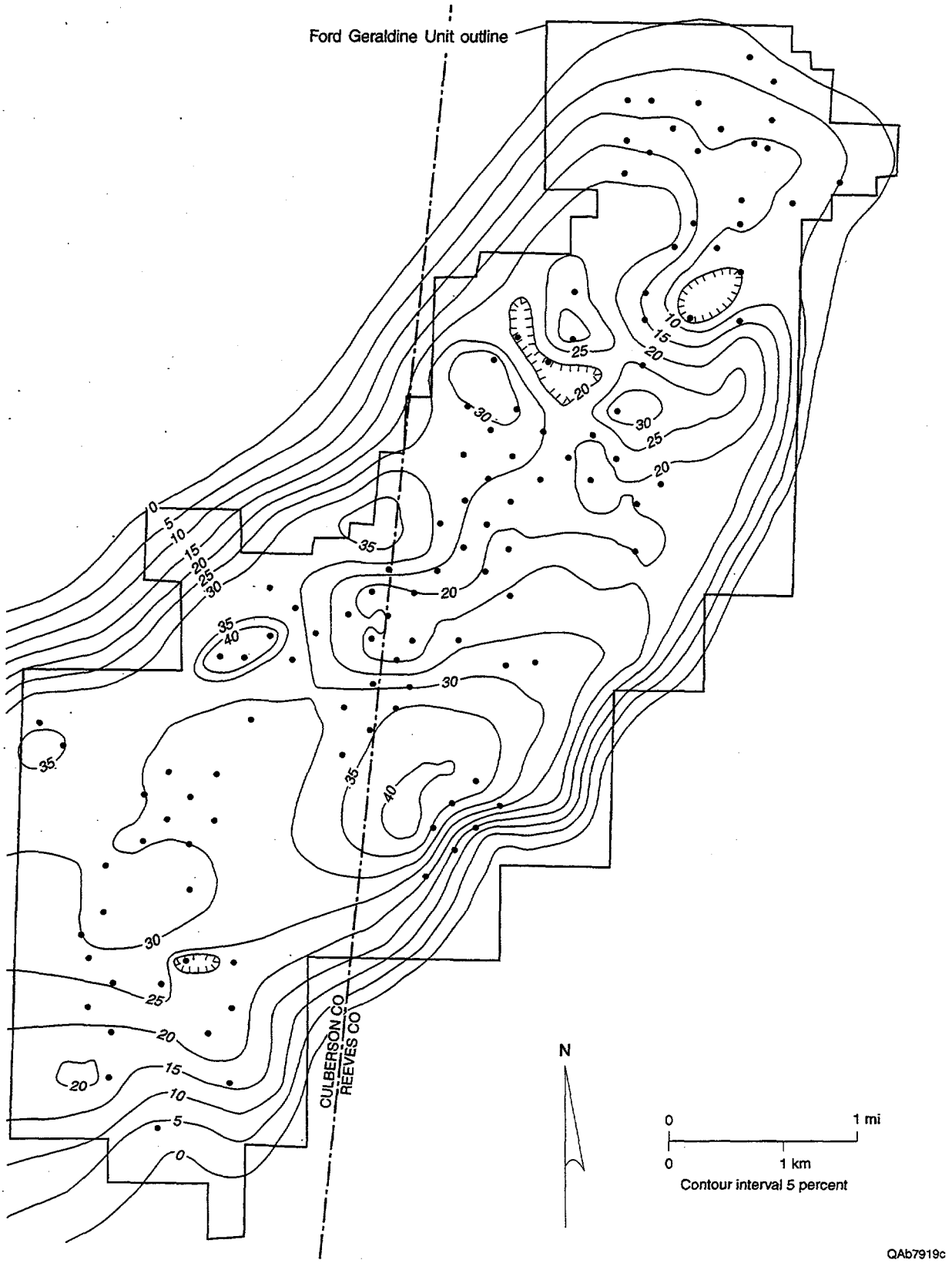

Figure 74. Map of mobile-oil saturation (MOS) for the Ramsey sandstone in the Ford Geraldine unit, Reeves and Culberson Counties, Texas. Higher values of MOS occur in the southwest part of the unit, which is structurally high.

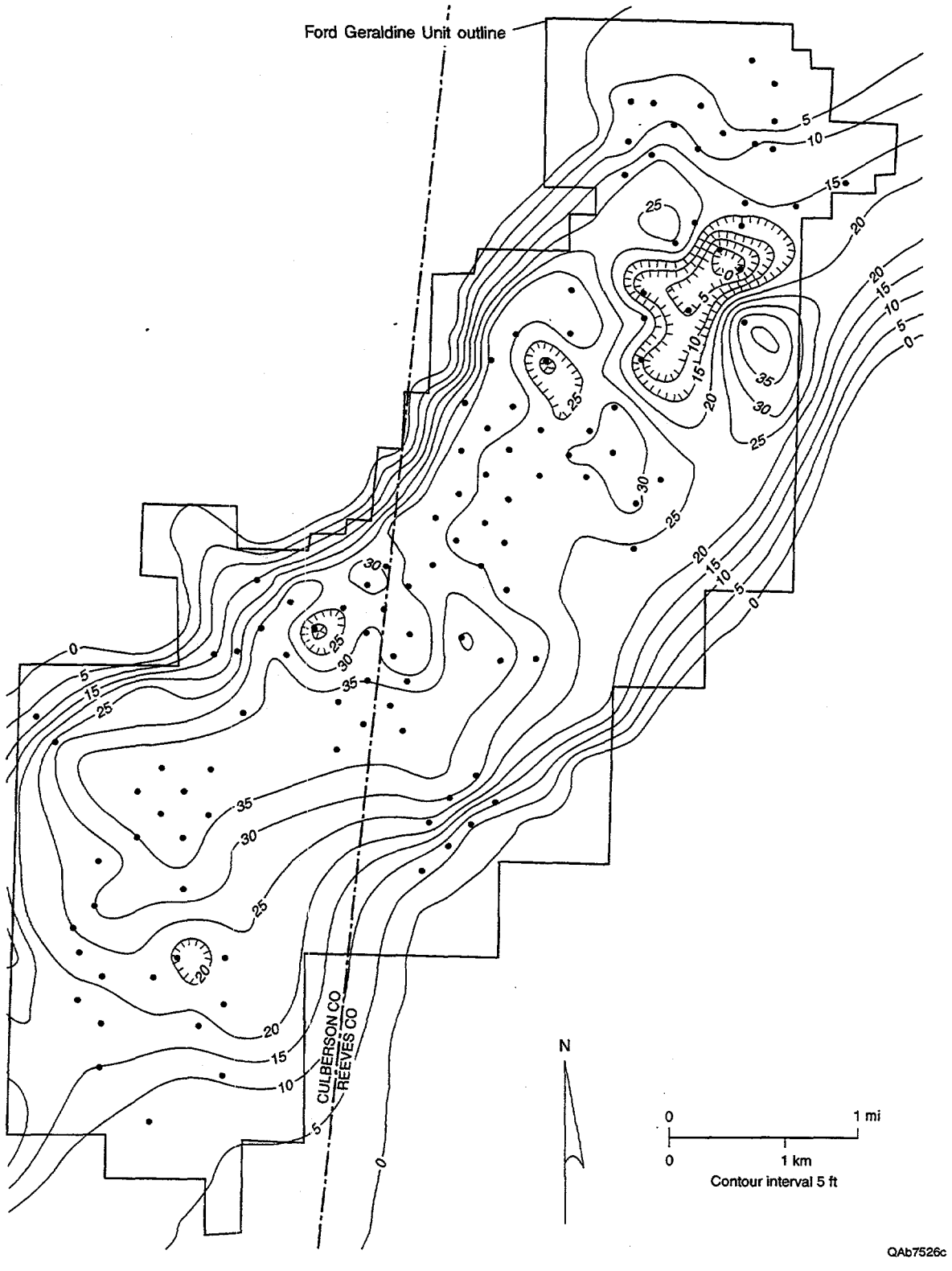

Figure 75. Map of net pay for the Ramsey sandstone in the Ford Geraldine unit, Reeves and Culberson Counties, Texas. The cutoffs for net pay were $V_{cl} \leq 15$ percent, $\emptyset \geq 15$ percent, and $S_w < 60$ percent.

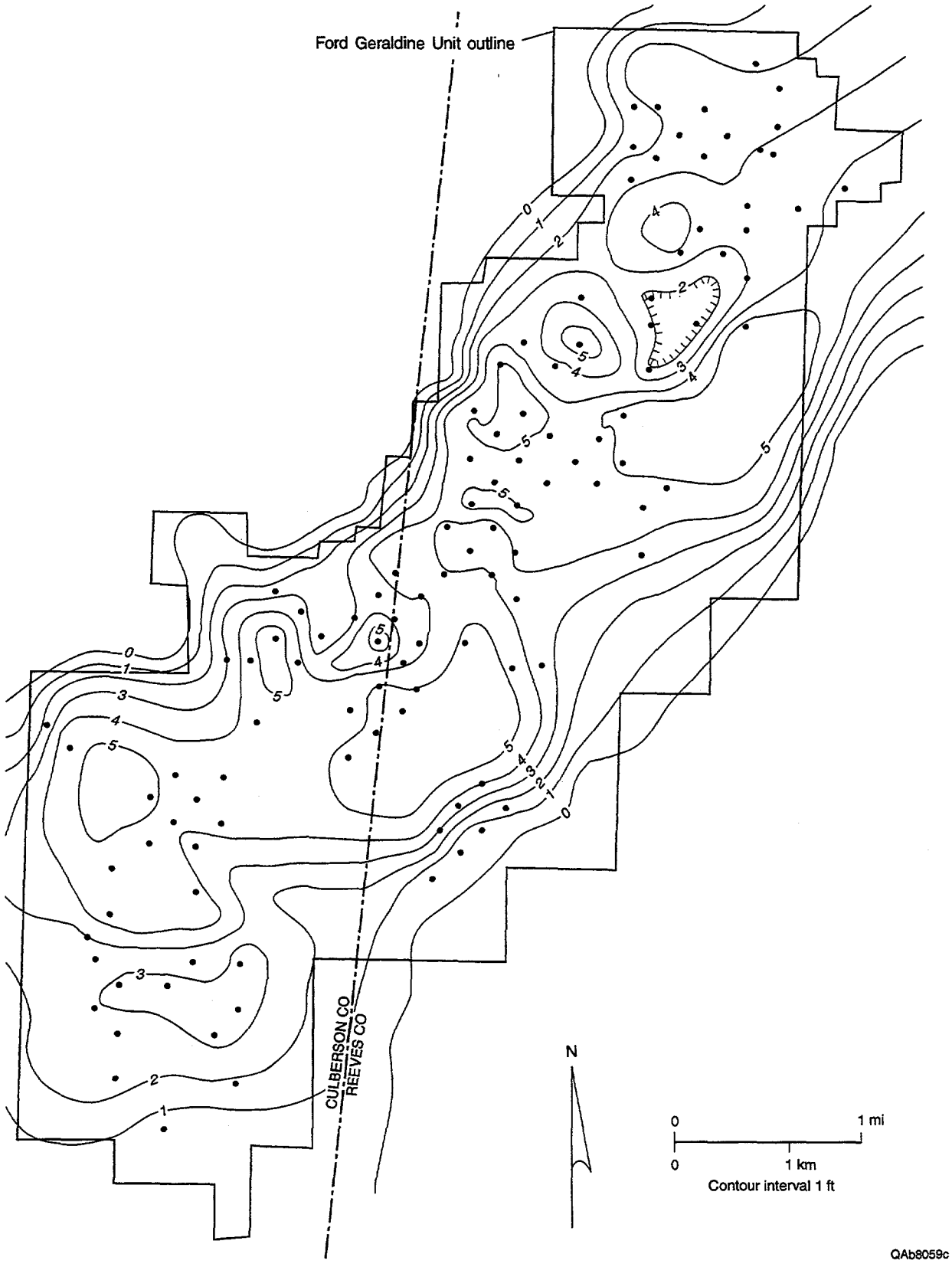

Figure 76. Map of hydrocarbon-pore-feet ($S_o \times \emptyset \times H$) for the Ramsey sandstone in the Ford Geraldine unit, Reeves and Culberson Counties, Texas. Higher $S_o \times \emptyset \times H$ values occur in the southwestern, structurally high part of the unit.

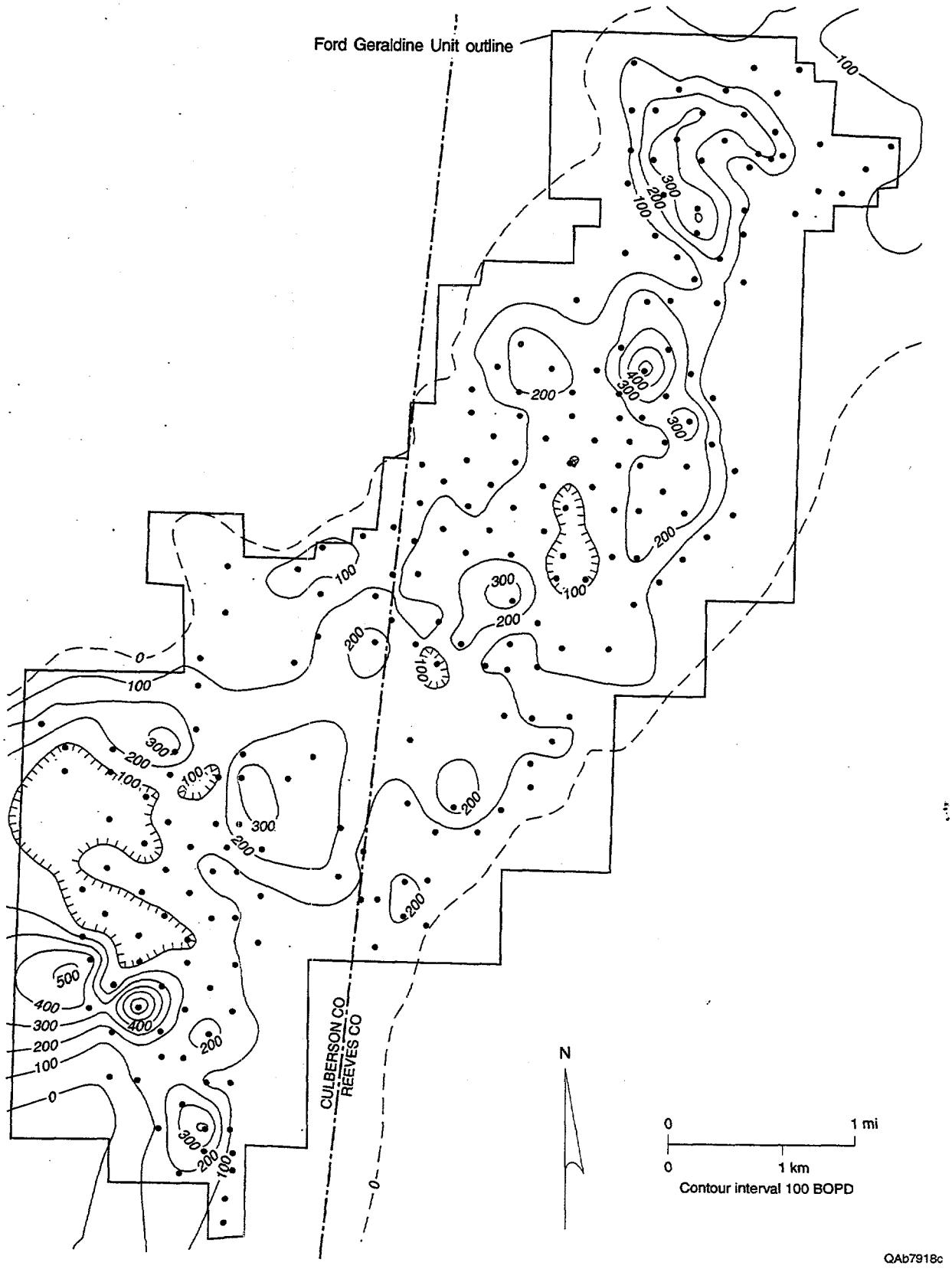

Figure 77. Map of initial potential of Ramsey sandstone in the Ford Geraldine unit, Reeves and Culberson Counties, Texas.

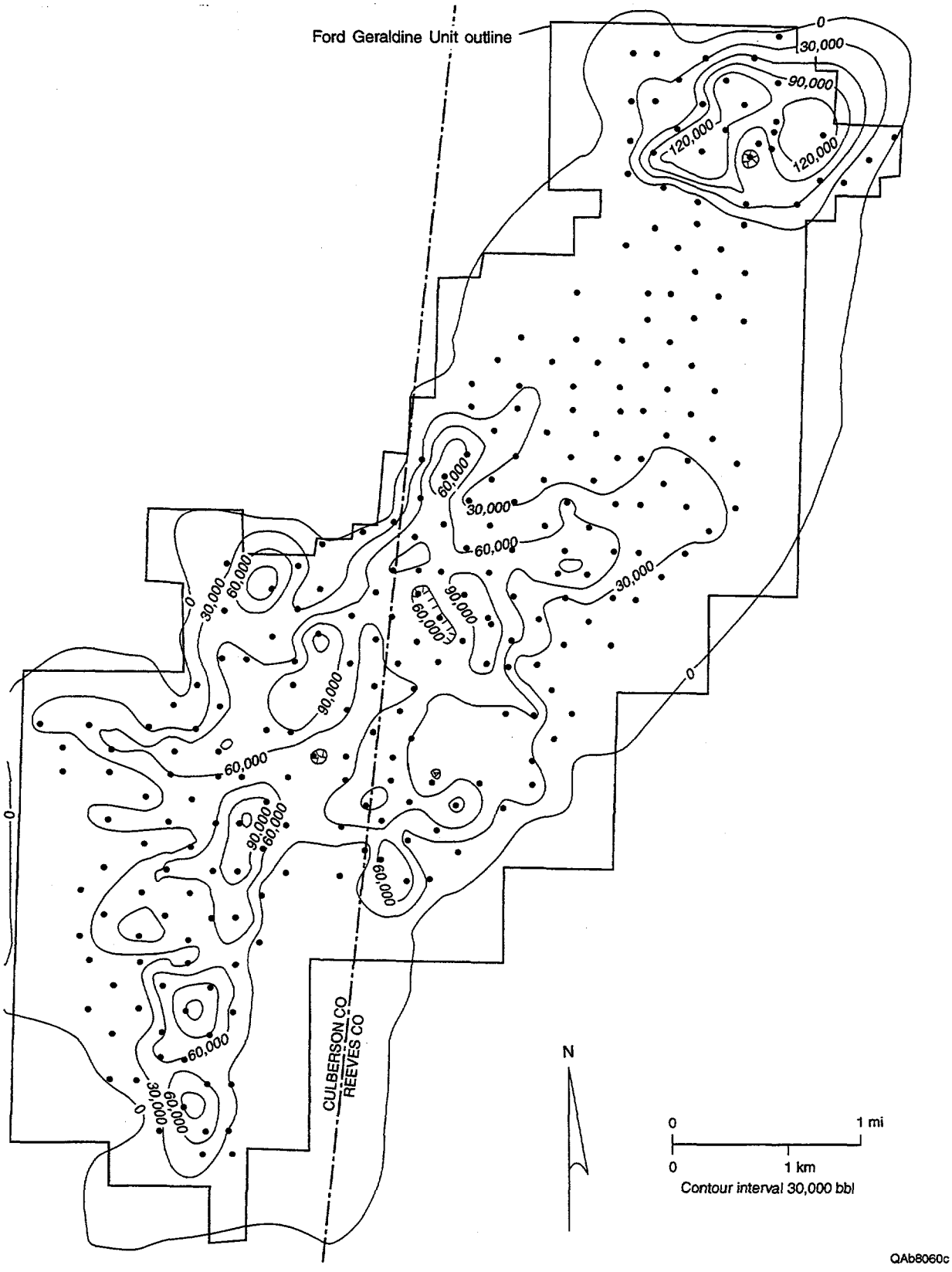

Figure 78. Map of primary recovery for the Ramsey sandstone in the Ford Geraldine unit, Reeves and Culberson Counties, Texas. The highest oil recovery is in the southwest part of the unit. To the northeast (down structural dip) there is an isolated area of high oil recovery. The high recoveries to the southwest are from the Ramsey 1 sandstone, and the high recoveries to the northeast are from the Ramsey 1 sandstone and the overlying Ramsey 2 sandstone. Because the Ramsey 2 sandstone is not developed to the southwest, the Ramsey 2 sandstone represents a separate trap.

Ramsey 1 sandstone and an upper Ramsey 2 sandstone. The high oil recoveries to the southwest are trapped in the Ramsey 1 sandstone that lenses out into a lower permeability facies to the southwest (fig. 35). The high recoveries to the northeast are from both Ramsey 1 and Ramsey 2 sandstones. Because the Ramsey 2 sandstone lenses out into a lower permeability facies near the central part of the unit (fig. 37), the oil in the Ramsey 2 is in a separate reservoir.

GEOPHYSICAL INTERPRETATION OF A BELL CANYON RESERVOIR USING 3-D SEISMIC DATA

The upper Bell Canyon Formation Ramsey sandstone was evaluated using 3-D reflection seismic data from a 36-mi^2 area (fig. 79). These data were acquired over the Geraldine Ford complex, which includes Bell Canyon and Cherry Canyon producing fields, to determine whether large-scale heterogeneities in the Delaware Mountain Group could be imaged using 3-D seismic data. This section summarizes the seismic interpretation of the Bell Canyon Ramsey sandstone and the relationship of the seismic data to the rock properties data.

Synthetic Seismograms and Wavelet Extraction

Synthetic seismograms were generated using the FGU-128 well and the Conoco G. E. Ramsey No. 6 well (figs. 80, 81) to correlate the seismic reflection character with the formation tops interpreted from well logs. Both wells penetrated the Ramsey interval, with the FGU 128 having Ramsey sandstone present and the Conoco G. E. Ramsey No. 6 having the Ramsey sandstone absent. The location of these two wells is shown in figure 82.

The FGU-128 well (fig. 80) is located on the east side of the field, and the synthetic seismogram shows in detail the picks associated with the Ramsey sandstone. This synthetic seismogram shows that the base of the Castile Formation salt and the top of the Lamar Limestone produce a peak response that will be referred as the Lamar peak. The trough below the Lamar peak was also picked to help characterize the Ramsey reservoir. This trough, which will be referred to

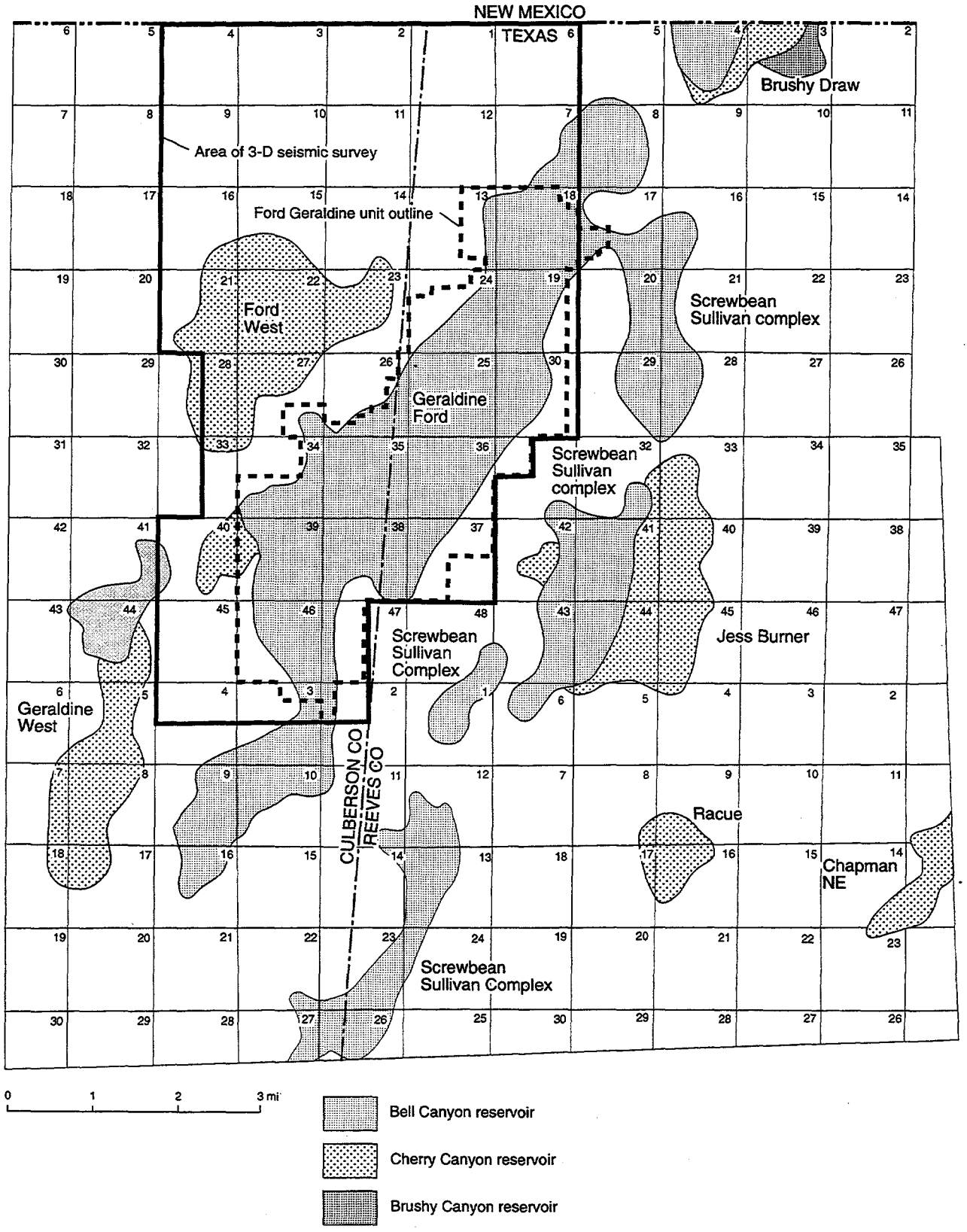

Figure 79. Outline of the area in which the 3-D seismic survey was acquired. Also shown are the locations of Ford Geraldine unit, West Ford field, and other nearby Bell and Cherry Canyon reservoirs.

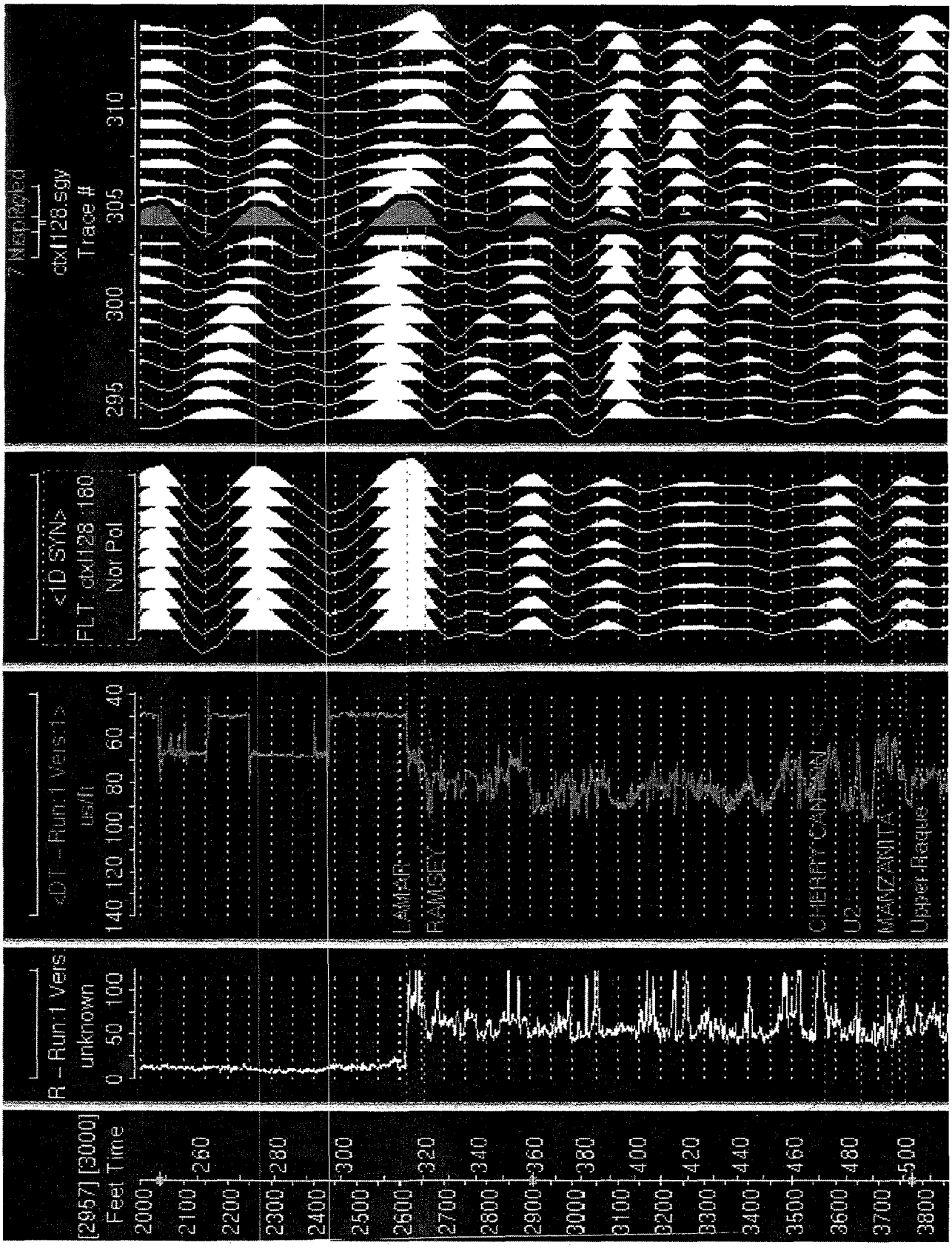

Figure 80. Synthetic seismogram of the FGU-128 well. Well location shown in figure 82. The horizon tops and their associated seismic responses are shown.

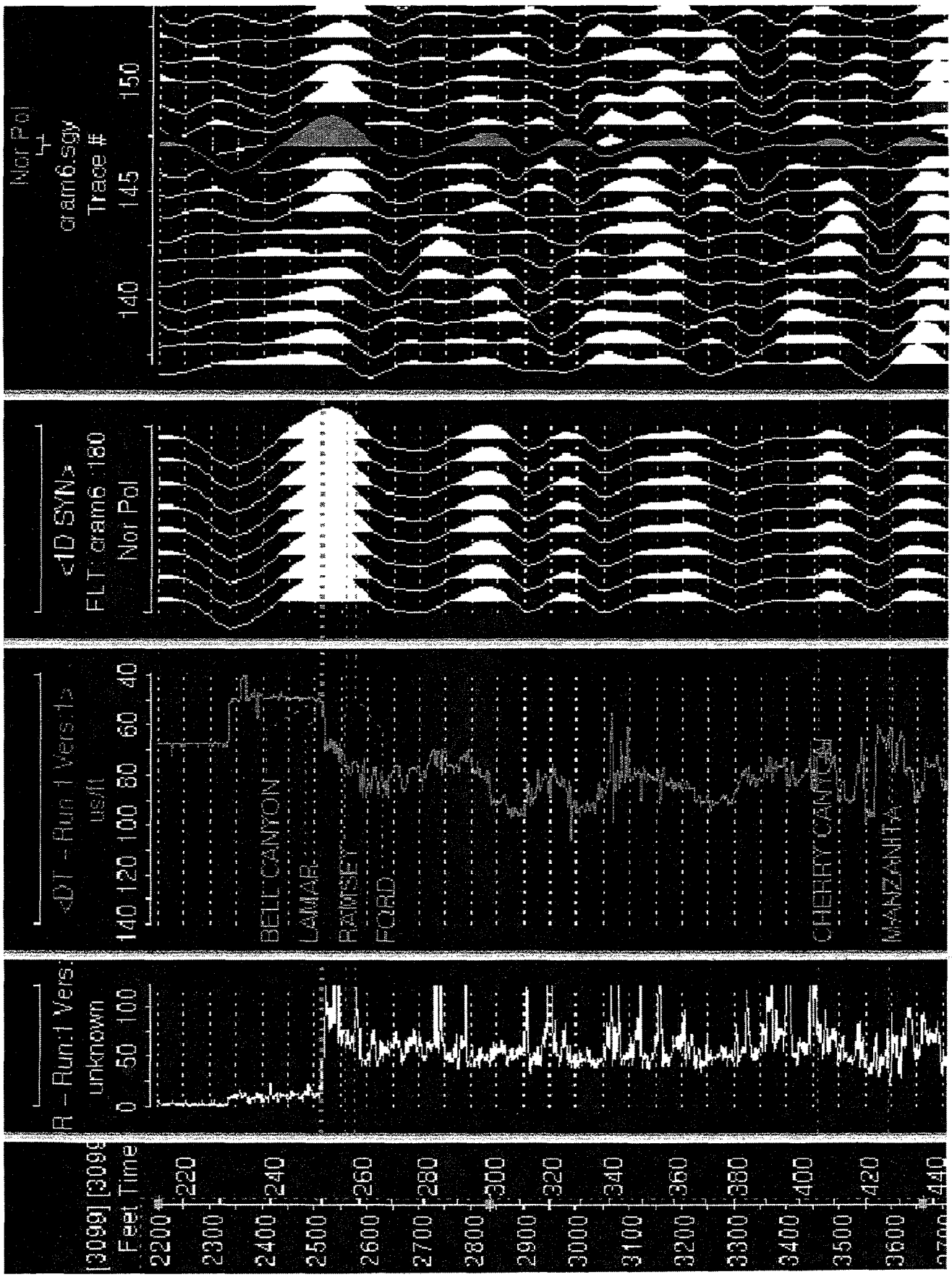

Figure 81. Synthetic seismogram of the Conoco G. E. Ramsey No. 6 well, which lacks Ramsey sandstone. Well location shown in figure 82.

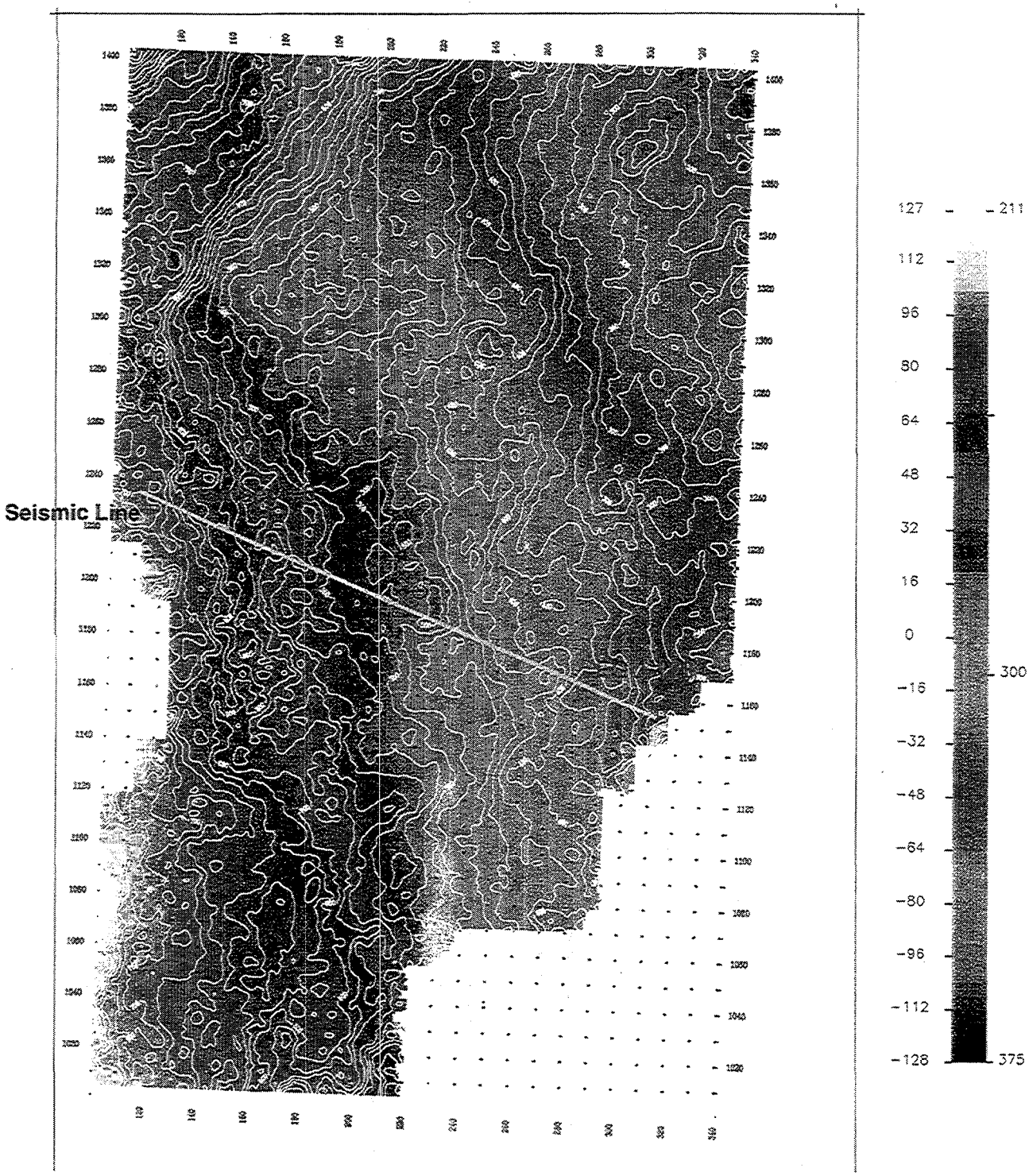

Figure 82. Top of Lamar interval in time showing location of the wells with synthetic seismograms (Conoco G. E. Ramsey No. 6 and FGU-128) and the location of the representative seismic line shown in figure 83.

as the Ramsey trough, is related to the base of the Ramsey and the top of the Ford siltstone. A representative seismic line (fig. 83) shows the seismic response of the Castile, Lamar, Ramsey, and Manzanita intervals. The Manzanita corresponds to the Cherry Canyon Manzanita Limestone, which underlies the main Cherry Canyon pay in Ford West field.

The FGU-128 well has 37 ft of Ramsey sandstone in an area of the field associated with 21-percent average porosity (fig. 67); the well has a cumulative production of approximately 50,000 bbl of oil. According to a wavelet derived from the seismic data (fig. 84), the Ramsey sandstone in this well is less than 1/4 wavelength thick. This wavelet was derived from the data set between 250 and 1,500 ms and was used to derive the seismograms. The wavelet has moderated side-lobe energy but is quite low frequency for imaging the Delaware Mountain Group. Ormsby (8-14-50-60 Hz) or Ricker (28 HZ) theoretical wavelets approximate the derived wavelet. The maximum thickness of the Ramsey sandstone in the field is 61 ft, which would be approximately 1/4 wavelength thick. Therefore, the Ramsey sandstone is always below the tuning thickness of this seismic data and would be considered a thin bed.

The Conoco G. E. Ramsey No. 6 well is located on the west side of the survey and has no Ramsey sandstone present. This allows a comparison of the seismic response of a well with Ramsey sandstone to a well without Ramsey sandstone. The peak amplitude at the top of the Lamar is 5 percent greater in the Conoco G. E. Ramsey No. 6 well's synthetic than that of the FGU-128 well. The Ramsey trough is a single broad trough in the well without sandstone and a doublet in the well with sandstone. The Ramsey trough also has 10-percent greater amplitude in the well without sandstone. The actual seismic data are too noisy, due to the shallow depth and lack of recovering high-frequency data in the area, to accurately detect the scale of amplitude differences needed to see between these synthetic models. The seismic data are probably too noisy to accurately differentiate between the shape of the trough from areas with sandstone and areas without sandstone. However, on the representative seismic line (fig. 83), the amplitudes of the Lamar peak and Ramsey trough are slightly greater at the Ramsey No. 6 location (well with

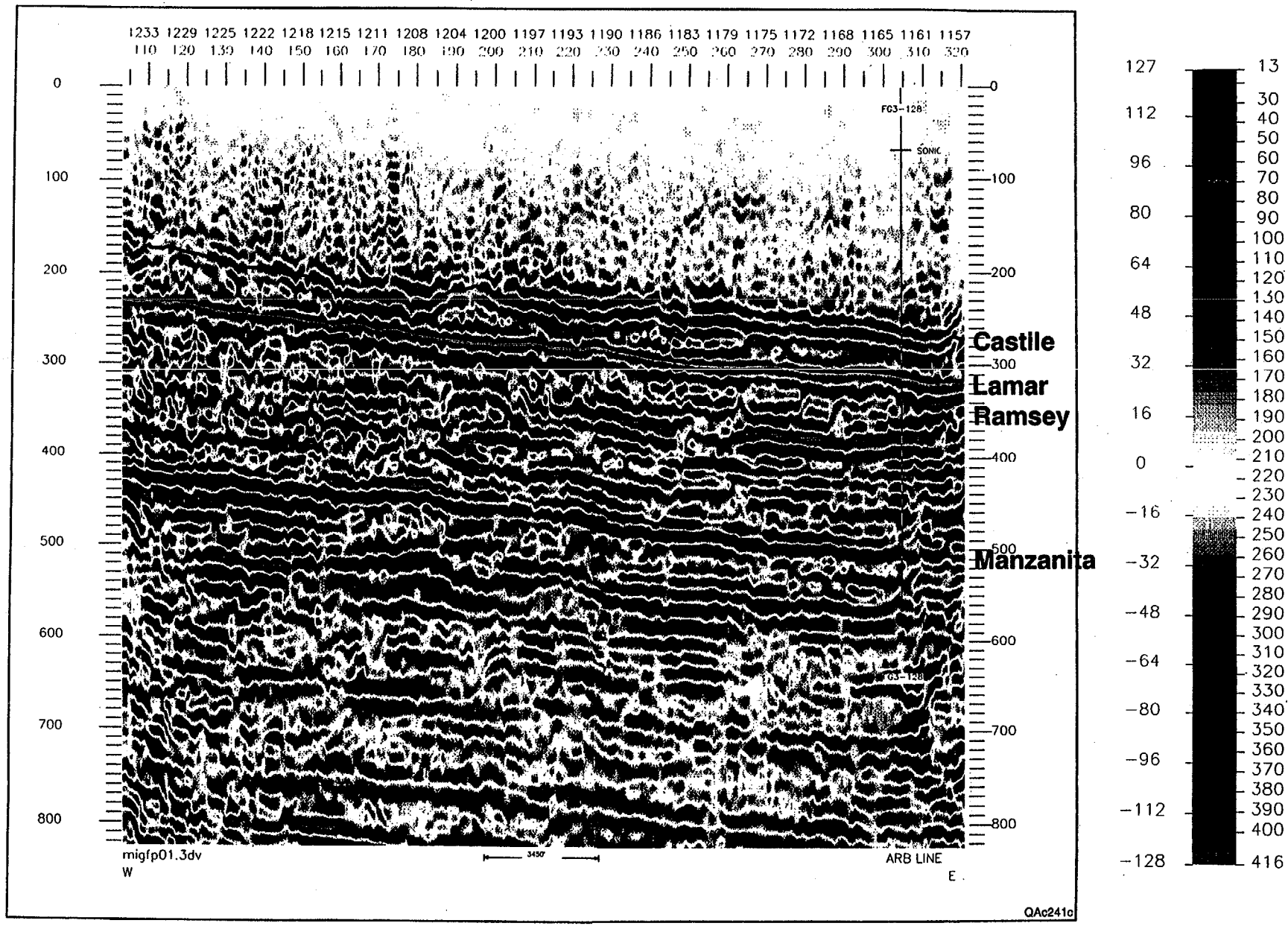

Figure 83. Representative seismic line showing the top of the Castile, Lamar, Ramsey, and Manzanita intervals.

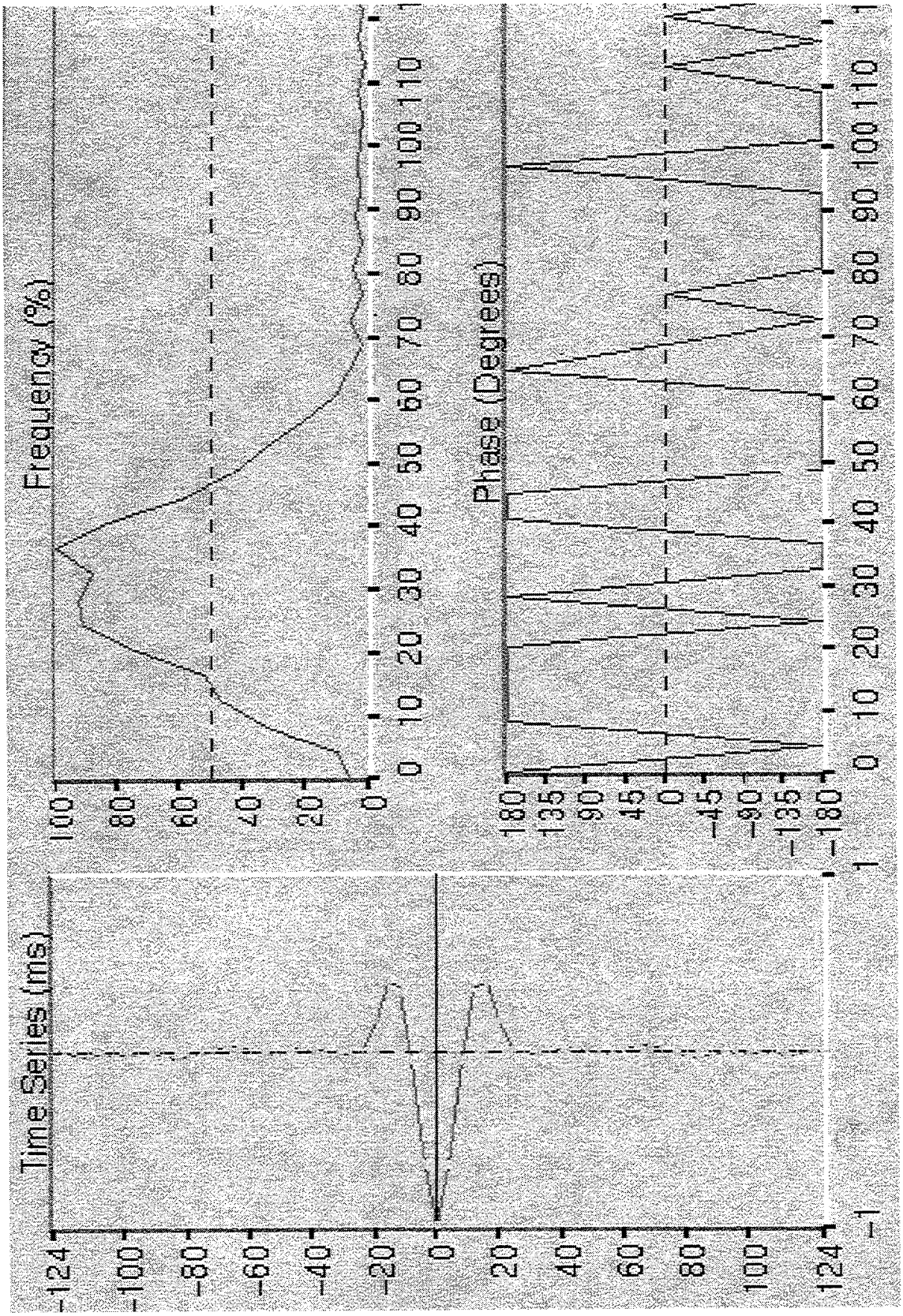

Figure 84. Seismic wavelet extracted from the seismic data set between 250 ms and 1,500 ms.

Ramsey sandstone absent) than at the FGU-128 location (well with Ramsey sandstone present). The location of this seismic line is shown on figure 82.

Structure, Amplitude, and Coherency Cube Maps

The top of the Lamar structure map (fig. 85) was made by depth converting the Lamar time horizon using an average velocity gradient calculated between the seismic datum and the Lamar. All wells were used in the calculation of the structure map. The structure map shows a gentle northeast dip into the deeper portion of the Delaware Basin. A structure map of the top of Ramsey sandstone was created in the same manner using the Ramsey time horizon (fig. 86). A residual map of the Lamar peak was generated by filtering the Lamar peak horizon with a 60 × 60 filter then subtracting the resulting smoothed horizon from the original horizon. The residual map shows localized high and lows. The residual accentuated the subtle high ridge in the structure map that is related to differential compaction over the main Ramsey 1 channel (fig. 35). Another residual high is present in the stage 5 area where the Ramsey 1 and Ramsey 2 channels stack.

The Ramsey amplitude map (fig. 87) on the Ramsey trough is simply an amplitude extraction on that seismic marker. The acquisition footprint can be seen along the edges of the survey and in the southern part of the survey in areas of less than full fold, but the amplitude extraction does have significance. The Ford Geraldine unit produces from the area of higher negative amplitudes, as can be seen on figure 87. The best part of the field, the stage 5 area (the pilot area), is located in the area of the highest amplitude to the north. A trend of slightly lower amplitudes extending through the axis of the field corresponds to a Ramsey sandstone thick.

The seismic volume was processed using the coherency cube transform in an attempt to identify channels, compartmentalization, or fracturing in the Delaware Mountain Group. Coherency cubes were derived using 3-, 5-, and 7-trace windows, and it was determined that the 5-trace window was best for imaging the upper Delaware section. The coherence extraction on the Lamar (fig. 88) does show a crude outline of the productive wells in the Ford Geraldine unit but

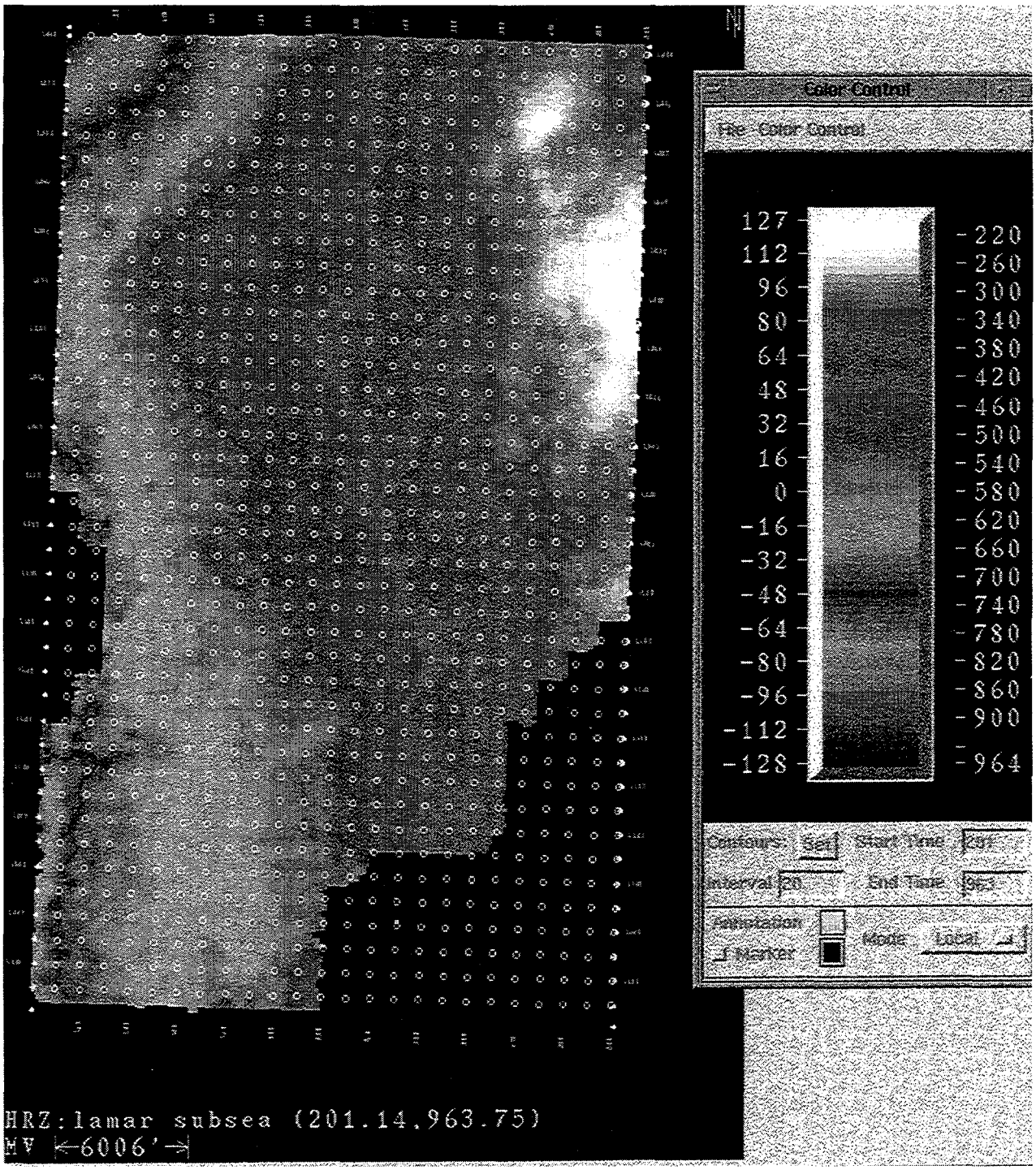

Figure 85. Top of Lamar structure map. Contour interval is 20 ft (each break in color represents a 20-ft contour).

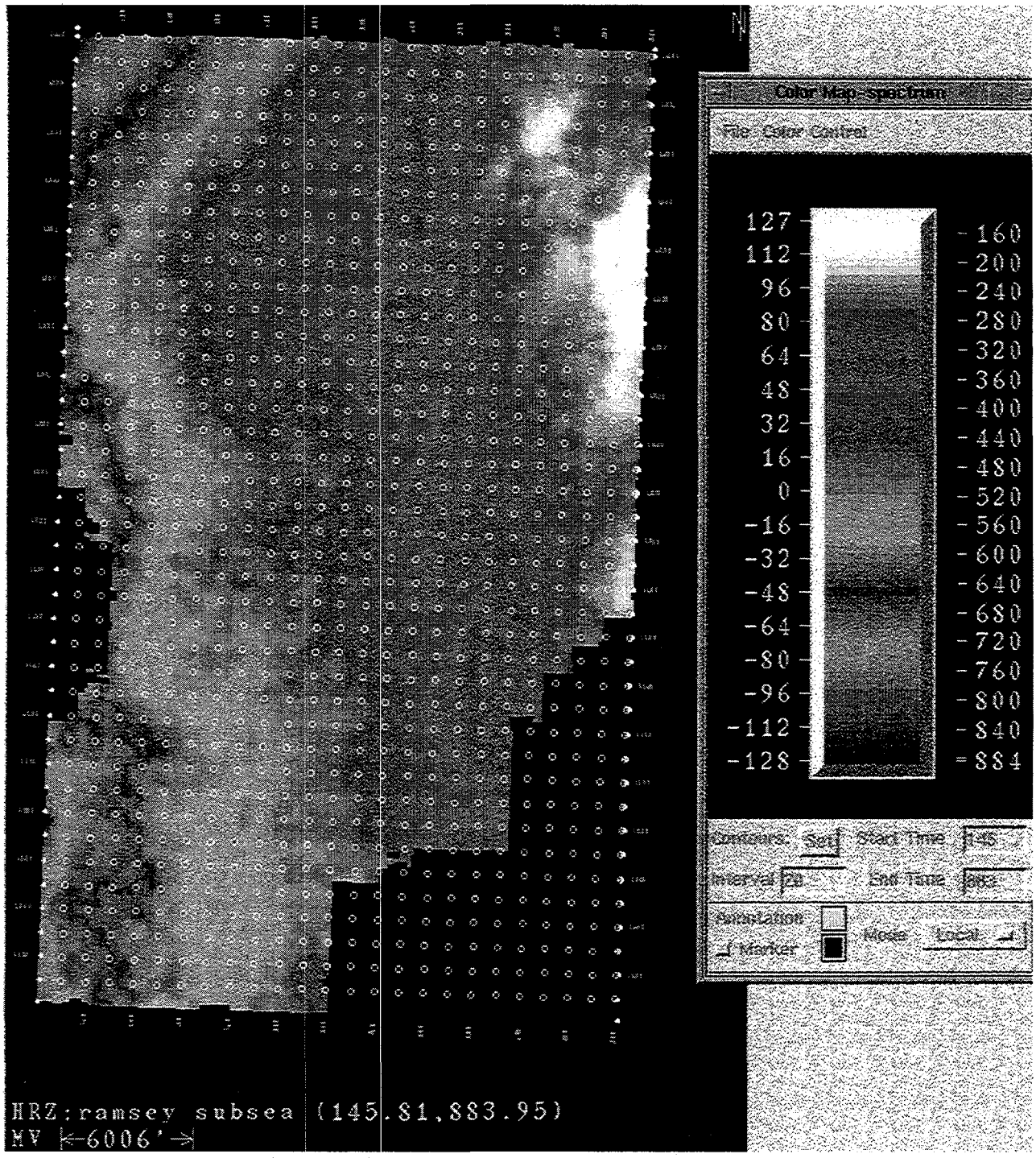

Figure 86. Top of Ramsey structure map. Contour interval is 20 ft (each break in color represents a 20-ft contour).

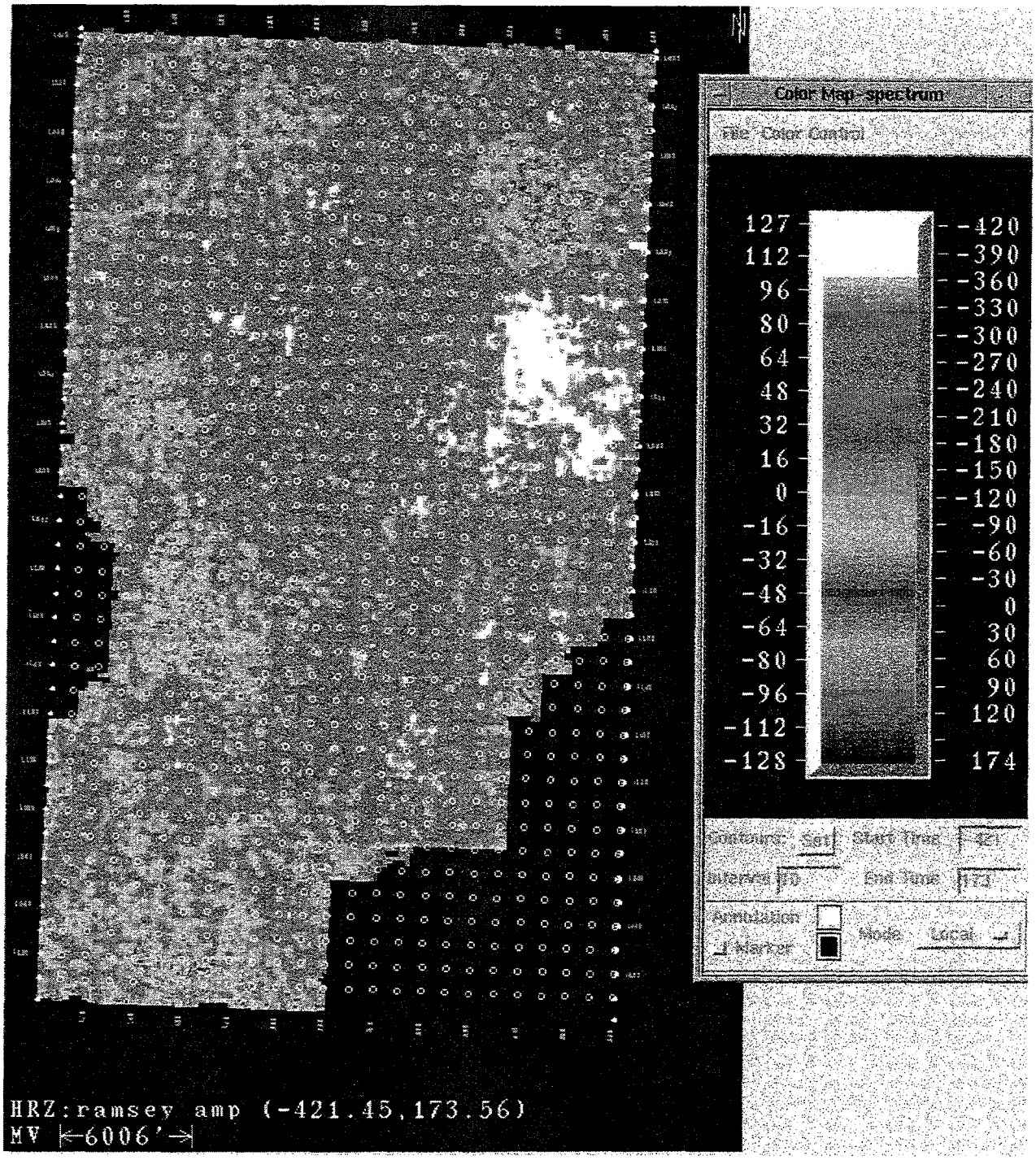

Figure 87. Ramsey amplitude map on the Ramsey trough seismic marker.

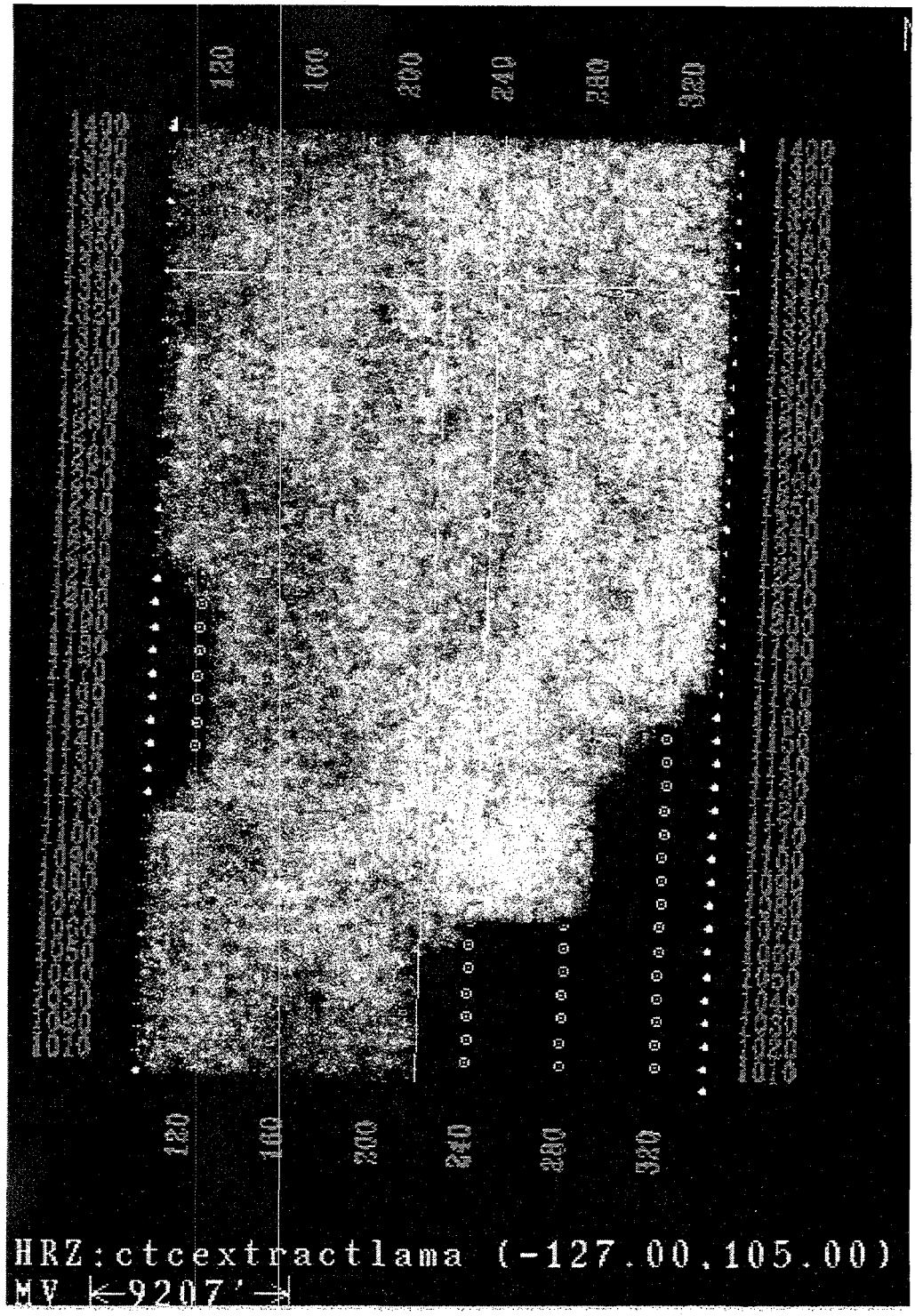

Figure 88. Coherence extraction on the top of the Lamar. Note the outline of the producing field in comparison with figure 79.

does not have the resolution to determine compartmentalization and did not indicate faulting in the Ramsey sandstone.

Correlation Coefficients and Cross Plots

Twenty-seven different seismic attributes were generated and cross plotted with various rock properties (such as porosity and permeability), production, and initial potentials over the entire field. Table 9 lists the top 24 correlation coefficients of the more than 300 correlation coefficients calculated. The best correlation coefficient of 0.49 was calculated using only the wells in the stage 5 area. The other correlation coefficients were calculated using the wells from the entire field. Consistently higher correlation coefficients were derived from cross plots of an amplitude attribute and porosity × thickness or average porosity. Attributes derived from the Ramsey trough had consistently higher correlation coefficients than those calculated from the Lamar peak, a composite amplitude, or a window encompassing both the trough and the peak.

The cross plot of Ramsey root-mean-square (RMS) amplitude against average porosity is presented in figure 89. The plot of Ramsey RMS amplitude (RMS amplitude extracted over a 10-ms window centered on the Ramsey trough) versus average porosity had the best correlation using the well data set from the entire field. The cross plot shows a wide scatter of points related to the low correlation coefficient of –0.39. In this case a high amplitude could correlate to a low or high porosity value and a low amplitude could correlate to a moderate or high porosity value. The porosity values from the field are limited in range, and a larger range of porosity samples might produce a higher correlation coefficient between the seismic amplitudes and porosity. The cross plot of Ramsey RMS amplitude against waterflood cumulative production to 1991 in the stage 5 area (fig. 90) shows the best correlation coefficient of 0.49. This shows that by limiting the data to the 45 wells in the stage 5 area, the correlation coefficient increased.

Table 9. Highest correlation coefficients calculated from the data set of seismic attributes cross plotted with various rock properties. Note highest correlation coefficient is 0.49.

	Well log data	Seismic data	Correlation coefficient
1	Waterflood cum 91	ramsey amp	0.49483
2	PHI avg	ramsey rms amp	–0.385492
3	PHI*h	ramsey rms amp	–0.3789
4	PHI*h	ramsey avg refl str	–0.377348
5	PHI*h	ramsey avg abs amp	–0.373124
6	PHI*h	ramsey avg trough	–0.370042
7	net pay >20%	ramsey rms amp	–0.36707
8	PHI avg	ramsey avg abs amp	–0.366438
9	PHI avg	ramsey avg trough	–0.365114
10	PHI avg	ramsey avg refl str	–0.36059
11	PHI*h	ramsey amp	0.360253
12	net pay >15%	ramsey comp	–0.351354
13	average perm	ramsey comp	–0.351354
14	net pay >15%	ramsey avg refl str	–0.349957
15	average perm	ramsey avg refl str	–0.349957
16	net pay >20%	ramsey avg abs amp	–0.34856
17	net pay >20%	ramsey avg refl str	–0.345852
18	net pay >15%	ramsey avg trough	–0.345775
19	average perm	ramsey avg trough	–0.345775
20	net pay >15%	ramsey rms amp	–0.345281
21	average perm	ramsey rms amp	–0.345281
22	net pay >15%	ramsey avg abs amp	–0.341708
23	average perm	ramsey avg abs amp	–0.341708
24	net pay >15%	ramsey amp	0.337709

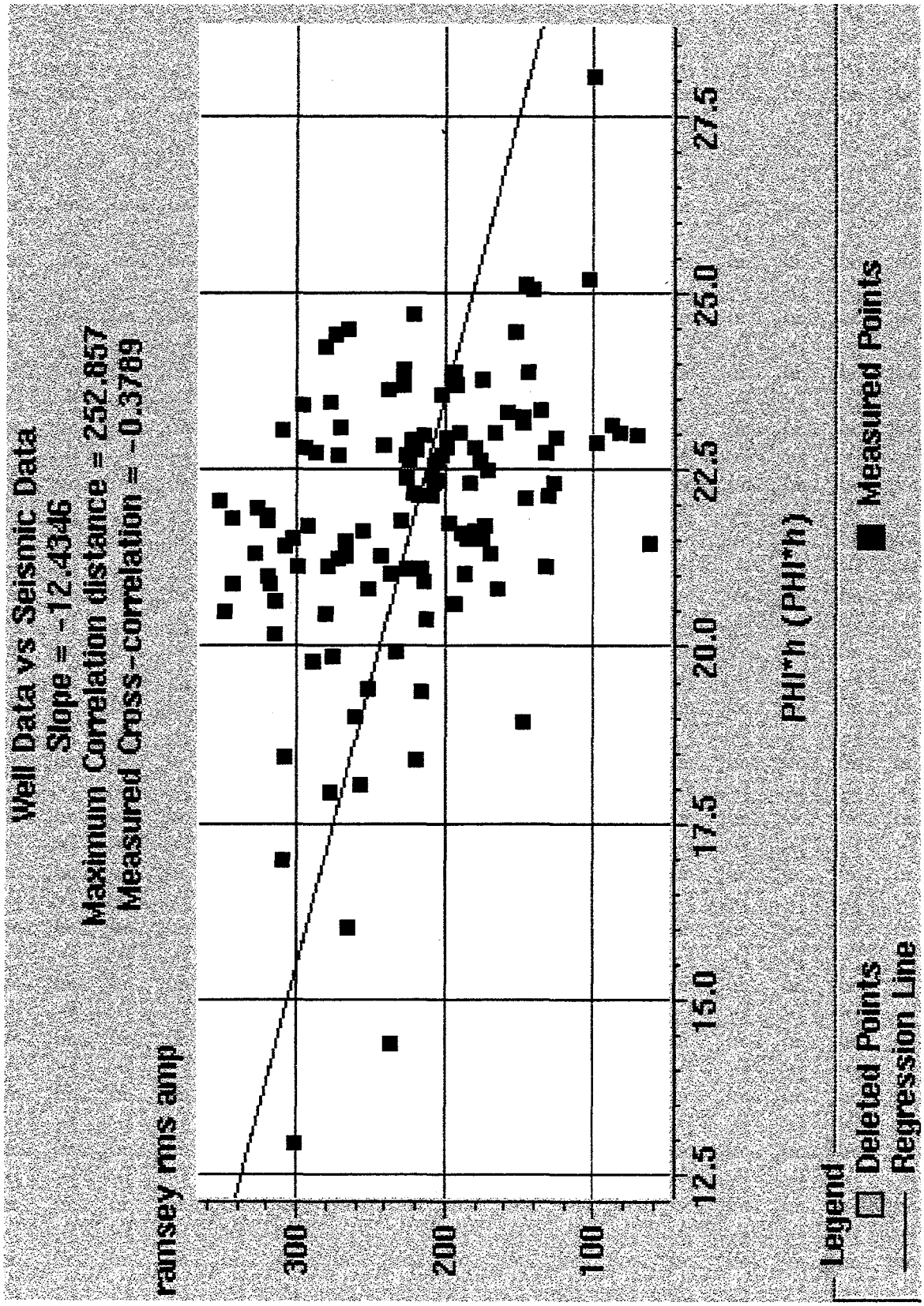

Figure 89. Cross plot of Ramsey RMS amplitude versus average porosity. Correlation coefficient is –0.39.

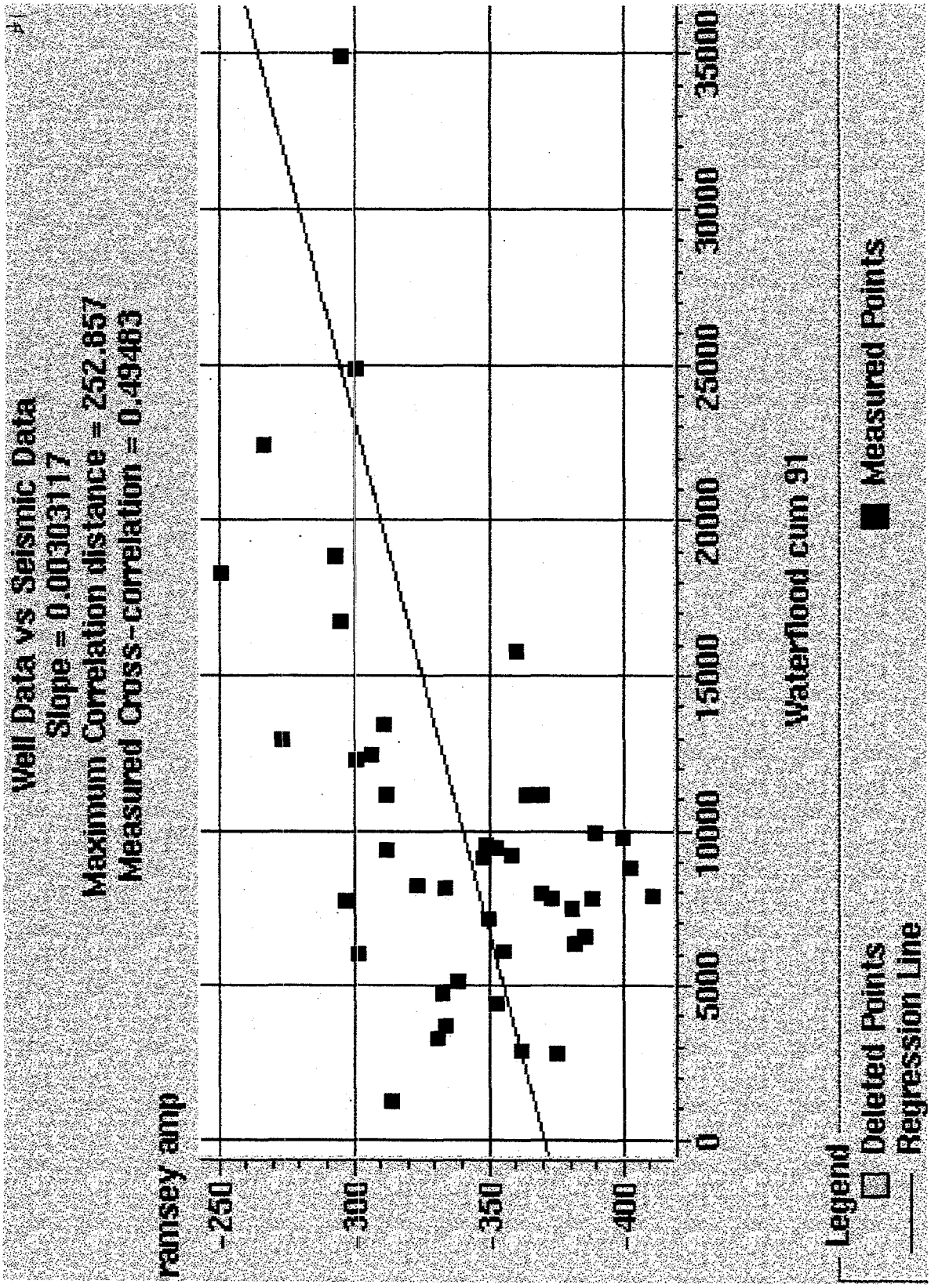

Figure 90. Cross plot of Ramsey RMS amplitude versus waterflood cumulative production to 1991 in the stage 5 area. Correlation coefficient is 0.49.

Conclusions

Accurately characterizing the Ramsey sandstone is difficult because Ramsey sandstone thickness is always ≤1/4 wavelength of the seismic data. This puts the Ramsey sandstone into the thin-bed category. Nonuniqueness becomes likely because other factors such as velocity and thickness of the Lamar limestone and composition of the Ford siltstone affect the seismic interval that is being used to characterize the Ramsey.

The coherency cube data are effective in delineating the field outline, but probably not as effective in detecting reservoir compartmentalization. More detailed comparison of reservoir properties and the subtle changes in coherency needs to be done to determine whether the coherency cube can help detect reservoir compartmentalization.

Residual mapping of the Lamar assisted in visualizing thick sandstones associated with the Ramsey 1 sandstone near the center of the field. Slight ridges can be seen in the structure map, but the residual maps make these ridges more obvious. Amplitude attributes were also effective in identifying the outline of the field. However, it was also observed that although high amplitudes identify the outline of the field, high amplitudes can also be associated with little or no sandstone, and low amplitudes are associated with the residual high and thick sandstone area in the center of the field. Detailed modeling, which was beyond the scope of this study, needs to be done to help resolve these conflicting observations.

Twenty-seven seismic attributes were calculated and cross plotted with various rock properties such as porosity and permeability, production, and initial potentials over the entire field. This resulted in a table with more than 300 rank correlations. The amplitude family of attributes consistently correlated best to reservoir properties. In addition, the rock properties of average porosity and porosity × thickness consistently correlated best to the seismic attributes. The cross plots of the best relationships between rock properties and seismic attributes exhibit significant scatter and have correlation coefficients of less than 0.4.

STOCHASTIC PERMEABILITY CHARACTERIZATION AND PRELIMINARY ENHANCED-RECOVERY PREDICTIONS OF PILOT AREA

The final task of the reservoir characterization phase will be to conduct a reservoir simulation of the demonstration area. To make reliable predictions of tertiary recovery from the demonstration area, fluid-flow simulations of CO_2 flooding will be conducted. These simulations will be based on stochastic permeability distributions and geologic characterization of the reservoir. They will predict the response of a demonstration CO_2 flood by testing various injector and producer well patterns to optimize design of the demonstration program.

The first step needed to simulate the pilot area is to generate interwell permeability distributions using geostatistical techniques. The methods used to do this are discussed in this section. Finally, although the simulation has not yet been conducted, production and other reservoir data were used to make preliminary estimates of tertiary recovery from the demonstration area with a CO_2 flood.

Geostatistical Permeability Modeling

Heterogeneity must be adequately represented to model subsurface reservoirs reliably. It is especially challenging to represent permeability heterogeneity because it cannot be directly mapped by any existing techniques. Geostatistical methods are commonly used now to generate interwell permeability distributions. In the technique called conditional simulation, the generated field honors the measured data, follows a desired correlation structure, and maintains reasonable heterogeneity (Journel and Huijbregts, 1978; Hewett, 1986; Lake and Malik, 1993; Malik, 1996).

Data Evaluation

For conditional simulation, the available data have to be examined to determine their distribution, and the cumulative distribution function (CDF) is a convenient tool for this purpose. The CDF of a data set with a normal distribution plots as a straight line on a linear scale on a

probability plot. Similarly, the CDF of a data set with a log-normal distribution plots as a straight line on a logarithmic scale on a probability plot. In the demonstration area, core permeability data are available for 21 wells with a total of 722 measured permeability values. The CDF of the permeability data plots almost as a straight line on log-probability coordinates (fig. 91), an indication that the permeability data in this field are distributed approximately log normally. The mean and standard deviation of log permeability are 1.036 and 0.805, respectively. The resulting coefficient of variation of 0.776 indicates that heterogeneity is of moderate degree (Jensen and Lake, 1988).

Autocorrelation

To determine the autocorrelation structure, vertical semivariograms (Jensen and others, 1997) of permeability and log permeability were plotted for the cored wells. Rescaled range (R/S) plots (Hewett, 1986; Malik, 1996) were also made to investigate the possibility of a power-law or fractal autocorrelation structure. Data in many wells indicated a spherical semivariogram, whereas a few wells appeared to support the possibility of a fractal or power-law semivariogram. The semivariograms of log permeability and their averages for three wells (FGU 6, 7, and 15) are shown in figure 92. These are some of the semivariograms with better structure. For wells FGU 6 and 7 the semivariograms can be interpreted to have approximately spherical autocorrelation structure with a dimensionless range of 0.3. The semivariogram for well FGU 15 has a continuously increasing trend, which is an indication of long-range autocorrelation typical of fractal or power-law semivariograms.

Because the semivariogram analysis did not indicate a well-defined autocorrelation structure, both types of semivariograms were tested in two vertical cross sections, and the resulting permeability distributions were compared with the geologic model of the reservoir. Dimensionless ranges of 0.3 and 0.5 were used for the spherical semivariogram, and intermittency or Hurst coefficients of H = 0.16 fGn and 0.7 fBm (derived from data from two different wells) were used for the power-law semivariogram in these cross sections. Two realizations of cross section G–G′

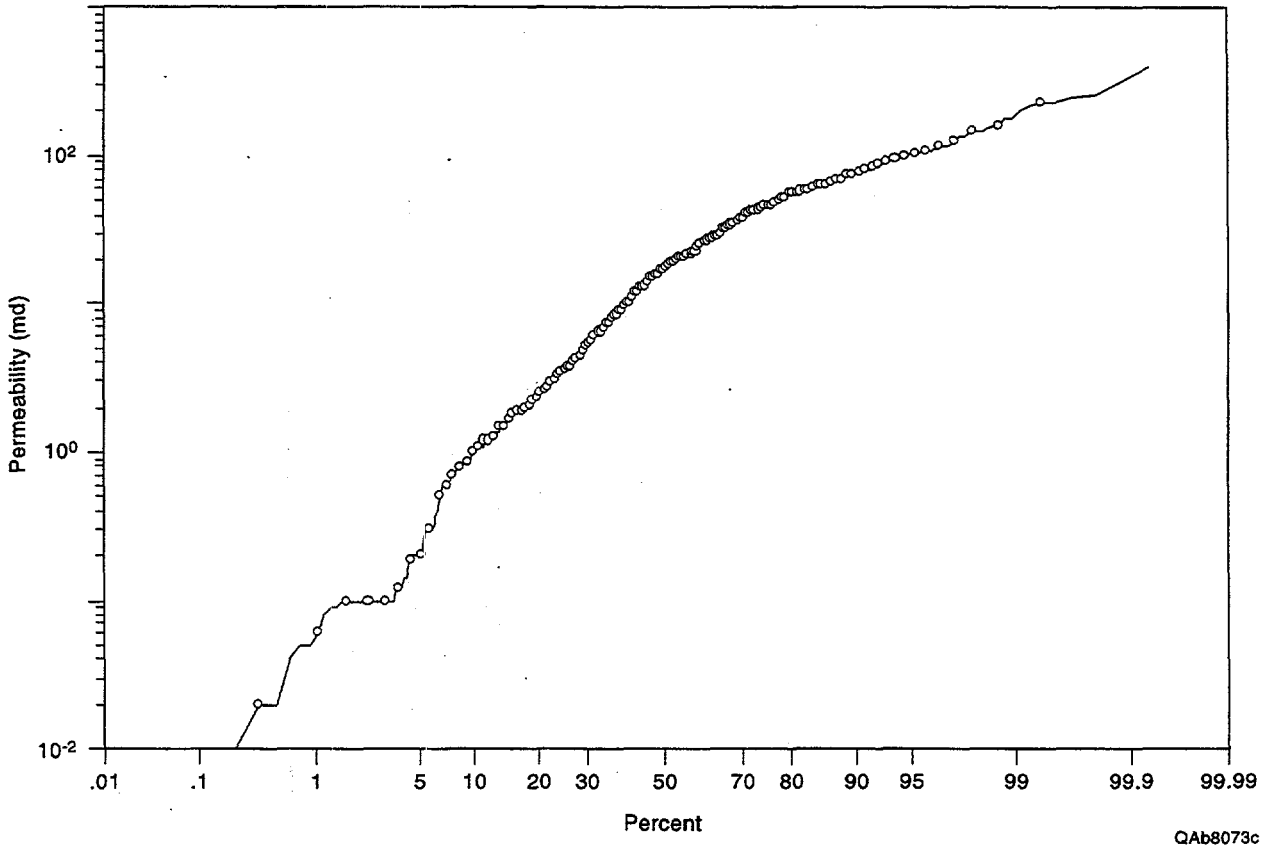

Figure 91. Cumulative distribution function of core-analysis permeability for 21 wells in the demonstration area.

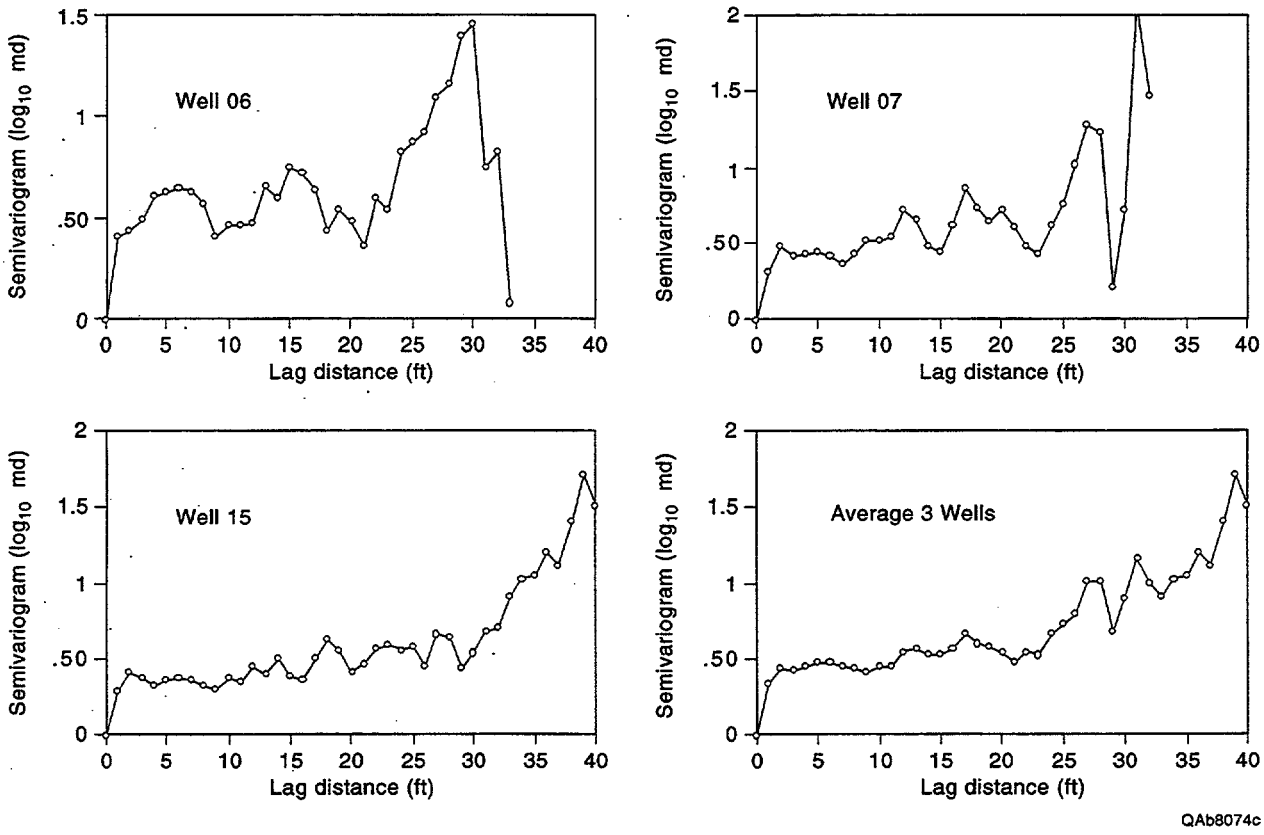

Figure 92. Vertical semivariograms for core-analysis permeability for wells FGU 6, 7, and 15 in the demonstration area, and the average for all three wells.

are shown in fig. 93. In this figure, the upper panel was generated by a spherical semivariogram with a dimensionless range of 0.3, whereas the lower panel was generated by a power-law semivariogram with H = 0.7 fBm. These realizations are log-normal, conditioned by data from wells FGU 3, 6, 11, 27, 312 and 24 (fig. 94). Both realizations are statistically equally probable, but they have to be evaluated with respect to the geology of the reservoir. Both Ramsey 1 and Ramsey 2 sandstones are present in the demonstration area, and between them is the low-permeability SH1 siltstone, which is continuous in the demonstration area. The lower panel in figure 93, although quite heterogeneous, is self similar everywhere and does not appear to mimic the dominant geological features. In the upper panel, however, the low-permeability laminated siltstone within the reservoir is reasonably represented by continuous low permeabilities in the middle horizontal portion. Above and below this unit, the heterogeneity is realistic, and extreme values are not predominant. These features are consistent with the characteristics of the two Ramsey sandstones. These observations indicated that a spherical semivariogram with a dimensionless correlation length of 0.3 is the preferable model for geostatistical permeability distribution in this field.

The demonstration area of the field (fig. 94) required 64,720 blocks for 3-D permeability distribution on the basis of a 150-ft-block size in each of the two areal directions (x and y) and 1 ft in the vertical (z) direction. A program based on the matrix decomposition method (MDM) (Fogg and Lucia, 1989; Yang, 1990) was used to generate the 3-D permeabilities. This method involves the inversion of a full matrix that is computationally intensive and time consuming. Therefore, the permeability distributions were generated in separate parts, each consisting of about 10,000 blocks.

Permeability Scale-Up

Although a block size of 150×150×1 ft is quite coarse compared with the subcentimeter-scale heterogeneity observed in sandstones, a total of 64,720 blocks is still too large for reservoir flow simulations to be performed economically. The generated permeabilities therefore had to be scaled

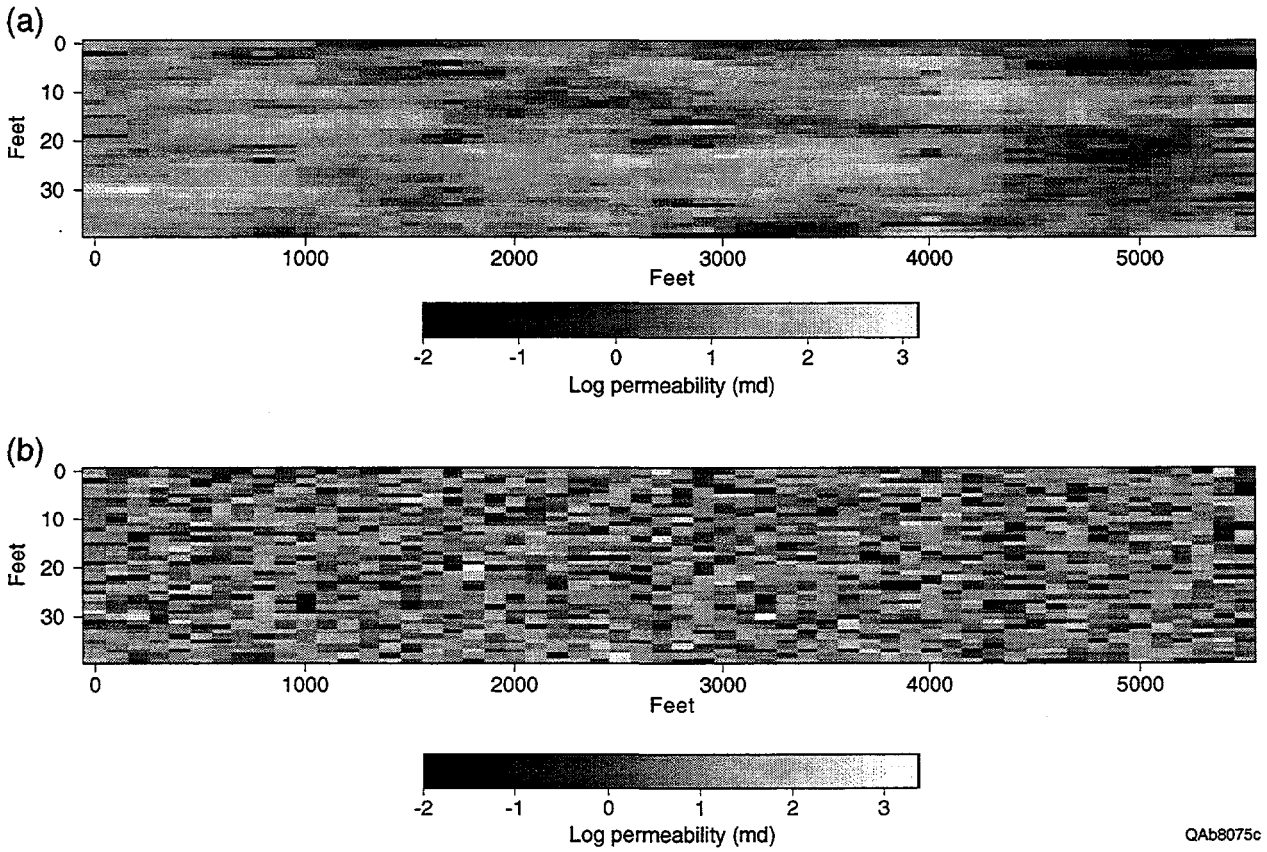

Figure 93. Two realizations of a 2-D cross section along line of section G–G′, which is shown in figure 4. (a) Realization made by a spherical semivariogram having dimensionless correlation length of 0.3. (b) Realization made by a power-law semivariogram with Hurst coefficient H = 0.7 fBm. Both cross sections are 56 × 40 blocks; blocks are 100 ft in the horizontal direction and 1 ft in the vertical direction.

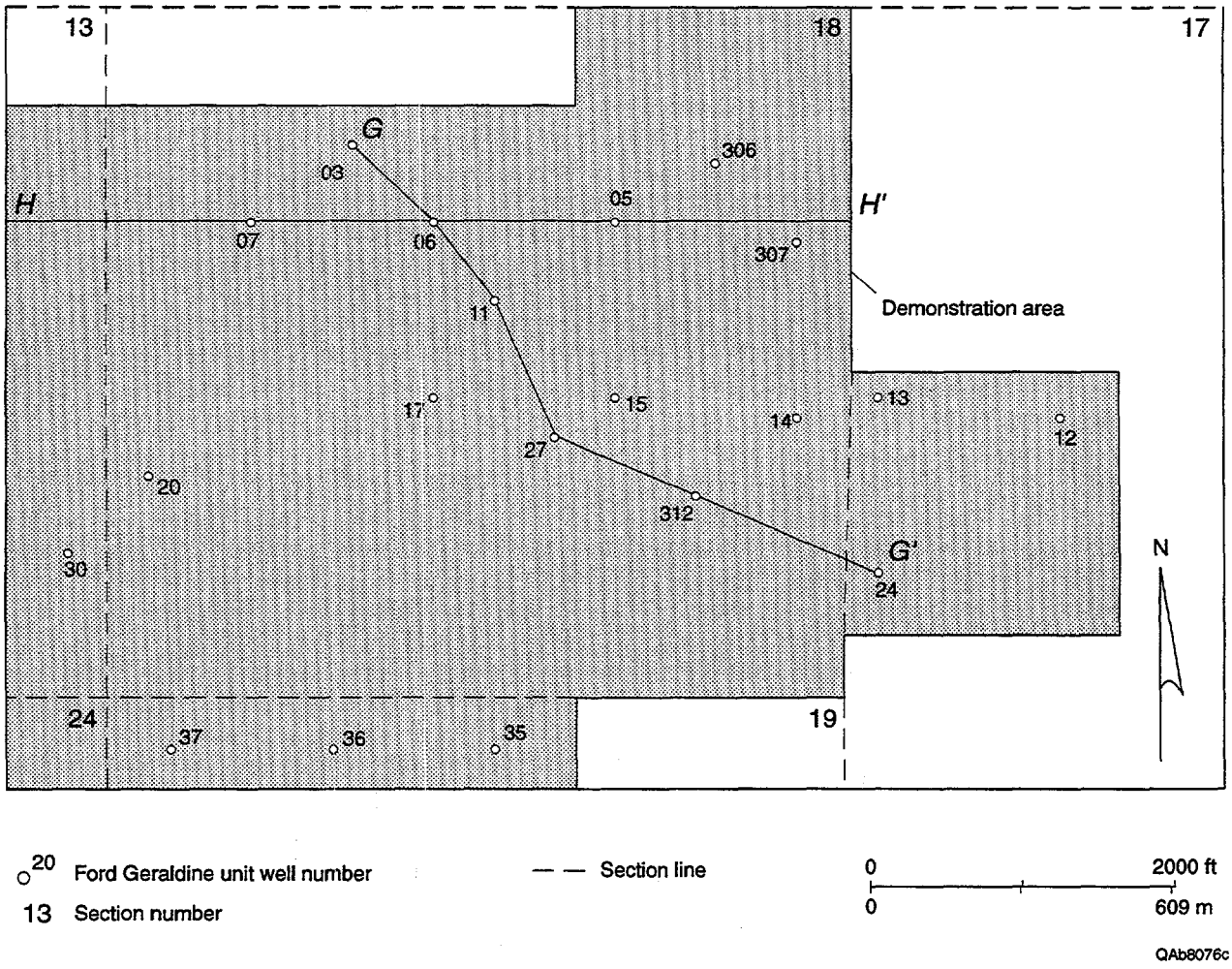

Figure 94. Map of demonstration area and location of wells used to generate the 3-D permeability distribution. The demonstration area occurs at the northern end of the Ford Geraldine unit.

up to bring the total number of blocks close to 10,000 for use in fluid-flow simulations. A 4×4×4 scale-up scheme appeared to be suitable.

Several permeability scale-up approaches are mentioned in the literature. They range from simple methods, such as geometric averaging, to more involved techniques, such as electrical network analogs (King, 1989). In a comparative study (Malik and Lake, 1997), it has been demonstrated that with a steady-state flow assumption, direct fine-scale simulation is accurate, flexible, and economical for permeability scale-up. An available 2-D code for this method was upgraded for 3-D cases to perform scale-up of the permeabilities generated for the demonstration area. In this method the coarse block is treated as a core and the initial conditions are set to irreducible water saturation in every fine-scale block. Buffer blocks are used at upstream and downstream ends of a course block for injection and production. A predetermined pressure drop is imposed to inject oil. Fluid-flow equations are numerically solved for only one time step to determine the single-phase flow rate with steady-state flow assumptions. Effective permeability of the coarse block is determined from Darcy's Law by using the imposed pressure drop, flow rate, flowing phase viscosity, and the length and cross sectional area of the coarse block.

The CDF's of scaled-up permeability and the corresponding fine-scale permeability are compared in figure 95 for a 40×4×40 fine-scale block portion of the reservoir along section G–G′ (fig. 94). The CDF of core permeability data is also shown for comparison. Despite the fine-scale permeabilities having been generated in parts, the CDF's of fine-scale permeabilities compare very well with the core-analysis data. The scaled-up permeability also follows the trend of the fine-scale permeability distribution. The averaging effect of scale-up noticeably affects the permeability values only in a small percentage of coarse blocks at the extreme ends.

Figure 96 shows a permeability image of a vertical cross section along section G–G′ (fig. 94) and the corresponding scaled-up cross section. Similarly figures 97 and 98 show fine-scale and corresponding coarse-scale areal cross sections from about the middle of the Ramsey 1 and 2 sandstones. In all three figures, reasonable heterogeneity is retained after scale-up. The fine-scale vertical cross section of figure 96 is more heterogeneous than the horizontal cross sections in

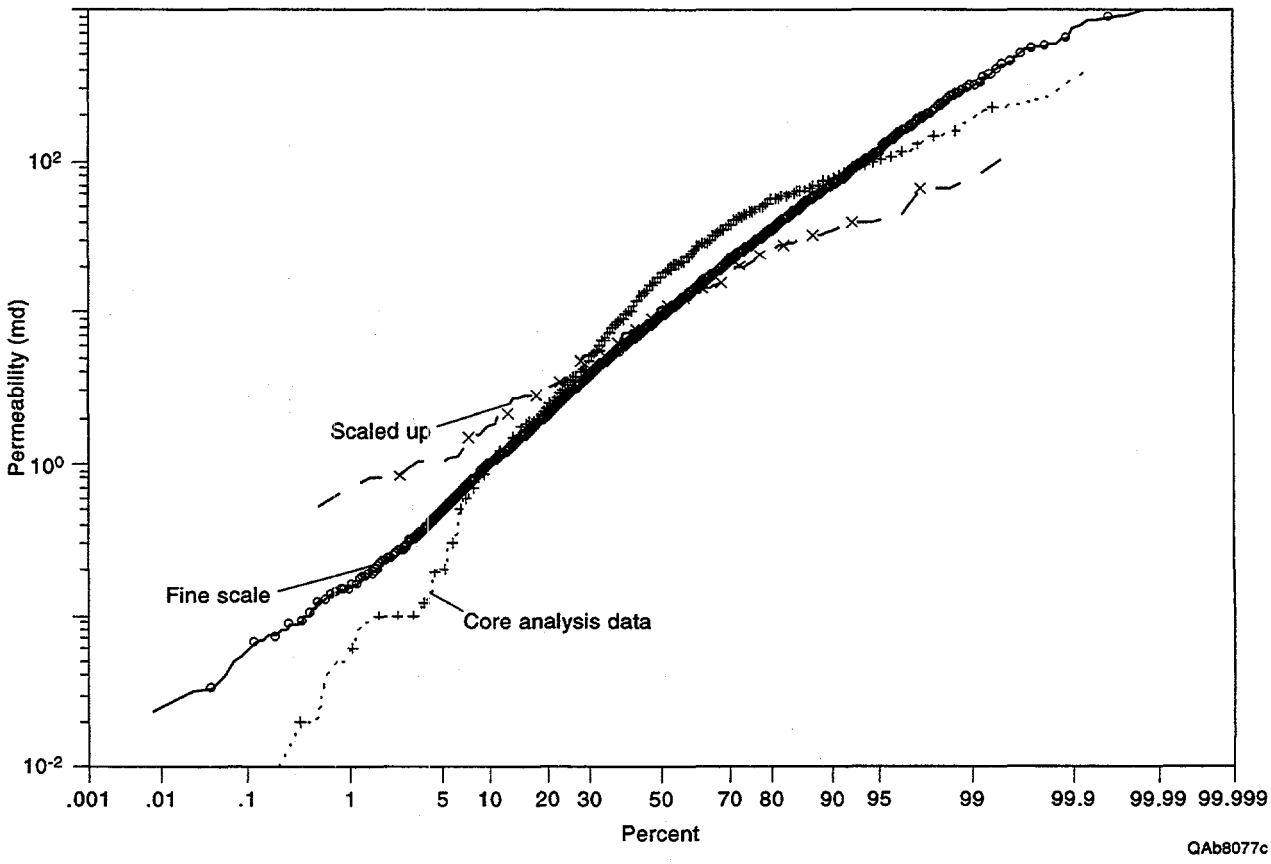

Figure 95. Cumulative distribution functions of permeability from (1) fine-scale permeability distribution, (2) scaled-up permeability distribution, and (3) permeability data from core analyses.

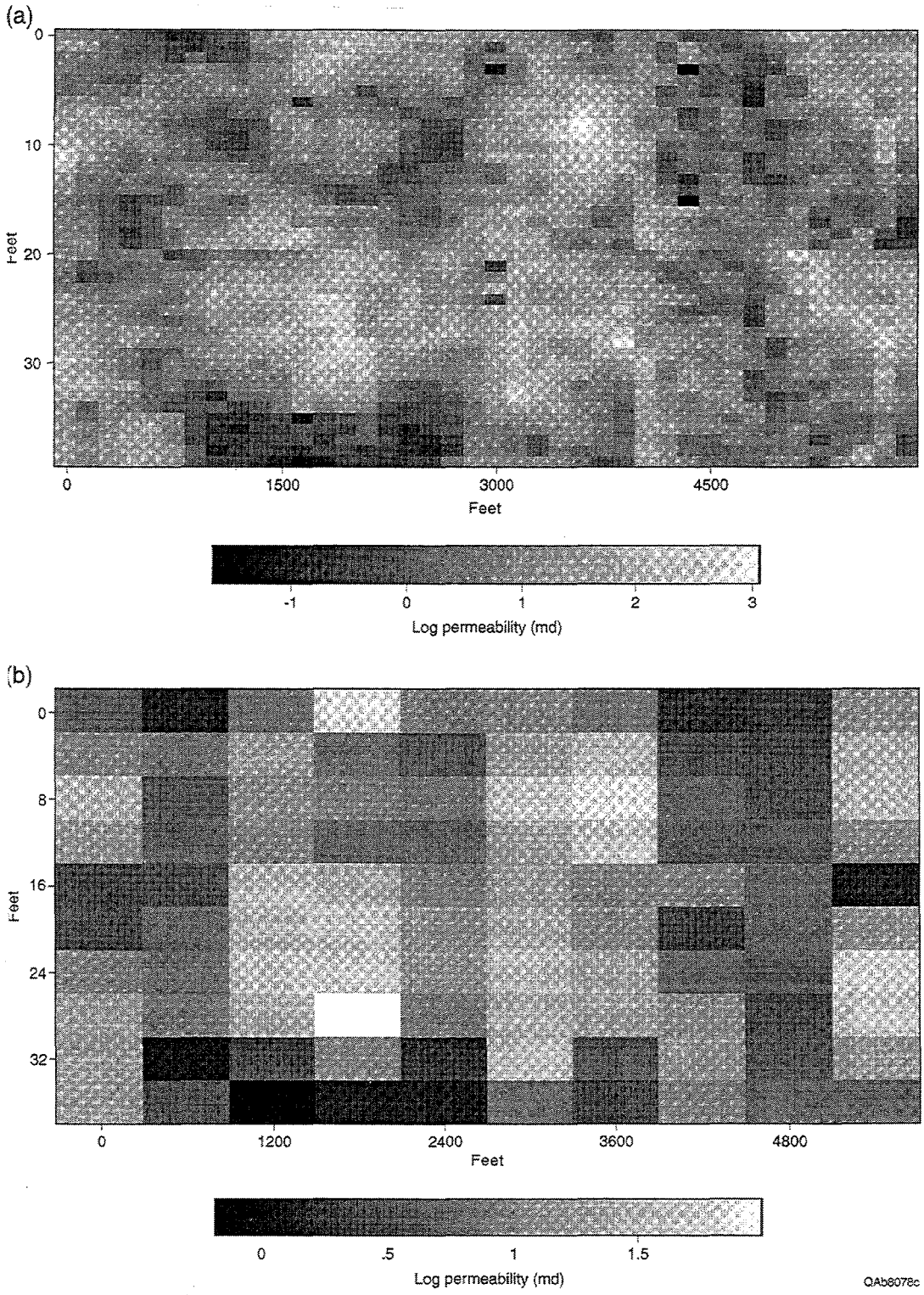

Figure 96. Vertical cross section showing permeability distribution along line of section H–H′ (fig. 4); permeabilities are from the 3-D permeability distribution. (a) Fine-scale permeability distribution in a 40 × 40 block, with a grid-block size of 150 ft in the horizontal direction and 1 ft in the vertical direction. (b) Scaled-up permeability distribution in a 10 × 10 block after performing a 3-D, 4 × 4 × 4 scale-up.

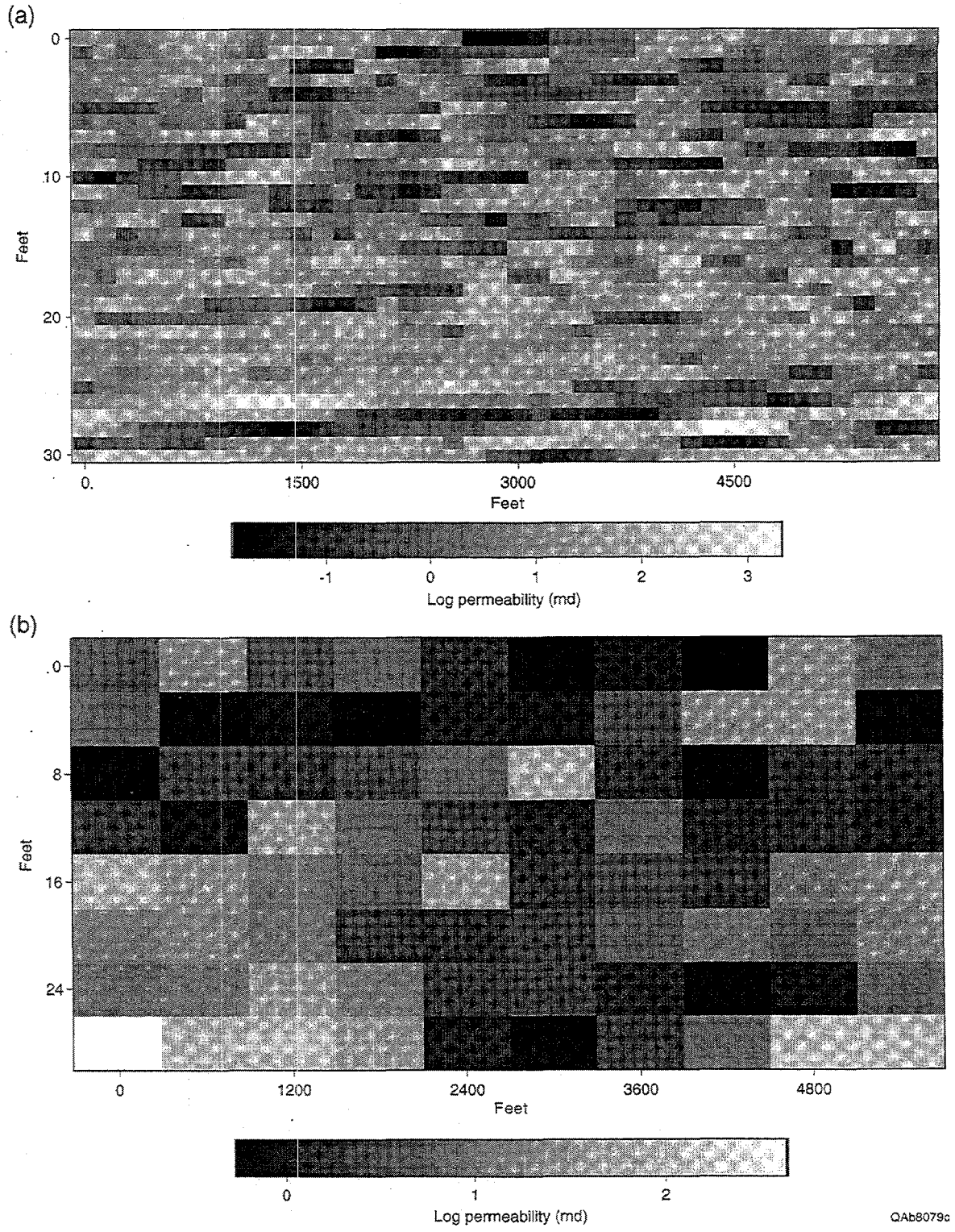

Figure 97. Areal cross section showing permeability distribution in the Ramsey 1 sandstone; permeabilities are from the 3-D permeability distribution. (a) Fine-scale permeability distribution in a 40 × 31 block, with a grid-block size of 150 ft in the horizontal direction and 1 ft in the vertical direction. (b) Scaled-up permeability distribution in a 10 × 8 block after performing a 3-D, 4 × 4 × 4 scale-up.

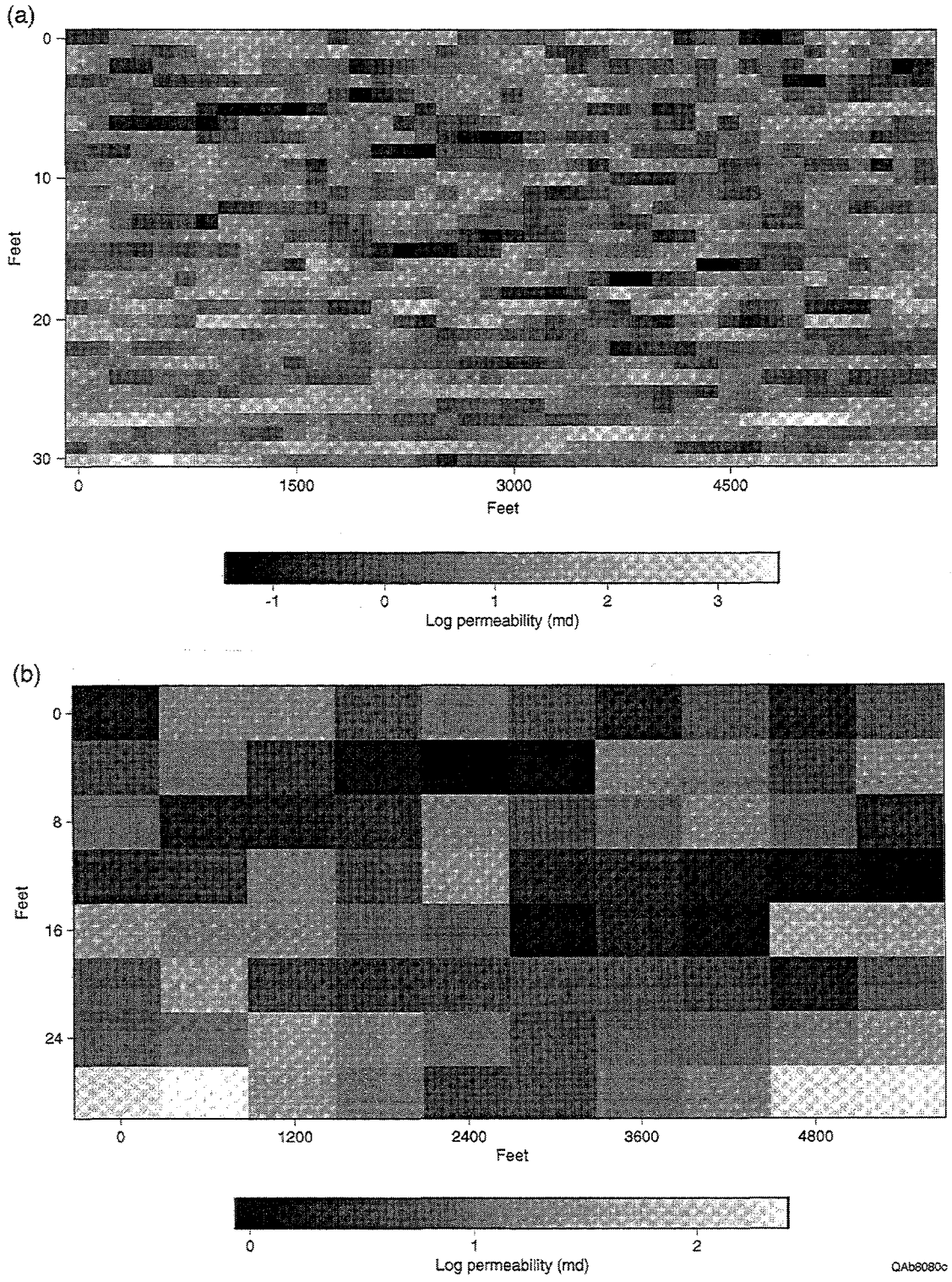

Figure 98. Areal cross section showing permeability distribution in the Ramsey 2 sandstone; permeabilities are from the 3-D permeability distribution. (a) Fine-scale permeability distribution in a 40 × 31 block, with a grid-block size of 150 ft in the horizontal direction and 1 ft in the vertical direction. (b) Scaled-up permeability distribution in a 10 × 8 block after performing a 3-D, 4 × 4 × 4 scale-up.

figures 97 and 98. This is consistent with the geology because the reservoirs are generally more heterogeneous vertically than laterally. Overall, the conditionally simulated stochastic permeabilities generated for the demonstration area appear to be in reasonable conformity with the main geologic features of the reservoir.

Preliminary Estimate of Tertiary Recovery

The Ford Geraldine unit has had a long production history. After primary production started to decline, a pilot waterflood was started in 1969 in area 1 (fig. 99). The waterflood was then extended to the entire field in the five stages marked in figure 99. The demonstration area was waterflooded in stage 5 in 1980. There is some evidence that during primary depletion, water from an adjoining aquifer encroached into this area. Therefore, most of the wells in area 5 were producing at high water cuts before the waterflood was started. In 1981, CO_2 injection was started for tertiary recovery in the central part of the reservoir and was gradually expanded into a major part of the reservoir. However, CO_2 flooding has not been implemented in the demonstration area

To make reliable predictions of tertiary recovery from the demonstration area, fluid-flow simulations of CO_2 flooding have been initiated. These simulations will be based on stochastic permeability distributions and geologic characterization of the reservoir. However, from the available production data and other information about the reservoir, preliminary estimates of tertiary recovery from the demonstration area can be made.

Original oil in place (OOIP) for areas 1 through 5 (fig. 99) is plotted in figure 100. Total OOIP is estimated to be 83.5 MMSTB. This is a conservative figure because in this reservoir, OOIP has been estimated as high as 110 MMSTB. Figure 101 shows primary, secondary, tertiary, and cumulative (primary+secondary or primary+secondary+tertiary) recovery by area as a percentage of OOIP. Area 5, the demonstration area, has only primary and secondary recovery. Area 3N is the only area with below-average production (fig. 101). The poor performance of this area is probably a result of the anomalous geologic and petrophysical features observed here. The 3N area includes the area of thin Ramsey 1 sandstone (fig. 35) and low average porosity (fig. 67),

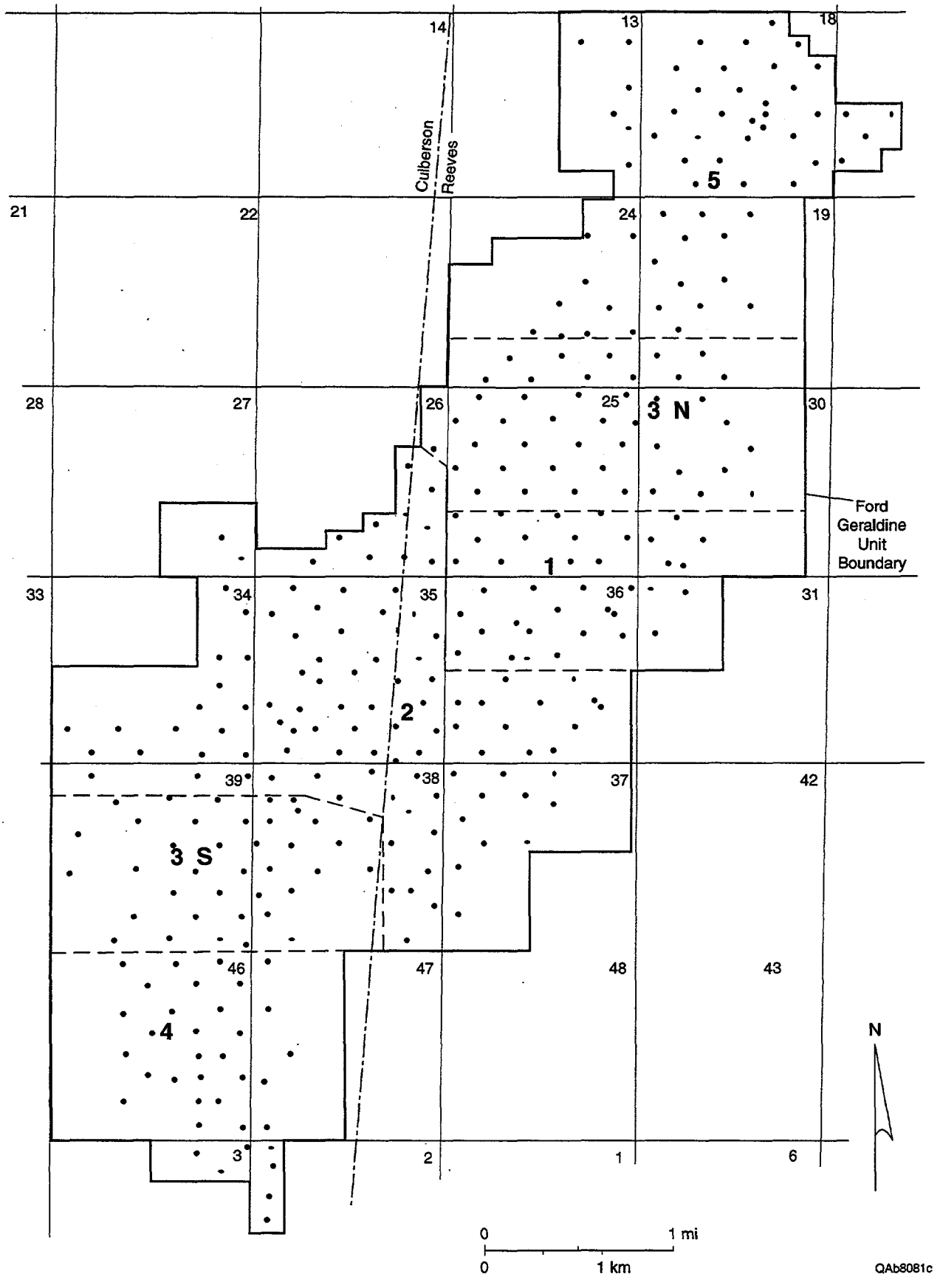

Figure 99. Waterflooding of the Ford Geraldine unit took place in five stages, in the areas shown.

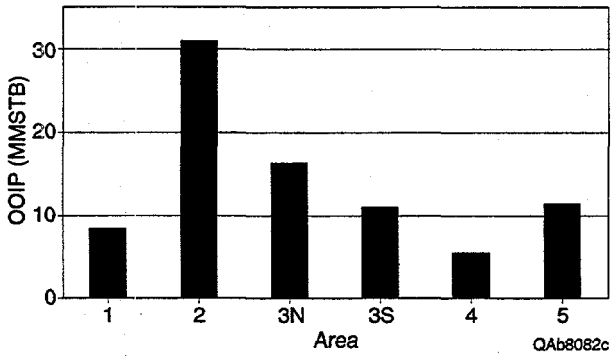

Figure 100. Original oil in place (OOIP) in waterflood areas 1 through 5. Areas are shown in figure 99.

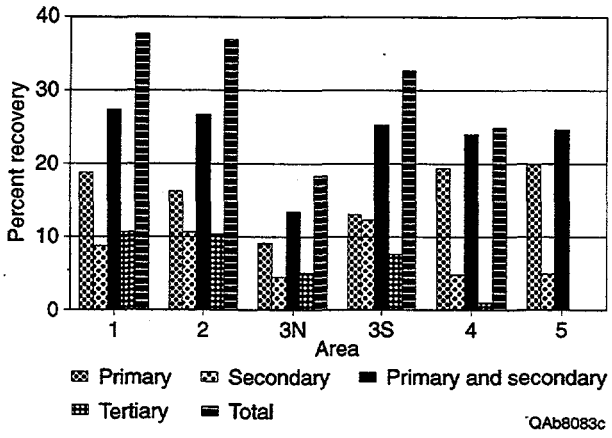

Figure 101. Primary, secondary, primary + secondary, tertiary, and total recovery through December 1995 as a percentage of original oil in place in areas 1 through 5. Areas shown in figure 99.

net pay (fig. 75) and $S_o \times \emptyset \times H$ (fig. 76). The primary and secondary recovery performance of the demonstration area is comparable to the other better producing areas of the reservoir. Postwaterflood oil saturations in the whole reservoir can be expected to be similar. Therefore, it is reasonable to assume that the demonstration area will perform similarly to the other areas in tertiary recovery.

Figure 102 shows the overall primary, secondary, and tertiary recovery to December 1995 in the reservoir as a percentage of OOIP. Tertiary recovery does not include the demonstration area. Using the average 7.9-percent tertiary performance of the rest of the reservoir, it is estimated that 904,000 STB of oil can be recovered from the demonstration area with a CO_2 flood (fig. 103). This is a conservative estimate; the results of the planned flow simulations are expected to confirm or exceed this estimate.

CONCLUSIONS

The research effort during the second year of the project concentrated on reservoir characterization of the Ford Geraldine unit and West Ford field. More of the work focused on the Ford Geraldine unit because it has more available data and a larger volume of oil in place than Ford West field, making it the more attractive target for enhanced recovery.

Interpretation of the processes that deposited the sandstones of the Delaware Mountain Group has long been controversial, and this controversy is of practical importance because different depositional models predict very different sandstone distribution, geometry, and continuity. A key component of our reservoir characterization effort was to investigate well-exposed analogs of the subsurface reservoirs in order to interpret the processes that deposited the reservoir sandstones in the Ford Geraldine unit and West Ford field and to develop a depositional model that could be used to interpret the subsurface data from those fields. Stratal relationships indicate that upper Bell Canyon sandstones exposed in outcrop were deposited by high- and low-density turbidity currents in a basinal deep-water setting. The fundamental depositional element is the channel with attached

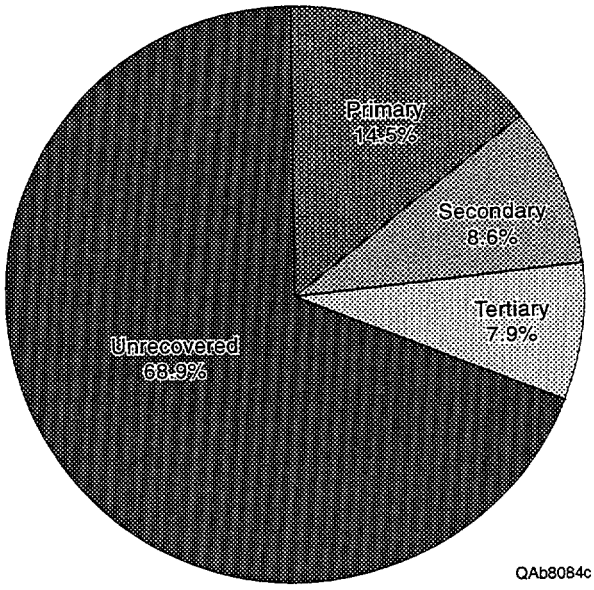

Figure 102. Primary, secondary, and tertiary recovery for all Ford Geraldine unit except area 5.

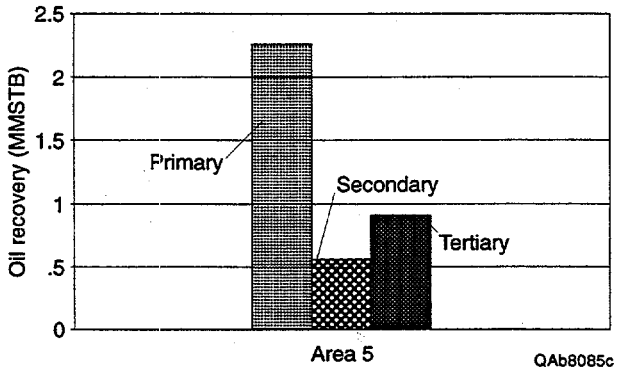

Figure 103. Primary and secondary recovery and projected tertiary recovery for area 5.

levees and lobes. The depositional model developed from outcrop for this project can be widely applied by operators to other reservoirs that produce from Delaware Mountain Group sandstones.

The model was used to interpret the processes that deposited the Ramsey sandstone reservoirs at the Ford Geraldine unit and to map the geometry and dimensions of the architectural elements within it. On the basis of core descriptions, subsurface mapping, and outcrop information, the Ramsey sandstones were interpreted as a channel-levee and lobe system. Reservoir sandstones consist of sheetlike lobe deposits overlain and incised by lenticular 1,200-ft-wide channels flanked by levee deposits. Ramsey sandstones are bounded by laterally continuous, organic-rich siltstones deposited by settling from suspension. The siltstone beds provide the greatest amount of depositional heterogeneity in the reservoir because of the grain size and permeability contrast between sandstones and siltstone facies. Because grain size is so uniform in the sandstone facies, the main control on reservoir quality is the volume of authigenic cement, particularly calcite and chlorite.

Upper Cherry Canyon and lower Bell Canyon B1 and B2 sandstone reservoirs at West Ford field are also interpreted as representing a channel-levee and lobe system deposited by turbidity currents. The grain size, detrital mineralogy, and cementation history of the West Ford reservoirs are similar to the Ramsey sandstones.

Special techniques were used to maximize the information that could be derived from the old geophysical logs at the Ford Geraldine unit. Using published information and log and core data, we determined net-pay cutoffs of volume of clay $\leq$ 15 percent, porosity $\geq$ 15 percent, and water saturation $<$ 60 percent for the Ramsey sandstone. Core-analysis and petrophysical data were used to construct maps of porosity, permeability, net pay, water saturation, porous hydrocarbon volume, and other reservoir properties.

The 3-D seismic survey that was done for this project was designed specifically to target Delaware Mountain Group reservoirs. For the first time, a key subsurface horizon above the Ramsey reservoir sandstone, the top of the Lamar Limestone, was imaged with 3-D seismic data. Residual mapping of the Lamar assisted in visualizing areas of thick Ramsey sandstone

development. Ramsey sandstone thickness in the Ford Geraldine unit is ≤1/4 wavelength of the seismic data. The amplitude family of attributes had the highest correlations with the reservoir properties of average porosity and porosity × thickness. Interpretation of the data included coherence cube evaluation to highlight discontinuities—a technique effective in delineating the field outline and perhaps one of the first uses of the coherency cube in a Delaware Mountain Group reservoir.

On the basis of reservoir characterization of the Ford Geraldine unit and West Ford field, the northern end of the Ford Geraldine unit was chosen as the proposed demonstration area. In preparation for simulation of the pilot area, conditional simulation was used to generate interwell permeability distributions.

The final task of the reservoir characterization phase will be to conduct a reservoir simulation of the demonstration area to make reliable predictions of tertiary recovery. These simulations will be based on stochastic permeability distributions and geologic characterization of the reservoir. The simulations will predict the response of a demonstration CO_2 flood and test various injector and producer well patterns to optimize design of the demonstration program. Preliminary estimates of tertiary recovery from the demonstration area were made using production and other reservoir data. It is estimated that 904,000 STB of oil can be recovered from the demonstration area with a CO_2 flood. This is a conservative estimate; the results of the planned flow simulations are expected to confirm or exceed this estimate.

ACKNOWLEDGMENTS

This research was funded by the U.S. Department of Energy under contract no. DE-FC22-95BC14936, by Conoco, Inc., and by the State of Texas under State Match Pool Project 4201 and as part of the State of Texas Advanced Resource Recovery project. The Bureau of Economic Geology acknowledges support of this research by Landmark Graphics Corporation via the Landmark University Grant Program. Research was assisted by Carlos Amaya, Radu Boghici, Janaka Paulus, and Mohammad Razi, whose hard work is gratefully acknowledged. Dr. R. P.

Major reviewed the manuscript. Drafting was by Christian T. Conly, Ruth E. O'Neal, Jana S. Robinson, Yvette Scott, Scott Schulz, David M. Stephens, and Tari Weaver of the Bureau of Economic Geology under the direction of Joel L. Lardon. Others contributing to the publication of this report were Susan Lloyd, word processing, Lana Dieterich, editing, and Susan Lloyd, pasteup.

REFERENCES

Archie, G. E., 1942, The electrical resistivity log as an aid in determining some reservoir characteristics: Petroleum Technology, v. 5, p. 54–62.

Asquith, G. B., 1979, Subsurface carbonate depositional models—a concise review: Tulsa, PennWell, 121 p.

Asquith, G. B., Thomerson, M. D., and Arnold, M. D., 1995, The recognition of possible oil and water wettability changes in the Permian Delaware Mountain Group sandstones from petrophysical well logs, *in* Martin, R. L., ed., In search of new Permian Basin oil and gas fields: West Texas Geological Society Fall Symposium, Publication 95-98, p. 39–50.

Asquith, G. B., and Gibson, C. R., 1982, Basic well log analysis for geologists: American association of Petroleum Geologists, Methods in Exploration Series, 216 p.

Atlas Wireline, 1985, Log interpretation charts: Houston, Texas, Atlas Wireline Services, Western Atlas International, Inc., 203 p.

Barton, M. D., 1997, Basin floor fan and channel-levee complexes, Permian Bell Canyon Formation: Dallas, Texas, 1997 American Association of Petroleum Geologists Annual Convention, Official Program, v. 6, p. A9.

Berg, R. R., 1979, Reservoir sandstones of the Delaware Mountain Group, southeast New Mexico, *in* Sullivan, N. M., ed., Guadalupian Delaware Mountain Group of west Texas and southeast New Mexico, Symposium and Field Trip Conference Guidebook: Society of Economic Paleontologists and Mineralogists (Permian Basin Section) Publication 79-18, p. 75–95.

Bureau of Economic Geology, 1993, State Lands Energy Resource Optimization Project Final Report, 89 p.

DeMis, W. D., and Cole, A. G., 1996, The Brushy Canyon play in outcrop and subsurface: concepts and examples: Guidebook, Permian Basin Section, SEPM, Publication No. 96-38, 188 p.

Dewan, J. T., 1984, Essentials of modern open-hole log interpretation: Tulsa, Oklahoma, PennWell Publishing Co. 345 p.

Dutton, S. P., Hovorka, S. D., and Cole, A. G., 1996, Application of advanced reservoir characterization, simulation, and production optimization strategies to maximize recovery in slope and basin clastic reservoirs, West Texas (Delaware Basin): The University of Texas at Austin, Bureau of Economic Geology, annual report prepared for the U.S. Department of Energy, DOE/BC/14936-5, 81 p.

Fischer, A. G., and Sarnthein, M., 1988, Airborne silts and dune-derived sands in the Permian of the Delaware Basin: Journal of Sedimentary Petrology, v. 58, p. 637–643.

Fogg, G. E., and Lucia, F. J., 1989, Stochastic simulation of interwell-scale heterogeneity for improved prediction of sweep efficiency in a carbonate reservoir: Dallas, NIPER/DOE Second International Reservoir Characterization Technical Conference, June 25–28.

Folk, R. L., 1974, Petrology of sedimentary rocks: Austin, Texas, Hemphill, 182 p.

Gardner, M. H., 1992, Sequence stratigraphy of eolian-derived turbidites: patterns of deep water sedimentation along an arid carbonate platform, Permian (Guadalupian) Delaware Mountain Group, West Texas, *in* Mruk, D. H., and Curran, B. C., eds., Permian Basin exploration and production strategies: applications of sequence stratigraphic and reservoir characterization concepts: West Texas Geological Society Publication 92-91, p. 7–12.

_____ in press, Reservoir characterization of deep-water siliciclastic reservoirs in the upper Bell Canyon and Cherry Canyon Formations of the northern Delaware Basin, West Texas, *in* Major, R. P., ed., Oil and gas on Texas State Lands: an assessment of the resource and characterization of type reservoirs: The University of Texas, Bureau of Economic Geology Report of Investigations No. 241.

Green, K. M., 1996, Water-flood feasibility study of the Brushy Canyon K-2 zone Red Tank field, Lea County, New Mexico: Texas Tech University, Master's thesis, 132 p.

Harms, J. C., 1968, Permian deep-water sedimentation by nonturbid currents, Guadalupe Mountains, Texas: Geological Society of America Special Paper 121, 127 p.

_____ 1974, Brushy Canyon Formation, Texas: a deep-water density current deposit: Geological Society of America Bulletin, v. 85, p. 1763–1784.

Harms, J. C., and Williamson, C. R., 1988, Deep-water density current deposits of Delaware Mountain Group (Permian), Delaware Basin, Texas and New Mexico: American Association of Petroleum Geologists Bulletin, v. 72, p. 299–317.

Hewett, T. A., 1986, Fractal distributions of reservoir heterogeneity and their influence on fluid transport: Society of Petroleum Engineers SPE Paper No. 15386.

Hilchie, D. W., 1979, Old electric log interpretation: Golden, Colorado, D. W. Hilchie Inc., 161 p.

Hills, J. M., 1984, Sedimentation, tectonism, and hydrocarbon generation in Delaware Basin, west Texas and southeastern New Mexico: American Association of Petroleum Geologists Bulletin, v. 68, p. 250–267.

Hiss, W. L., 1975, Stratigraphy and groundwater hydrology of the Capitan aquifer, southeastern New Mexico and western Texas: University of Colorado, Ph.D. dissertation, 396 p.

Holtz, M. H., and Major, R. P., 1994, Geological and engineering assessment of remaining oil in a mature carbonate reservoir: an example from the Permian Basin, West Texas: Society of Petroleum Engineers Permian Basin Oil and Gas Recovery Conference Proceedings, SPE Paper No. 27687, p. 565–576.

Jenkins, R. R., 1961, Characteristics of the Delaware Formation: Society of Petroleum Engineers, SPE Paper No. 44, p. 151–195.

Jensen, J. L., and Lake, L. W., 1988, The influence of sample size and permeability distribution upon heterogeneity measures: Society of Petroleum Engineers Reservoir Engineering, v. 3, p. 629–637.

Jensen, J. L., Lake, L. W., Corbett, P. W. M., and Goggin, D. J., 1997, Statistics for petroleum engineers and geoscientists: Upper Saddle River, New Jersey, Prentice Hall, 390 p.

Journel, A. G., and Huijbregts, C. J., 1978, Mining geostatistics: San Diego, Academic Press.

Kerans, Charles, Fitchen, W. M., Gardner, M. H., Sonnenfeld, M. D., Tinker, S. W., and Wardlaw, B. R., 1992, Styles of sequence development within uppermost Leonardian through Guadalupian strata of the Guadalupe Mountains, Texas and New Mexico, *in* Mruk, D. H., and Curran, B. C., eds., Permian Basin exploration and production strategies: applications of sequence stratigraphic and reservoir characterization concepts: West Texas Geological Society Publication 92-91, p. 1–6.

Kerans, Charles, Lucia, F. J., and Senger, R. K., 1994, Integrated characterization of carbonate ramp reservoirs using Permian San Andres Formation outcrop analogs: American Association of Petroleum Geologists Bulletin, v. 78, no. 2, p. 181–216.

King, P. R., 1989, The use of renormalization for calculating effective permeability: Transport in Porous Media, v. 4, p. 37–58.

Kneller, B., 1996, When is a turbidity current not a turbidity current? A question of mobility? (abs.): American Association of Petroleum Geologists Annual Convention, Official Program, v. 5, p. A76.

Lake, L. W., and Malik, M. A., 1993, Modeling fluid flow through geologically realistic media, *in* North, C. P., and Prosser, D. J., eds., Characterization of fluvial and aeolian reservoirs: Geological Society Special Publication, The University of Aberdeen.

Linn, A. M., 1985, Depositional environment and hydrodynamic flow in Guadalupian Cherry Canyon Sandstone, West Ford and West Geraldine fields, Delaware Basin, Texas: Texas A&M University, Master's thesis, 152 p.

Lowe, D. R., 1982, Sediment gravity flows: II. Depositional models with special reference to the deposits of high-density turbidity currents: Journal of Sedimentary Research, v. 52, p. 279–297.

Malik, M. A., 1996, Geostatistical reservoir characterization and scale-up of permeability and relative permeabilities: The University of Texas at Austin, Ph.D. dissertation, 174 p.

Malik, M. A., and Lake, L. W., in press, A practical approach to scaling-up permeability and relative permeabilities in heterogeneous permeable media: Society of Petroleum Engineers, SPE Paper No. 38310.

Meissner, F. F., 1972, Cyclic sedimentation in Middle Permian strata of the Permian Basin, west Texas and New Mexico, *in* Cyclic sedimentation in the Permian Basin, 2nd ed.: West Texas Geological Society, p. 203–232.

Mutti, E., and Normark, W. R., 1987, Comparing examples of modern and ancient turbidite systems: problems and concepts, *in* Leggett, J. K., and Zuffa, G. G., eds., Marine clastic sedimentology: concepts and case studies: London, Graham and Trotman, p. 1–38.

Payne, M. W., 1976, Basinal sandstone facies, Delaware Basin, west Texas and southeast New Mexico: American Association of Petroleum Geologists Bulletin, v. 60, p. 517–527.

Pittaway, K. R., and Rosato, R. J., 1991, The Ford Geraldine unit CO_2 flood—update 1990: Society of Petroleum Engineers Reservoir Engineering, v. 6, no. 4, p. 410–414.

Ruggiero, R. W., 1985, Depositional history and performance of a Bell Canyon sandstone reservoir, Ford-Geraldine field, west Texas: The University of Texas at Austin, Master's thesis, 242 p.

_____ 1993, Depositional history and performance of a Permian Bell Canyon sandstone reservoir, Ford-Geraldine field, West Texas, *in* Rhodes, E. G., and Moslow, T. F., eds., Marine clastic reservoirs: New York, Springer-Verlag, p. 201–229.

Ruppel, S. C., Kerans, Charles, Major, R. P., and Holtz, M. H., 1995, Controls on reservoir heterogeneity in Permian shallow-water-platform carbonate reservoirs, Permian Basin: implications for improved recovery: The University of Texas, Bureau of Economic Geology Geological Circular 95-2, 30 p.

Schneider, F. N., 1987, Three procedures enhance relative permeability data: Tulsa, Oklahoma, Oil and Gas Journal, March, p. 45–51.

Slatt, R. M., Jordan, D. W., D'Agostino, A. E., and Gillespie, R. H., 1992, Outcrop gamma-ray logging to improve understanding of subsurface well log correlations, *in* Hurst, A., Griffiths, C. M., and Worthington, P. F., eds., Geological applications of wireline logs II: Geological Society Special Publication No. 65, p. 3–19.

Sonnenfeld, M. D., 1991, High-frequency cyclicity within shelf-margin and slope strata of the upper San Andres sequence, Last Chance Canyon, *in* Meader-Roberts, Sally, Candelaria, M. P., and Moore, G. E., eds., Sequence stratigraphy, facies and reservoir geometries of the

San Andres, Grayburg, and Queen Formations, Guadalupe Mountains, New Mexico and Texas: Permian Basin Section, Society of Economic Paleontologists and Mineralogists Publication 91-32, p. 11–51.

Thomerson, M. D., 1992, Petrophysical analysis of the Brushy Canyon Formation, Hat Mesa Delaware field, Lea County, New Mexico: Texas Tech University, Master's thesis, 124 p.

Tyler, Noel, Barton, M. D., Bebout, D. G., Fisher, R. S., Grigsby, J. D., Guevara, Edgar, Holtz, M. H., Kerans, Charles, Nance, H. S., and Levey, R. A., 1992, Characterization of oil and gas heterogeneity: U.S. Department of Energy final report, no. DE92001072, 219 p.

Tyler, Noel, and Gholston, J. C., 1988, Heterogeneous deep-sea fan reservoirs, Shackelford and Preston waterflood units, Spraberry Trend, West Texas: The University of Texas, Bureau of Economic Geology Report of Investigations No. 171, 38 p.

Walling, S. D., 1992, Authigenic clay minerals in sandstones of the Delaware Mountain Group: Bell Canyon and Cherry Canyon Formations, Waha field, West Texas: Texas A&M University, Master's thesis, 63 p.

Williamson, C. R., 1977, Deep-sea channels of the Bell Canyon Formation (Guadalupian), Delaware Basin, Texas–New Mexico, *in* Hileman, M. E., and Mazzullo, S. J., eds., Upper Guadalupian facies, Permian reef complex, Guadalupe Mountains New Mexico and west Texas: Society of Economic Paleontologists and Mineralogists (Permian Basin Section) Publication 77-16, p. 409–431.

_____ 1978, Depositional processes, diagenesis and reservoir properties of Permian deep-sea sandstones, Bell Canyon Formation, Texas-New Mexico: The University of Texas at Austin, Ph.D. dissertation, 262 p.

_____ 1979, Deep sea sedimentation and stratigraphic traps, Bell Canyon Formation (Permian), Delaware basin, *in* Sullivan, N. M., ed., Guadalupian Delaware Mountain Group of west Texas and southeast New Mexico, Symposium and Field Trip Conference Guidebook: Society of Economic Paleontologists and Mineralogists (Permian Basin Section) Publication 79-18, p. 39-74.

Yang, An-Ping, 1990, Stochastic heterogeneity and dispersion: The University of Texas at Austin, Ph.D. dissertation, 241 p.

Zelt, F. B., and Rossen, C., 1995, Geometry and continuity of deep-water sandstones and siltstones, Brushy Canyon Formation (Permian) Delaware Mountains, Texas, *in* Pickering, K. T., Hiscott, R. N., Kenyon, N. H., Ricci Lucchi, F., and Smith, R. D. A., eds., Atlas of deep water environments, architectural style in turbidite systems: London, Chapman & Hall, p. 167–183.